

Mechanisms of color processing in the retina

Dissertation

for the award of the degree

“ Doctor of Philosophy ”

Division of Mathematics and Natural Sciences

within the doctoral program

Neurosciences

of the Georg-August University School of Science (GAUSS)

submitted by

Mohammad Hossein Khani

from: Tehran, Iran

Göttingen, 2018

Thesis committee

First referee and supervisor

Prof. Dr. Tim Gollisch

Department of Ophthalmology,
University Medical Center Göttingen

Second referee

Prof. Dr. Tobias Moser

Institute for Auditory Neuroscience & Inner Ear Lab
University Medical Center Göttingen

Third referee

Prof. Dr. Siegrid Löwel

Systems Neuroscience Group
Johann-Friedrich-Blumenbach-Institute of Zoology and Anthropology
Bernstein Focus for Neurotechnology
University of Göttingen

Further members of the examination board

Prof. Dr. Stefan Treue

German Primate Center
Dept. of Cognitive Neurosciences
University of Göttingen

Dr. Marion Silies

Visual Processing group
European Neuroscience Institute Göttingen (ENI)

Prof. Dr. André Fiala

Schwann-Schleiden Research Centre
Dept. of Molecular Neurobiology of Behavior
University of Göttingen

Date of oral examination: 14 December 2017

Declaration

I declare that this thesis is an original report of my research, has been written by me and the experimental work is entirely my own work. This work has not been submitted for any previous degree. Except where states otherwise by reference or acknowledgment, the work presented is entirely my own.

Mohammad Hossein Khani

Göttingen, October 2017

To my grandmother

Acknowledgements

I am truly and deeply grateful to many people who supported me during this project. First and above all, I would like to thank my advisor Tim Gollisch for his continuous support of my PhD. I am grateful to him for his patience, motivation, enthusiasm, great knowledge and above all his trust in me for managing my project. His guidance throughout my work helped me to become a better researcher and scientist.

Beside my advisor, I would like to thank the members of my thesis committee, Prof. Dr. Tobias Moser and Prof. Dr. Siegrid Löwel for their encouragements, hard questions, insightful comments, and support during the 4 years of my PhD. I am very grateful to all my fellow lab mates in the sensory processing in the retina lab. I like to thank them for the amazing atmosphere of the lab and all the great scientific discussions that we had. I would like to thank Helene Schreyer, Diasuke Takeshita, Michael Weick, Vidhyasankar Krishnamoorthy, Fernando Rozenblit, Norma Kühn, Jian Liu, Dimokratis Karamanlis, Sebastian Bemme, Larissa Lauterbach, Luis Giordano Ramos Traslosheros López, Michael Siebrecht, Daniela Proto, Omar Diaz and Christiane Westermann for their great support over the years. In addition, I like to thank all the rotation students, Lucas Weiss, Alina Heukamp, Yunus Can Erol, Clara Tepohl and Deniz Yüzak. I would especially like to express my gratitude to Helene Schreyer for her great patience, motivation, and amazing understanding throughout my PhD. Her amazing support and encouragement was in the end what made this dissertation possible.

I would like to thank the coordination team of the International Max Planck Research School (IMPRS) for Neurosciences, Prof. Dr. Michael Hörner and Sandra Drube for their awesome support throughout the years. Additionally, I like to thank my IMPRS neuroscience family and my classmates for all the great discussion and fun that we had together. Last but not least, I would like to thank my parents and my brothers for supporting me throughout my life.

Abstract

In the sensory system, many neurons are specified to detect different environmental signals and transfer the signals to downstream neurons. These downstream neurons integrate the detected signals and generate an output that is evolutionally relevant for the organism. In the retina, the photoreceptors are specified to detect light from the environment at different wavelength, thus separating the input light into different chromatic channels. The chromatic signals from the photoreceptors are integrated by downstream bipolar and ganglion cells. Although chromatic properties of the photoreceptors and the bipolar cells are relatively known, it is not clear how retinal ganglion cells integrate their chromatic inputs.

In this project, we studied the properties of chromatic signal integration in the mouse retina. We used the mouse retina because of its dichromatic light sensitivity to both UV (ultra-violet) and green light. We first built a new projection system that allowed us to stimulate both s-cones (UV sensitive) and m-cones (green sensitive) of the mouse. We designed a new stimulation approach that allowed us to probe the question of chromatic integration. In this stimulation approach, we showed opposing contrasts of the UV and green light simultaneously and checked the responses of the ganglion cells with multi-electrode arrays. We focused on the stimulus combinations where the opposing contrasts of UV and green could effectively cancel each other out (cancellation point). Based on the responses of the ganglion cells at the cancellation point, we asked whether ganglion cells integrate their chromatic inputs linearly or nonlinearly. The chromatically linear cells did not showed any different responses from their spontaneous activity at the cancellation point. The nonlinear cells, on the other hand, showed reliable responses at the cancellation point. Moreover, we found a separation between the responses of the On and Off nonlinear cells. The Off cells showed increased firing rates at the cancellation point. The On cells, however, showed suppressive responses by reducing their activity below their spontaneous firing rates. Next, we classified the ganglion cells based on the chromatic integration properties and their responses to the preferred and non-preferred light stimulus. Further, we used computational models to simulate both linear and nonlinear chromatic integration. In the final step of this thesis, we looked into potential mechanisms of nonlinear chromatic integration. We used

a grating variant of our color integration stimulus that allowed us to stimulate the center of the receptive more effectively than the surround. We observed that by reducing the effect of the surround the chromatically linear cells do not change their integration properties while the nonlinear cells become linear. Thus, we concluded that the nonlinearity of the chromatic integration is induced by the receptive field surround of the ganglion cells.

To conclude, we found a new type of nonlinear computation in the mouse retina, which can assist the current functional classifications schemes of the retinal ganglion cells that usually ignore the chromatic integration properties. Furthermore, we believe that our experimental approach could potentially be used in other sensory systems to investigate the nonlinear computations of neurons.

Contents

Overview.....	1
1. Chromatic processing and signal integration in the retina.....	7
1.1. The retina.....	7
1.2. Similarities and differences between mouse and primate retina.....	11
1.3. Color processing in the retina.....	14
1.4. Signal integration in the retina.....	15
1.5. Center-surround structure of the receptive field.....	17
1.6. Aim of this study.....	20
2. Experimental methods.....	21
2.1. Animals.....	21
2.2. Retina preparation.....	22
2.3. Visual stimulation.....	24
2.4. Electrophysiology.....	24
2.5. Spike sorting.....	25
2.6. Analysis of ganglion cells response to the chromatic integration stimulus.....	26
2.6.1. The cancellation point.....	27
2.6.2. Polarity of the responses.....	28
2.6.3. Rectification of the non-preferred stimulus.....	28
2.7. Classification of retinal ganglion cells based on their chromatic integration characteristics.....	31
2.7.1. Monochromatic index.....	31
2.7.2. Nonlinearity index.....	31
2.7.3. On-Off bias.....	33
2.7.4. Rectification index.....	33
2.8. Measuring the properties of chromatic integration responses.....	34
2.8.1. Green-UV index.....	34
2.8.2. Transient-sustained index.....	34
2.9. Measuring properties of the strongest response.....	35
2.10. Spike-triggered analysis.....	36
2.10.1 Spike-triggered average.....	37
2.11. Receptive field estimation.....	37
2.12. Linear-nonlinear Poisson model.....	39
2.13. Nonlinear-linear-nonlinear model.....	40
3. Projection System.....	43
3.1. Building a new projection system.....	43
3.2. Selection of the projector.....	44
3.3. Preparation of DLP lightcrafter projector for UV-green stimulation.....	45

3.3.1 Finding a matching UV LED.....	46
3.3.2. Replacing the blue LED.....	48
First step: separating the light engine from the projection circuitry:	48
Second step: replacing the blue LED with the UV LED.....	49
3.4. Building a new lens system.....	54
3.5. Mounting platform and optical cage system.....	58
3.6. Brightness adjustment of the projection system.....	63
3.6.1 Brightness adjustment with different filters	63
3.6.2 Brightness adjustment through the software.....	64
3.7. Calibration and gamma correction of lightcrafter projector.....	65
3.8. Isomerization and cone-isolation.....	68
3.8.1. Isomerization	68
3.8.2. Cone-isolation.....	69
4. Linear & nonlinear chromatic integration in the mouse retina.....	71
4.1. Chromatic integration stimulus.....	71
4.2. Analysis of chromatic integration stimulus.....	73
First: The cancellation point.....	75
Second: Polarity of the responses	75
Third: Rectification of the non-preferred stimulus.....	76
4.3. Diversity of chromatic signal integration among retinal ganglion cells.....	78
4.3.1. Chromatically linear ganglion cells.....	78
4.3.2. Chromatically nonlinear ganglion cells.....	82
4.3.3. Monochromatic, On UV-sensitive and unclassified ganglion cells.....	87
4.4. Classification of retinal ganglion cells based on their chromatic integration characteristics.....	90
First: Monochromatic index.....	90
Second: Nonlinearity index	91
Third: On-Off bias	93
Fourth: Rectification index	93
Fifth: Classification	93
4.5. Population analysis of the chromatic integration classes.....	95
4.5.1. Population analysis based on the chromatic integration curves.....	95
First: Contrast combination at the crossing point	95
Second: Rectification index of the nonlinear cells.....	96
Third: Contribution of the s- and m- opsins on the response of the ganglion cells	97
Fourth: Transient vs sustained cells.....	98
Fifth: Relative proportion of each class.....	98
4.5.2. Population analysis based on the strongest response.....	99
First: Dynamics of the response	99
Second: Peak of the firing rate.....	100
Third: Decay time and Final to peak response.....	101
Fourth: Baseline rate.....	101
5. The impact of the receptive field surround on chromatic integration.....	103
5.1. Modelling chromatic signal integration using a nonlinear- linear- nonlinear cascade model.....	104
5.2. The role of the receptive field surround in the chromatic signal integration.....	109
5.3. Chromatic grating stimulus.....	110
5.4. Analysis of chromatic grating stimulus.....	112
5.5. Surround contribution to the chromatic integration of linear and nonlinear ganglion cells.....	115

5.5.1. Linear rectifying and non-rectifying cells.....	116
5.5.2. Nonlinear cells.....	116
5.5.3. Linear On-Off cells.....	116
5.5.4. Population comparison between the chromatic integration classes.....	117
5.6. Receptive field properties of the chromatically linear and nonlinear ganglion cells	121
5.6.1. Temporal properties of chromatic integration classes.....	122
5.6.2. Ganglion cell's location and its chromatic integration.....	122
5.6.3. Receptive field properties across the population	126
6. Discussion.....	127
6.1. Linear chromatic integration	128
First: Potential circuitry of the linear chromatic integration:.....	129
Second: rectification properties of linear cells	132
6.2. Nonlinear chromatic integration.....	133
6.3. Functional roles of chromatic linearity and nonlinearity	135
6.4. Inference of integration nonlinearities with iso-response measurements	136
6.5. Comparison to other color processing studies.....	137
6.6. UV stimulus and the mouse retina.....	138
6.7. Classification of the ganglion cells beyond chromatic integration.....	139
7. Outlook	141
Closure	143
Bibliography	145

List of figures

Chapter 1:

Figure 1.1. Schematic structure of the eye and the retina.	9
Figure 1.2. Different arrangements of photoreceptors in the mouse and human retina.	13
Figure 1.3. Linear and nonlinear spatial integration in the cat retina.....	16
Figure 1.4. Center-surround structure of the receptive field of a ganglion cell.....	18

Chapter 2:

Figure 2.1. Schematic illustration of the experiment procedure, projection system and the electrophysiology setup.....	23
Figure 2.2. Chromatic integration curves and the cancellation point of green-on, UV-off and green-off, UV-on contrast combinations.....	27
Figure 2.3. Response polarity of On, Off and On-Off cells.	29
Figure 2.4. Rectification of the non-preferred stimulus for non-rectifying, rectifying and On-Off cells.....	30
Figure 2.5. Measurement of the nonlinearity index from the chromatic integration curves.	33
Figure 2.6. Measuring the properties of the strongest response.....	36
Figure 2.7. Measuring properties of the ganglion cell receptive field.....	40

Chapter 3:

Figure 3.1. DLP lightcrafter and its input/output ports.	45
Figure 3.2. Spectrum and architecture of the red, green and blue LEDs that are used in the light engine of the DLP lightcrafter projector and the spectrum and architecture of the replaced UV LED.	48
Figure 3.3. Systematic guide to open the light engine from the lightcrafter projector.	52
Figure 3.4. Details of the lightcrafter light engine.....	55
Figure 3.5. Schematic design of the lens system.....	57
Figure 3.6. Reflectance curves and schematic view of the lenses used inside the lens system.	58
Figure 3.7. Mounting platform and the optical cage system of the projector.	60
Figure 3.8. Transmittance of the filters used in the lens system of the projection system.	65
Figure 3.9. Gamma correction of the lightcrafter projector and examples of cone-isolated stimuli.	68

Chapter 4:

Figure 4.1. Schematic view of the chromatic integration stimulus.....	73
Figure 4.2. Chromatic integration stimulus was designed based on the classical stimulus that was used to study spatial integration in the retina.....	74
Figure 4.3. Chromatic integration responses and its analysis.	77
Figure 4.4. Response characteristics of a chromatically linear rectifying Off ganglion cell.....	80
Figure 4.5. Response characteristics of chromatically linear, non-rectifying ganglion cell.....	81
Figure 4.6. Response characteristics of a chromatically nonlinear Off ganglion cell.	84
Figure 4.7. Response characteristics of a chromatically nonlinear On-Off ganglion cell.	85
Figure 4.8. Response characteristics of a chromatically nonlinear On ganglion cell.	86
Figure 4.9. Examples for each ganglion cell types based on their chromatic integration properties.	90

Figure 4.10. Classification of the ganglion cells based on their chromatic integration, response polarity and rectification features.	92
Figure 4.11. Basic properties of the different ganglion cell groups that were classified based on their chromatic integration curves.	97
Figure 4.12. Population analysis based on the strongest response to the chromatic integration stimulus. ...	100
Chapter 5:	
Figure 5.1. Structure of the nonlinear-linear-nonlinear (NLN) model.	105
Figure 5.2. Output of the NLN model using different nonlinear functions for $N1(.)$ and $N2(.)$	108
Figure 5.3. Schematic view of the chromatic grating stimulus.	111
Figure 5.4. Examples of linear and nonlinear chromatic integration in response to the chromatic grating stimulus.	114
Figure 5.5. The effects of receptive field surround on the chromatic integration properties of the nonlinear cells.	118
Figure 5.6. Different integration properties of the On-Off linear cells in response to the chromatic grating stimulus.	119
Figure 5.7. Reducing the effects of the receptive field surround linearize the chromatic integration of the nonlinear cells.	121
Figure 5.8. Receptive field properties of the chromatic integration classes.	124
Figure 5.9. Receptive field properties of the chromatic integration classes.	125

Overview

As we browse scenes with our eyes and with every image that we see, countless number of light photons enter our eyes. The light is passed through the pupils and is focused by the cornea and lens onto the retina where the photons get absorbed by the photoreceptors of the retina. Each photoreceptor then transforms the light input into electrical activity. Mammalian retinas have different types of photoreceptors. Each photoreceptor type has a specific opsin that is sensitive to a certain spectrum of light and allows each photoreceptor to convert a certain wavelength of the input light into electrical signals. Thus, the retina breaks apart each image into its chromatic components at its very first synapse. These separated input signals are then transferred to different bipolar cells and the signals split further into more parallel input streams. These different inputs are transferred to the retinal ganglion cells in a way that each ganglion cell pools information from many bipolar cells. The inhibitory cells such as horizontal cells at the synapse of the photoreceptors and bipolar cells, and the amacrine cells at the synapse of the bipolar and ganglion cells modulate the input signals. These modulations add even more complexity to the functions of the retina. As a result, for every image that we see, such as the text of this page, our retina processes different features of the image such as color, brightness, edge etc. in a way that the output of the retina is a good representative of that image. The retina achieve these capabilities through mechanisms such as parallel processing of the input signals, convergence and divergence of signals, adaptation and sensitization to different brightness levels and contrast of the stimulus. Moreover, the retina has nearly 100 specific types of neurons (Masland, 2012; Euler et al., 2014; Seung and Sumbul, 2014; Sanes and Masland, 2015; Baden et al., 2016; Franke et al., 2017) with unique anatomical and functional properties along with many different types of nonlinear operations that allow the retina to process each visual scene (Gollisch and Meister, 2010).

Therefore, to understand the visual processing of the retina, we need to first understand the mechanisms involved in the processing of the image at different levels of the retina. Moreover, it is important to go beyond the structure and anatomy of the cells and study the functional nonlinearities

that are used by the retina. Finally, the operations that are done by the retina such as nonlinear signal processing, signal integration, adaptation etc. are common among many other neurons as the fundamental functional features of the nervous system. Thus, understanding these operations and mechanisms in the retina would guide us to have a better understanding of the functional properties of the nervous system.

In this thesis, we aim to study mechanisms of the chromatic signal integration in the retina. In this project, we investigated two fundamental features of the retina, chromatic processing and signal integration.

The photoreceptors of the retina break each image into its chromatic components and the ganglion cells receive the chromatic information from tens to hundreds of photoreceptors through bipolar cells and integrate these inputs into their spiking output. Therefore, studying how chromatic inputs are processed by the ganglion cells helps us, on the one hand, to get a better understanding of the chromatic signal processing in the retina and on the other hand, to elucidate the signal integration features of the retina. Furthermore, we hope that by studying chromatic signal integration, we get a better understanding of the functions of the retina in particular and the nervous system in general.

We used the mouse retina as the model for studying chromatic signal integration. Mouse is an established model for vision research (Huberman and Niell, 2011; Baker, 2013; Seabrook et al., 2017). The mouse retina has two types of cone photoreceptors (dichromatic vision), with peak sensitivity to either ultraviolet (360 nm) or green light (508 nm). These two photoreceptors separate the input light into two chromatic signal channels, which is an advantage for studying signal integration in the retina. The chromatic signals from the photoreceptors are transferred to the bipolar cells. Most bipolar cells of the mouse retina make non-specific connection to both types of cones and few bipolar cells receive inputs from one type of cones (Haverkamp et al., 2005; Behrens et al., 2016). Therefore, some bipolar cells integrate the chromatic inputs while others keep the signals separate. The ganglion cells receive chromatic signals from different bipolar cells and integrate these signals to generate their output.

In this project, we ask how each ganglion cell integrates its chromatic inputs. We approach this question by asking whether the ganglion cells integrate chromatic signals linearly or nonlinearly. This approach has been used extensively in investigating the spatial integration in the retina. Previous studies have reported spatially linear and nonlinear ganglion cells in the retinas of different species such as cat (Enroth-Cugell and Robson, 1966), guinea pig (Demb et al., 1999; Zaghoul et al., 2007), rabbit (Caldwell and Daw, 1978; Hamasaki et al., 1979; Famiglietti, 2004) and monkey (de Monasterio, 1978; Petrusca et al., 2007; Crook et al., 2008). Beyond that, other studies showed the effects of the nonlinear spatial integration on specific functions of the retina such as object-motion detection (Olveczky et al., 2003; Baccus et al., 2008). In these studies, the presence of different forms of spatial integration in the retina and their influence on the functional output of the retina was shown. Unlike spatial integration, little is known about the chromatic signal integrations in the retina. Previous

studies relevant to chromatic processing in the retina were mainly focused on the color opponent ganglion cells. These studies found chromatic opponent ganglion cells in the primate with red-green and blue-yellow opponency (Dacey and Lee, 1994; Dacey, 1996, 1999; Dacey and Packer, 2003; Diller et al., 2004; Packer et al., 2010; Crook et al., 2011). In the guinea pig and mouse retina, the ganglion cells with UV-green opponency have been found (Yin et al., 2006, 2009; Chang et al., 2013). However, in both mouse and guinea pig the opponent cells constitute small population of the ganglion cells. Moreover, these opponent cells were found in specific regions of the retina, dorsal and ventral edge of the retina for guinea pig (Yin et al., 2006, 2009) and center of the retina for the mouse (Chang et al., 2013). Thus, beyond the opponent cells, not much is known about chromatic processing of the other ganglion cells.

In this thesis, we used multi-electrode array recording of the ganglion cells in isolated retina of the mouse. Multi-electrodes recording is a powerful tool that allowed us to record from different regions of the retina. This way we could gather information about chromatic integration properties of different ganglion cells. To stimulate both s- and m-cones of the mouse retina effectively, we built a new projection system that allowed us to activate individual s- and m-cones independently. We designed and used a specific stimulus that helped us to check for the linearity and nonlinearity of the chromatic integration. We found that the majority of the ganglion cells in the retina integrate their chromatic inputs linearly. Additionally, we found certain population of the ganglion cells that showed nonlinear chromatic integration. In the next step, we searched for the potential mechanisms of linear and nonlinear chromatic integration. Previous studies about the spatial integration showed that the nonlinearity of the integration is caused by the synapse between the bipolar cells and the ganglion cells with the influence of the amacrine cell and the receptive field surround (Zaghloul et al., 2007; Baccus et al., 2008; Molnar et al., 2009; Werblin, 2010). In this study, we investigated the mechanisms of chromatic integration by analyzing the role of the receptive field surround in the chromatic integration characteristic of the ganglion cells. We studied the role of the surround with both modelling and experimental approaches. We found that the receptive field center showed mostly linear chromatic integration properties. For the nonlinear cells, the receptive field surround likely influences the center and creates the nonlinearity of their chromatic integration.

This thesis is organized in six chapters.

In the first chapter, we describe the anatomy and functions of the retina. We start by describing organizational layers and different cell types of the retina. We then explain the functional roles of each cell type in the retina. Next, we compare the features of the mouse retina to the primate retina. Furthermore, we provide an overview of the color processing properties of the retina and highlight the most important findings. We then continue with the signal integration features of the retina and make an overview about different findings regarding signal integration in the retina. Moreover, we provide a brief description about the receptive field structure of retinal ganglion cells. Finally, we explain the

main goal of this thesis by focusing on the chromatic signal integration properties of the retinal ganglion cells.

In the second chapter, we describe the general methods that we used in this project. We start the chapter by describing the experiments. We first explain the procedure of the retina preparation followed by description of the electrophysiological methods that were used in this study. After that, we describe the analytical approaches and methods that were used to interpret the experimental data.

The third chapter is a specific method chapter. A significant part of this PhD project was devoted to develop new approaches and techniques that allowed us to study chromatic integration in the mouse retina. In this work, we built a new projection system that allowed us to activate the s- and m-cones of the retina independently. This projection system consists of a UV-green projector, a new UV-fusing lens system, and a mounting system. The third chapter serves as a guideline for building similar projection systems, which can be used in studies of mouse visual system especially in cases where stimulating the s-cones of the mouse retina is important. After describing the technical parts of this chapter, we explain the necessary steps for calibration, brightness adjustments, and gamma-correction of the projector. Finally, we describe the approach we used to generate cone-isolating stimuli that was used systematically in this project.

In chapter four, we present the first part of the results of this thesis. We introduce a stimulation paradigm that we designed to study chromatic integration in the retina. With this stimulation approach, we studied whether the ganglion cells integrate their chromatic inputs linearly or nonlinearly. Next, we describe the analytical approaches we used to measure the linearity and nonlinearity of the chromatic integration. Based on the chromatic integration, and other properties of the ganglion cells such as the polarity of the response and the rectification of the non-preferred stimulus, we classified the recorded ganglion cells into different classes. We then look at the properties of the classes on the population level and focus on features that show the difference between the classes. Therefore, chapter four serves as a descriptive part of the results where we describe our findings about linear and nonlinear chromatic integration in the retina. Moreover, we show the diversity of the chromatic integration and beyond that, we show how other properties of the ganglion cells are relevant to their chromatic integration.

In chapter five, we present the second part of the result. In this chapter, we aim to investigate the potential mechanisms of linear and nonlinear chromatic integration. We attempt to simulate the responses of the chromatically linear and nonlinear ganglion cell by using the nonlinear-linear-nonlinear (NLN) model. From our modelling studies, we speculate about the role of receptive surround in the chromatic integration. We therefore check the influence of the surround on chromatic integration by designing and using a grating variant of the stimulus that we used to study color integration. The use of grating allowed us to stimulate the center more effectively than the surround. We found that reducing the activity of the surround changes the response of the chromatically nonlinear cells and

makes them linear. The chromatically linear cells, on the other hand, remain mostly linear even after weakening the influence of their receptive field surround.

In chapter six, we summarize and discuss the results of this thesis and we propose potential mechanisms for the linearity and nonlinearity of the chromatic integration. We conclude this thesis with the outlook section where we put forth some new ideas and future directions for the output of this thesis.

1.

Chromatic processing and signal integration in the retina

In this chapter, we look into the anatomical organization and functions of the retina and we highlight the chromatic processing and signal integration in the retina. We start by introducing the structure and functional properties of the retina. Since this work is done in the mouse retina, we focus on the features and properties of the mouse retina. Additionally, we compare the mouse retina to the primate retina to show the similarities and the differences between the two species. We then look into the chromatic processing aspects of the retina. We continue by looking at how the retina integrates its inputs at the level of the ganglion cells and we focus on different integration features of the ganglion cells. We then briefly introduce the concept of the receptive field for the retinal ganglion cells and provide more information about their anatomical structure and their relevance for chromatic signal integration.

1.1. The retina

Vision starts when the light enters the eye and goes to the retina in the back of the eye. The anatomy and structure of the eye is evolved to effectively pass the light to the retina with little to no distortion in the input (figure 1.1.A). The retina is a thin layer of nervous tissue that absorbs the light and transfers it to electrical activity. The retina however is not just a simple light sensor. Instead, what retina does goes beyond the simple sensation of light and includes complex computations and elaborate processing of the input light (Olveczky et al., 2003; Munch et al., 2009; Gollisch and Meister, 2010). In this work, we focus on one of the many computations that is done by the retina, which is chromatic signal integration.

Photoreceptors in the back of the retina absorb the input light. There are two different types of photoreceptors in the vertebrate retina, rods and cones. Both of these types hyperpolarize to light with rods being more sensitive to light (Baylor, 1996). Rods are activated even with single photons of light and they are active during night vision (scotopic light level) when the brightness is limited. Cones, on the other hand, are active during the daylight (photopic light level) and brighter environment where the rods are mostly saturated. At the intermediary level (mesopic light) such as twilight, daybreak, or in-door light, both rods and cones are active (Yin et al., 2006). Each photoreceptor type has a different photopigment (opsin and chromophore) which defines its spectral sensitivity. Based on the spectral sensitivity of the photoreceptors, they respond to specific wavelengths of light. The mouse retina is dichromatic. The dichromatic vision in the mouse retina is common among many mammals. However, some species of primates such as macaques, chimpanzee, and human have trichromatic vision with an extra class of cone photoreceptors. One type of the cones in the mouse retina is sensitive to short wavelength (s-cone) and responds to ultra-violet (300-400 nm, peak sensitivity at 360 nm) light spectrum. Another type of cone photoreceptor (m-cone) is sensitive to the middle part of the visual spectrum or green (450-550 nm, peak sensitivity at 508 nm) light. The cone photoreceptors of the mouse are arranged in an opposing gradient along the dorsal-ventral axis of the retina (Szel et al., 1996) (figure 1.2.A). This mosaic pattern of cone opsin expression has been found in other species such as guinea pigs, rabbits, hyenas, guppies, dragonflies and honey bee (Rohlich et al., 1994; Lukats et al., 2005; Peichl, 2005; Yin et al., 2009). In the mouse and some of the other animals with regionalized retinas, the m-cone opsin is highly expressed in the dorsal part of the retina and s-cone opsin is expressed in the ventral two thirds (figure 1.2.F). The middle region of the retina has the cones that have co-expression of s- and m-opsins (Rohlich et al., 1994; Lukats et al., 2005). Therefore, the mouse retina has three different regions: a s-cone dominated ventral retina (UV sensitive), m-cone dominated dorsal retina (green sensitive) and an opsin transition zone in between these regions where cones have co-expression of the s- and m-opsins (Rohlich et al., 1994; Chang et al., 2013). The main theory behind the regionalized pattern in the mouse retina is that this arrangement is evolved to sample the environment optimally.

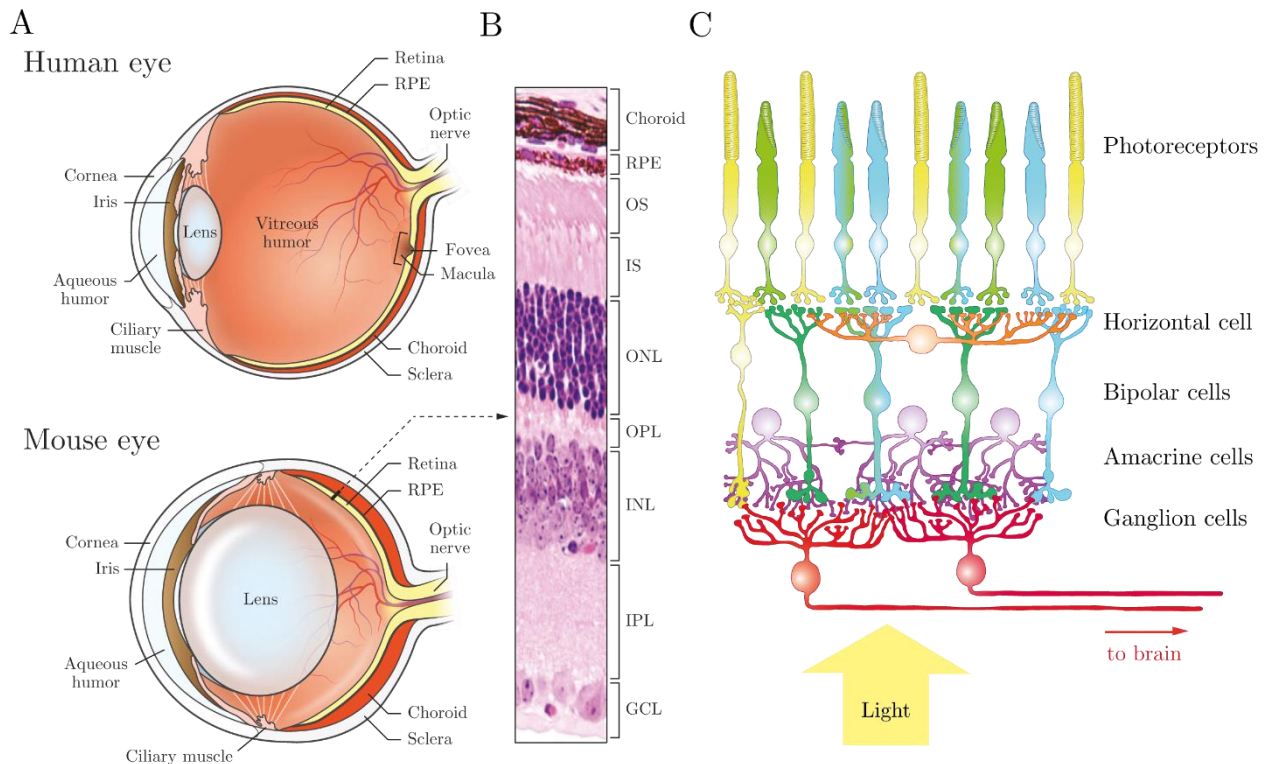


Figure 1.1. Schematic structure of the eye and the retina. A. Schematic cross-section of the human and mouse eyes. The light passes through the cornea and lens to reach the retina in the back of the eye. B. Image of the mouse retinal section stained with hematoxylin and eosin shows different layers of the retina. The outer part of the retina (including outer (OS) and inner (IS) segments of the photoreceptors, outer nuclear layer (ONL) and outer plexiform layer (OPL)) contains the photoreceptors. The inner part of the retina (including inner nuclear layer (INL) and inner plexiform layer (IPL)) includes horizontal cells, bipolar and amacrine cell. The last part of inner retina is the ganglion cells layer (GCL). The plexiform layers contain the synaptic regions. C. Illustration of the different cell types of the retina. The light passes through the retina and is absorbed by the photoreceptors. They transfer the light into electrical activity, which is then sent to the bipolar cells and after that to the ganglion cells. The horizontal and amacrine cells provide lateral inhibition to the excitatory signals of the photoreceptors, bipolar cells and ganglion cells. Part A and B of the image are adapted from (Veleri et al., 2015).

Therefore, the ventral retina with s-opsins, maximize the sampling of the sky (UV) and the dorsal retina with m-opsins, samples the terrestrial light sources, efficiently (Baden et al., 2013).

The mid-region provides the basis for complex dichromatic responses (Haverkamp et al., 2005; Chang et al., 2013). Cones account for 3-4% of the photoreceptors of the mouse retina and nearly 96-97% of mouse photoreceptors are rods (Jeon et al., 1998). This ratio is similar to trichromatic primate and human retina with rods to cone ratio of 20-30 to one (Wikler et al., 1990; Jonas et al., 1992).

Unlike cones, rods interspace the retina in a random order. Taken together, the first layer of the retina encodes the intensity and spectral differences of the input light.

After detection of the light from the photoreceptors, their output activates the bipolar cells (figure 1.1.C). Similar to the photoreceptors, bipolar cells are divided into two types of rod and cone bipolar cells. Based on the response properties of the cone bipolar cells, they are further divided into On and Off types. The On bipolar cells respond to the onset of the light and Off cells to the offset (Kolb, 1994; Boycott and Wässle, 1999; Euler et al., 2014). The difference between the On and Off bipolar cells comes from their different receptors at their dendrites. The On bipolar cells have metabotropic glutamate channels that invert the signals of the photoreceptors. The Off bipolar cells, on the other hand, have ionotropic glutamate receptors that preserve the sign of the photoreceptor's signal. The rod bipolar cells are On type. Beyond the differences in the glutamate receptors, the axons of On and Off bipolar cells terminate in different layers (strata) of the retina. The mouse retina has 14 different types of bipolar cells (Franke et al., 2017). Some bipolar cells make connections with both types of cones (cone-unspecific) and others make cone-specific contacts to either s- or m-cones. The mouse retina has two types of cone-specific bipolar cells; one green-off (type 1) and one UV-on cone (type 9) (Haverkamp et al., 2005; Breuninger et al., 2011; Behrens et al., 2016). Therefore, with its cone-specific and cone-unspecific bipolar cells, the retina splits the input light into different chromatic and achromatic channels after the photoreceptors. The output signal of the bipolar cells activates the retinal ganglion cells.

The retinal ganglion cells are the output layer of the retina (figure 1.1.B-C). They receive inputs from many bipolar cells and integrate these inputs to generate their output. The output of the ganglion cells are spikes that are sent via the optic nerve to the brain. Unlike the ganglion cells, other neurons of the retina such as photoreceptors, most bipolar cells and the majority of the inhibitory neurons of the retina do not generate action potential (spikes). Instead, these cells have graded membrane potential. The ganglion cells are divided into On, Off and On-off types based on their response to increment and decrement of light. The On ganglion cells respond to an increase of light (On stimulus) while the Off cells respond to the decrement of light (Off stimulus). Moreover, the On-off cells respond to both On and Off part of the stimulus (Hartline and Ratliff, 1957; Kolb and Nelson, 1993). Mouse retina has nearly 40 types of ganglion cells (Baden et al., 2016). Each type of ganglion cells process specific features of the input image. This notable diversity of the ganglion cells shows the functional diversity of the retina and its ability to process complex features of the input image.

In addition to excitatory neurons such as photoreceptors, bipolar and ganglion cells, the retina has intricate network of inhibitory cells. Horizontal and amacrine cells form this inhibitory network and they control the signal processing properties of the bipolar and ganglion cells. The horizontal cells are found at the synapses between the photoreceptors and bipolar cells and provide negative feedback at these synapses. Moreover, horizontal cells are coupled through gap junctions, which allow them to control the signal over larger areas in the retina (Weiler et al., 2000; Thoreson and Mangel, 2012).

Previous studies have shown that the inhibitory outputs of the horizontal cells are involved in the generation of the antagonistic center-surround structure of the receptive field (Kolb, 1994; Thoreson and Mangel, 2012). There are typically two types of horizontal cells and both are GABAergic neurons (Guo et al., 2010; Puller et al., 2014). The first type is the A-type that has an axon (HI in primates) and the second type is the B-type that has no axon (HII in primates). Mouse retina has only the B-type horizontal cells (Jeon et al., 1998; Masland, 2012). Previous studies reported different mechanisms for the feedback inhibition of the horizontal cells. In addition to conventional GABAergic synaptic inhibition (Puller et al., 2014), it has been shown that the horizontal cells induce inhibition by either changing the pH at the synaptic terminals of the photoreceptors (Davenport et al., 2008; Wang et al., 2014) or through gap junctions by changing the current at the synaptic clefts (Thoreson and Mangel, 2012; Vroman et al., 2014). In the mouse retina, it has been shown that the horizontal cells are involved in generating chromatically opponent responses between rods and cones at lower light levels (Joesch and Meister, 2016).

Amacrine cells are the other class of inhibitory neurons that are found in the inner retina. These cells modulate the signals between the bipolar and the ganglion cells. Some amacrine cells have smaller dendritic trees (narrow-field) and modulate the signals locally while other amacrine cells have larger dendritic trees (wide-field) and mediate long-range synaptic interactions. The narrow-field amacrine cells are typically glycinergic and wide-field cells are mostly GABAergic (Zhang and McCall, 2012; Franke and Baden, 2017). Previous studies showed that the narrow-field amacrine cells are more involved in fine-tuning the local output of the bipolar cells. An example about this role of the narrow-field amacrine cells was shown in the crossover inhibition where the nonlinearity of the bipolar cell's synapse is linearized by an amacrine cell (Molnar et al., 2009; Werblin, 2010). Wide-field amacrine cells seem to be involved more in the surround generation (in addition to horizontal cells) and more complex nonlinear properties of the ganglion cells. For example, wide-field amacrine cells have been reported to be involved in direction selectivity (Barlow and Levick, 1965; Fried et al., 2005; Lee and Zhou, 2006), object motion sensitivity (Olveczky et al., 2003; Baccus et al., 2008), color opponency (DeVries et al., 2006; Li and DeVries, 2006; Sher and DeVries, 2012; Chang et al., 2013) and other specific functions of the retina. The mouse retina has nearly 50-60 different types of amacrine cells and little is known about the functional properties of each type.

1.2. Similarities and differences between mouse and primate retina

The mouse retina has dichromatic vision with two types of cones (s- and m-cones). Humans and most old world primates have trichromatic vision. This means that they have three different types of cone photoreceptors besides rods. In addition to s-cone and m-cone, trichromatic animals have one more class of cones that is more sensitive to long wavelength (l-cones) (Nathans et al., 1986; Nathans, 1999).

Therefore, humans and other trichromatic primate can see longer wavelength (red color) compared to the mouse retina.

Another difference between primate and mouse retina is the sensitivity spectrum of the s-cones. Primate's s-cones are sensitive to blue light (400-500 nm, peak sensitivity at 445 nm) while mouse s-cones are sensitive to the ultra-violet light ranges (300-400 nm, peak sensitivity at 360 nm). Furthermore, the distribution of the cones differs between primate and mouse retina. The cone photoreceptors of the mouse are arranged in an opposing gradient along the dorsal-ventral axis of the retina (Szel et al., 1996) (figure 1.2.A). In the primate retina, the photoreceptors are distributed mostly in a random fashion with few areas of organization (figure 1.2.H). The central part of the retina or foveola is packed with only m and l-cones. In the region around the foveola (fovea), s-cones become integrated into the photoreceptor mosaic. Both foveola and fovea (figure 1.2.M) are devoid of rods. Rods start to appear in the macular region (region around the fovea) all the way to the posterior pole (figure 1.2.N). In posterior regions (figure 1.2.N.4-5), rods are more dominant than cones (Ahnelt, 1998; Roorda and Williams, 1999; Roorda et al., 2001). Apart from the described differences, there are similarities between the mouse and primate retina. For example, the bipolar cells and ganglion cells of mouse and primates have comparable characteristics (Field and Chichilnisky, 2007). In this project, we used the mouse retina to study the features of chromatic signal integration. The mouse retina is dichromatic, which makes it a good model for studying chromatic integration since we can compare the impact of each cone type on the activity of the ganglion cells.

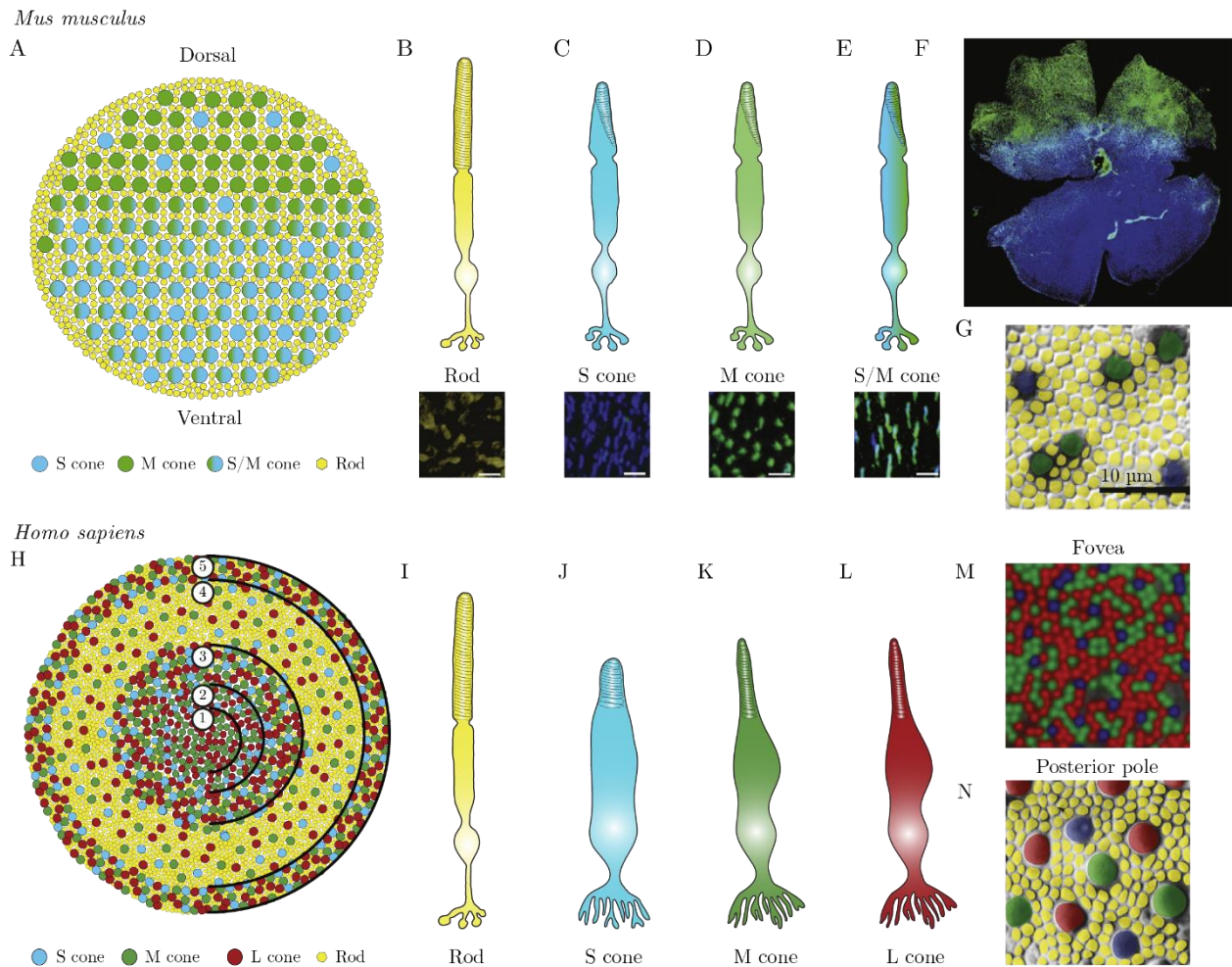


Figure 1.2. Different arrangements of photoreceptors in the mouse and human retina. A. Schematic picture of the mouse photoreceptors mosaics. The ventral retina is dominated by s-cones and the dorsal retina has more m-cones. The central part of the retina contains photoreceptors that co-express both s- and m-opsins. This image is not to scale. B-E, schematics of different photoreceptor types of the mouse retina. These includes Rods (B), UV sensitive s-cone (C), green sensitive m- cone (D) and s/m cone (E) which is sensitive to both UV and green light. Below the schematics are the labeled immunostaining of each photoreceptor type. F. Immunostaining of the whole mount retina, the s-cones are colored as blue and m-cones as green. G. False colored differential interference contrast (DIC) section of the retina that shows the distribution of the rods and cones in the mouse retina. The colors are attributed arbitrarily for s- and m-cones. Adapted from (Jeon et al., 1998; Viets et al., 2016). H. Schematic view of human photoreceptors patterning. In the center of human retina, photoreceptors have regionalized distribution where foveola (1) has only m- and l-cones. In fovea, (2) and macula (3) s-cones are distributed along with m- and l-cones. The posterior pole (4) and peripheral rim (5) are dominated with rods while the cones are distributed in a random fashion. I-L. Schematic view of human photoreceptors, rods are depicted in yellow (I) and s-, m- and l-cones (J-L) are shown in blue, green and red colors. M. False color adaptive optics image of the human fovea. The human fovea has high density of cones while it is devoid of rod photoreceptors. Here s-cones are colored as blue and red and green colors are arbitrary assigned to m- and l-cones. Image is adapted from (Williams,

2011). N. False colored image of human photoreceptors in the posterior pole. This region and other non-fovea region are dominated by rods, while cones have larger size and they are distributed sparsely. Image adapted from (Curcio et al., 1991). Different parts of this figure are adapted from (Viets et al., 2016).

1.3. Color processing in the retina

Color processing in the retina starts from the first synapse. The cone photoreceptors separate the light into different chromatic channels. Classical studies of color processing have mainly focused on the fovea of the primate retina. In the primate fovea, the signal from each cone is transferred to a single bipolar cell and then to a single ganglion cell (Kolb, 1970; Kolb and Dekorver, 1991). The midget cells of the fovea process the color information with m- vs l-cone (red-green) opponency and the bistratified ganglion cells have s-cone vs l- plus m-cone (blue-yellow) opponency. In these cases, the receptive field center receives chromatic input from one type of cones. The inhibitory surround, on the other hand, receives inputs from different cones with opposite color sensitivity and response from the center. The result of this structure is a center-surround receptive field with color opponent properties (Lee et al., 2010). The color opponent surround for these midget cells is formed by the horizontal cells (Dacey et al., 2000; Dacey and Packer, 2003; Diller et al., 2004; Packer et al., 2010; Crook et al., 2011). The midget cells in the periphery of the primate retina receive inputs from many bipolar cells in their receptive field center and show no selective wiring to the bipolar cells (Crook et al., 2011). In these peripheral ganglion cells, the input to the center shows a relative bias to one cone type (l- or m-cone) and the surround has random connection to l- and m-cone inputs. Thus, this bias in the cone selection generates the center-surround color opponent response for the midget cell of the primate periphery (Field et al., 2010).

Besides the trichromatic primates, color opponent cells have been reported in the retinas of dichromatic mammals such as guinea pig (Yin et al., 2006, 2009), ground squirrel (DeVries et al., 2006; Li and DeVries, 2006; Sher and DeVries, 2012) and the mouse (Chang et al., 2013). In the guinea pig, similar to the fovea of the primates the horizontal cells induce the opponency. However, for the mouse and the ground squirrel, the chromatic opponency is enabled with the intervention from the amacrine cells. In the mouse retina, the color opponent ganglion cells have been found in the middle part of the retina. These cells receive inputs from the cones that express both s- and m-opsins in their center. The surround for these cells is generated by wide-field amacrine cells that provide opponent signals from the ventral and dorsal part of the retina (Chang et al., 2013). Beside the color opponent cells in the retina, not much is known about the chromatic integration properties of the retinal ganglion cells. This is specifically interesting for dichromatic mammals, because in these animals the opponent cells are only a small fraction of the whole ganglion cell population (1-5%) (Yin et al., 2006, 2009; Chang et al., 2013). Similar scarcity of opponent cells has been reported in the lateral geniculate nucleus of the

mouse where nearly 10% of the cells are color opponent (Denman et al., 2017). Thus, this raises the questions about the chromatic properties of the ganglion cells. Is color opponency the only way of processing chromatic inputs in the retina? What about the other non-opponent ganglion cells? How do they process chromatic information? In this project, we aim to find answers to these questions by studying how the chromatic inputs from the s- and m-cones are integrated by different ganglion cells in the mouse retina.

1.4. Signal integration in the retina

Retinal ganglion cells pool inputs from many bipolar cell types with various number of synapses (Masland, 2012) and integrate these inputs to generate their outputs. One of the well-studied signal integration features of ganglion cells is their spatial integration, which is how each ganglion cell responds to stimuli with different spatial structures or patterns inside their receptive field. In the classical studies of spatial integration, a spatial grating with alternating black and white bars was shown to the cat retina for a short period of time and the response of the neurons was measured (Enroth-Cugell and Robson, 1966). This stimulus was repeated for different spatial phases so that each ganglion cell saw different spatial parts of the stimulus (figure 1.3). Using this stimulus, the ganglion cells were categorized into two major groups of X and Y cells.

The X cells did not respond when the two opposing contrasts were in the receptive field and they averaged the stimulus inside their receptive field (figure 1.3.A). The Y cells, on the other hand, responded strongly even when each half of the receptive field was covered by opposing contrasts (figure 1.3.C). Thus, X cells integrate the spatial stimulus linearly in their receptive field. Y cells, on the other hand, integrate the stimulus nonlinearly and respond to different combinations of contrasts in their receptive field.

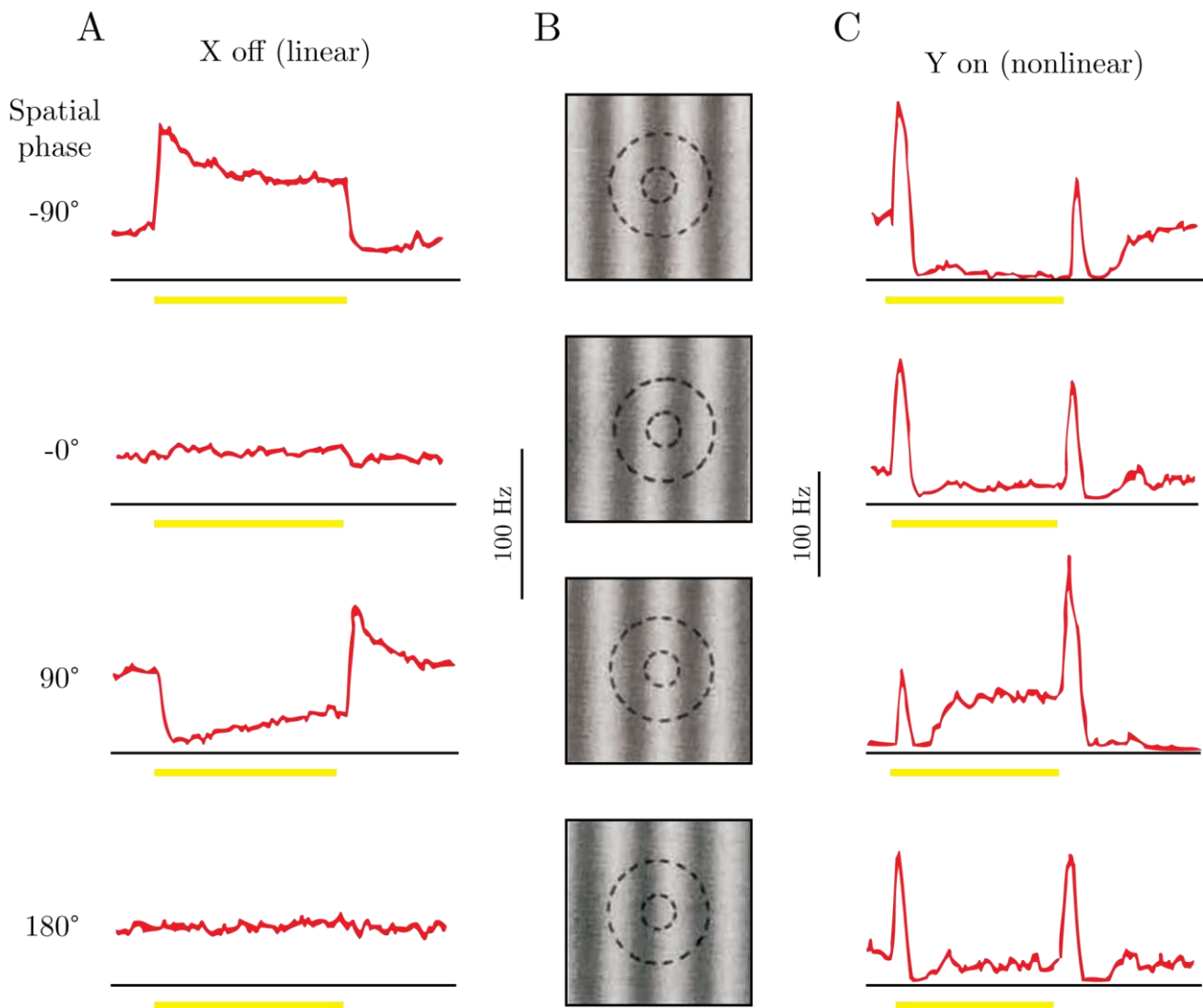


Figure 1.3. Linear and nonlinear spatial integration in the cat retina. A. Responses of an X cell in the cat retina shows linear integration of the spatial stimulus. When each half of the receptive field is covered by black and white bars (0 and 180 degree), the cell does not respond. This is because this cell integrates the stimulus linearly and averages the black and white contrasts. B. Sinewave grating stimulus with different spatial phases was shown to the retina. C. Response of a Y cell shows nonlinear integration of the spatial stimulus. Here, unlike the X cell, the ganglion cell still responds strongly when each half of the receptive field faces a different contrast. In this example, the X cell is an Off center and the Y cell is an On center ganglion cell. The vertical yellow bars show the time in which the stimulus pattern was presented. The data shown here is from the recordings in the cat retina from (Enroth-Cugell and Robson, 1966, 1984) and the image is adapted from (Shapley, 2009).

The same types of spatially linear and nonlinear ganglion cells were found in the retina of other species such as guinea pig (Demb et al., 1999; Zaghoul et al., 2007), rabbit (Caldwell and Daw, 1978; Hamasaki et al., 1979; Famiglietti, 2004) and monkey (de Monasterio, 1978; Petrusca et al., 2007; Crook et al.,

2008). Many studies ensued this work to find the mechanisms and functional relevance of the linear and nonlinear spatial integration. These studies showed that the source of nonlinear integration is the synapse between the bipolar and ganglion cells. (Katz and Miledi, 1967; Baccus et al., 2008; Molnar et al., 2009; Werblin, 2010; Schwartz et al., 2012; Borghuis et al., 2013). Nonlinear spatial integration is fundamental to many complex functions of the retina. Previous studies showed the role of nonlinear spatial integration in object motion sensitivity (Olveczky et al., 2003; Baccus et al., 2008), detecting approaching (looming) objects (Munch et al., 2009) and detecting homogenous patterns (Bolinger and Gollisch, 2012). Beyond that, it has been shown that the nonlinearities in the retina are involved in other functions such as motion sensitivity (Barlow and Levick, 1965; Levick, 1965; Fried et al., 2005) and local edge detection (Levick, 1965; van Wyk et al., 2006). Taken together, retinal ganglion cells integrate their inputs from bipolar cells linearly or nonlinearly. Both linear and nonlinear integration provides the retina with complex and intricate computational capabilities that go beyond simple light detection. Investigating these nonlinearities therefore helps us to get a better understanding about the neuronal code of the visual system.

1.5. Center-surround structure of the receptive field

One of the common concepts in studying sensory systems is the concept of the receptive field. In the visual system, the receptive field of a neuron is a region of the visual space in which a stimulus activates that neuron (Hartline, 1938). The definition of the receptive field generally goes beyond the spatial responsiveness of a cell, and it incorporates the temporal course of the response (spatio-temporal receptive field) and the relation between different locations of the receptive field (center-surround). This relation between different locations of the receptive field is generally described as the antagonistic center-surround structure of the receptive field. In this structure, the receptive field receives excitatory inputs in the center and inhibitory inputs in the surround. Retinal ganglion cells have complex receptive fields (figure 1.4). They, on the one hand, receive inputs from many bipolar cells, which give them linear or nonlinear sub-fields in their center. On the other hand, the modulations from the amacrine cells at their dendrites provide them with a linear or nonlinear surround.

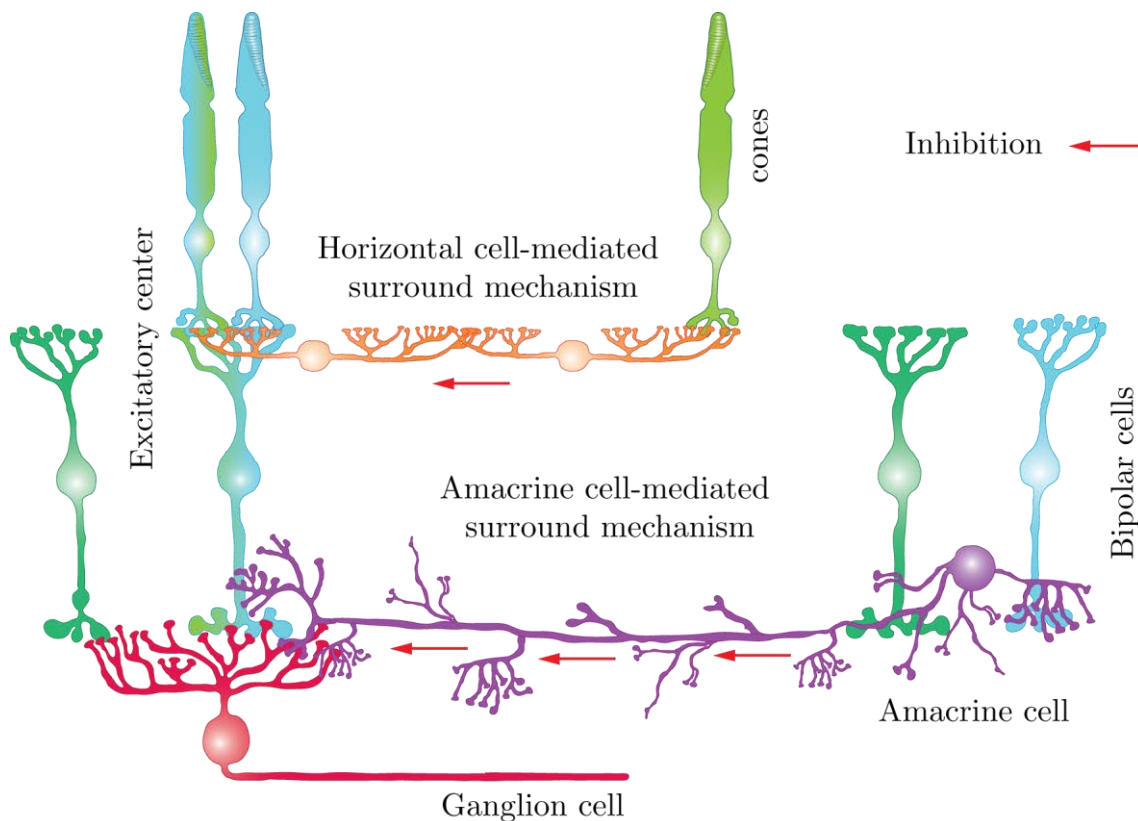


Figure 1.4. Center-surround structure of the receptive field of a ganglion cell. The center of the receptive field receives excitatory inputs from the bipolar cells. Lateral inhibition from the horizontal cells and the amacrine cells form the inhibitory surround of the receptive field. The outline of this image is adapted from (Zaghloul et al., 2007). The colors of the photoreceptors and bipolar cells were chosen arbitrarily.

Until now, we described different examples about features of the receptive field's center and surround. Many of the spatial integration attributes of the ganglion cells are done by their center such as linear and nonlinear spatial integration (Enroth-Cugell and Robson, 1966). In addition to the center, many chromatic processing features of the ganglion cells are attributed to their receptive field surround. Chromatic opponency in the fovea of the primates and the central region of the mouse retina is caused through interactions of the receptive field center and surround (Dacey, 1996, 1999; Chang et al., 2013). The inhibitory cells of the retina contribute to the receptive field surround of the ganglion cells. The horizontal cells mainly influence the receptive field of the bipolar cells (Thoreson and Mangel, 2012) but their effects can go beyond a few synapses through their electrical couplings (Weiler et al., 2000; Thoreson and Mangel, 2012). This way, they contribute to the receptive surround of the ganglion cells too (Mangel, 1991; Crook et al., 2011). In addition to the horizontal cells, the amacrine cells also play a major role in creating the receptive field surround of the ganglion cells. The contribution of the amacrine cells to the receptive field surround and their influence on the center has been shown in object motion sensitive cells (Olveczky et al., 2003), direction selective cells (Vaney et al., 2012; Vlasits

et al., 2014) and color opponent cells in the mouse retina (Chang et al., 2013). Classic models of the receptive field assume a linear relation between the receptive field center and its surround (Enroth-Cugell and Robson, 1966; Dayan and Abbott, 2001). In these models the center-surround interaction was described with difference of two Gaussians (Rodieck, 1965) or with linear-nonlinear models (Chichilnisky, 2001). However, later studies showed the nonlinear effects that happen beyond the scope of the receptive center. For example moving a grating pattern outside the receptive field and far from the center seems to influence the center nonlinearly (Shapley and Victor, 1979; Passaglia et al., 2001; Solomon et al., 2006; Passaglia et al., 2009). Recent studies reported spatial nonlinear properties in the receptive field surround of the salamander ganglion cells (Takeshita and Gollisch, 2014). Therefore, the receptive field surround could potentially add more nonlinearity to the functions of the center and provides more functionality for the overall receptive field of the ganglion cells. In this study, we focus on the chromatic integration properties of the ganglion cells and we check whether the ganglion cells integrate their chromatic inputs linearly or nonlinearly. Furthermore, we look at the influence of the receptive field surround on the center for the integration properties of the ganglion cells.

1.6. Aim of this study

Retinal ganglion cells show complex and diverse functional properties and at the core of these functions reside many nonlinear processes. In this thesis, we focus on one of these processes and investigate how ganglion cells integrate their chromatic inputs. The approach we chose for this investigation was inspired by earlier studies that were done about the linear and nonlinear spatial integration of the ganglion cells. Based on these studies, we focus on two main questions in this thesis. First, whether the ganglion cells integrate their chromatic inputs linearly or nonlinearly and second whether the receptive field surround plays a role in the integration characteristics of the ganglion cells. In the first part of this study, we talk about the technical methods that we developed in order to be able to inspect the chromatic integration properties of the ganglion cells (chapter 2 and 3). We then look at the integration properties of the ganglion cells (chapter 4) and finally we investigate the role of the receptive field surround in the chromatic integration (chapter 5). We hope this study provides new insights about the functional nonlinearities involved in the chromatic processing of the ganglion cells. Beyond that, we hope that the technical and analytical methods along with the output of this thesis can help us to have a better understanding about the integration properties of the retinal ganglion cells and other sensory neurons.

2.

Experimental methods

To study the mechanism of chromatic signal integration in the mouse retina, it is important to gather data from many types of retinal ganglion cells. Thus, one can probe the question of the chromatic signal integration by comparing the responses of a population of ganglion cells to different chromatic stimuli. In this project, we used the multi-electrode array recording technique to measure the output of mouse ganglion cells. We studied the response of the ganglion cells with different analytical approaches. In this chapter, we describe the details of the experimental and analytical methods that were used in this project.

2.1. Animals

All the experiments of this study were done on the retina of the adult mice (*Mus musculus*, C57BL6/J). Mouse retina is a commonly used model system for studying early vision. In terms of processing chromatic information, the mouse has a dichromatic retina with two types of cone photoreceptors (Applebury et al., 2000). Having two type of cones was an advantage in our project where we aimed to study chromatic signal integration. Moreover, the anatomical and functional properties of the mouse retina are reasonably known (Sanes and Masland, 2015; Baden et al., 2016). Many studies have been done on different characteristics of mouse retinal ganglion cells (Wassle, 2004; Baden et al., 2016). This is helpful in terms of assigning different chromatic integration features to specific cell types and then predicting the potential mechanisms based on the known functional and anatomical characteristics. Moreover, in terms of diversity, mouse retina has similarities to the primate retina (Field and Chichilnisky, 2007; Volgyi et al., 2009). With around 14 types of bipolar cells (Franke et al., 2017) and nearly 40 types of retina ganglion cells (Baden et al., 2016) the mouse retina is nearly as diverse as the primate retina. Thus, it is possible to do comparative analysis between the mouse

and primate retina. Finally, the availability of the mouse retina compared to primate retina is another advantage that motivated us to use the mouse as the animal model for our experiments.

2.2. Retina preparation

The retinas were obtained from mice aged between 8-12 weeks. Both male and female mice were used for the experiments without any preference to either gender. Before each experiment, a mouse was dark adapted for 1-2 hours. After the dark adaptation, the animal was sacrificed via cervical dislocation. All the experimental procedures were done in accordance with institutional guidelines of animal experimentation of the University Medical Center Göttingen. The eyes of the mouse were immediately enucleated and transferred to small preparation container. As soon as the eyes were detached from the animal body they were kept in a solution that was perfused constantly with oxygenated (95% O₂ and 5% CO₂) Ames' medium (Sigma-Aldrich, St. Louis, USA; Ames and Nesbett 1981). This ensured the survival of the retina for a long period of each experiment. To prevent the effects of pH fluctuations and maintain the pH of 7.4 during the whole experiment, the solution was buffered with 22 mM of NaHCO₃. Moreover, 6 mM of D-glucose was added to the solution that provided extra nutrition for the cells during the experiment. After enucleation, the outer part of each eye including the cornea and lens was cut and detached from the eyecup. Subsequently, the vitreous inside each eye was carefully extracted to have direct access to the retina. In the next step, the retina was carefully removed from the eyecup and separated from the pigmented epithelium. For some experiments, the whole retina was used for the multi-electrode array recording (whole-mount) while for other experiments, the retina was dissected into two halves and each half was used for one recording session (half-mount). Whether the whole retina was used or half of it depended on the type of multi-electrode array that was used.

For the experiments with half of the retina, before enucleation of the eyes, a small burn-mark was introduced with a surgical cautery pen (Praxisdienst Medizinprodukte) on the dorsal part of each eye.

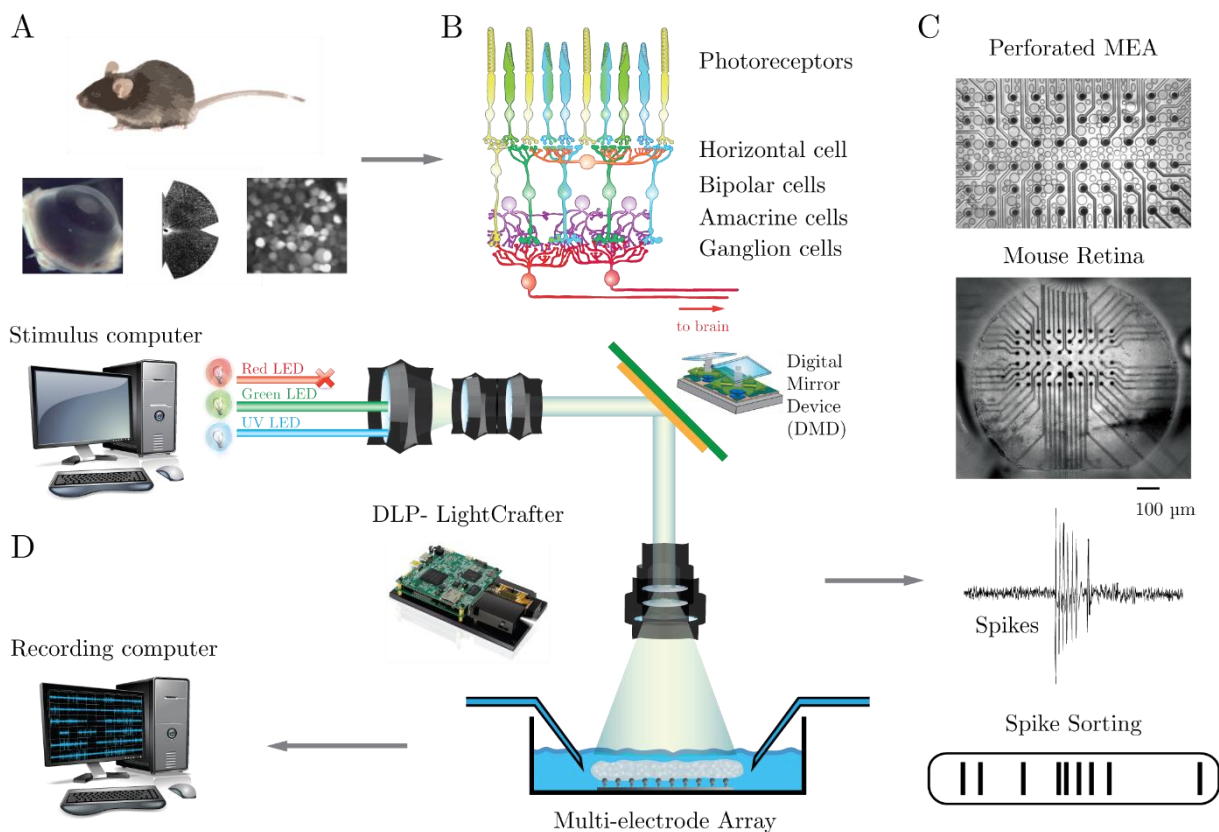


Figure 2.1. Schematic illustration of the experiment procedure, projection system and the electrophysiology setup. A. Schematic illustration of the retina preparation. Before each experiment, the mouse was dark-adapted for 1-2 hours and it was sacrificed with cervical dislocation. The eyes were enucleated and the retina was removed from each eyes and cut into two pieces. Each piece of the retina was mounted on a multi-electrode array. B. Illustration of the different layers of the retina. C. Image of the perforated multi-electrode array (top). Image of a piece of retina mounted on top of the multi-electrode array. D. Schematic illustration of the projection system. The visual stimulus was generated by the stimulus computer and the stimulus was displayed to the retina with the projector. The projection system has Green and UV LEDs and it stimulates both s- and m-cones of the mouse retina. The activity of the ganglion cells were recorded and stored by the recording computer. The stored data was analyzed off-line and after the spike sorting. The images of the mouse eyes were adapted from (Pitulescu et al., 2010), the image of the ganglion cells was adapted from (Chang et al., 2013). The image of the DLP Lightcrafter projector was adapted from Texas Instruments webpage and Texas Instruments DLP Lightcrafter Evaluation Module (EVM) user's guide.

This landmark was used to find the ventral-dorsal orientation of the retina during preparation and mounting of the retina. For the experiments with the whole retina, the ventral-dorsal axis was defined based on the response characteristics of the ganglion cells. After removal of the retina, it was mounted on a multi-electrode array (see electrophysiology section). The remaining piece of the retina (in case of half mount preparation)

was stored in the perfused solution for further recording. Previous studies have shown that the retina in the ex-vivo preparation can be responsive and healthy up to eight hours after the preparation (Wei et al., 2010; Reinhard et al., 2014). Based on our experience from previous recordings in the lab, with good perfusion, the retina stays healthy and responsive up to 12 hours after the preparation. As a result, we were able to record high quality and reliable data during the long period of each experiment. The dissection and retina preparation was done under infrared illumination with a stereo-zoom microscope (SZX7, Olympus, Japan). This microscope was equipped with a night vision goggles (PS-14, ATN Corporation, San Francisco, USA) to have clear vision during preparation without stimulating the retina. All the experimental procedures, from dark adaptation of the mouse to the retina preparation and electrophysiological recording were performed in a dark room. In case of necessity, a portable red light source or a portable infrared goggle was used for controlling the experimental procedures.

2.3. Visual stimulation

Visual stimuli of all the experiments were displayed on a custom-built green-UV projection system. This projection system is a modified version of the DLP lightcrafter projector (evaluation module (EVM) from Texas Instruments Company, USA). The projector was gamma-corrected to linearize its output. Moreover, all the stimuli were cone isolating, and they were presented at 60 Hz refresh rate (for more details see chapter 3). The projection system displayed the stimuli to the photoreceptor layer of the mouse retina. The output image of the projector was de-magnified in a way that each pixel of the projector had a diameter of 8 μm . The whole projection system and electrophysiological setup were inside a Faraday cage that was covered with a dark curtain. This protective cover blocks any lights from outside to enter the experimental setup. Thus, the activity of the retina was only driven by the stimuli shown via the projector. All the visual stimuli were generated and controlled through a custom-made software based on visual C++ and OpenGL libraries. All the stimuli were presented on a background with equal green and UV brightness (mean level of green and UV light). For all the experiments, the stimuli were presented at the photopic light level with mean irradiance at 8.2 or 9.1 mW/m^2 . In terms of isomerization, the rod isomerization was equal to $(1.92 \times 10^4 \text{ R}^*/\text{rod}/\text{s})$. For more details about individual cone isomerization levels and visual stimulation, see chapter 3.

2.4. Electrophysiology

For all the experiments, the spiking activities of retinal ganglion cells were recorded using different planar multi-electrode arrays. In this project, two different types of multi-electrode arrays were used. These include perforated multi-electrode array and conventional multi-electrode array (both from Multi Channel Systems, Reutlingen Germany). For perforated multi-electrode recording, the arrays have 60 electrodes with 100- μm gaps between them and 30- μm electrode diameter. The retina was mounted on these arrays using a nitrocellulose membrane and kept in place via negative pressure from

a suction pump below the retina. The suction from the below provides stability and good contact to the electrodes while the perfusion through the retina kept the retina healthy and responsive for a long period of the experiment. The unique perfusion system of these perforated arrays provide stable and high quality recordings (Reinhard et al., 2014). In some experiments, the conventional multi-electrode arrays were used. These arrays have 252 electrodes with the same dimension and distance between electrodes as the perforated arrays. The advantage of this system is its bigger recording area. The retina was mounted on these conventional multi-electrode arrays via a transparent membrane and then held over the electrodes using poly-D-Lysine (PDL, Merck-Millipore Company, A 003-E). PDL increases the adhesion between tissues, and we used it as a biological glue to keep the retina over the array.

After mounting, the retina was continually perfused with oxygenated Ames' medium (220-250 ml/hour). This solution was constantly heated-up close to physiological temperature (31-34 °C) by an inline and a base-plate heater (PH01 for perforated MEA, PH01 and MEA1060INV for 252 MEA). After mounting the retina over the multi-electrode array and into the recording chamber, we let the retina lay in the recording chamber for 45-90 minutes while a black screen was presented to the retina. After this resting period, the retina was exposed to 10-15 minutes of the background light. The resting period and the background light exposure provide better contacts between the electrodes and the retina and allow the retina to adapt to the experiment light level. After this, the visual stimulation and data acquisition were started. The acquired voltage traces were amplified and filtered with a band-pass filter (between 300 Hz to 5000 Hz). The filtered data was then stored at 25 kHz for perforated multi-electrode arrays, 10 kHz for 252 multi-electrode arrays systems. These data were stored and used for off-line analysis after the spike sorting.

2.5. Spike sorting

Extracellular recording with multi-electrode arrays is a powerful technique that allowed us to record many retinal ganglion cells, simultaneously. Having a huge population of neurons helped us to investigate chromatic integration properties of different types of the ganglion cells. Moreover, we were able to compare the responses based on the location of the ganglion cells along the ventral-dorsal axis of the retina. These advantages came along with challenges in data management and data analysis. From each experiment, voltage traces of tens to hundreds of neurons were recorded for 5-12 hours of visual stimulation. To analyze the responses of individual ganglion cells, it is important to extract the spiking activity of each ganglion cell from the voltage traces. It is possible that the signal of one ganglion cell is recorded at multiple electrodes or one electrode records the signal of multiple ganglion cells (Lewicki, 1998). To address these issues and correctly assign the recorded signals to each individual ganglion cell, we used the analytical method of spike sorting. Spike sorting tries to group

spikes into clusters based on the similarity of their spike shapes and their refractory periods (Lewicki, 1998). These specific characteristics of a neuron are defined by the morphology of their dendritic tree and the distance and orientation of each cell relative to the recording electrode (Gold et al., 2006). For this study, spike sorting was done using a custom-made software package developed by Dr. Ofer Mazor (Harvard University, USA) in Igor Pro program (WaveMetrics, Lake Oswego, USA) based on a Gaussian mixture model and an expectation maximization algorithm (Pouzat et al., 2002). The output of the spike sorting was controlled and checked and only ganglion cells with very good and reliable responses and high quality spike sorting were used for further data analysis.

2.6. Analysis of ganglion cells response to the chromatic integration stimulus

To study the properties of the chromatic integration, we designed the chromatic integration stimulus (chapter 4). This stimulus has 22 combinations of green and UV contrasts that were presented simultaneously. To distinguish chromatically linear cells from nonlinear cells, we searched for the cancellation point in response of the cell to the chromatic integration stimulus. Therefore, in our analysis, if we found a cancellation point for a ganglion cell, we considered that ganglion cell to be chromatically linear. If no cancellation point was found, it indicates nonlinear chromatic integration. In the following section, we first explain how we measured the cancellation point and then we describe additional measurements such as the polarity and the rectification that we calculated from the chromatic integration stimulus.

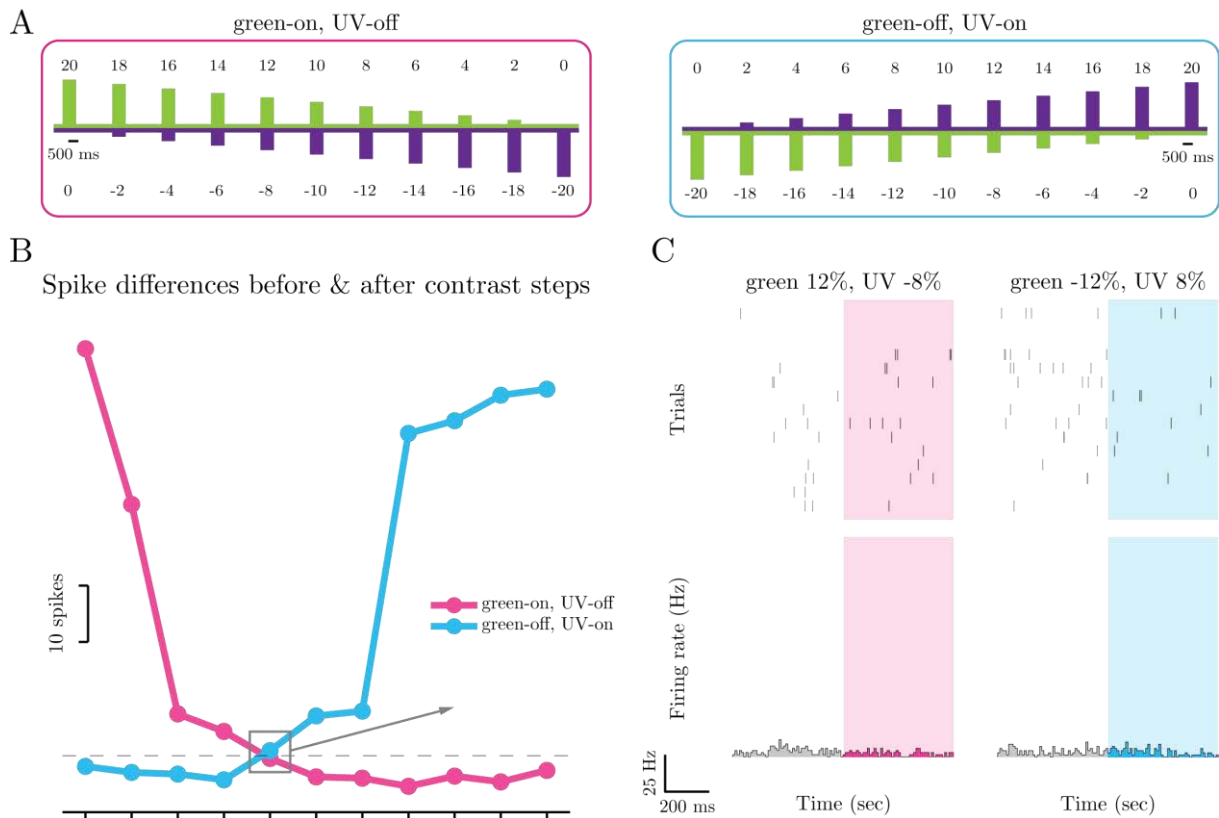


Figure 2.2. Chromatic integration curves and the cancellation point of green-on, UV-off and green-off, UV-on contrast combinations. A. The chromatic integration stimulus (chapter 4). This stimulus has 22 different contrast combinations, that are grouped in two sets; green-on, UV-off (pink) and green-off, UV-on. B. The chromatic integration curves show the response of a ganglion cell to the different contrasts of green-on, UV-off (in pink) and green-off, UV-on stimuli (in blue). C. The right panel shows the response of the cell at the crossing point of the two chromatic integration curves. At this crossing point, the cell's response has no difference from the background. Therefore, the two opposing contrasts cancel each other out.

2.6.1. The cancellation point

The cancellation point was deduced as follows: For all the trials, we measured the spiking activity of each ganglion cell in response to the 22 contrast combinations of the stimulus. We then constructed a peri-stimulus time histogram (PSTH) with 10 ms time bin resolution for each contrast step of the stimulus and the background light that comes before each contrast step.

Therefore, for each ganglion cell, we had 22 contrast-driven PSTHs and 22 PSTHs from the background light. For each contrast-driven PSTH, we took the average of the responses in the time window of 50 to 250 ms after the onset of the contrast step and we refer to this as the contrast-driven response

(figure 2.2.B). We chose a 200 ms time window to consider the response delay and avoid adaptation effects. We then took the average over 200 ms before the onset of the contrast step from the PSTHs of the background activity. This background driven response is used to find the baseline or spontaneous activity of a ganglion cell. We calculated the difference between the contrast-driven response and the background (baseline activity) response and we refer to this as the chromatic integration response. Since we presented 22 different UV-green contrast combinations, we measured 22 values of chromatic integration responses for each cell. We grouped these 22 values into two sets:

1. *green-on, UV-off*
2. *green-off, UV-on*

To compare these opposing contrasts, we plotted these two groups of responses with separate curves as shown in the figure 2.2. This way of grouping and presenting the responses is not only the same as the stimulus grouping (figure 2.1.B) but also it allows us to present and compare chromatically opposing contrasts easily (for example: 12% green, -8% UV vs -12% green, 8% UV).

2.6.2. Polarity of the responses

One of the fundamental features of the ganglion cells is their response polarity. Some ganglion cells respond to an increase in the brightness of the stimulus (On cells), some respond to the decrease of brightness (Off cells) and some respond to both (On-Off cells) (figure 2.2). (Hartline, 1938). In this project, we defined the polarity of each ganglion cell based on the strongest response to the chromatic integration stimulus (chapter 4). In this stimulus, we have two contrast combinations that have only $\pm 20\%$ of one color and no contrast of the other color. These stimuli include green On (green 20%, UV 0% of the green-on, UV-off curve), green Off (green -20%, UV 0% of the green-off, UV-on curve) and likewise for the UV On and Off stimuli. We then looked at the response of each ganglion cell to these contrast combinations and from them we chose the strongest response as the one with highest peak firing rate. On cells responded strongly to green On (20%) and UV On (20%) contrasts of the stimulus and Off cells to both Off (-20%) contrasts while On-Off cells responded to On and Off contrasts. These include, green $\pm 20\%$, UV 0% and green 0%, UV $\pm 20\%$.

2.6.3. Rectification of the non-preferred stimulus

Beside chromatic integration features and the polarity (On, Off and On-Off), we further assessed from the chromatic integration curves how each ganglion cell encodes the non-preferred contrast. From this analysis, we gained the information whether a ganglion cell rectifies its inputs or not. For a rectifying cell, the non-preferred stimulus does not elicit any responses.

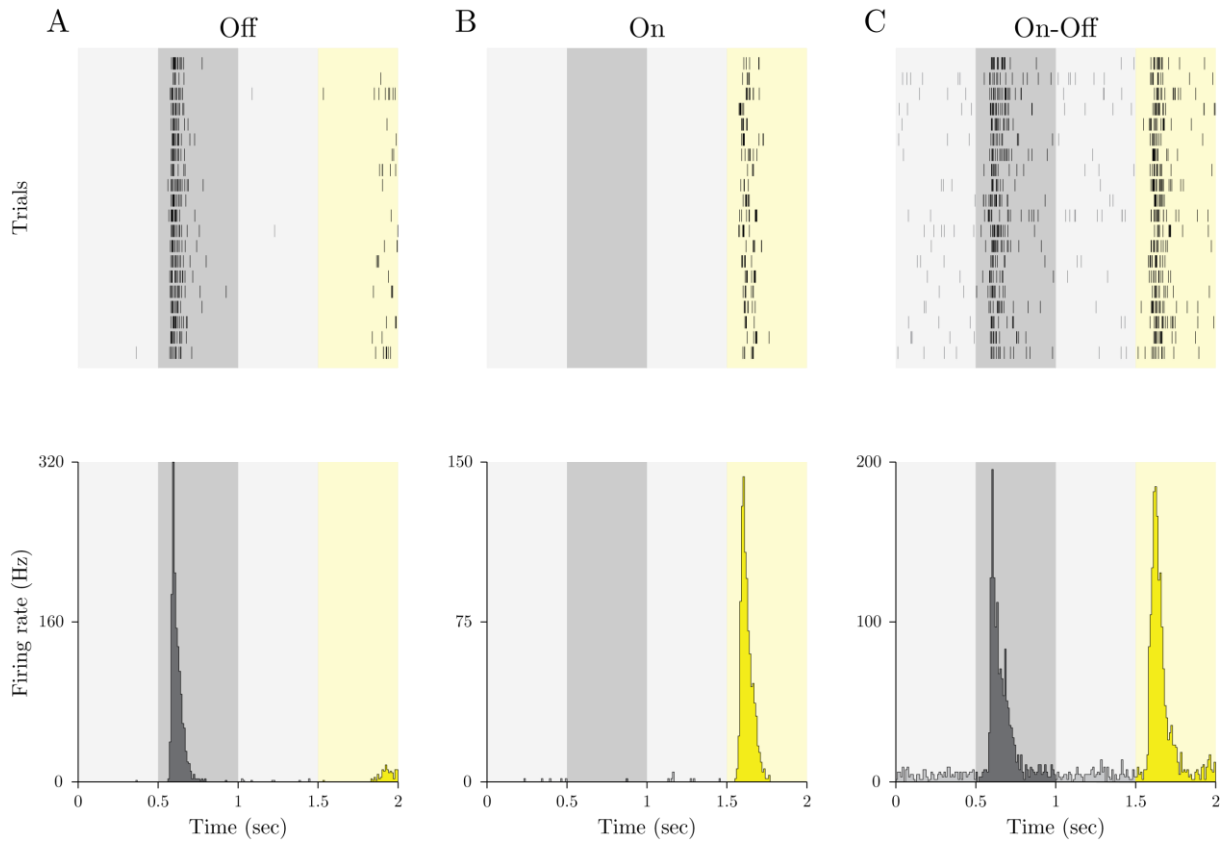


Figure 2.3. Response polarity of On, Off and On-Off cells. A. Response of Off ganglion cell to the On-Off square wave stimulus. Between the On and Off part of the stimulus the mean light was shown (gray shades). B. Response of an On ganglion cell. C. same as A and B but for an On-Off ganglion cell.

For example, if we stimulate an Off rectifying ganglion cell with a bright spot of light or an On stimulus, we will not see any differences in the activity of the ganglion cell from the baseline (figure 2.3.B). This is because the ganglion cell has a thresholding output function so that the non-preferred stimuli are rectified. However, for a non-rectifying ganglion cell, the non-preferred stimuli will cause the cell to reduce its firing rate below the spontaneous activity (figure 2.3.A). Similar to the analysis of chromatic integration responses, here we first need to subtract response of the cell from its spontaneous activity and then look at the cell's response to the non-preferred stimuli. For the analysis of the rectification, similar to the analysis of ganglion cell's polarity, we looked at the corner responses but to the non-preferred stimuli. If a ganglion cell's response to the non-preferred stimuli is close to zero, it is a sign of rectification of the non-preferred contrast.

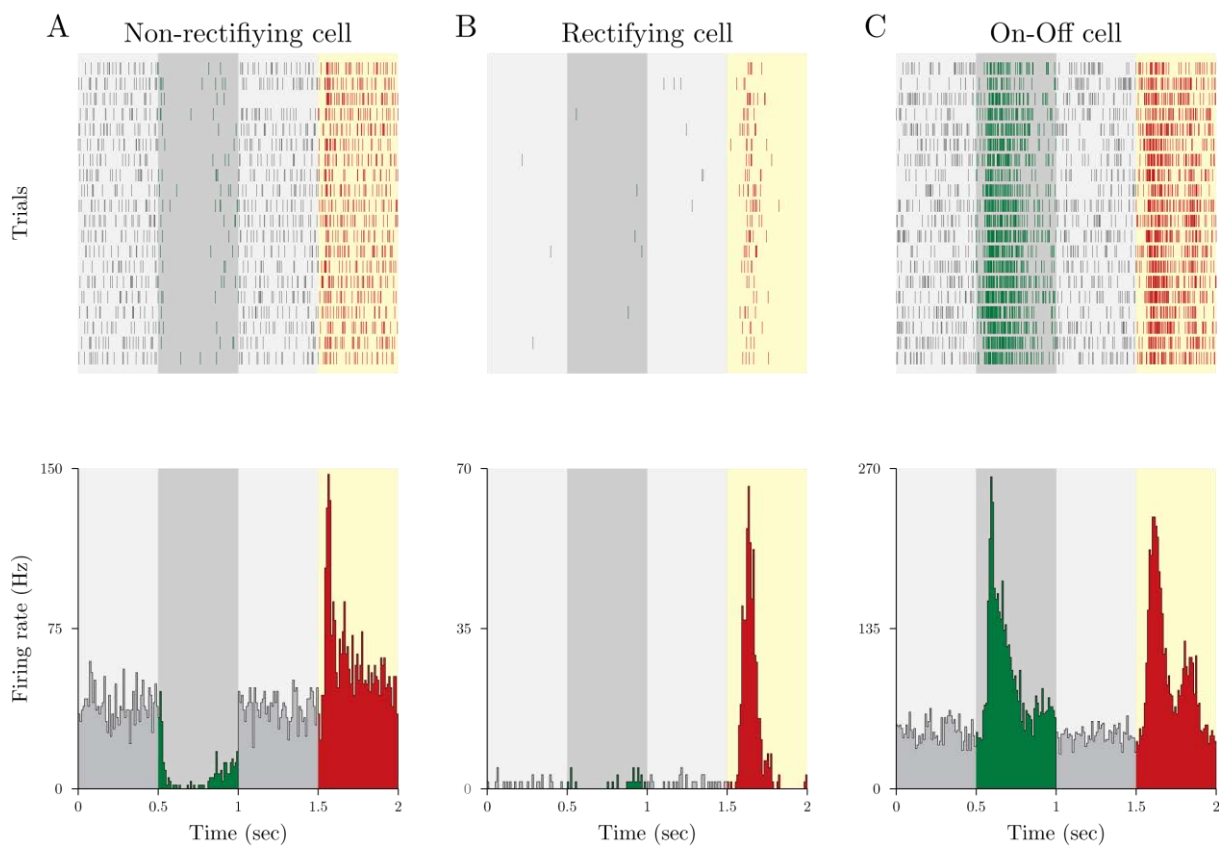


Figure 2.4. Rectification of the non-preferred stimulus for non-rectifying, rectifying and On-Off cells. A. Response of an On non-rectifying ganglion cell shows clear response to the On stimulus (preferred stimulus). The Off stimulus, on the other hand suppresses the activity of the cell (non-preferred stimulus). B. Response of an On rectifying ganglion cell show strong response to the On stimulus but little to no response to the Off stimulus. This cell rectifies the non-preferred stimulus. C. Response of an On-Off ganglion cell shows strong activity for both On and Off stimulus (no rectification). In this project, we did not use this measure to separate the On-Off cells from the rest. Instead, we used the response polarity and On-Off bias to recognize the On-Off cells. Here the dark shades correspond to Off stimulus and yellow shade are for On stimulus. The bright gray shades are for background before each stimulus.

However, if the chromatic integration curves of a ganglion cell have negative values at the corner stimuli, it is due to the suppression caused by the non-preferred stimuli. For these cells, the contrast encoding is not rectified. Finally, if a ganglion cell responds to both On and Off contrasts of each color, it is considered an On-Off ganglion cell with no rectification of the opposing contrast.

Taken together, for each recorded retinal ganglion cell, we calculated a chromatic integration function based on their responses to the chromatic integration stimulus and their baseline activity. From the chromatic integration function of each ganglion cell, we defined first, whether each cell integrates chromatic stimuli linearly or nonlinearly. Second, we defined the response polarity for each ganglion cell (On, Off or On-Off). Last, we defined whether the cell rectifies the non-preferred stimuli or not.

From these criteria, we were able to classify the recorded ganglion cells into different chromatic integration groups.

2.7. Classification of retinal ganglion cells based on their chromatic integration characteristics

For objective classification of the recorded ganglion cells, we looked at three different features of their responses to the chromatic integration stimulus. These features were the crossing point of the chromatic integration curves, the polarity and the rectification of the responses (see section 2.6). Now based on the mentioned three criteria we defined a series of indices that allowed us to classify, objectively, the entire population of the recorded ganglion cells.

2.7.1. Monochromatic index

This index separates the ganglion cells that respond to both green and UV colors (dichromatic) from the monochromatic ganglion cells. The monochromatic index was defined as the difference between the absolute value of the responses to the strongest green and UV stimuli divided by the sum of them.

$$\textit{monochromatic index} = \frac{\left| \textit{green}_{\textit{strongest response}} \right| - \left| \textit{UV}_{\textit{strongest response}} \right|}{\left| \textit{green}_{\textit{strongest response}} \right| + \left| \textit{UV}_{\textit{strongest response}} \right|}$$

The maximum green stimuli are green 20%, UV 0% and green -20%, UV 0%. The maximum UV stimuli are the 20% and -20% UV with 0% green contrast. For this index, the monochromatic ganglion cells that responded only to UV stimulus have values close to -1 and monochromatic green cells have the index close to 1. The ganglion cells that integrate both colors on the other hand, have monochromatic indices that are different from 1 and -1. We then used the threshold of -0.8 to 0.8 to separate the cells that integrate both colors from the monochromatic cells.

2.7.2. Nonlinearity index

The aim of this index is to separate the chromatically linear cells from the nonlinear cells. To do so, first, we needed to find the crossing point of the two green-on, UV-off and green-off, UV-on curves. For each stimulus set, we had 11 data points and we first linearly interpolated between these points to get the smooth curves. We then searched for the intersection (crossing point) of the green-on, UV-off and green-off, UV-on curves. For an intersection, we needed four different data points to be positioned in a way that the line passing through two points crosses the line that pass through the other two points. After finding the intersection of the two curves, we looked at the four data points

around the crossing point. For each curve at the crossing point, we had one stronger response and one weaker response (figure 2.5). We defined the upper bound of the crossing point as the two stronger (maximum) responses from the four data points around the crossing point of the green-on, UV-off and green-off, UV-on curves (figure 2.5.A and B). Similarly, the lower bound was defined as the weaker (minimum) responses at the crossing point (figure 2.5.C and D). We calculated a nonlinearity index for each ganglion cell as the maximum of the lower bound at the crossing point divided by the strongest response (maximum response to all the combinations of chromatic integration stimuli) of the cell (figure 2.5).

$$\text{nonlinearity index} = \frac{\max(\text{lower bound})}{\text{strongest response}}$$

Our measurement here is a conservative approach to get the nonlinearity. We chose the lower bound over the crossing point to ensure that for the nonlinear cells even the weaker response was still away from zero. For the linear cells, both the lower bound and crossing point were close to zero. We chose the threshold of 0.1 and -0.1 to separate the linear cells from the nonlinear ones. This is equivalent to 10% of the maximum activity of the cell. Therefore, the chromatically linear cells have nonlinearity index between -0.1 and 0.1 (figure 4.9.B-inset). Nonlinear cells with robust responses at the crossing point have a nonlinearity index bigger than 0.1 and the suppressive nonlinear cells have a nonlinearity index smaller than -0.1.

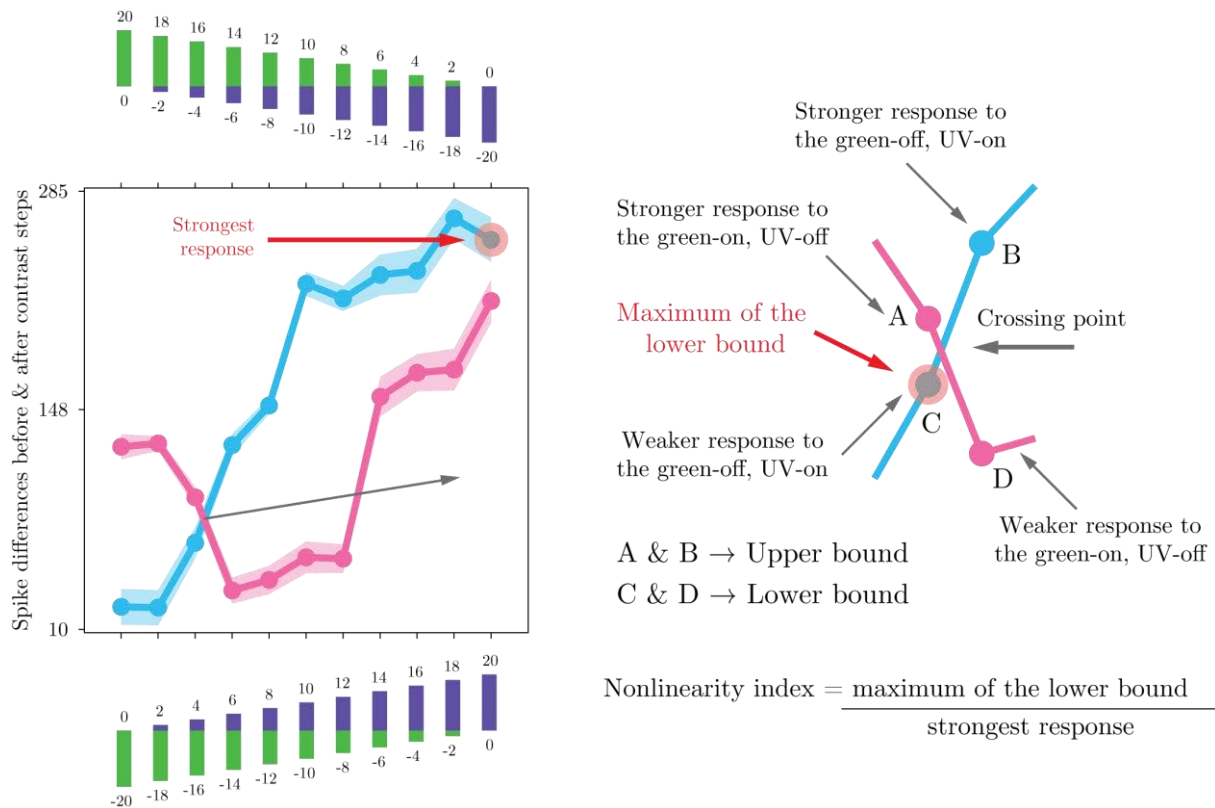


Figure 2.5. Measurement of the nonlinearity index from the chromatic integration curves. For each ganglion cell, we found the crossing point of the green-on, UV-off and green-off, UV-on curves (right panel). At the crossing point, we searched for the upper and lower bounds, which we defined as the stronger and weaker responses to opposing contrast combinations. For each cell, we calculated a nonlinearity index as the ratio of maximum of the lower bound (C) and the strongest response (upper data point in left panel).

2.7.3. On-Off bias

After the nonlinearity indices, we classified the ganglion cells based on their response polarity. In this classification, we used an On-Off bias for the strongest response to either UV or the green stimulus. To calculate the On-Off bias, we first subtracted the baseline activity of the cell from its strongest response (e.g. 20% green or UV for On cell) and its opposite counterpart (e.g. -20% green or UV). We calculated the On-Off bias as the difference of the absolute responses during On and Off stimulus divided by the sum of the two. The On-Off bias was defined as:

$$\text{On-off bias} = \frac{|R_{on}| - |R_{off}|}{|R_{on}| + |R_{off}|}$$

Here, R_{on} is the cell's response to the On stimulus and R_{off} is the response to the Off stimulus. The On-Off bias ranges from -1 for the Off cells to 1 for the On cells and On-Off cells have On-Off bias closer to 0 (figure 4.9.D). We classified any cells with an On-Off bias between -0.6 and 0.6 as On-Off cells, cells with an On-Off bias bigger than 0.6 as On cells and cells with an On-Off bias smaller than -0.6 as Off cells.

2.7.4. Rectification index

We checked how each ganglion cell responded to its non-preferred stimulus. As shown before, some ganglion cells rectify the non-preferred stimulus (figure 2.4.B) while others suppress their activity in response to non-preferred stimulus (figure 2.4.A). Therefore, to separate the ganglion cells further, we defined a rectification index. This index is based on how each ganglion cell responds to the non-preferred stimulus. Here, similar to the On-Off bias, we first found the strongest response among all the different contrast combinations and then defined a rectification threshold as the 10% of the strongest response. After this, we looked at the response of the cell to the stimulus with opposite contrasts of the strongest response (non-preferred stimulus). We then defined a rectification index as the response to the stimulus with non-preferred contrast divided by 10% of the strongest response.

$$\text{rectification index} = \frac{\text{response to the non - preferred stimulus}}{0.1 \times \text{strongest response}}$$

Based on this index the cells that rectify their non-preferred stimulus have a rectification index between -1 and 1, while the non-rectifying cells have a rectification index smaller than -1 and On-Off cells have a rectification index bigger than 1. For example, the rectification index for a ganglion cell that responds to the green On stimulus with 240 Hz firing rate and to the green Off (non-preferred stimulus) with 10 Hz is 10 divided by 24 (10% of 240Hz) or 0.42.

2.8. Measuring the properties of chromatic integration responses

In addition to the indices that were mentioned before, we defined two more indices to further measure the properties of the chromatic integration classes.

2.8.1. Green-UV index

This index shows the contribution of s- and m-cones to the output of the chromatic integration classes. To calculate this index, we looked at the contrast combinations of the chromatic integration stimulus that had only one color (green $\pm 20\%$, UV 0% and green 0%, UV $\pm 20\%$). For each color, we take the maximum of the response from either the On or Off stimulus. We then calculated the green-UV index as the maximum of the response to green stimulus subtracted from maximum response to the UV stimulus and divided by the sum of the two. The green-UV index was defined as follows:

$$\text{green-UV index} = \frac{R_{\text{green}} - R_{\text{UV}}}{R_{\text{green}} + R_{\text{UV}}}$$

where R_{green} and R_{UV} are the maximum responses to the green and UV stimuli, respectively. This index ranges from -1 to 1 and for the cells with stronger green response, it is closer to 1 and for the cells with stronger UV response, this index is closer to -1.

2.8.2. Transient-sustained index

As a metric for transience of the responses, we defined a transient-sustained index. Similar to many of the previous indices, this index was measured from the strongest response. For each ganglion cell, we defined a transient-sustained index as the difference between the peak and the average response divided by the sum of the two. Here the peak response was measured as the maximum response in the time

windows of 50-250 ms after the onset of the stimulus. Thus, the transient-sustained index was defined as:

$$\text{transient} - \text{sustained index} = \frac{R_{peak} - R_{mean}}{R_{peak} + R_{mean}}$$

Here, R_{peak} is the peak of response and R_{mean} is the average of the response during stimulation. For a transient ganglion cell, this index would be close to 1 and for sustained cells close to zero.

2.9. Measuring properties of the strongest response

The chromatic integration stimulus consists of 22 different contrast combinations. From these stimulus combinations, we defined the strongest response as the combination that has the highest peak firing rate. We studied the properties of the strongest response with the following measurements. First, we found the location of the peak from the PSTH of the strongest response (figure 2.6). From the peak, we measured the latency of the response as the time from the onset of the stimulus to the peak. Moreover, we measured the peak rate as the maximum of the firing rate from the PSTH. Next, we measured the decay time, which shows how fast the response declines from the peak. To measure the decay time, we fitted an exponential function between the peak and last time bin of the PSTH and from the fit parameters, we calculated the decay time (figure 2.6). To measure the transience of the response, we calculated the ratio of the response at the offset of stimulus and peak response (final response divided by peak rate in figure 2.6.). For the transient cells, this value is small and close to zero and for sustained cells this value is higher and closer to 1. Finally, we measured the spontaneous activity of each ganglion cell as the average of the last 200 ms of the background stimulus that was presented before the onset of the stimulus. Here, we calculated the baseline activity from the background stimulus that came before the stimulus that caused the strongest response. Since the same background stimulus was shown before each contrast, it is possible to use any background stimulus for calculating the baseline rate.

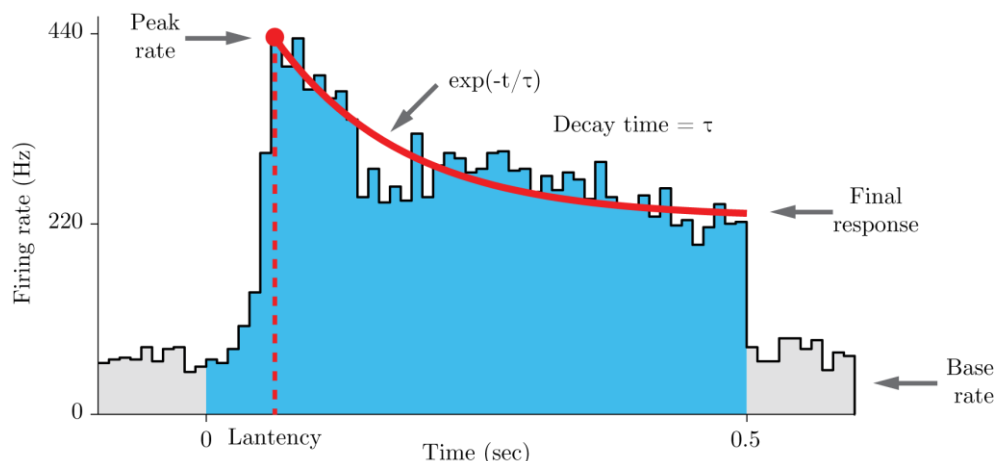


Figure 2.6. Measuring the properties of the strongest response. For each cell, we found the strongest response. We then measured the peak firing rate, final response, latency of the response (time-to-peak), base rate and decay time from the PSTH of the strongest response. To measure the decay time, we fitted an exponential function between the peak and final point of the PSTH. From the parameters of the fit, we calculated the decay time.

2.10. Spike-triggered analysis

Retina ganglion cells respond to a diverse range of stimuli. To define the response characteristics of a ganglion cell, it is desirable to stimulate it with as many different stimuli as possible. Stimuli such as the chromatic integration stimulus that was used in this thesis limit the stimulation to a handful of contrast values. To get a better insight about the response characteristics of different ganglion cells and especially their chromatic response properties, one should use a broader and more diverse set of stimuli. One approach to have a better estimate of the response characteristics of a ganglion cell is to use the method of spike-triggered analysis. The premise of this method is to stimulate the retina with a huge set of random contrast values and record the spiking activity of each ganglion cell. Then, for each individual spike, one looks into the stimulus that elicited that spike. This is done by defining a specific time window before each spike and looking at the stimuli inside that time window. The stimuli that were presented before each spike are the ones that triggered the spikes and they are called the spike-triggered stimulus ensemble. This spike-triggered stimulus ensemble is then investigated with different statistical methods such as average (spike-triggered average, STA) or covariance (spike-triggered covariance). Moreover, the spike-triggered stimulus ensemble represents filtering properties of a ganglion cell and it can be used as part of different modelling approaches such as linear-nonlinear Poisson (LNP) model (Chichilnisky, 2001), linear-nonlinear-linear-nonlinear Poisson (LNLNP) model and semi-nonnegative matrix factorization (STNMF) model (Liu et al., 2017).

The stimuli that we used for the spike-triggered analysis were chromatic versions of a temporal or spatio-temporal white noise. All white-noise stimuli that we used in this study had combinations of

green and UV contrast values that were drawn from two sets of pseudorandom numbers. Since both of these colors were presented simultaneously, for each ganglion cell we calculated two spike-triggered stimulus ensembles. The chromatic temporal white noise stimulus consisted of a full-field (no spatial structure) stimulus with green-UV contrasts. The values of the contrasts were drawn from two Gaussian distributions. The spatio-temporal stimuli have spatial structures (a checkerboard structure (48 μm to the side)). For each spatial element, they have combinations of green and UV colors. The contrast of the green and UV values for the spatio-temporal white noise stimuli were drawn from two sets of binary random distributions. The advantage of using temporal or spatio-temporal stimuli is in generation of a wide range of stimuli that could be presented to a large population of ganglion cells (Chichilnisky, 2001). At the same time, with this method it is possible to extract the response characteristics of individual ganglion cells.

To calculate the spike-triggered stimulus ensemble, one assumes that the spiking activity of a ganglion cell in response to white noise stimuli is elicited by a temporal length of stimuli preceding the spike (Schwartz et al., 2006). This sets of stimulus before each spike i is put together in the vector s_i . The spike-triggered stimulus ensemble for each ganglion cell is the collection of all the stimuli set preceding the spikes of that cell. Since the white noise stimuli had two colors, we measured two sets of spike-triggered ensemble, one for green and one for UV color.

2.10.1 Spike-triggered average

A simple way to analyze the ganglion cell's response to the white noise stimuli is to take the average of the spike-triggered ensemble. Therefore the spike-triggered average (STA) for each ganglion cells would be:

$$STA = \frac{1}{N} \sum_{i=1}^N s_i$$

In this equation, N is the total number of spikes and s_i is the stimulus vector that elicited the spike i . With this method, the spike-triggered stimulus ensemble is collapsed into one dimension along which the cell has the strongest response. In this project, the spike-triggered average is used to measure the receptive field area of each ganglion cell and to check the polarity of the ganglion cell response (On vs Off).

2.11. Receptive field estimation

The receptive field of an individual ganglion cells is a region of visual field in which a stimulus can modify the response of that ganglion cell (Kuffler, 1953). The receptive field of most retinal ganglion

cells has a center-surround structure. The center of the receptive field is excitatory and receives inputs from bipolar cells. Similar to the ganglion cells, the bipolar cell receptive field center integrates inputs from the photoreceptors. The receptive field surround of a ganglion cell is mostly inhibitory, and amacrine cells are the main inhibitory cells that form the receptive field surround. The classical approach to measure the receptive field of a ganglion cell was used in single-cell recordings. Spots of light with varying size were projected to a ganglion cell, and the receptive field borders of the cell were measured. However, this approach is not applicable to multi-electrode recordings, because many cells are being stimulated and recorded simultaneously. One approach to find the receptive field of the ganglion cells in the multi-electrode recordings is to stimulate the retina with long and diverse sets of stimuli such as Gaussian or binary white noise that has a spatial structure (checkerboard or stripe pattern). The spatio-temporal receptive field is then calculated by measuring the spike-triggered average (STA) of the stimuli that elicit the response of each ganglion cell (Chichilnisky, 2001). This spatio-temporal receptive field is in fact a movie of the stimuli that shows both the spatial location of the receptive field and at the same times its temporal dynamics. The temporal dynamics here correspond to the changes in response over time (response latency and time-course of the response).

For each recorded ganglion cell, we measured a receptive for green and one for UV color. We stimulated the retinal ganglion cells with flickering white noise stimuli with spatial (checkboard) pattern that has combinations of green and UV colors. We calculated the spike-triggered average for each stimulus and got two sets of spatio-temporal receptive fields. We broke down each spatio-temporal receptive field into its spatial and temporal components using singular value decomposition (SVD). The spatial component of the receptive was approximated with a 2D-Gaussian function:

$$RF(x, y) = \frac{1}{2\pi\sigma_x\sigma_y} e^{-\left(\frac{(x-\mu_x)^2}{2\sigma_x^2} + \frac{(y-\mu_y)^2}{2\sigma_y^2}\right)}$$

where parameters σ_x and σ_y correspond to the width of the receptive field while μ_x and μ_y represent the location of receptive field center. After fitting the spatial component of the receptive field with a 2D Gaussian function, the receptive field was defined as the area that is enclosed by an ellipse at 1.5 standard deviations of the Gaussian (figure 2.7). For each ganglion cell, one receptive field for green color and one for UV were measured. The temporal component of the receptive field is then used to check the polarity (On vs Off) of the ganglion cell. Furthermore, for each ganglion cell, we studied the temporal kinetics of the response by calculating the time-to-peak for each temporal component of the receptive field. To measure the time-to-peak, we fit the region around the peak with a second-order polynomial function and from the fit function, we calculated the time-to-peak for each temporal component. Beside the time-to-peak, we measured the biphasicness of the temporal filters (Zaghloul et al., 2007). For this measurement, we calculated a biphasic index as the ratio of absolute value for the size (filter strength) of second to first peak. Here, similar to the time-to-peak measurement, the values for first and second peaks were found after fitting the temporal components with second-order

polynomials. Finally, it is important to mention that for our population analysis of the receptive field properties, we mainly compared the receptive fields of the cell in response to the UV stimulus. This is due to stronger and more robust responses of the ganglion cells to the UV stimulus in comparison to the green. Furthermore, we had a considerable population of UV sensitive cells that did not respond to the green stimulus, while we rarely found cells that responded only to green. Thus, in our analysis of the receptive field, our measurements were done based on the UV stimulus.

2.12. Linear-nonlinear Poisson model

The linear-nonlinear Poisson (LNP) model is a simplified functional model that is used to describe the response properties of a neuron especially in the early visual system (Chichilnisky, 2001). The LNP model consists of three different stages. The first stage is a linear filter that describes how a neuron integrates stimulus intensity over space and time. This linear filter is calculated with the spike-triggered average. As shown in the receptive field estimation part, this linear filter already shows the location and temporal dynamics of a ganglion cell receptive field. In the second stage of the LNP model, the linear filter output of the first stage is then passed through a nonlinear function. This nonlinear function maps the instantaneous response of the filters to the firing rate of the neuron. In the third stage of the model the output of the second stage is used to generate spikes according to an inhomogeneous Poisson process (Schwartz et al., 2006).

The linear filtering of the LNP model shows the feature selectivity of a ganglion cell by reducing the multi-dimensional stimulus space to a low dimensional feature space (STA). The nonlinearity is generated by convolving the stimulus ensemble with the ganglion cell filter and then comparing the histogram of filtered stimulus signal with the histogram of the firing rate of the ganglion cell. Thus, the nonlinearity converts the filtering output of a ganglion cells to its non-negative firing rate and it corresponds to nonlinear features of a neuron such as spike-threshold (rectification) and saturation of the response. The output of the nonlinearity is a firing rate, and the Poisson spike generator converts the firing rate to a series of spike times. The main assumption about the spike generation is that the probability of having a spike at a certain time point depends on the instantaneous firing rate. In this project, the LNP model is used to calculate the chromatic filtering properties of each ganglion cell and the nonlinearities are used to measure the sensitivity changes of a ganglion cell in response to different chromatic stimuli.

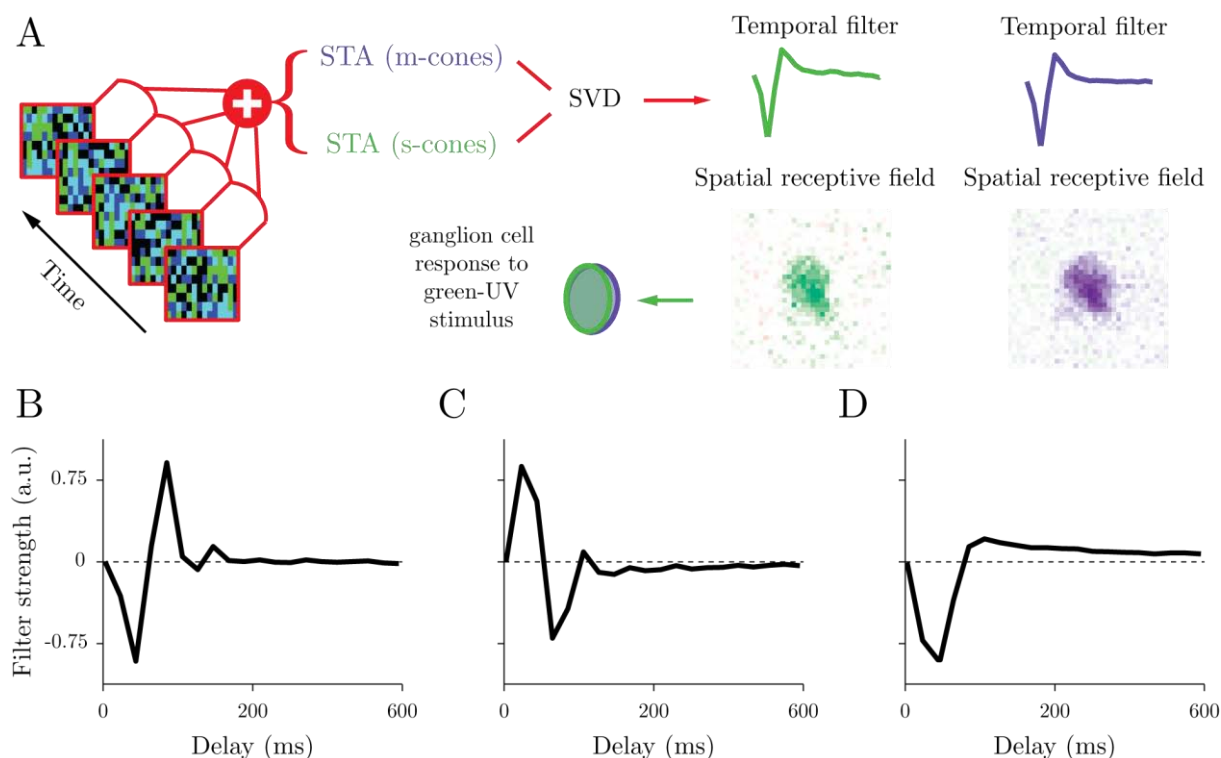


Figure 2.7. Measuring properties of the ganglion cell receptive field. A. Schematic presentation of the chromatic white-noise stimulus that was used to estimate the spatio-temporal receptive field of each ganglion cell. We calculated the spike-triggered average (STA), for both green and UV colors from the white-noise stimulus. The spatio-temporal receptive field was separated to its temporal and spatial components with the method of singular value decomposition (SVD). For each ganglion cell, we measured two temporal and spatial components of the receptive field. The spatial components of the receptive field were fitted with a 2D Gaussian function to estimate the location and diameter of the receptive field. Temporal component of the receptive field was used to measure the polarity, and biphasicness of the receptive field. B. An example for the temporal component of the receptive field for an Off ganglion cell. C. same as B but for an On ganglion cell. Here both B and C have biphasic filters. D. Example of the temporal component for an Off ganglion cell that is monophasic.

2.13. Nonlinear-linear-nonlinear model

The nonlinear-linear-nonlinear (NLN) model is an extension of the LN model. In the LN model, the input to the model is considered a linear filter. When the LN model is used to study the properties of ganglion cells, this linear filter is corresponded to all the input signals that come to the ganglion cells. However, in the retina the inputs to ganglion cells are generated and modified by the photoreceptors, bipolar cells, horizontal cells and amacrine cells. Therefore, the linear filtering stage of the LN model oversimplifies the way the inputs are conveyed in the ganglion cells. To overcome this limitation of

the LN model, many models were evolved based on the LN model to consider different properties of the retinal circuitry.

NLN model is an example of such models that can be used to model the signal integration features of the retina. The NLN model has two stages. The first stage considers multiple inputs and each input is passed through its own nonlinear function and after that all the inputs are summed together. In the second stage of the NLN model, the summed inputs are passed through the second nonlinear function to generate the output of the model. The advantage of NLN model lies in its ability to have multiple types of inputs and assign a separated nonlinear function for each input. This is advantageous in this project and in general for studying signal integration.

In this project, we had two types of chromatic inputs, one for the green and another for the UV color. We thus defined two inputs to the model and each input was passed through a nonlinear function. This function (first stage nonlinearity) corresponded to the nonlinearities of the bipolar cell's synapse. In our usage of the NLN model in this thesis, we did not consider the inhibitory circuit of the retina. However, we were able to simulate some properties of the chromatic integration with the NLN model. Taken together, the NLN model is a powerful model to study chromatic integration and in general, signal integration. Therefore, with this model we were able to simulate different aspects of chromatic signal integration.

3.

Projection System

The main goal of this project is to study the mechanism of chromatic signal integration in the mouse retina. To do so, it is necessary to stimulate the mouse s-cones (UV-sensitive) independently of the m-cones (green-sensitive) and measure how each chromatic input signal contributes to the overall output of a ganglion cell. Common light projectors do not have UV LEDs or high spatial resolution projection capabilities. To overcome these issues, we built a new UV-green projector that allowed us to display UV-green stimuli at micrometer resolution. In this chapter, first, we focus on the technical aspects of building a UV-green projector. Then, we explain how the calibration was done on the output of the projector. In the last part of this chapter, we explain how and why the cone-isolation was implemented and used for our experiments. The aim of this chapter is to provide a guideline or protocol to build a UV-green projection system. This projection system can be used in studying different aspects of the mouse visual system.

3.1. Building a new projection system

In the design of experiments, it is important to consider the features of the animal that is being studied. One of these features in vision research is the sensitivity of the photoreceptors. As mentioned before, mouse s-opsins are sensitive to UV light (300-400 nm), which is different from blue sensitive (450-495 nm) s-cones of primates. This difference motivated us to develop a new projection system that is able to project UV light with a spectrum very similar to the mouse s-cone sensitivity spectrum. Moreover, mice have smaller eyes and relatively smaller photoreceptors compared to primates (Remtulla and Hallett, 1985; Lapuerta and Schein, 1995; Oyster, 1999; Schmucker and Schaeffel, 2004). The small size of mouse photoreceptors (5-10 μm) required us to design a custom-built lens system that demagnifies the projector pixels to the resolution of mouse photoreceptors. This custom-built projection

system allowed us to stimulate effectively the mouse photoreceptors independent of one another. We assembled the projection system along with its lens system onto a custom-built mounting system. This mounting system was used to install the UV-green projector inside the electrophysiological setup. For the first part of this chapter, we focus on the technical parts involved in building of the UV-green projection system. We discuss in more details the lens system and the mounting system. In the second part of this chapter, we will focus on the calibration, gamma-correction and preparation of the projection system for our experiments.

3.2. Selection of the projector

To select a projector for our experimental setup we considered two main features. First, the projector must have three separate red, green and blue LEDs. Second, the projector should be small, so it can be used inside the electrophysiological setup of our lab. In addition to these requirements, the projector should be affordable and not very bright so it can be used in the experiments without bleaching the photoreceptors. Regarding these criteria, most conventional cellphone projectors are suitable for our projection setup. However, there is another important issue to consider and that is the mechanism for light generation in the projector. This light generation mechanisms should be linear. One of the main features of the modern projectors including cellphone projectors is that they are equipped with a nonlinear color correction circuit. Color correction circuit is an internal circuitry of a projector that adjusts the color of the picture to optimize it for human color vision. This circuitry adjusts the color hues (e.g. blue vs green) relative to each other in a nonlinear fashion so that the output color is more pleasant for the human observer. In addition, the color correction circuitry changes different contrasts of the same color nonlinearly (e.g. different shades of green). Therefore, from bright to dark and from one color to another the adjustment is different. Since color correction circuitry introduces nonlinearities in the chromatic output of a projector, for our experiment it is important to choose a projector that does not have a color correction circuitry. Taken together, a suitable projector for our experiments should be a color projector with three LEDs, small, affordable, not very bright and without any complex color or brightness control circuitry.

Considering all these requirements, we chose DLP lightcrafter™ projector evaluation module (EVM) from Texas Instruments Company (figure 3.2). This is a developmental projection kit and it uses DLP (digital light projection) technology for image generation. This projector has many useful features that make it a good pick for our experimental setup. These features include an RGB light engine with not very bright LEDs that generates 20-lumen light output. It can display images or videos up to WVGA (854 x 480) resolution.

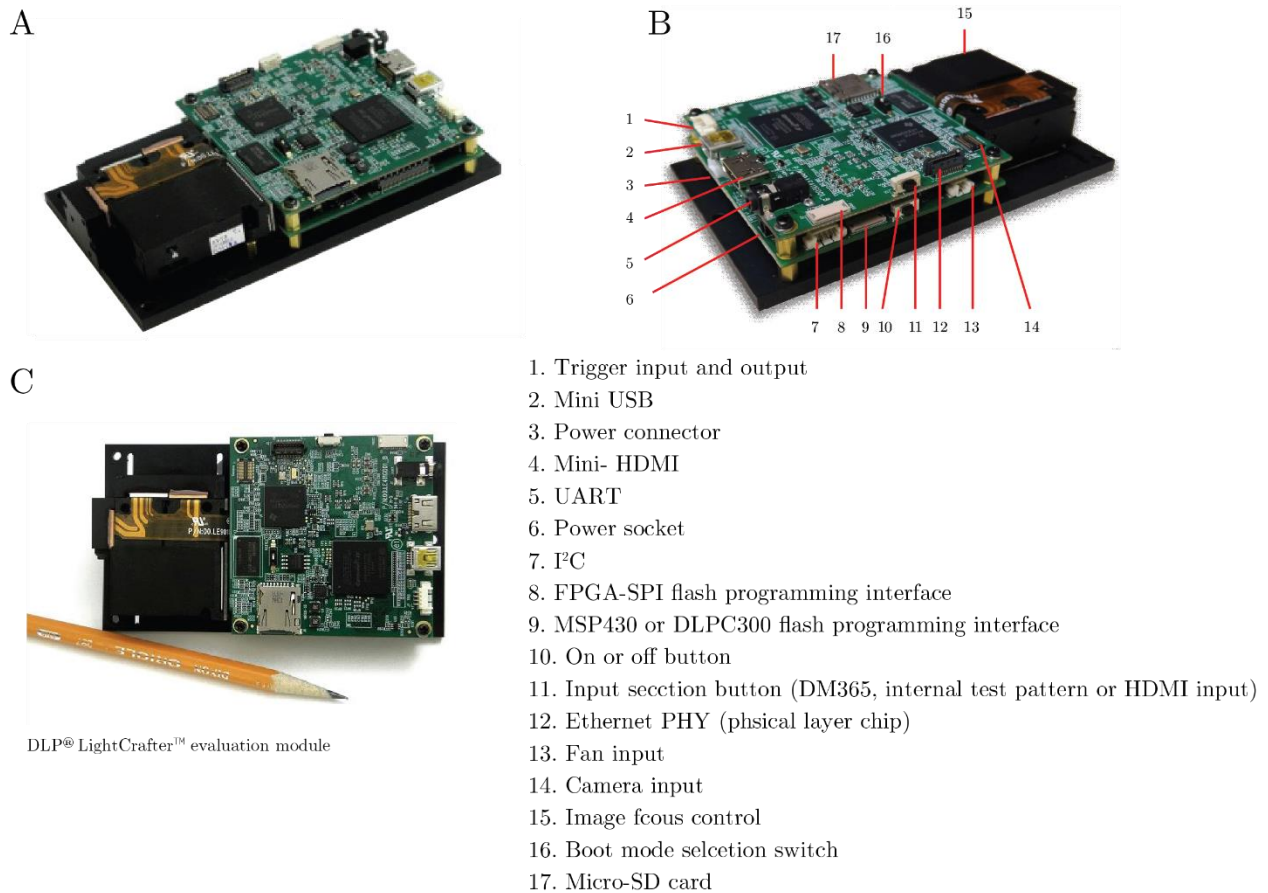


Figure 3.1. DLP lightcrafter and its input/output ports. A. Picture of Texas Instruments DLP lightcrafter projector that is used in this project for light stimulation. B. Full list of all input/output interfaces of the lightcrafter projector. A strong feature of the lightcrafter projector is its diverse input/output ports, which makes it adaptable to different applications. C. Comparative small size of the lightcrafter projector makes it a good pick for a stimulation system inside any electrophysiological setup. The images and the corresponding labels are acquired and adapted from the Texas Instruments webpage (September 2017) and Texas Instruments DLP Lightcrafter Evaluation Module (EVM) user's guide.

The lightcrafter has diverse port interfaces such as USB, Mini HDMI and UART. It has simple and practical graphical user interface (GUI) and USB-based API that allows the user to control many features of the lightcrafter such as individual LED brightness, aspect ratio, resolution etc. Finally, the lightcrafter's compact size of 117mm x 65mm x 23mm allowed us to use it inside the conventional electrophysiological setups of our lab.

3.3. Preparation of DLP lightcrafter projector for UV-green stimulation

The lightcrafter projector like many other commercial projectors has red, green and blue LEDs. To adjust this projector for the stimulating mouse retina, we had to exchange its blue LED with a UV (ultra-violet) LED and block its red LED. Changing the blue LED to UV LED consists of two crucial

steps. First, finding a UV LED that match the heatsink architecture of the light engine of the lightcrafter and second opening the light engine and replacing the blue LED with the UV LED.

3.3.1 Finding a matching UV LED

The light engine of lightcrafter is developed and manufactured by Young Optics International. All three LEDs of this light engine are produced by Osram Company (figure 3.3). These include:

1. red Osram Ostar compact LED- LE A Q9WN
2. green Osram Ostar compact LED- L CG H9RN
3. blue Osram Ostar compact LED- LE B Q9WN

Both red and blue LEDs have very similar architecture (figure 3.3.C and I). A suitable UV LED to replace the blue LED of the lightcrafter's light engine needs to have a similar soldering pad as the blue LED. Moreover, it must operate with the same forward current and must be relatively as bright as the green LED of the lightcrafter projector. Finally, an acceptable UV LED for our experiments should have a peak spectrum as close as possible to the peak sensitivity of mouse s-cones. After extensive search, we found and used the Nichia NCSU276A UV LED to replace the blue LED of the lightcrafter projector. Both Nichia NCSU276A and blue Osram LE B Q9WN have forward current of 700 mA. The peak wavelength of Nichia LED is between 360-370 nm, close to mouse s-cone peak sensitivity (360 nm) (Wang et al., 2011). However, it is important to point out that the soldering pads of the two LEDs have slightly different architecture (compare figure 3.3.C to 3.3.L). We will address this problem in section 3.6.8. Another issue with this particular UV LED and most commercially available UV LEDs is that they are not very bright compared to most conventional RGB LEDs.

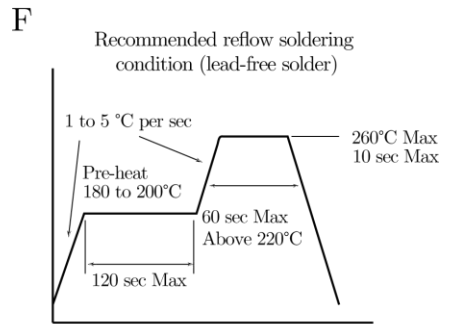
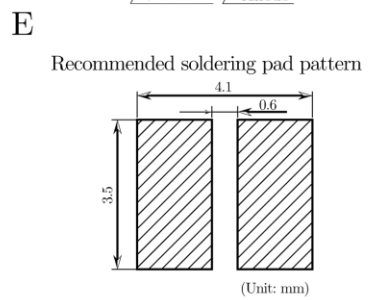
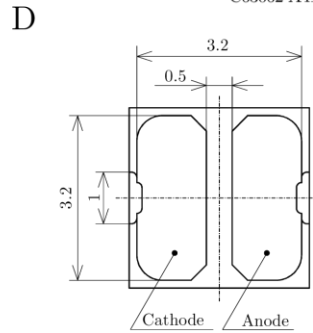
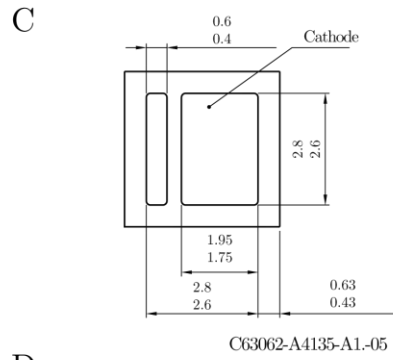
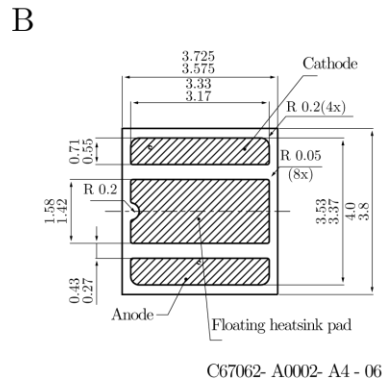
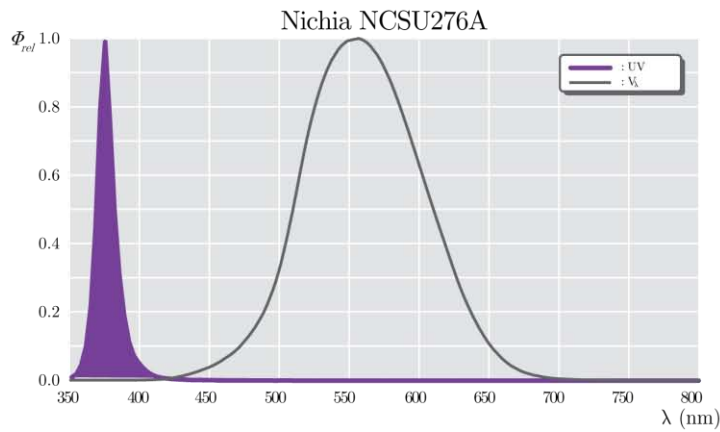
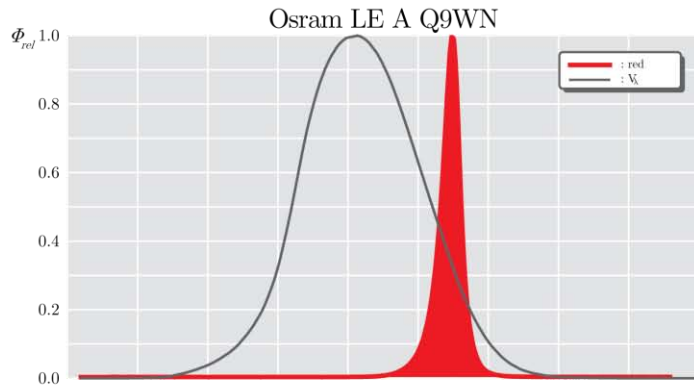
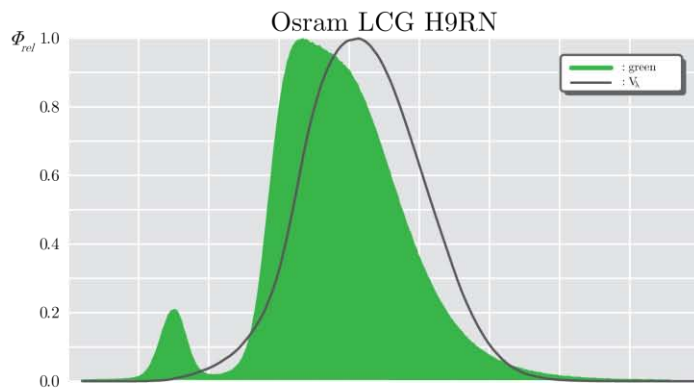
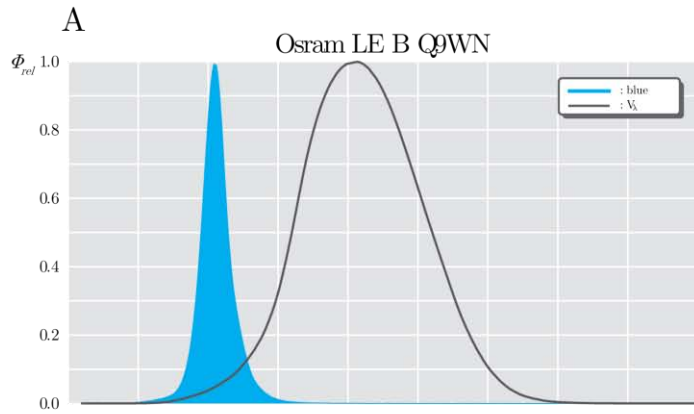


Figure 3.2. Spectrum and architecture of the red, green and blue LEDs that are used in the light engine of the DLP lightcrafter projector and the spectrum and architecture of the replaced UV LED. A. Spectrum of the blue, green and red LEDs of the lightcrafter. Below is the spectrum of Nichia NCSU276A UV LED. The peak spectrum of this UV LED is at 365 nm. V_λ is the photopic luminous efficiency function that describes the average spectral sensitivity of human visual perception of brightness at photopic light level. B shows the architecture and soldering pad structures of the blue and red LEDs. These two LEDs have same base architecture. D. Soldering pad and architecture of the green LED. The soldering pad of the green LED is different from the blue and red LEDs. E. Base design and recommended soldering pad pattern of the UV LED. Note that the UV LED has two soldering pads compared to three soldering pads of the blue LED. To overcome this issue during soldering we blocked the middle part of the UV LEDs' soldering pads with a shrinkage rubber so that the base of the UV LED match the base of the blue LED. F. The recommended soldering conditions for the UV LED. It is important to limit the soldering temperature up to 260 °C while soldering the UV LED in the place of the blue LED. All the spectrums and images are adapted from the data sheets of red Osram Ostar compact LED (LE A Q9WN), green Osram Ostar compact LED (L CG H9RN), blue Osram Ostar compact LED (LE B Q9WN) and Nichia NCSU276A UV LED datasheets and user manuals.

In case of the lightcrafter projector, the green LED is very bright (up to 1.8 W) and relatively brighter than the other onboard blue (0.63 W) and red (up to 0.44 W) LEDs. To balance the brightness of UV vs green LEDs, we used different color filters which we will discuss in more details in the section 3.6.12.

3.3.2. Replacing the blue LED

After finding a desirable UV LED, the next step was to open the lightcrafter light engine and replace the blue LED with the UV LED. Since the lightcrafter projector has a very small form factor with a very delicate light engine the opening of the light engine should be done with caution. This procedure consists of three steps. The first step is to separate the light engine from the DMD (digital mirror device) and circuit board of the lightcrafter projector. The second step is to open the light engine, detach the blue LED and then solder the UV LED in its place. The last step consists of putting back the light engine and re-assemble it together with the circuit board of the lightcrafter projector. These steps are shown in the figure 3.4 and 3.5. Below is a systematic guide about how to separate the light engine and replace the blue LED with UV LED.

First step: separating the light engine from the projection circuitry:

1. Remove the system board (top layer board) from the projector by un-screwing the four corner post screws (figure 3.4.A). These can be done with a Phillips P00 screwdriver.

2. Remove the three screws from the top of the light engine. Two screws are on one side close to the ribbon cable and the third screw is in the gap between light engine and corner post (figure 3.4.B).
3. Remove the screws from the bottom of the thermal plate (figure 3.4.C). These screws are the main screws that hold the light engine from below. Hold the light engine while opening; otherwise, the weight of the light engine is on the DMD board and ribbon cable. This weight may tear apart the ribbon cables and any damage makes the light engine inoperative.
4. Rotate the projector and gently remove the ribbon cables from the driver board (bottom layer board). To do this, first pull up the white plastic tab and then slowly take out the connecting ribbon cables that connect the driver board to the light engine (figure 3.4.D). These ribbon cables are very fragile and easy to break while pulling, so be very cautious.
5. Remove the two small back screws of the DMD board that hold the light engine from behind (figure 3.4.E). The DMD board is the vertical board behind the light engine that connects to the driver board.
6. Now, gently take off the light engine from the base thermal plate. The light engine stands on top of small support posts. To release it, one has to raise the light engine slightly and pull it from the driver board. In this step, the DMD comes off together with the light engine.
7. Separate the DMD from the light engine by removing the two screws behind the light engine (figure 3.4.F). To access the DMD, take out the DMD board behind the light engine and then carefully remove the DMD. The DMD is very delicate, and it is an essential part of the projector. Do not touch its surface because this might damage the micro-mirrors. To avoid any damage to the DMD, it is important to mount it back on the DMD board by putting it into the DMD socket on the board. It is important to mount the DMD in a correct orientation. To check this, the large square notch on the DMD should be to the left side of the projector and the triangular notch should be to the right side of the projector close to the mounting post (figure 3.4.G).
8. Now, the light engine should be completely separated from the projector. To access the internal parts of the light engine, remove the black tape that covers the top part of the light engine (figure 3.4.H). To do this, slowly lift one corner of the tape and pull the rest. Be careful not to tear apart the tape cover. It is needed to cover the light engine after changing the LEDs. After removing the tape cover, one should be able to see the focus lens of the lightcrafter and the three red, green and blue LEDs with their supportive heatsinks (figure 3.4.H).

Second step: replacing the blue LED with the UV LED

After opening the light engine, the internal parts of the light engine are visible (figure 3.5). Figure 3.5.A shows the top view of the light engine where the three LEDs (red, green and blue) are shown along with the connecting ribbon cable. The light beam emitted from each LED is passed through an optical collimator that makes the beam narrower. These narrow beams of light pass through series of

dichroic mirrors. These dichroic mirrors reflect one range of wavelengths while allowing others to pass. Moreover, they combine all three-color beams into one co-linear beam (figure 3.5.B). This recombined light is then passed through a fly-eye lens and condenser lenses, which together provide uniform light intensity over space. Finally, the uniform light intensity beam is directed to a mirror that reflects the light toward the DMD.

Figure 3.5.C shows details of the light path inside the light engine. It is important to note that the collimator, dichroic mirrors, fly-eye lens, condenser lenses and the DMD are all made of glass, and they slightly absorb the UV light. These glass components also slightly shift the spectrum of the UV LED.

Since these parts are specifically made for this light engine, it is very difficult to find identical UV-fusing lenses and dichroic mirrors. Therefore, we kept these internal glass components of the light engine. However, from the DMD onward we replaced all the lenses (focus lens in figure 3.5.A) with a new UV-fusing lens system. The result of keeping the internal lenses and DMD is a slight shift (10-20 nm) in the spectrum of the UV illumination. We will address this issue in the calibration part of this chapter. The following section contains the technical steps to remove the blue LED from the light engine and replace it with the UV LED:

1. Remove the LED's heat sink from the sides of the light engine (figure 3.5.A) by opening the four screws and slowly pull out the heat sink. Now the light engine should look like figure 3.5.C.
2. The LEDs are soldered to a copper sheet that dissipates the heat to the LED heat sink. Each LED copper sheet is connected to the light engine with a ribbon cable. Carefully put the tip of the soldering gun on the copper sheet of the blue LED below the connection point of the ribbon cable (figure 3.5.F). The heat from the soldering gun melts the soldering tin and release the LED copper sheet from the ribbon cable. Be careful not to tear apart or burn the ribbon cable. Otherwise, the light engine becomes dysfunctional. Now the blue LED with its copper sheet is separated from the light engine.
3. Remove the blue LED from the copper sheet by heating the copper sheet up to 250 °C. It is easy to put the LED with its copper sheet on a hot plate and with a small forceps pull the LED away from the copper sheet.
4. Replace the UV LED in the location of the blue LED on the copper sheet. As mentioned before the soldering pad of the Nichia NCSU276A UV LED has a different design than the blue Osram LE B Q9WN LED (compare figure 3.3.C with 3.3.L). To solve this issue, put a small soldering shrinkage rubber in between the two soldering pads of the UV LED (figure 3.3.L). This rubber will cover the middle pad position of the copper sheet of the blue LED (figure 3.3.C). Therefore, the two side pads of the blue LED copper sheet match the two soldering pads of the UV LED. To solder the UV LED, first cool down the copper sheet that we separated from blue LED. Then, cut a small piece of the shrinkage rubber with the same size as the

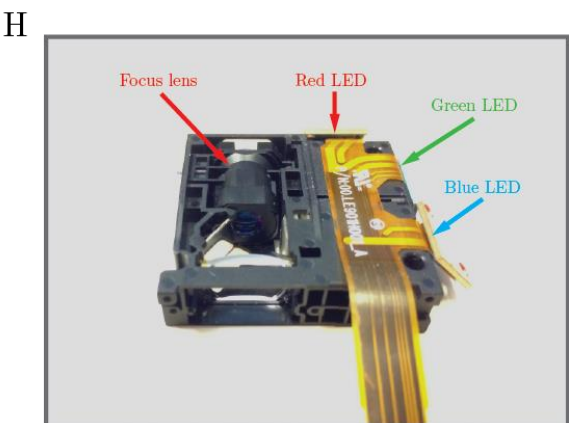
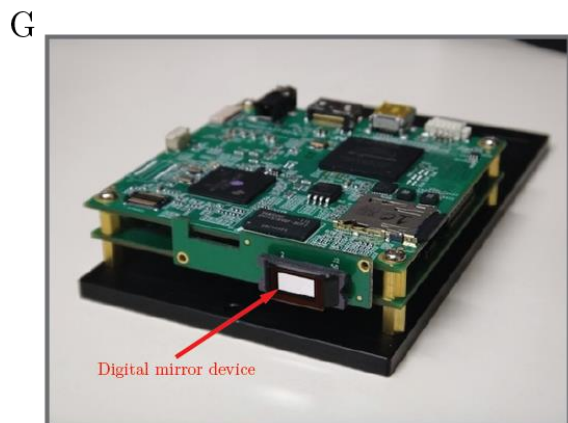
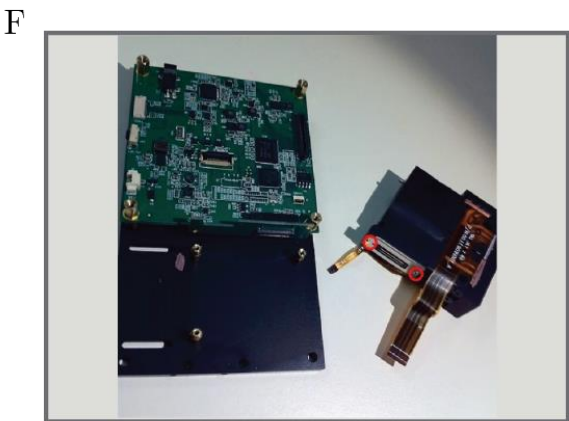
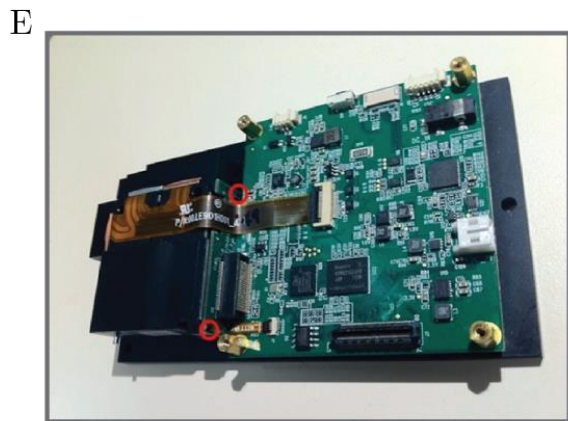
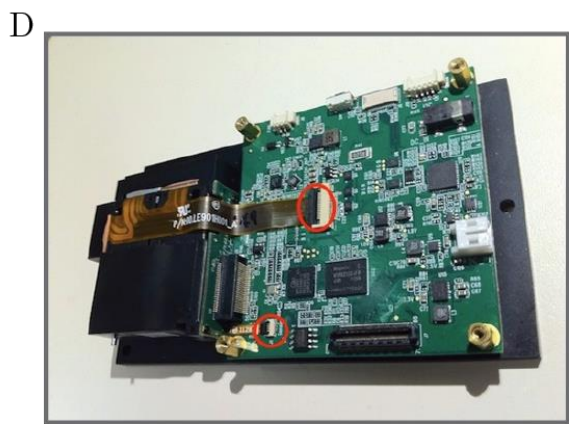
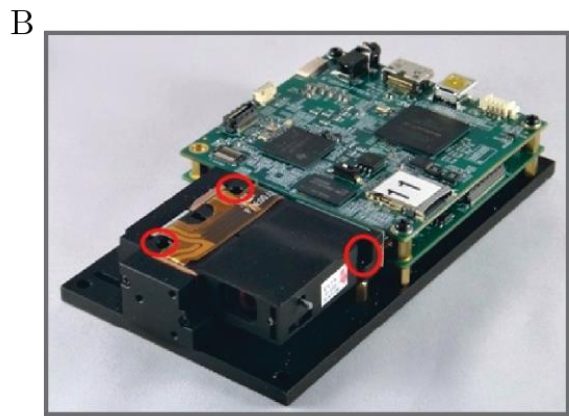
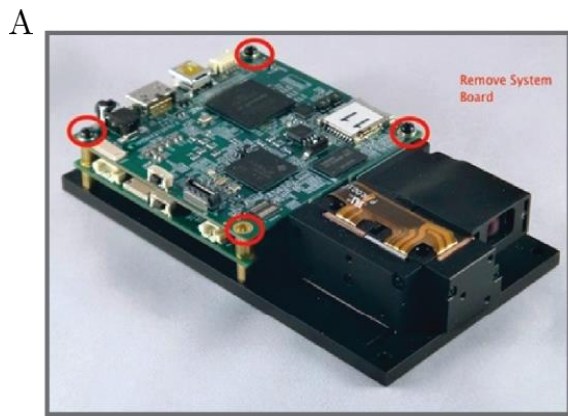
middle pad on the copper sheet of the blue LED. Before putting the shrinkage rubber, put two small drops of soldering tin on the side pads (cathode and anode) of the copper sheet. These should get solid fast and they will be used to hold the UV LED. Now heat up the hot plate close to 250 °C. Put the copper sheet on the heated hot plate and wait until the soldering tins on the side pad start to melt. Check the UV LEDs position of the cathode and anode on the soldering pad. These should match the positions of the copper sheet. Hold the UV LED in the correct direction with a forceps. As soon as the soldering tin on the side pads starts to melt, put the small shrinkage rubber that was cut before on the middle pad, and then put the UV LED on copper sheet and apply small pressure with the forceps to the UV LED. Now it is necessary to cool down the copper sheet very fast so the soldering tin solidify and holds the UV LED. Moreover the shrinkage rubber in between should not shrink a lot or burn. Since it takes time to cool down the hot plate, it is helpful to put few drops of water on the copper sheet and LED and then quickly push the LED away from the hot plate. This way the soldering tin holds the UV LED on the copper sheet. Otherwise, if the soldering tin is still in the liquid form, the LED will come off the copper sheet. After quick cooling of the copper sheet make sure that, the LED is attached perfectly to the copper sheet and no water droplet left on the LED. In the last step use a multimeter and measure the forward voltage and current of the soldered LED. Make sure that the current is passing from LED's cathode to its anode. If the multimeter does not show any current flow, it is a sign that the soldering was not good or the shrinkage rubber is not blocking the middle pad of the copper sheet effectively. This means that the LED will not work. To solve this issue re-heat the copper sheet and disconnect the LED and re-solder it again in same way as before. Always before assembling the light engine make sure, that the UV LED has forward current otherwise the LED will not work.

5. Connect the UV LED's copper sheet back to the ribbon cable. To do so, put a small amount of soldering tin on the connecting surface of the copper sheet, heat the sheet from below with the soldering gun, and carefully attach the free ribbon cable to it. Again, use the multimeter to make sure that there is a current flow in the UV LED.
6. Re-assemble the light engine by putting back the LEDs heat sink first and then connect the light engine to the DMD board.
7. Connect the light engine to the driver and system boards of the lightcrafter with the ribbon cables and put back all the screws that holds light engine in its place.

In the final step, use a 5-volt electrical adapter to power the lightcrafter projector and use the on/off button (figure 3.2.10) to turn on the projector. After a few seconds, the projector runs its internal booting check-up program and if all the previous steps were done without any mistake, no error should show up at this point. After the start-up routine, the lightcrafter shows a default screen with three bars, one for each LED. Now hold a white sheet of paper in front of the projector and three color bars should appear: one red bar, a green bar and a faded violet bar. This violet bar is from the UV LED.

If there is no violet bar try again with a UV-sensitive florescent surface or use a spectrometer to measure the UV signal. If still there is no UV light, re-open the light engine and check for possible errors.

Figure 3.3. Systematic guide to open the light engine from the lightcrafter projector. First, open the system board (A) and then remove the screws of the light engine from the thermal plate (B and C). Next, disconnect the ribbon cables (D) and remove the screws of the DMD board (E). Finally, de-tach the light engine from the thermal plate and the DMD board (F and G). Internal parts of the lightcrafter light engine (H). Images are acquired (September 2017) and adapted with permission from Texas Instrument's e2e community as part of the forum for DLP lightcrafter development platform.



3.4. Building a new lens system

Until now, we have explained the steps to change the lightcrafter projector to be able to emit UV light. To use this projector for our experiments, we needed to de-magnify the image in a way that each pixel output of the projector is the same size or smaller than the receptive field of a typical mouse photoreceptor. To do so, we removed the focus lens set that is in the light engine and replaced it with a new UV-fusing lens system that not only allowed UV light to pass through but also de-magnified the image. Nevertheless, before moving to the new lens system, first the original focus lens should be removed (figure 3.5.A). To do so, we removed first the focus handle (small screw) from the lens. After that, the lens is held in place with two longitudinal metal bars. It is possible to see them close to the end of the lenses of the projector. We used a forceps with a very small tip and slowly pushed each metal bar out. One can see the bars coming out from the front of the light engine. When nearly one third of the bar is out, the rest of the bars can be pulled out by using a long nose plier. If the metal bar was stuck in the light engine, we used a hot metal forceps or heated tip of a scalpel to melt the plastic slightly around the metal bar. This way the longitudinal bars can be moved easier. One needs to be very careful not to damage the plastic parts of the light engine that lead to light leakage that may contaminate the output light. After removing the original focus lens of the lightcrafter projector, we had to design a new lens. This new lens system should have certain properties. These include:

1. The lenses inside the lens system should allow UV light to pass or be UV fusing. Due to the small form factor of the original lens system of the lightcrafter, it is very difficult to find a commercial UV-fusing lens that has the same dimensions as the original.
2. The lens system should de-magnify the output image in a way that each pixel is as small as the average mouse photoreceptor receptive field (5-10 μm).
3. The minimum object distance from the first lens should be 38 mm. This is the distance from the DMD (inside the light engine) to the outer border of the light engine. This border of light engine is where the light is emitted out from the projector.
4. The image distance of the last lens that is inside the lens system should be bigger than 50 mm. This is because the components of the electrophysiological setup have together a height of around 40-50 mm (multi-electrode array, amplifier and solution inlet & outlet).
5. The lens system should not contain lenses with very long focal length so it can fit inside the electrophysiological setup.
6. The lens system should have as few lenses as possible to avoid distortion and chromatic aberration.

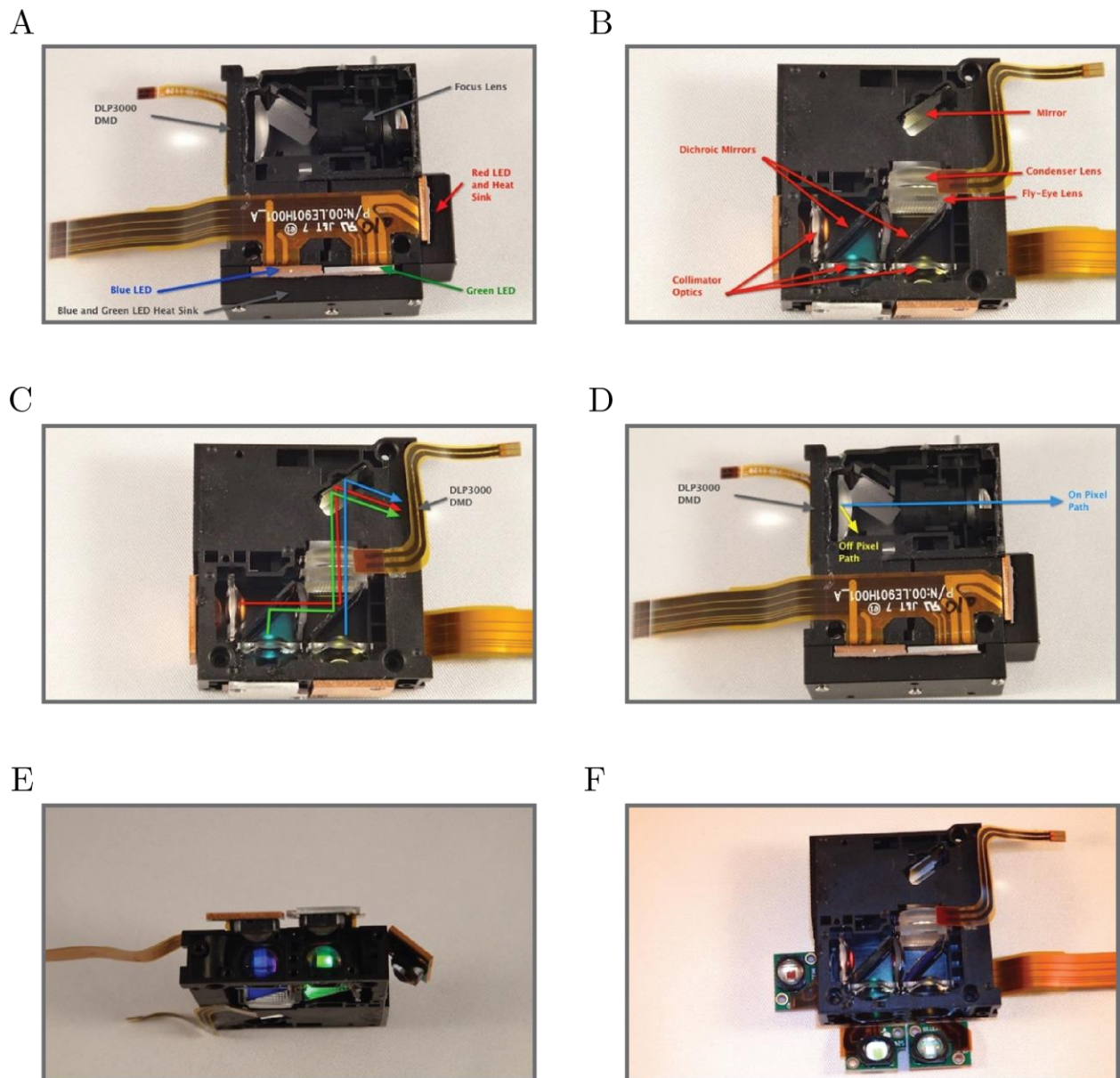


Figure 3.4. Details of the lightcrafter light engine. A. Top view of the internal part of the light engine where the ribbon cable connects to each LED. B. Bottom view of the light engine where the dichroic mirrors, fly-eye lens and condenser lens are shown. C and D. Light path of each LED inside the light engine to DMD and through focus lens to the outside of the light engine. E. A side view of the light engine after removal of the blue and green LED heat sink. F. A bottom view of the light engine after removal of the LEDs heat sink. Images are acquired (September 2017) and adapted with permission from Texas Instrument's e2e community as part of the forum for DLP lightcrafter development platform.

Considering all these issues, we used WinLens3D Basic software to design our lens system. This is a free version of WinLens3D software offered by Qioptiq Company. A great feature of this software is

its comprehensive database of most commercially available lenses and optical component. Therefore, one can design, model, test and simulate different optical components. We put all our design constrains (UV-fusing, object size, image size, back focal length, focal length, limited images distortion and chromatic aberration) into this software and built a lens system model using the information from different commercially available lenses (figure 3.6.A). Moreover, we could simulate green and UV light with the same wavelength as the LEDs we used to measure how they were affected by different parameters of the lens system (figure 3.6.B). Based on our optical design we used three lenses inside our lens system. These include:

1. UV plano-convex lens with UV-AR coating (catalog number: 48286).
2. Near UV achromatic lens with UV-VIS coating (catalog number: 65978).
3. Near UV achromatic lens with UV-VIS coating (catalog number 65978- same as 2).

All three lenses are UV fusing with 25mm diameter and are produced by Edmund Optics. We chose this three-lens design based on our simulations of lens system (figure 3.6). For the design of the lens, the fewer the lenses the smaller the light distortion and chromatic aberration. In our case, a single or even two lens system was not enough because we wanted the lens system to de-magnify the input image. Moreover, we wanted the lens system to be cost-effective and made of commercially available lenses. After considering these points and from many different simulations of lens arrangements that we tried with the WinLens3D Basic software, we found this three-lens system to be sufficient and reliable for our experiment.

In this lens system, the first lens is a UV-AR coated, plano-convex lens (figure 3.7.B) with back focal length (BFL) of 97.4 mm that is bigger than the distance from DMD to the edge of the light engine. The effective focal length (EFL) of this lens is 100 mm. The next two lenses of the lens system are identical. These lenses are compound lenses that consist each again of two fused lenses, a double concave lens fused with another convex-concave lens (figure 3.7.D). The back focal length of these lenses is 71.09 mm and the effective focal length is 75 mm. All three lenses of the lens system are designed for green and UV light stimulation (figure 3.7.A and C for reflectance curves).

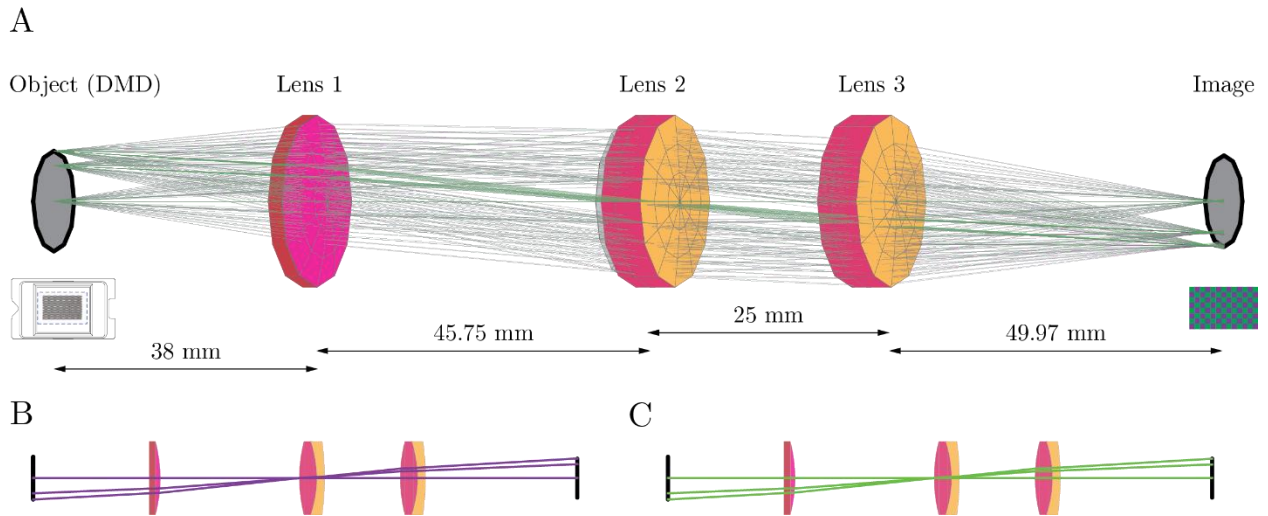


Figure 3.5. Schematic design of the lens system. A. main design of the lens system with simulated green and UV light beams. The light beam is emitted from the DMD inside the light engine and travel through the three different lenses to generate an image with 0.75 magnification scale. B. Simulation of three UV light beams from center, close to the edge and edge of the DMD passed through the lens system (A) which arrives at the positions shown on the image. C. same as B but for green light. The schematic image of the DMD on left is adapted from the Texas Instruments DLP Lightcrafter Evaluation Module (EVM) user's guide.

To get a sharp, focused output image, each of these lenses should be precisely at a fixed distance from one another (figure 3.6.A). The values for the distance between the lenses were acquired from the simulations of lens system that was done with the WinLens3D Basic software (figure 3.6). The first lens should be at 38 mm from the DMD inside the light engine. We used the first lens in a reverse position so that the flat, planar side of the lens facing the DMD and the convex side of the lens is toward the second lens. This way the image is focused towards the second lens.

The second lens should be exactly at 45.75 mm distance from the first lens with the double convex side facing the first lens and the concave-convex side towards the third lens. The third lens should be positioned 25 mm away from the second lens with the same orientation as the second lens. By putting the lenses in this distance and orientation, the image is in focus at 49.97 mm or close to 5 cm away from the last lens. The magnification ratio of this lens system is 0.75. Each pixel of the light crafter DMD has a diameter of $10.8 \mu\text{m}$. For the de-magnified output image of the lens system, each pixel has roughly $8 \mu\text{m}$ diameter. Therefore, each pixel of the output image is projected at the resolution of a typical mouse photoreceptor's receptive field.

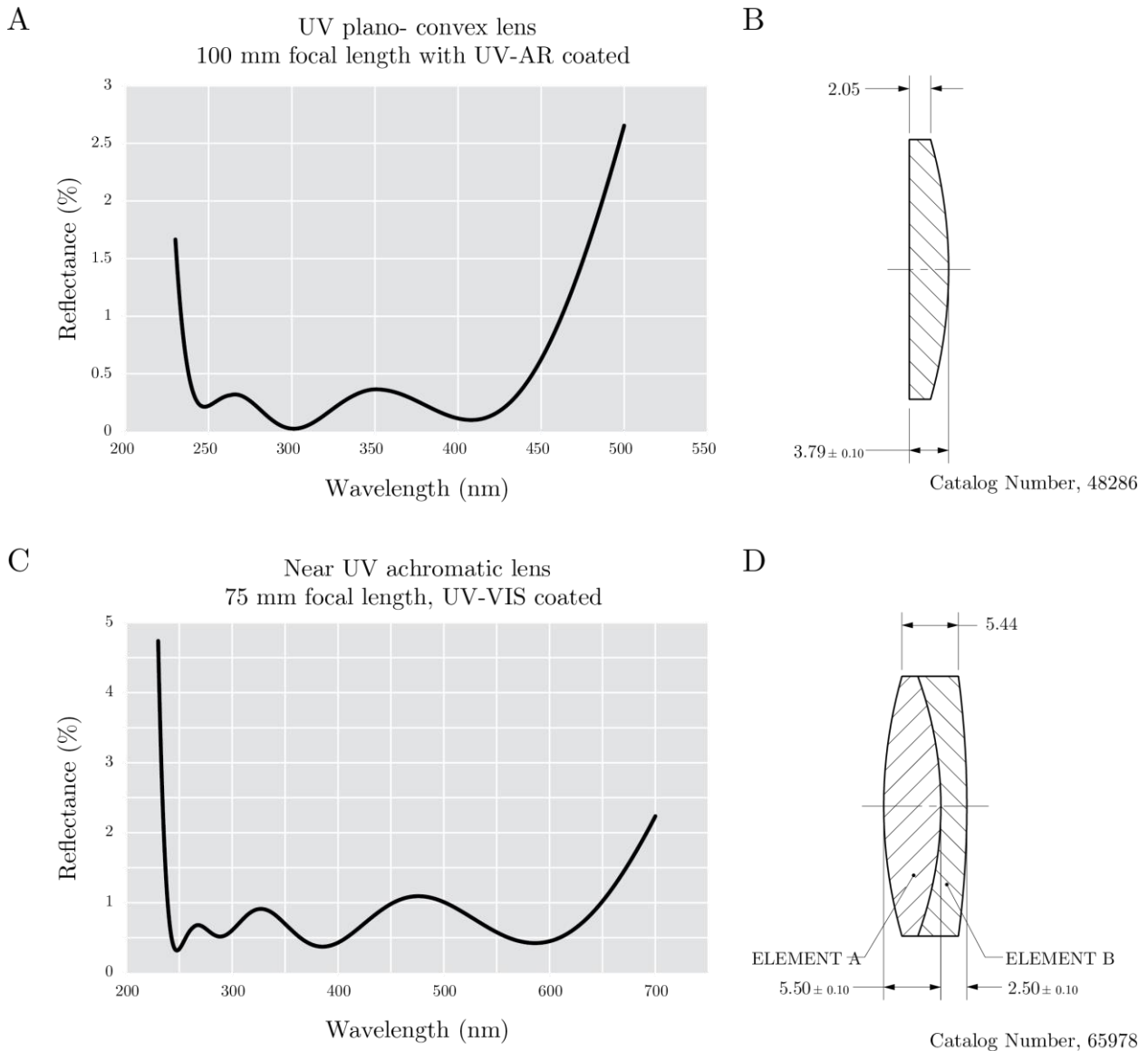


Figure 3.6. Reflectance curves and schematic view of the lenses used inside the lens system. A. Reflectance curve of the UV plano-convex lens. As shown here, this lens reflects less than 1% of its inputs. B. Schematic view of the same lens as A. The diameter of this lens is 25 mm. C. Reflectance curve of the near UV achromatic lens. This lens is used as the second and third lens of the lens system. Same as A this lens has less than 1% reflectance to either UV or green light. D. Schematic view of the second and third lens of the lens system. This lens is a compound lens with a double concave lens (element A) that is fused to a convex-concave lens (element B). The diameter of this lens is 25 mm. All the images and data are acquired and adapted from the Edmund Optics lens catalog (2017).

3.5. Mounting platform and optical cage system

After designing the new lens system and simulating its output, the lenses were assembled together in an optical cage system that is attached to the lightcrafter projector. Optical cage systems are a collection of mechanical components that are designed to serve as the structure that holds the optical parts (lenses and filters). The step after assembling the optical cage system was to put together the lightcrafter projector with a mounting platform and mechanical controllers inside the electrophysiological setup. This was to keep the projector at a correct distance from the multi-electrode array and to have a projection setup that can be used for experiments routinely. Figure 3.8 shows the overall mounting system and lens-cage system that is attached to the lightcrafter projector. We mounted the retina on the multi-electrode array with ganglion cells attached to the electrode and the photoreceptors facing upwards. Thus, we positioned the lightcrafter projector on top of the amplifier in a way that it stimulates the photoreceptors first. This arrangement makes the projector perpendicular to the multi-electrode array and its amplifier. Thus, the mounting system needs to be stable enough to hold the weight of the projector and its lens system. The mounting system consists of different mechanical components that allow fine control over the angle and position of the projector. This is useful to focus the image perfectly on the photoreceptor layer of the retina. The whole projection system together with the lens-cage system and its mechanical holders were put on a stable mounting stage and post that keep the projector at a correct distance from the recording area. This mounting stage platform also allows the experimenter to move the projection system towards or away from the recording area. This is a practical feature in our experimental setup since one needs to move parts of the amplifier up to put the multi-electrode array inside the amplifier. Table 3.1 shows the detail information about different components of the mounting system. Most components of the mounting system are commercially available. However, it is important to note that the base thermal plate of the lightcrafter projector does not have a standard screw thread. This unique design of the thermal plate makes it incompatible to other mechanical components of the mounting system mainly the kinematic prism mount (figure 3.9.A5) that is used to hold the lightcrafter. To solve the issue, we ordered a custom-made adapter plate (figure 3.9.A4) that was built in the local university workshop to match the screw threads of the lightcrafter projector and the kinematic mount prism. The remaining components of the mounting system are available commercially as pointed out in table 3.1.

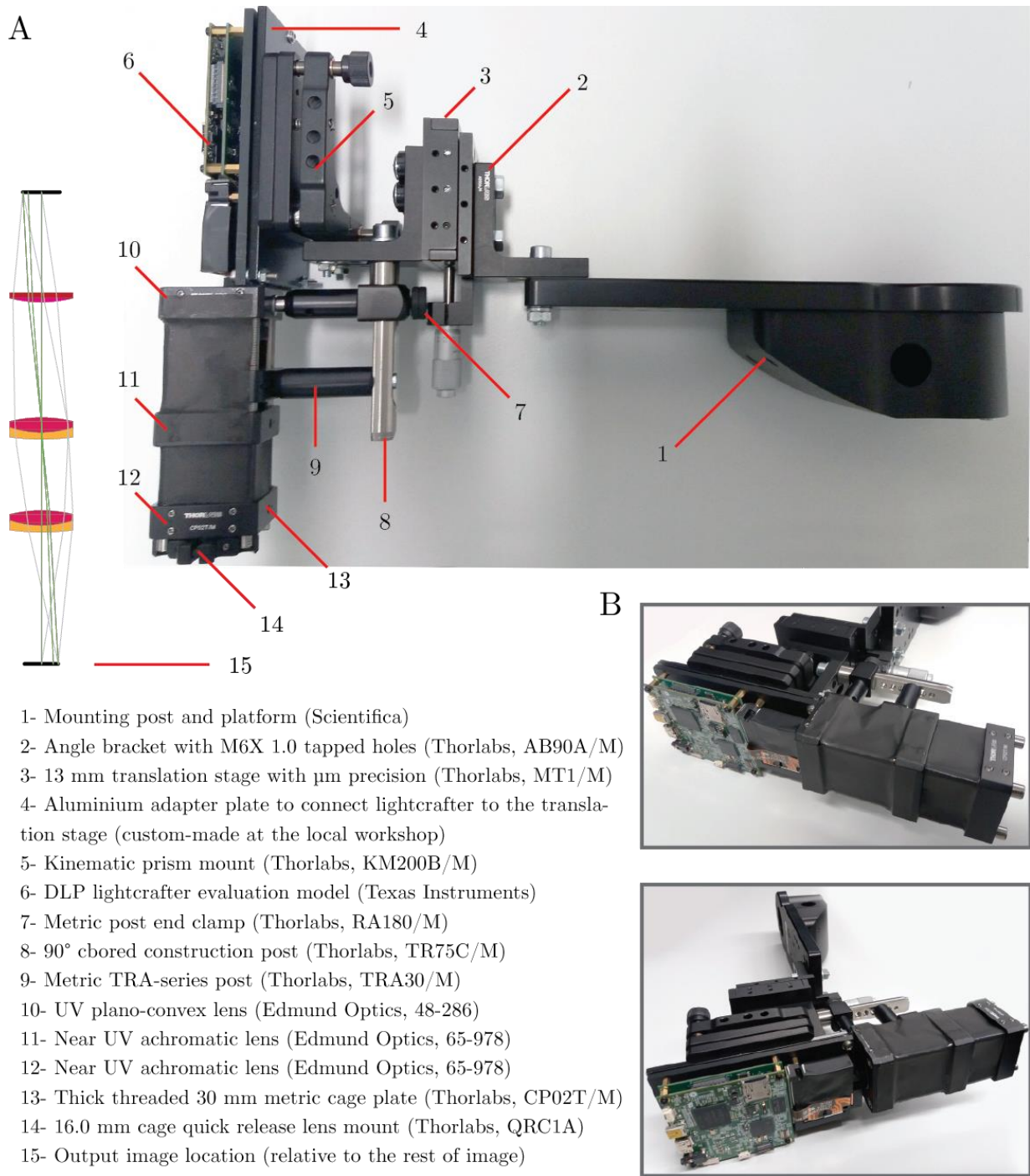


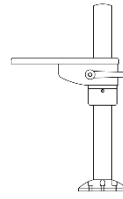
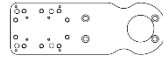
Figure 3.7. Mounting platform and the optical cage system of the projector. A. An overall view of the mounting system of the projection system with the mechanical components that are mentioned by number 1 to 14. Next to the optical cage system, there is an illustration of the lens system same as figure 3.7 where it shows the position of each lens with respect to the optical cage system and the rest of the mounting system. B. Different views of the projection system along with all the components of the mounting system.

Part: Mounting post and platform, (figure 3.9.A1)

Company: Scientifica

Weight: 8.8 Kg

Dimensions: 393 x 189 x 100 mm (height x width x depth)



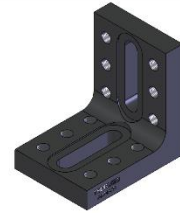
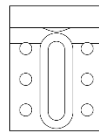
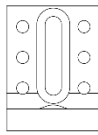
Part: Angle bracket with M6X 1.0 tapped holes, (figure 3.9.A2)

Company: Thorlabs

Catalog Number: AB90A/M

Weight: 0.07 Kg

Dimensions: 50.8 x 50.8 x 38.1



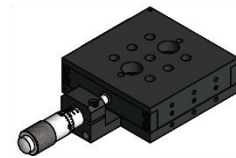
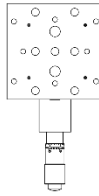
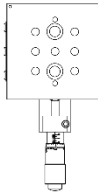
Part: 13 mm translation stage, (figure 3.9.A3)

Company: Thorlabs

Catalog Number: MT1/M

Weight: 0.20 Kg

Dimensions: 20.6 x 61.0 x 61.0



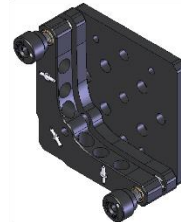
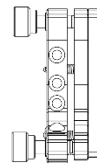
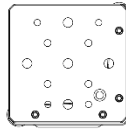
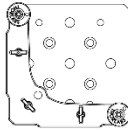
Part: Kinematic prism mount, (figure 3.9.A5)

Company: Thorlabs

Catalog Number: KM200B/M

Weight: 0.50 Kg

Dimensions: 44.4 x 76.5 x 76.5



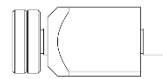
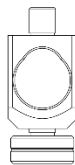
Part: Metric post end clamp, (figure 3.9.A7)

Company: Thorlabs

Catalog Number: RA180/M

Weight: 0.018 Kg

Dimensions: 15.7 x 35.7 x 15.7



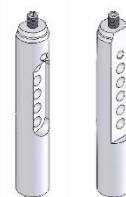
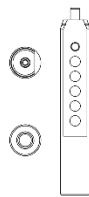
Part: 90° cored construction post, (figure 3.9.A8)

Company: Thorlabs

Catalog Number: TR75C/M

Weight: 0.05 Kg

Dimensions: 75 x 12.7 x 12.7



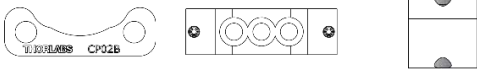

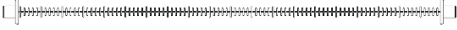

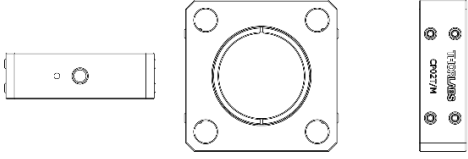

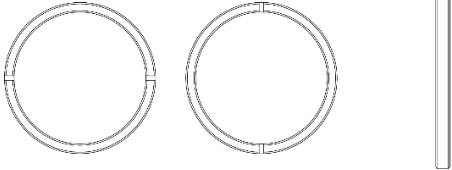

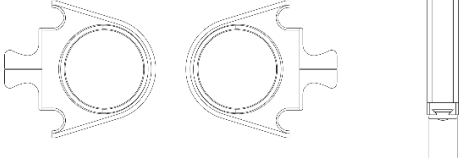

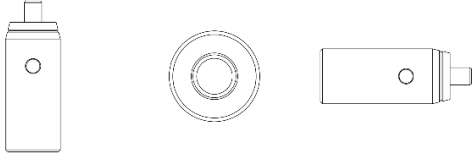

<p>Part: 30 mm cage mounting bracket Company: Thorlabs Catalog Number: CP02B Weight: 0.01 Kg Dimensions: 13.4 x 12.7 x 41.9</p>		
<p>Part: 100 mm extension rod engraved Company: Thorlabs Catalog Number: ER4E Weight: 0.02 Kg Dimensions: 101.6 x 6.0 x 6.0</p>		
<p>Part: Thick threaded 30 mm cage plate, (figure 3.9.A13) Company: Thorlabs Catalog Number: CP02T/M Weight: 0.03 Kg Dimensions: 40.6 x 40.6 x 12.7</p>		
<p>Part: 1.035-40 retaining ring (holds lenses inside the cage) Company: Thorlabs Catalog Number: SMIRR Weight: 0.0108 Kg Dimensions: 2.0 x 22.9 x 22.9</p>		
<p>Part: 16 mm cage quick release lens mount, (figure 3.9.A14) Company: Thorlabs Catalog Number: QRC1A Weight: 0.0045 Kg Dimensions: 40.1 x 58.4 x 7.6</p>		
<p>Part: Metric TRA-series post, (figure 3.9.A9) Company: Thorlabs Catalog Number: TRA30/M Weight: 0.01 Kg Dimensions: 30.0 x 12.7 x 12.7</p>		

Table 3.1. Detail view of the components used in the mounting system of the projection system. All images are acquired and adapted from Scientifica (for the mounting post) and Thorlabs company catalog (2017).

3.6. Brightness adjustment of the projection system

After exchanging the UV LED and building the mounting system, the next steps are to adjust the brightness level of the two LEDs and to calibrate the projector. This way we made sure that the output of the projector is linear and activates the mouse photoreceptors equally. In this section, we explain the approaches we chose to control the brightness of each LED. Since the main goal of our project is to study the integration of s- and m-cone signals, it is necessary that the brightness or the amount of the photons emitted from green and UV LEDs are similar. We were able to control the brightness level of the green and UV LEDs with two different ways. The first way was to use different color glass and neutral density filters. The second way was to control the amount of current sent to each LED with the accompanying software of the lightcrafter projector.

3.6.1 Brightness adjustment with different filters

One of the challenges that we faced in choosing the UV LED was that most of the commercially available UV LEDs that match the dimensions of the lightcrafter light engine were relatively dimmer than the original LEDs of the projector. Besides, the green LED of the lightcrafter was the brightest LED among the three LEDs of the projector. This difference in the brightness level was to a degree that we could not correct them with lightcrafter software. In other words, the minimum brightness level of the green LED was still more than 10 fold brighter than the maximum brightness of the UV LED. To overcome this issue, we used a special band-pass colored glass filter called UG-5 from Schott Company. This filter has a unique transmittance (figure 3.9.A). It allows nearly 90% of UV light (300 to 380 nm) to pass but only 1-5% of the green light. UG-5 filter blocks the majority of the input green light while most of the UV light could pass through. As a result, it balances the brightness of the green and UV LEDs. As part of this project we wanted to do the experiments at lower photopic and mesopic light levels. After measuring the brightness of the two LEDs with only UG-5 filter in the light path, we found that both LEDs were still very bright and they would bleach the photoreceptors very fast in the experiment. To dim down both LEDs, we used two different neutral density filters. One is a reflective UV-fusing neutral density filter with optical density of 1.0 (10% transmittance, figure 3.9.C) and the other one is an absorptive neutral density filter with optical density of 0.4 to 0.6 (40% and 25% transmittance, respectively, figure 3.9.B). We used these two different types of neutral density filters because most UV-fusing filters are reflective which means they reflect back most of the input light to the DMD. This may cause distortion in the output image of the projector. To avoid this issue, we chose an UV-fusing filter with very low reflectance (figure 3.9.C) and the other filter to be absorptive and non-UV fusing (figure 3.9.B). We had two reasons to choose an absorptive non-UV-fusing filter. The first was to slightly dim down the UV light, because the UG-5 filter makes the UV light slightly brighter than the green light. The absorptive neutral density filter can compensate for this difference by balancing the green and UV light by allowing 5-10% UV light vs 25-40% of the green light to pass.. The second reason to have one absorptive filter was to put this filter before the reflective

filter to block most of the reflected light from the reflective filter. In addition to the previous filters, we used another temperature balancing filter, because the UG-5 filter transmittance after 650 nm starts to rise from 5% to nearly 80% (figure 3.9.A 650 to 1000 nm region). A small part of the green LED's spectrum is extended beyond 650 nm. As a result, the output of the green LED after the UG-5 filter has two peaks, one around 500 nm and another one around 680 nm. To block the second artificial peak that is caused by UG-5 filter we used temperature-balancing filter that allows 60 to 80% transmission from 250 to 600 nm and blocks most of the light from 600 to 1000 nm (figure 3.9.D). We chose the temperature-balancing filter from Thorlabs with -132 mireds with 25 mm diameter. We arranged these filters in the following order inside the lens-cage system between the first and second lenses:

1. UG-5 colored glass bandpass filter (Edmund optics– catalog number: 84897)
2. UV-near IR neutral density filter, OD 1.0 (Edmund optics– catalog number: 88272)
3. Absorptive neutral density filter, OD 0.6/0.4 (Edmund optics– catalog number: 46214)
4. Temperature-balancing filter, -132 mireds (Thorlabs– catalog number: FGT165).

It is important to mention that we used these filters to optimize the projector for our experiments in the lower photopic light level. For our experiments in the mesopic light level, we used another reflective UV-fusing neutral density filter with 0.3/0.4 optical density to reduce the brightness to the mesopic light level.

3.6.2 Brightness adjustment through the software

To have precise control over the brightness of each LED in the lower photopic light level, we adjusted the forward current of each LED with the software of the lightcrafter projector. This is to ensure that the isomerization rates of the s- and m-cones were similar. The values for the photopic light level are as follow:

1. UV LED input current at photopic light: 250 μ A (value 105 in the software (1- 274 range))
2. Green LED input current at photopic light: 150 μ A (value 85 in the software (1-274 range))

These values are optimized to generate cone-isolating stimuli. For a cone-isolating stimulus, what matters is the isomerization ratio between the s- and m-opsins. Therefore, it is important to have constant and precise control over the brightness of green and UV lights. We describe cone-isolating stimuli and its relevance in this project in the following sections.

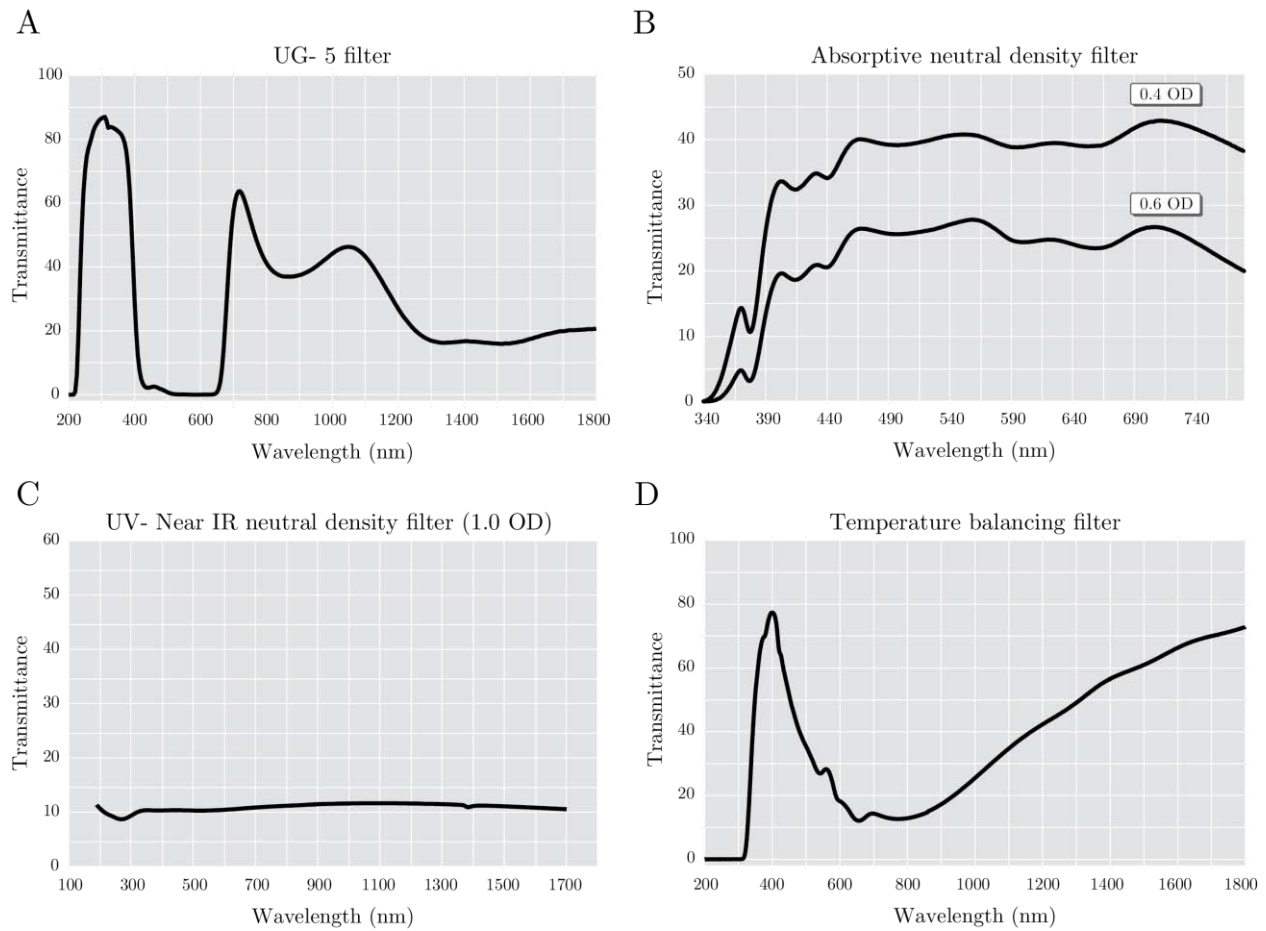


Figure 3.8. Transmittance of the filters used in the lens system of the projection system. A. Transmittance of the UG-5 colored glass bandpass filter. This filter allows nearly 90% of the UV light to pass while only 5% of green light. This is the main filter we used to balance the brightness of the dimmer UV LED and brighter green LED. B. Transmittance of the absorptive neutral density filter. For one projector a filter with OD 0.4 was used and for the second projector a filter with OD 0.6. This is due to slight manufacture variances of the UV LEDs. C. Transmittance of the second neutral density filter. This filter is UV-fusing and partially reflective. The reflected light from this filter is attenuated with the absorptive filter that was placed on top of it inside the lens system. This is to reduce image distortion and chromatic imbalance. The optical density of this filter is 1.0 and only 10% of the input light passes through it. D. Transmittance of the temperature-balancing filter. This filter was used to reduce the output of UG-5 filter for wavelength of 600 to 1000 nm. This filter narrows the spectrum of the green LED and limits to a region close to 500 nm. All the images and data are acquired and adapted from the Edmund Optics lens catalog (2017).

3.7. Calibration and gamma correction of lightcrafter projector

After adjusting the brightness level of the two LEDs, the next step was to calibrate the projector and do gamma-correction for each LED. This step was necessary to make sure that the output of the projector is linear for each color. For most conventional projectors, the light output is an exponential

function with power or gamma value close to 2.2. This is because the humans perceive light and color in a nonlinear manner. Therefore, the projector producing companies adjust the output of their projectors to be nonlinear. This way the output images are more pleasant for the human vision (Poynton, 2003). For experiments with visual system, it is necessary to correct the output function of the projector with an inverse exponential function to get a linear output. To gamma-correct the lightcrafter projector, first we measured the output of each LED with a photodiode (PDA- 750 Photodiode Amplifier, Terahertz Technologies Inc.). Since in our stimulus-generating computer of our lab we used an 8-bit graphic card, we generated 256 steps of brightness from black to maximum brightness of the green and UV LEDs. Then, we measured the amount of photons released at each brightness level with the photodiode (figure 3.10.A, left, gamma function). From this measurement, we made a look-up table that correctly translates the digital values sent from the stimulation program into new values that effectively compensate for the particular characteristics of the lightcrafter projector (figure 3.10.A, middle, inverted gamma function). This way we made sure that the output of the projector for each color is linear (figure 3.10.A, right, corrected gamma function). One of the surprises we had during the calibration was that the lightcrafter projector, unlike many conventional projection systems, cannot generate 256 shades of each color at 60 Hz refresh rate. In other words, the output of the projector was not an exponential function that is found in many commercial projectors and monitors, but a step-wise nonlinear function (figure 3.10.A). After conferring this issue with Texas Instruments, we were notified that this is one of the limitation of the lightcrafter projector. Because the driver board of the projector requires a minimum of 8.33 ms to display a true 8-bit color and for three LEDs (RGB) 8x3 (24 bits) around 25 ms is needed. Since the lightcrafter projector operates at 60 Hz (16.67 ms), the duration between two frames is not enough to display the three colors. Thus, an internal algorithm from the FPGA (field-programmable gate array, an integrated circuit of the projector designed to control the output of the lightcrafter projector) of the projector, reduces the output steps from 256 steps to nearly 130 steps to compensate for the time that is required to display the three colors.

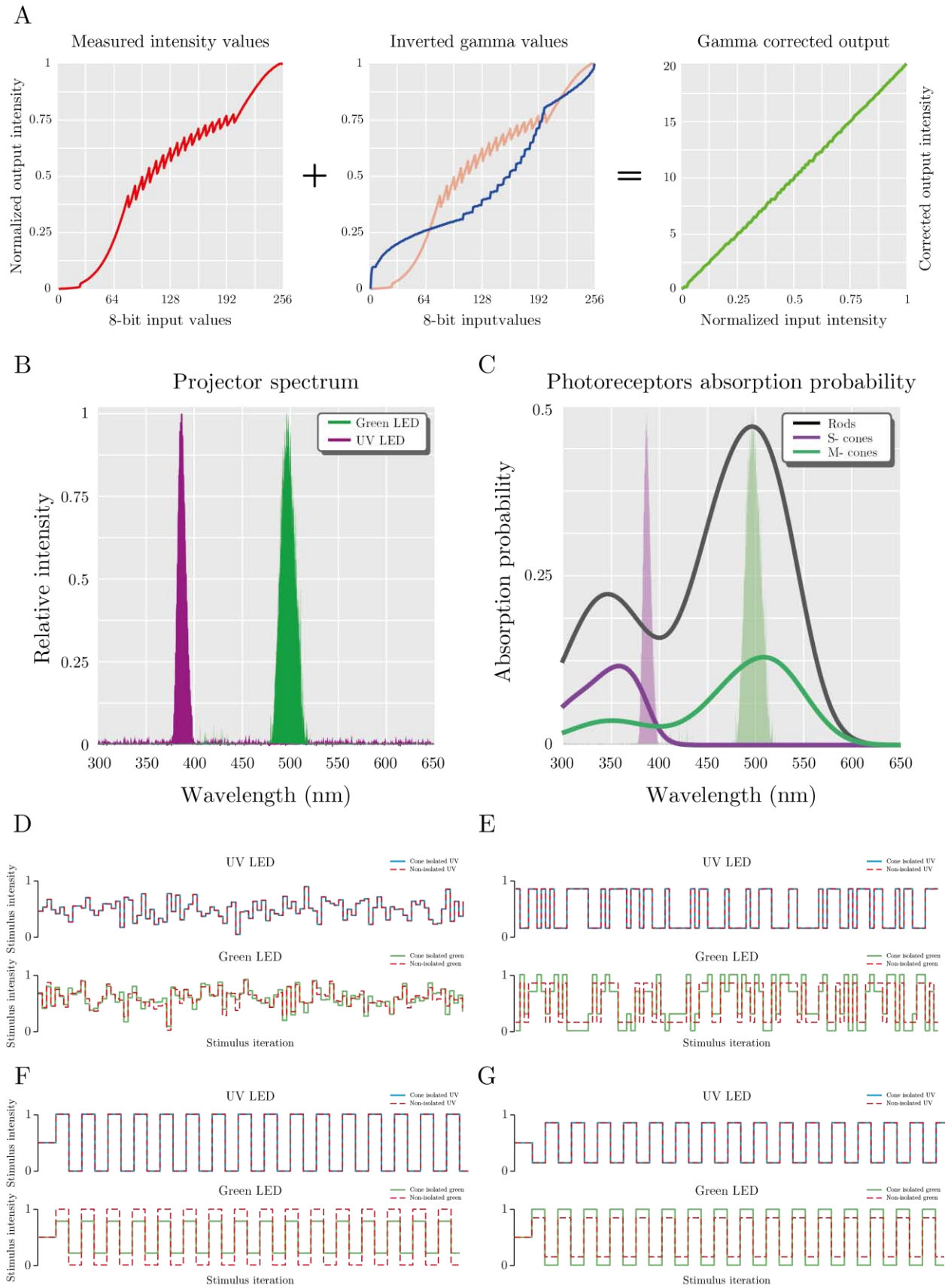


Figure 3.9. Gamma correction of the lightcrafter projector and examples of cone-isolated stimuli. A. First plot shows the output of the lightcrafter projector measured with a photodiode. The peculiar shape of this curve is due to internal optimizing mechanisms of the lightcrafter projector. The second plot shows the inverted gamma-table calculated in a way to compensate the fluctuation and nonlinearities of the output function. The right plot is the measured output of the lightcrafter projector after gamma correction. B. Output spectrum of the projection system measure with a spectrometer. The peak spectrum of the UV LED is at 380 nm and the peak spectrum of green LED is at 500 nm. C. The absorption probability of the mouse photoreceptors. The s-cone's sensitivity peak is close to 360 nm and m-cone sensitivity is close to 504 nm. The output spectrum of the projector is depicted in the background. As it is shown, the UV LED activates both s- and m-cones. However, the green LED is only activating m-cones with little to no effect on s-cones. To solve the problem of the UV LED, the difference in the activation is corrected with the method of silent substitution. D- G. Simulation of different cone-isolated stimuli to show how the contrast of green LED is corrected so that the overall isomerization of m- opsin stays constant. The simulations show the contrast changes of the stimuli: spatially uniform flickering stimulus (D), spatio-temporal flickering stimulus (E), on-off steps with contrast changes in the same phase for green and UV lights (F) and on-off steps with alternating contrast of green and UV lights (G).

As a result, the lightcrafter projector can produce around 130 different brightness steps of each color. This contrast resolution is reliable for our experiments because it is below 1% contrast difference and not far from the smallest contrast differences that can be generated by an 8-bit graphic card. However, this algorithm adds more nonlinearity and complexity to the output of the projector.

To rectify the nonlinearities caused by the FPGA algorithm (figure 3.10.A, indentation of the middle section), we developed a new algorithm that compensated the FPGA algorithm. What this new algorithm does, is to find whether the digital output value is a real value that is emitted by the projector or is a value that is corrected by the projector's FPGA algorithm. If the digital output from the stimulation program is not the real output of the projector and it is corrected by FPGA, our algorithm would find the closest real value that the projector can create and use this value as the output instead. The comparison between the real and the FPGA-corrected values is done based on the look-up table from the gamma correction (figure 3.10.A middle plot). After using this algorithm and gamma correction the output of the projection system is approximately linear (figure 3.10.A, right plot).

3.8. Isomerization and cone-isolation

3.8.1. Isomerization

After calibration and gamma correction, the output of the projection system was approximately linear. The final step before the experiment was to see how the green and UV LEDs of the projector drive

the s- and m-cones of the mouse retina. This means to calculate the isomerization rate of the s- and m- opsins and rhodopsin for either UV, green or combination of the green and UV light. We measured the intensity of each LED per area with a photodiode and the output spectrums of the two LEDs (figure 3.10.B). To do this, we positioned the photodiode in the focal plane of the projector. We then showed a stimulus that starts from lowest intensity of each LED and gradually increased its brightness to the maximum brightness in 256 steps. We measured the energy that was emitted from each LED at each brightness level with the photodiode. Next, we used a stimulus, which had a small square with maximum brightness over the black background. The square in this stimulus increased its area in some steps until it fits the whole screen. We measured the energy emitted by each LED per area, with this stimulus. Afterwards, we put a spectrometer in the focal plane of the projector and measured the spectrum of each LED. Therefore, for each LED we measured the intensity at different brightness levels, the intensity per area and its spectrum. From these measurements, we calculated the irradiance of the projector and from that, we calculated the isomerization rates of mouse opsins. We used the isomerization modules of the Psychophysics toolbox (Brainard, 1997; Govardovskii et al., 2000) that has measured values of absorption probability of each photoreceptor (figure 3.10.C). The measured isomerization values for photopic light level for both LEDs are as follows:

	Wavelength peak (nm)	UV LED (R*/s-cone/s)	Green LED (R*/m-cone/s)	UV&Green LEDs (R*/s & m-cone/s)
m-cone	508	962.9	2387	3234
s-cone	360	2071	3.28	2170
rod	496	7561	12080	19184

Table 3.2. Isomerization values for s-cone, m-cone and rod photoreceptors caused by green and UV LEDs of the projection system.

Here, the values show the number of photoreceptors opsins that are being isomerized per second (R*/s) for each LED. The rhodopsin isomerization values are used to separate the photopic light level from the mesopic and the scotopic. Previous studies showed that the rod saturation begins when the illumination is larger than 5000 (R*/rod/s) (Hood and Finkelstein, 1986; Farrow et al., 2013). Here, the UV and the green LEDs can saturate the rods adequately. The cone isomerization values were used to generate cone-isolating stimuli for our experiments.

3.8.2. Cone-isolation

The main objective of our project is to study how different signals from s- and m-cone photoreceptors are integrated by mouse retinal ganglion cells. To approach this objective it is necessary that we stimulate s-cones and m-cones independently. However, the spectral sensitivity of s- and m-cones of

mouse has a considerable overlap. This overlap is mainly between 380 to 450 nm (figure 3.10.C). This means that a stimulus generated only with the UV LED (peak spectrum at 380 nm), could still co-activate the m-cones effectively. It is indeed challenging to use a UV output from the projector that has its peak spectrum similar to the mouse s-cone with little to no effect on the m-cones (figure 3.10.C, purple line). This is due to the technical limitations such as internal glass components of the light engine.

To solve this problem, we used the method of silent substitution (Estevez and Spekreijse, 1982) to generate cone-isolating stimuli in all our experiments. The idea behind the silent substitution is to compensate for the UV light-induced co-activation of the m-opsins with changes in the brightness of the green LED. To do this compensation all the stimuli should be defined as relative contrast from the mean level of brightness that has both green and UV light. When a stimulus has positive contrast of the UV light (increase in brightness compare to background) there is an increase for UV photons compared to what was emitted at background light level and at the same time, some green light photons that are being emitted in the background. What silent substitution does is to measure how much the UV photons excite m-opsins and reduce this amount of photons from the one emitted from the green LED by making green LED dimmer. In other words, an increase in UV brightness is accompanying by a decrease in green brightness in a way that the isomerization of the m-opsin would be the same as the background light. Similarly, a decrease in the UV light contrast is compensated with an increase in the green contrast. The compensation ratio comes directly from the measured isomerization values. As it is shown in the table 3.2, the UV light can co-activate the m-opsin up to 30% while the green light has little to no effect on the s-opsin. Figure 3.10.C shows the spectral sensitivity curve of the mouse retina for s-, m-cones and rods where one can see the overlap between the s-cone and m-cones around 380 nm where it is the peak of UV LED. Similar to gamma correction, we implemented an algorithm that generates the cone-isolating stimulus by correcting the changes in brightness of green and UV LEDs automatically. The core of this algorithm is a simple arithmetic operation to correct the output brightness value of the LEDs based on the isomerization ratio of s- and m-cones. To ensure that this algorithm generates cone-isolated stimuli we did a series of simulations of the stimuli that we planned to use in our experiments. In these simulations, we gave the contrast values that we wanted to display as an input to the algorithm and then checked for the output of it. As shown in figure 3.10.D-G regardless of the stimulus design the algorithm can adjust the brightness of green LED along with changes in the UV LED's output.

4.

Linear & nonlinear chromatic integration in the mouse retina

The aim of this study is to investigate properties of chromatic signal integration in the mouse retina. In the previous chapters, we introduced the main experimental and computational methods that we used in this study. In this chapter, we address the question of chromatic signal integration in detail, from the design of the stimulus to the analysis of the data acquired from our experiments. We measured responses of isolated mouse retina using multi-electrode arrays recording while stimulating the retina with a series of stimuli that have different chromatic (UV vs green) contrast. We used a new stimulation approach that let us investigate whether the mouse ganglion cells integrate their chromatic input linearly or nonlinearly. We found that a majority of the ganglion cells integrate their chromatic inputs linearly while a certain population of ganglion cells encodes chromatic stimuli nonlinearly. We then classified the ganglion cells based on their chromatic integration properties. Further, we focused on the features of each ganglion cell class and investigated the different properties both chromatically linear and nonlinear cells.

4.1. Chromatic integration stimulus

The mouse has a dichromatic retina with two types of cone photoreceptors, which makes it a suitable model to study chromatic signal integration. To study chromatic integration, it is necessary to use a

stimulus that drives both s-cones (UV sensitive) and m-cones (green sensitive), effectively. Therefore, we developed a new projection system (chapter 3) that allowed us to display different contrast combinations of both green and UV lights. With the option of stimulating both s- and m-cones, we were ready to tackle the challenge of chromatic integration. We started this quest by asking the question whether mouse retinal ganglion cells integrate their chromatic inputs linearly or nonlinearly. For a linear chromatic integration, we hypothesized that a stimulus, which has an increase in UV contrast (UV-on stimulus), can be counter-acted by a simultaneous green stimulus with opposing contrast (green-off stimulus). This combination of opposing contrasts would reduce the ganglion cell's firing rate to the baseline activity. For a nonlinear chromatic integration, however, there is no combinations of green and UV stimuli with opposing contrasts that leads to the baseline activity. To test these assumptions, we designed a stimulus that is composed of 22 steps of combinations of green and UV contrasts always with opposite polarity (On vs Off).

Since this stimulus is designed to probe the question of chromatic integration, for the rest of the text, we use the term chromatic integration stimulus to describe this stimulus (figure 4.1). We used 11 different contrasts for both green and UV light that were assigned to two sets:

1. The first stimulus set is a green-on, UV-off stimulus. This stimulus starts by presenting green-on with 20% positive green contrast and 0% UV contrast. In the next step, 18% of green contrast is presented simultaneously with -2% of UV contrast. In every steps of this stimulus set, the green-on contrast is reduced by 2% and at the same time, the contrast of the UV-off stimulus is reduced by 2% contrast. This reduction in contrast continues until the green-on contrast reaches 0% and the UV-off reaches -20% contrast (figure 4.1.B pink border).
2. The second stimulus set is a green-off, UV-on stimulus. This is the opposite of the green-on, UV-off stimulus set. Here the starting contrasts are -20% of green (off) and 0% of UV (on) that goes up to 0% green and 20% UV with 2% increase in contrast per step (figure 4.1.B blue border).

Taken together, the chromatic integration stimulus consists of 22 steps that expand from -20% to 20% contrasts of green and UV light. At each step of this stimulus, one combination of the UV-green contrasts (for example -12% green-off with 8% UV-on) is presented for 500 milliseconds. After each presentation, a background light with 0% contrast of green and UV light is shown for 2 seconds (figure 4.1.C).

The order of the color integration stimulus was selected randomly to avoid any adaptation effects. For each retina piece around 50- 60 trials of each step of the color integration stimulus were presented to provide strong statistical information about the ganglion cells responses. It is worth mentioning that we presented the chromatic integration stimulus as a full-field stimulus without any spatial structure (figure 4.1.A). This was done to avoid potential nonlinearities that might be caused by the nonlinear spatial features of some mouse ganglion cells (Enroth-Cugell and Robson, 1966; Schwartz et al., 2012).

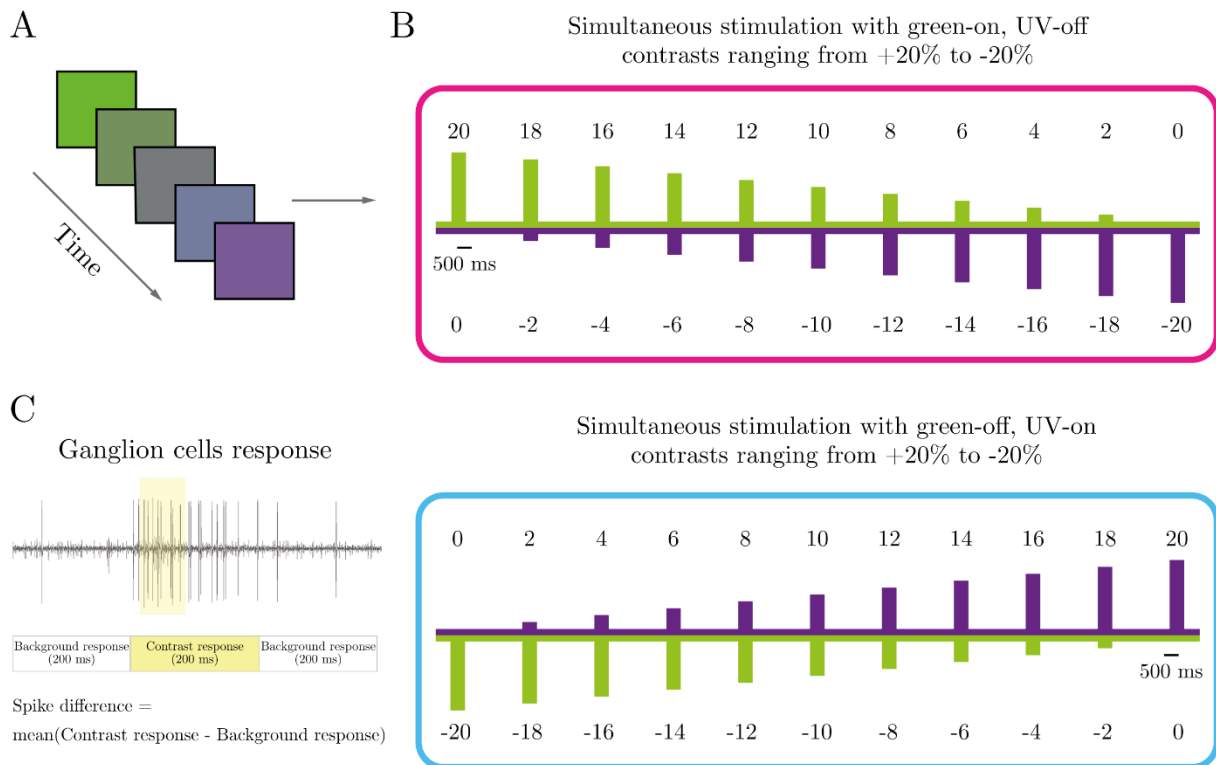


Figure 4.1. Schematic view of the chromatic integration stimulus. This is a full-field stimulus (A) that consists of 22 contrast steps that are presented in two sets. The first set is green-on, UV-off (B- pink border) and the second set is green-off, UV-on (B- blue border). Each step has a combination of green and UV contrast that are presented with opposing contrast for the duration of 500 ms. Between the stimulation steps the background stimulus (mean intensity of green and UV light) is presented for 2 seconds. For analyzing the responses of the retinal ganglion cells to this stimulus, we measured the difference between the responses of each cell in the time window of 50- 250 ms after the onset of the stimulus (contrast response in C) and the 200 ms preceding the stimulus (background response in C).

4.2. Analysis of chromatic integration stimulus

We analyzed the chromatic integration stimulus based on the premise of finding a combination of contrasts that leads to the baseline activity for each ganglion cell. If this premise holds for a ganglion cell, it is an evidence of linear chromatic integration because one color (e.g. UV) contrast is cancelled out by the other color contrast (e.g. green) with opposite polarity (On vs Off). Therefore, in our analysis, if we found a cancellation point for a ganglion cell, we considered that ganglion cell to be chromatically linear. If no cancellation point was found, it indicates nonlinear chromatic integration.

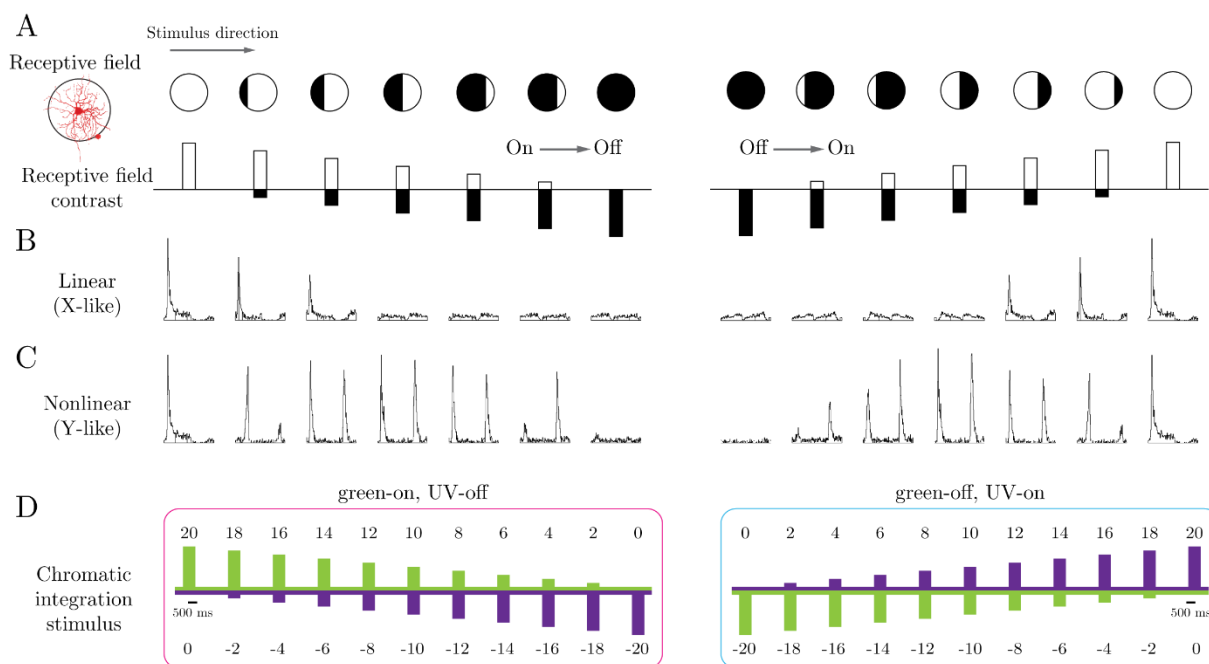


Figure 4.2. Chromatic integration stimulus was designed based on the classical stimulus that was used to study spatial integration in the retina. A. Schematic illustration of the grating stimulus with alternating contrast that covers the receptive field center with different black and white ratio. Below is the schematic representation of the contrast that covers the receptive field. B. Illustration of the response of an X cell. This cell does not respond when opposing contrasts cover the receptive field. Therefore, this cell integrates its spatial stimulus linearly. C. illustration of the response of a Y cell. Unlike the X cell, this cell responds to every combination of On and Off stimuli in the receptive field. D. Chromatic integration stimulus was designed based on the premise of the stimulus that was used to study spatial integration. The outline of our analysis was also inspired by the analysis that was used to find the X and Y cells. The image of the ganglion cell in A was kindly provided by Helene Schreyer.

The design of the chromatic integration stimulus here and the outline of our analysis were inspired from classical studies of the spatial integration in the cat retina (Enroth-Cugell and Robson, 1966, 1984). In these studies, a spatial grating stimulus with alternating contrast was shown to the retina and the responses of the ganglion cells were recorded (chapter 1.4 and figure 1.3).

This measurement was repeated for different spatial phase of the grating in a way that different regions of black and white cover the receptive field (figure 4.2.A). Based on the recorded responses, the ganglion cells were categorized into X and Y cells. The X cells did not respond when both black and white parts of the grating covered the receptive field. The Y cells, on the other hand responded to different combinations of black and white contrasts that covered the receptive field. Figure 4.2.A is an illustration of the stimulus that was used to study spatial integration over the receptive field at different phases. For X- and Y-cells, the responses are depicted below (B and C). As shown in part D, the outline of the chromatic integration stimulus that we used in this project is analogous the stimulus that was used for studying spatial integration. Similarly, our analysis about the linearity and

nonlinearity of chromatic integration is inspired by the analysis of spatial integration. For the chromatically linear cells, similar to X-cells, we speculate to find a contrast combination (e.g. 12% green, -8% UV) and its inverted combination (-12% green, 8% UV) to cause no change in the cell's activity from the baseline (cancellation point). For the nonlinear cells, similar to Y-cells, we speculate that the ganglion cell would respond to a stimulus with specific contrast of green and UV, and the inverse of the same stimulus with opposing UV and green contrasts.

In the following section, we first explain how we measured the cancellation point for each ganglion cell and then we describe two additional measurements (polarity and rectification) that we computed from the chromatic integration stimulus.

First: The cancellation point

In this study, we used the cancellation point as the measure for linearity vs nonlinearity of the chromatic integration. To find the cancellation point, we measured the spiking activity of each ganglion cell in response to the chromatic integration stimulus. We constructed 22 PSTHs, one for each contrast combination (see methods). For each PSTH we took the average activity of the cell during the time window of 50-250 ms after the onset of the stimulus and subtracted this value from the average of the 200 ms spontaneous activity before the stimulus. We measured 22 values and grouped these values into two sets: (1) green-on, UV-off and (2) green-off, UV-on. To compare these opposing contrasts, we plotted these two groups of responses with separate curves as shown in the figure 4.3.

What information can we get from the chromatic integration curves shown in figure 4.3? The first important point is the crossing point of the green-on, UV-off (figure 4.3. pink curve) and green-off, UV-on (figure 4.3. blue curve) curves. This crossing point shows the two combinations of contrast that are equally effective. For example, if the crossing point for a ganglion cell is at 16%, -4% contrast, it means that this cell responds in the same way to 16% green, -4% UV and -16% green, 4% UV contrasts. Now if the crossing point is very close to zero it shows the combination of opposing contrast that cancel each other out. We considered this cancellation point (crossing point close to zero) as the sign for linear chromatic integration (figure 4.3.A- center raster and PSTH plots). Since we subtracted the contrast responses from the background activity, the point zero of the chromatic integration curves is an indicator of baseline (spontaneous) activity. If, on the other hand, the crossing point is away from zero, it shows nonlinear chromatic integration.

Second: Polarity of the responses

In addition to the crossing and possible cancellation point, we defined the polarity of the ganglion cell's responses from the chromatic integration curves (see methods). On cells respond strongly to green On and UV On contrasts of the stimulus and Off cells to both Off contrasts while On-Off cells respond to On and Off contrasts.

Third: Rectification of the non-preferred stimulus

Beside chromatic integration features and the polarity (On, Off and On-Off), we looked at how each ganglion cell encode the non-preferred contrast and we asked whether each cell rectifies its inputs or not (see methods). For a rectifying cell, the non-preferred stimulus does not elicit any responses. For example, if we stimulate an Off rectifying ganglion cell with a bright spot of light or an On stimulus, we will not see any differences in the activity of the ganglion cell from the baseline. This is because the ganglion cell has a thresholding output function so that the non-preferred stimuli are rectified. However, for a non-rectifying ganglion cell the non-preferred stimuli will cause the cell to reduce its firing rate below the spontaneous activity. Since in the analysis of chromatic integration responses, we compared the stimuli driven responses to the spontaneous activity of the cells, we can analyze rectification properties of the ganglion cells.

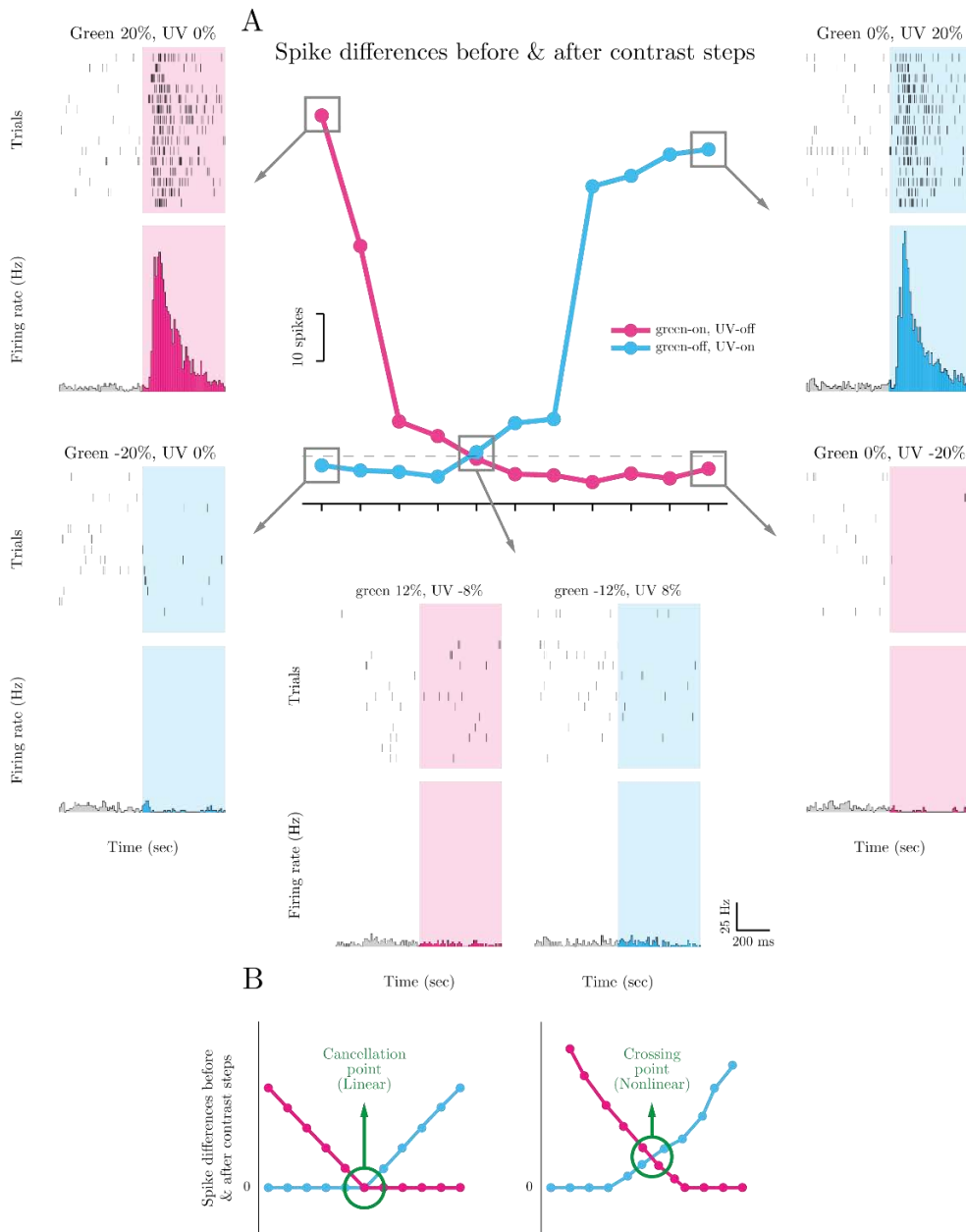


Figure 4.3. Chromatic integration responses and its analysis. A. The chromatic integration curves in the center show the response of a ganglion cell to the different contrasts of green-on, UV-off (in pink) and green-off, UV-on stimuli (in blue). As shown in the side raster and PSTH plots, this cell responds strongly to green and UV On stimuli (two upper PSTHs) while it does not respond to the Off stimulus (two lower PSTHs). The center panel shows the response of the cell at the crossing point of the two chromatic integration curves. At this crossing point, the cell's response has no difference from the background. Therefore, the two opposing contrasts cancel each other out. This is because this cell integrate chromatic signals in a linear fashion. B. schematic view of the analysis of chromatic integration stimulus. If the crossing point of the two curves is close to zero, it is an evidence for linear integration while a crossing point that is away from zero indicates nonlinear chromatic integration.

Taken together, for each recorded retinal ganglion cell, we calculated chromatic integration function based on their responses to the chromatic integration stimulus and their baseline activity. From the

chromatic integration function of each ganglion cell, we defined first, whether each cell integrates chromatic stimuli linearly or nonlinearly. Second, we defined the response polarity for each ganglion cell (On, Off or On-Off). Last, we defined whether the cell rectifies the non-preferred stimuli or not. From these criteria, we were able to classify the recorded ganglion cells into different chromatic integration groups. In following sections, we first focus on the diversity of the responses (4.4) and then we classify the ganglion cells based on their chromatic integration features (4.5).

4.3. Diversity of chromatic signal integration among retinal ganglion cells

We recorded 543 retinal ganglion cells from 12 retinas of adult mice. We stimulated these cells with the chromatic integration stimulus and recorded their response to this stimulus. Based on the responses to the chromatic integration stimulus we found different response types among the recorded retinal ganglion cells. For each response type, we checked whether a ganglion cell is chromatically linear or nonlinear, whether it is On or Off or On-Off ganglion cell and whether it rectifies the stimulus contrast or not.

4.3.1. Chromatically linear ganglion cells

After analyzing the responses of the recorded ganglion cells to the chromatic integration stimulus, we found ganglion cells that showed linear chromatic integration. All these linear cells had a cancellation point in their response, which means, that the activation elicited by the s-cone input was balanced with the activation induced by the opposing m-cone input. The way these linear cells integrate green and UV colors is similar to how X-cells in the cat retina and X-like cells in other animals integrate spatially heterogeneous stimulus (Enroth-Cugell and Robson, 1966; Caldwell and Daw, 1978; de Monasterio, 1978; Demb et al., 1999).

We investigated these linear cells by looking at the other features of the chromatic integration curves (see section 4.2). The first distinctive feature was the response polarity. This feature separates the ganglion cells into On, Off and On-Off groups. The second feature we checked was the rectification property. Based on this feature we found both rectifying and non-rectifying cells. Figure 4.4 shows a typical example of a linear ganglion cell. For this cell both 12% green, -8% UV and -12% green, 8% UV stimulus elicit no responses different from the baseline activity. In other words, for each of these two stimuli, the response that is induced by one color was cancelled out by the other opposing color (e.g. 12% green cancels out -8% UV) (figure 4.4.B). Furthermore, by looking at the responses to the first and the last stimulus it becomes clear that this example ganglion cell prefers Off contrasts. Therefore, it is considered as an Off ganglion cell. We then looked at the non-preferred stimulus (on stimulus in this case) and observed little to no change in the ganglion cell responses compared to its baseline activity. This means that this cell rectifies the On stimulus. Taken together, based on the

chromatic integration, response polarity and rectification features, we labeled this cell as an Off linear rectifying ganglion cell. Similar to the Off linear rectifying cells in our population, we found On linear rectifying ganglion cells (figure 4.9.B). Moreover, we found On-Off linear cells (4.9.E) that showed similar chromatic integration properties but with On-Off response polarity. As mentioned before, the On-Off cells do not have rectification since they respond to both On and Off part of the stimulus.

In addition to the linear rectifying cells, we found that a certain number of linear ganglion cells were not rectifying the non-preferred contrast. These cells instead suppress their activity below their spontaneous firing rate. Figure 4.5 shows an example of such a linear ganglion cell that showed suppressed output. Since this cell has a cancellation point at 12% green, -8% UV and -12% green, 8% UV stimulus combinations, it is chromatically linear. What set this cell apart from the previous example is how it responds to the non-preferred (in this example Off stimulus) contrast (figure 4.5 A&B). Since these cells suppress their activity for the non-preferred stimulus, they are therefore labeled as non-rectifying linear cells. Another feature of these linear non-rectifying cells, that further separates them from the linear rectifying cells, is their high spontaneous activity (compare 4.4.C and 4.5.C). It is possible that these linear non-rectifying cells need high level of spontaneous activity to achieve linear contrast (On vs Off) integration. For the linear non-rectifying cells, we found both Off and On linear cells among our recorded ganglion cells (figure 4.9.C and 4.9.D for examples of linear non-rectifying cells).

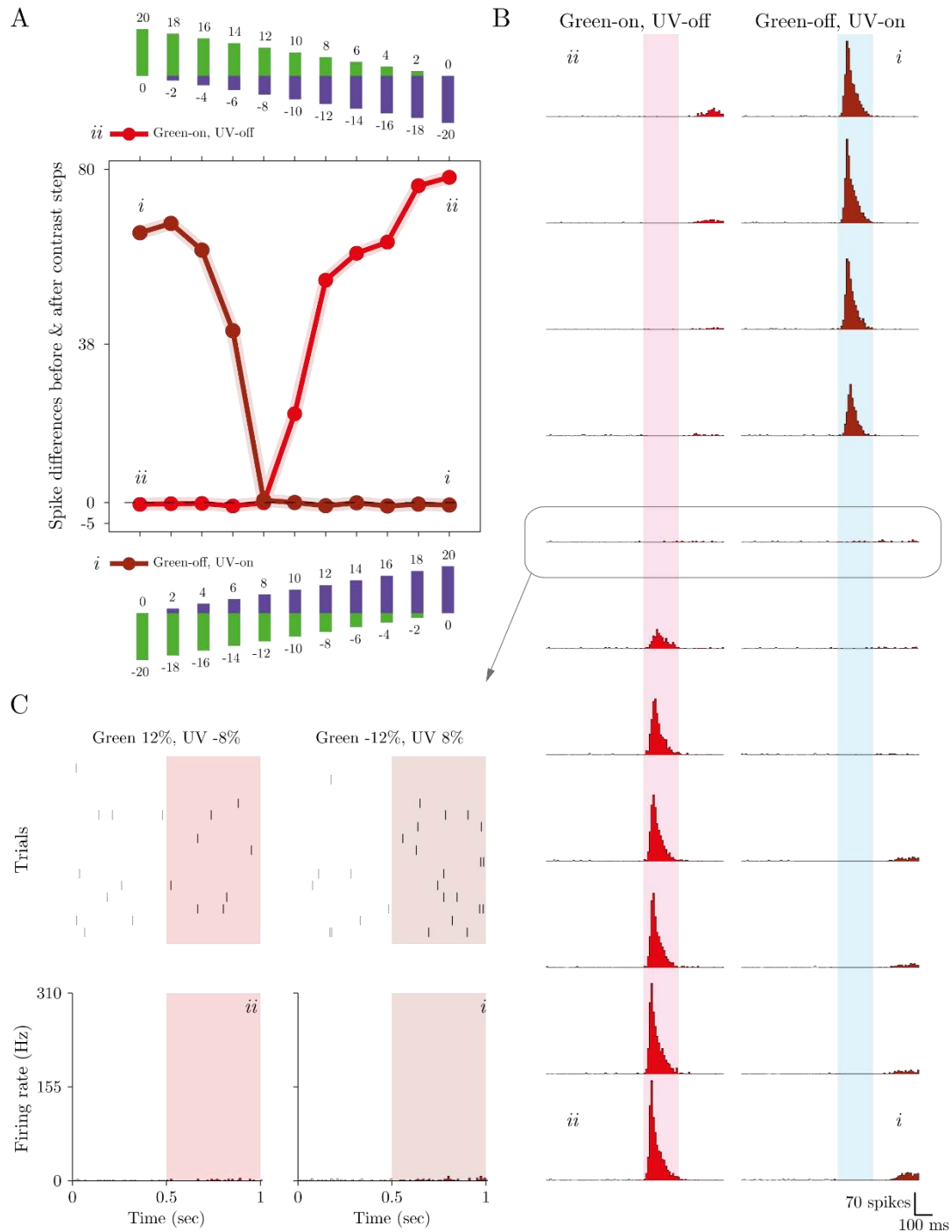


Figure 4.4. Response characteristics of a chromatically linear rectifying Off ganglion cell. A) Chromatic integration curves of an Off linear rectifying cell. For this cell, the crossing point is at zero that shows the linear nature of its chromatic integration. Shades around the data is \pm SEM. B) PSTHs of the responses of the ganglion cell to the chromatic integration stimulus. As shown here this cell has a clear preference for Off-green (top row, right) and Off-UV (bottom row, left). C) Raster plots and PSTHs of the crossing point. For this cell there is little to no response at the crossing point. Darker shades correspond to green-off, UV-on stimulus and lighter shades represent green-on, UV-off stimulus set.

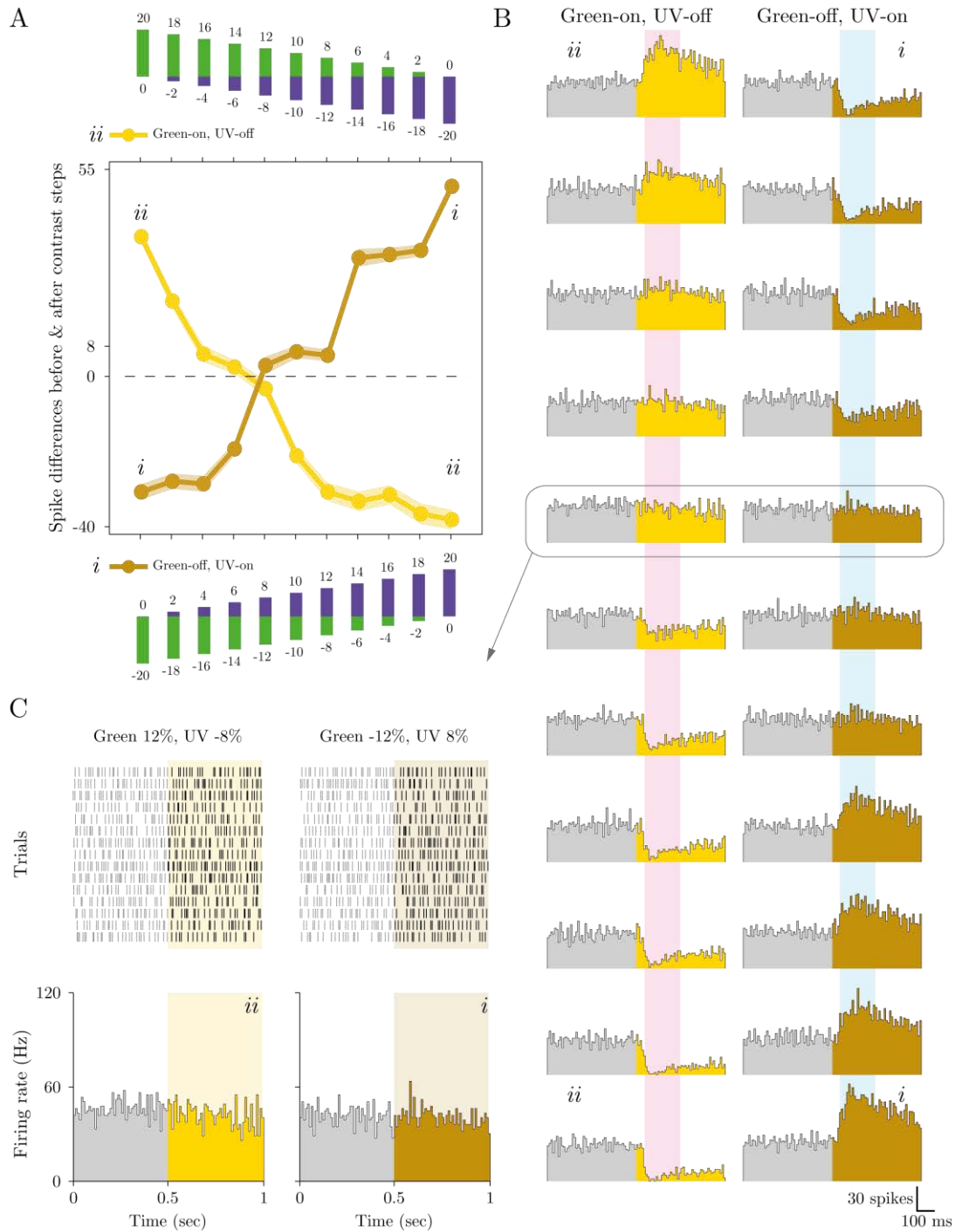


Figure 4.5. Response characteristics of chromatically linear, non-rectifying ganglion cell. A) The chromatic integration curves of this cell shows linear chromatic integration. B) PSTHs of the responses of the cell show its preference to On stimulus. What is unique for this cell is its response to the Off stimulus. For this cell, the non-preferred stimulus suppresses the activity of the cell below the spontaneous activity. C) Responses of the ganglion cell *ii* at the crossing point of chromatic integration curves. Due to the linear nature of the chromatic integration, the response of the cell at the cancellation point stays at the spontaneous level.

4.3.2. Chromatically nonlinear ganglion cells

Besides the chromatically linear cells, we found ganglion cells that responded to every contrast combinations of the chromatic integration stimulus. The hallmark of these cells is that they did not have any cancellation point. This means, that the activation elicited by the s-cone input cannot be counteracted by the activation induced from the opposing m-cone input. In other words, these ganglion cells integrate their s-cone inputs different from their m-cones. The chromatic integration characteristics of these nonlinear cells is similar to Y cells in the cat retina and Y-like cells in other animals, that integrate spatially heterogeneous stimulus nonlinearly (Enroth-Cugell and Robson, 1966; Caldwell and Daw, 1978; de Monasterio, 1978; Demb et al., 1999; Zaghloul et al., 2007). Based on the chromatic integration properties and the polarity of the ganglion cells we observed three different types of responses.

1. Off nonlinear ganglion cells: Figure 4.6.A shows the chromatic integration curve of an Off nonlinear cell. A look at the crossing point of the green-on, UV-off and green-off, UV-on curves shows that this cell responded to a combination of stimulus and its opposite (inverted) combination in a positive fashion. Thus, this cell had strong firing rate, even at the point, where the two opposing combinations of green and UV stimuli were equally effective (around 25 Hz more than the baseline, Figure 4.6 B & C). Therefore, this cell integrates its chromatic inputs nonlinearly and thus it has no cancellation point. Moreover, the response polarity of this cell shows that it is an Off ganglion cell and the non-preferred On stimulus suppress the activity. It is important to mention, that at the crossing point the firing rate of the cell is lower than at the preferred (off) corner stimulus. This is expected, because the crossing point has weaker preferred contrast (-6% or -14%) compared to the preferred corner contrast (-20%).
2. On-Off nonlinear ganglion cells: Figure 4.7 shows an example of On-Off nonlinear cell. This cell is similar to the Off nonlinear cell by showing strong spiking activity at the crossing point (figure 4.7.C and 4.6 C). However, unlike the Off nonlinear cell, this cell shows a peculiar response polarity to On and Off stimuli. A closer look at the PSTHs of the corner stimuli (figure 4.7.B top and bottom rows) shows the On-Off profile of this cell in response to UV-on and UV-off stimuli. Here, we see stronger responses to the green-off stimulus compared to the green-on stimulus. The potential reason for this unique asymmetry of the response could be the different sensitivity of this ganglion cell to green and UV stimulus. It is plausible that this cell is more sensitive to UV and as result, both UV-on and UV-off can elicit strong response. However, for the green, although the response to the green-off stimulus is robust, it is possible that the sensitivity to green-on stimulus is different from green-off. The effect of the asymmetry in the chromatic sensitivity can be seen at the location of the crossing point on the x-axis of the chromatic integration plot. For the On-Off nonlinear cell in figure 4.6, a high contrast of the green stimulus ($\pm 16\%$) was needed to compensate the $\pm 4\%$ of the UV contrast. This shows the high sensitivity of the On-Off nonlinear cell to the UV contrasts.

3. On nonlinear ganglion cells: One of the surprising findings we had was the lack of any On ganglion cell that had chromatically nonlinear characteristics similar to Off and On-Off nonlinear cells. In other words, our data was devoid of any On ganglion cell that had strong response at the crossing point of the green-on, UV-off and green-off, UV-on curves. However, we found a group of On ganglion cells that had a crossing point that is noticeably smaller than zero. This means that these On ganglion cells integrate their chromatic input nonlinearly but by suppressing instead of increasing their firing rate at the crossing point. As a result, when a set of equally effective stimuli with opposing colors (green vs UV) is shown to these cells, they suppress their activity to a level below their spontaneous activity. The magnitude of this suppression is different for identical opposing contrasts (e.g. -14% green, 6% UV and 14% green, -6% UV). Figure 4.8 shows the chromatic integration curves of such a chromatically nonlinear On ganglion cell. As shown in the panel 4.8.B, this cell has a crossing point that is noticeably below zero. A comparison of this cell's responses along the different contrast sets indicates that this cell is non-rectifying by showing suppression to the Off contrast. A pattern that we have seen with On, Off linear non-rectifying, and Off nonlinear cells. Finally, similar to linear non-rectifying cells, this ganglion cell has strong spontaneous activity. This high spontaneous activity could potentially play a role in the specific integration properties of this cell. We will discuss this observation in the following sections.

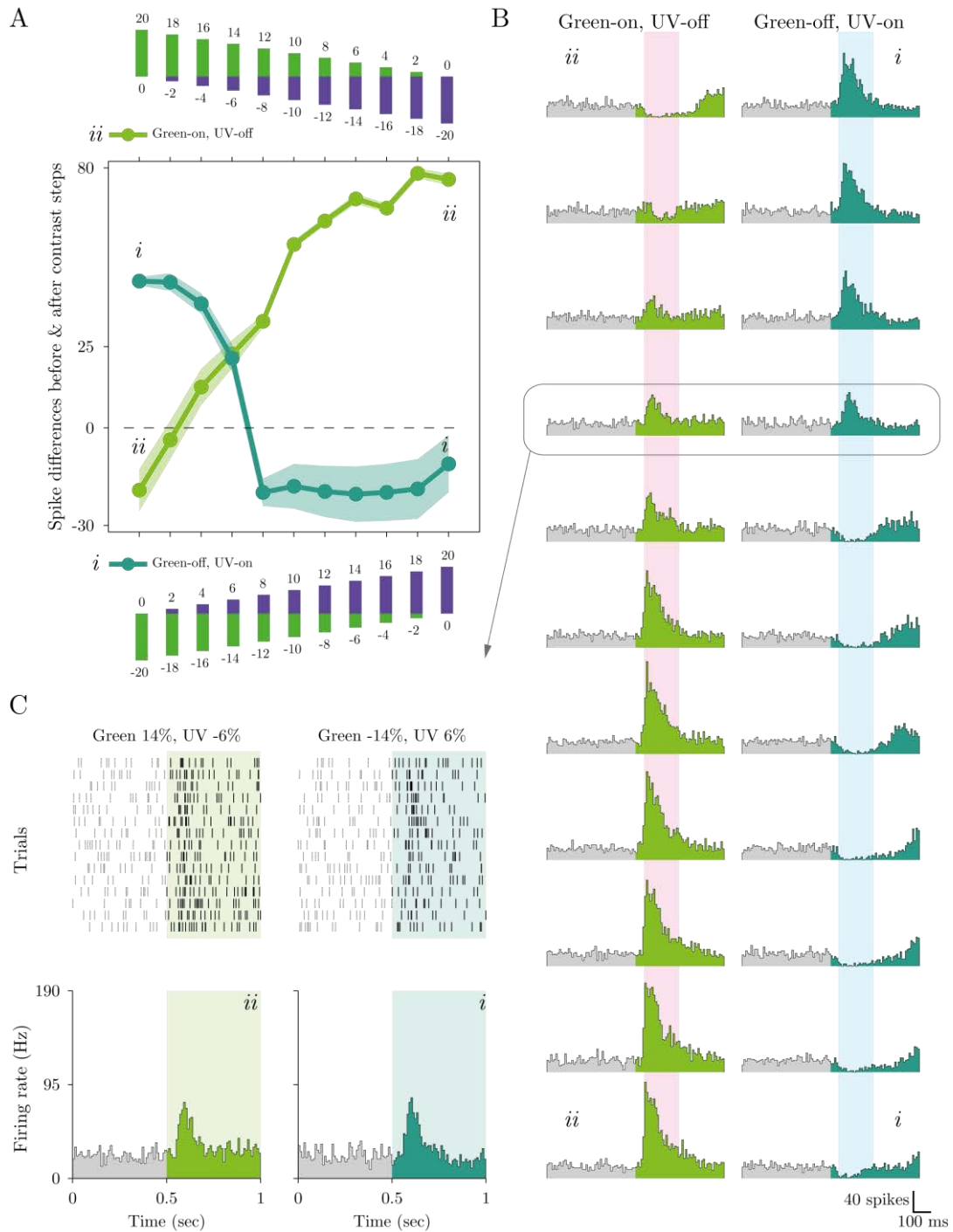


Figure 4.6. Response characteristics of a chromatically nonlinear Off ganglion cell. A) Chromatic integration curves of an Off nonlinear cell. This cell shows strong responses at the crossing point of the green-on, UV-off (bright shades) and green-off, UV-on (dark shade) curves. Therefore, this cell unlike the linear cell has no cancellation point. B) PSTHs from the response of this cell show its preference to Off stimulus. The On stimulus slightly suppresses the activity. C) Rasters and PSTHs of the crossing point shows strong activity for this nonlinear example cell.

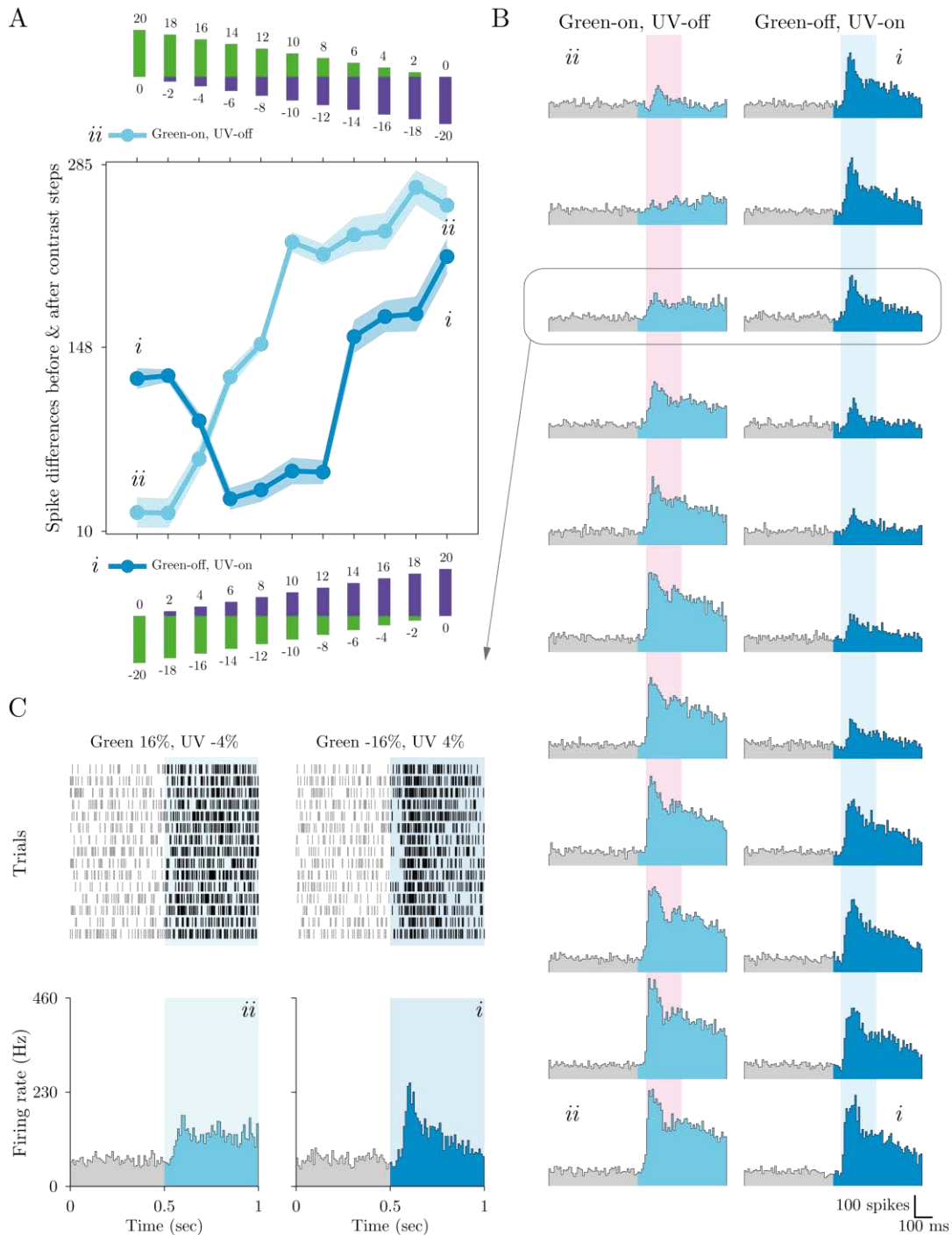


Figure 4.7. Response characteristics of a chromatically nonlinear On-Off ganglion cell. A) Chromatic integration curves of an On-Off nonlinear cell. This cell has strong activity at the crossing point of the two chromatic integration curves. Moreover, this cell respond to every combination of the stimulus. B) The PSTHs of the cell's responses to different contrasts of green and UV. The sensitivity of this cell to the UV stimulus is more than the green stimulus. C) Rasters and PSTHs of the crossing point shows strong activity for this nonlinear cell. Darker shades corresponds to green-off, UV-on stimulus and lighter shades represent green-on, UV Off stimulus set.

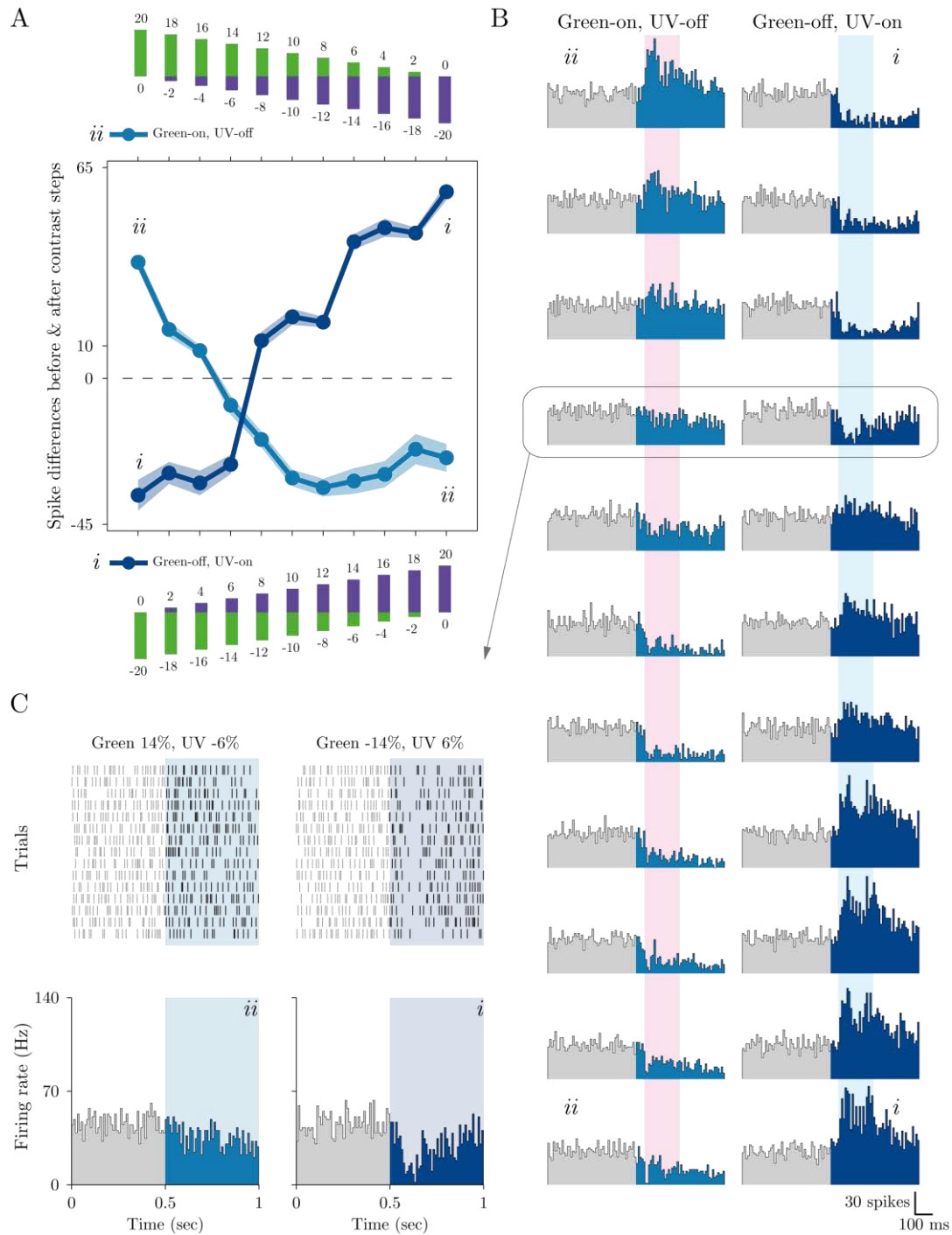
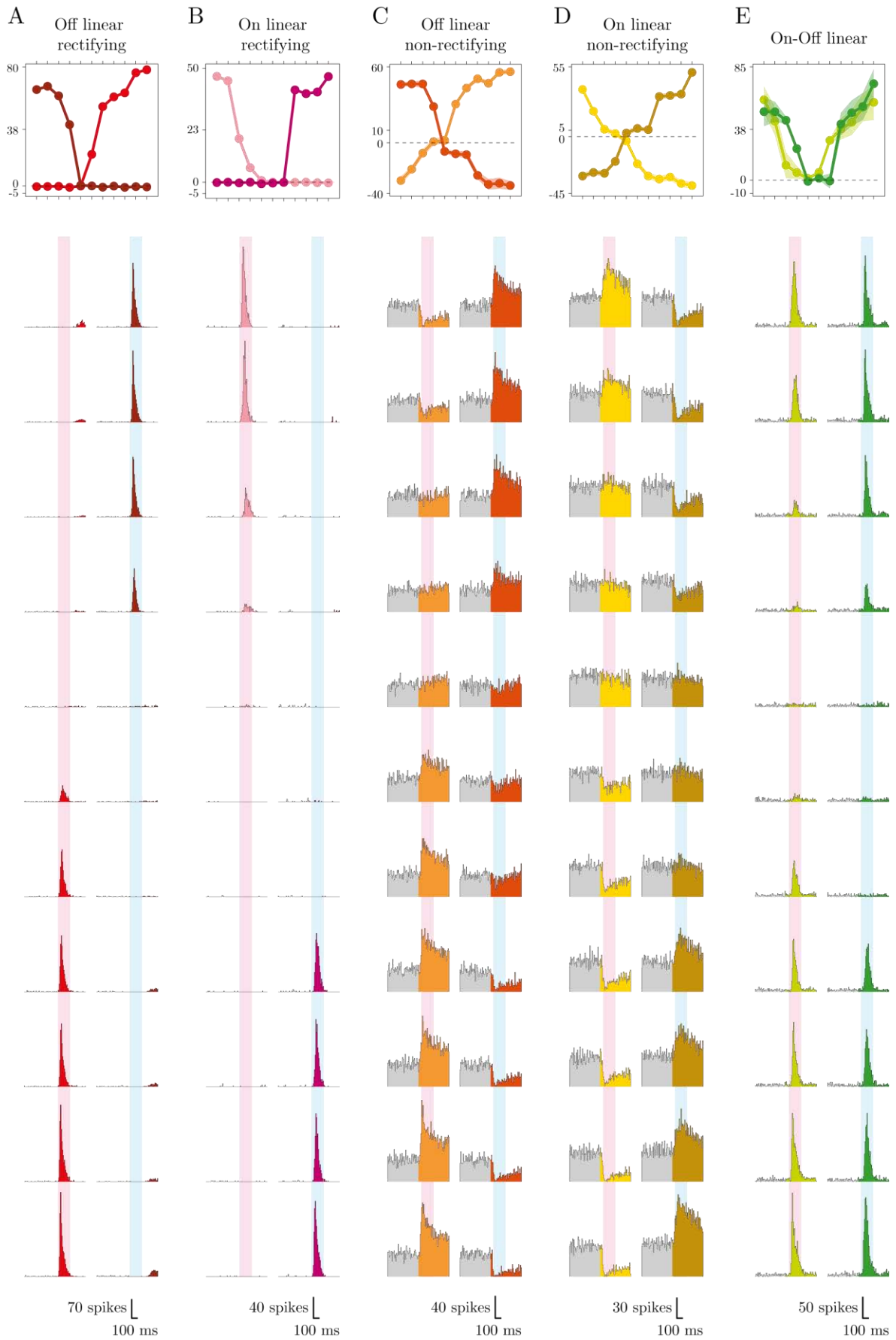


Figure 4.8. Response characteristics of a chromatically nonlinear On ganglion cell. A. Chromatic integration curves of an On nonlinear cell. This cell suppresses its activity at the crossing point of the green-on, UV-off and green-off, UV-on curves (C). B. A look at the PSTHs of this cell shows clear preference to On stimulus and strong suppression in response to Off stimulus.

4.3.3. Monochromatic, On UV-sensitive and unclassified ganglion cells

Until now, we focused mainly on the ganglion cells that showed clear responses to both green and UV stimuli (dichromatic cells). In addition, we found ganglion cells that responded only to one color of the chromatic stimulus (either UV or green, figure 4.8.J). Since mouse retina has a gradient of opsin expression along the ventral-dorsal axis (chapter 1.2), we hypothesized that these monochromatic cells are more likely to be found slightly away from the center of the retina. We will test this hypothesis in the following sections. In our experiments, we found more UV-sensitive cells than green sensitive cells. Since these monochromatic ganglion cells only responded to either green or UV stimulus, they had no chromatic integration characteristics. As a result, the cancellation point for these cells was at the stimuli that had no contrast of the preferred color. For example, for a cell that responds to the UV stimulus, the green 20%, UV 0% and green -20%, UV 0% stimulus would elicit no response different from the baseline activity. We therefore used the cancellation point at the corner stimulus as the indicator to group the monochromatic ganglion cells from the rest of the dichromatic cells. It is worth mentioning that we observed different polarity of responses among the monochromatic cells such as On, Off, and On-Off. We also found cells with high sensitivity to small contrast changes of a single color (figure 4.8.J the cell starts responding from 2% UV-off contrast). Further investigation, beyond the scope of this project, would be needed to study the properties of these monochromatic ganglion cells.

In addition, we found a small group of ganglion cells that had similar responses to the UV monochromatic cells but with small response to the green stimulus (figure 4.8.I). For these cells, only the high contrast of the green stimulus (18-20%) could activate them and even this level of activation was less than the activation from the equivalent UV contrast. In terms of chromatic integration, these cells were linear with a crossing point close to zero. The crossing point for these cells was close to the highest contrast of the green stimulus. This unbalance response to green and UV is likely caused by different sensitivity to green and UV stimulus. Since our chromatic integration stimulus only covers the contrast ranges of $\pm 20\%$, a stronger stimuli could potentially drive these cells more effectively. We found the On UV-sensitive cells mostly in the recordings that were done from the ventral retina of the mouse. Since these cells show distinct response features that lie between On linear rectifying cell and monochromatic UV sensitive cells, we classify them into a separate group with the label of On UV-sensitive cells.



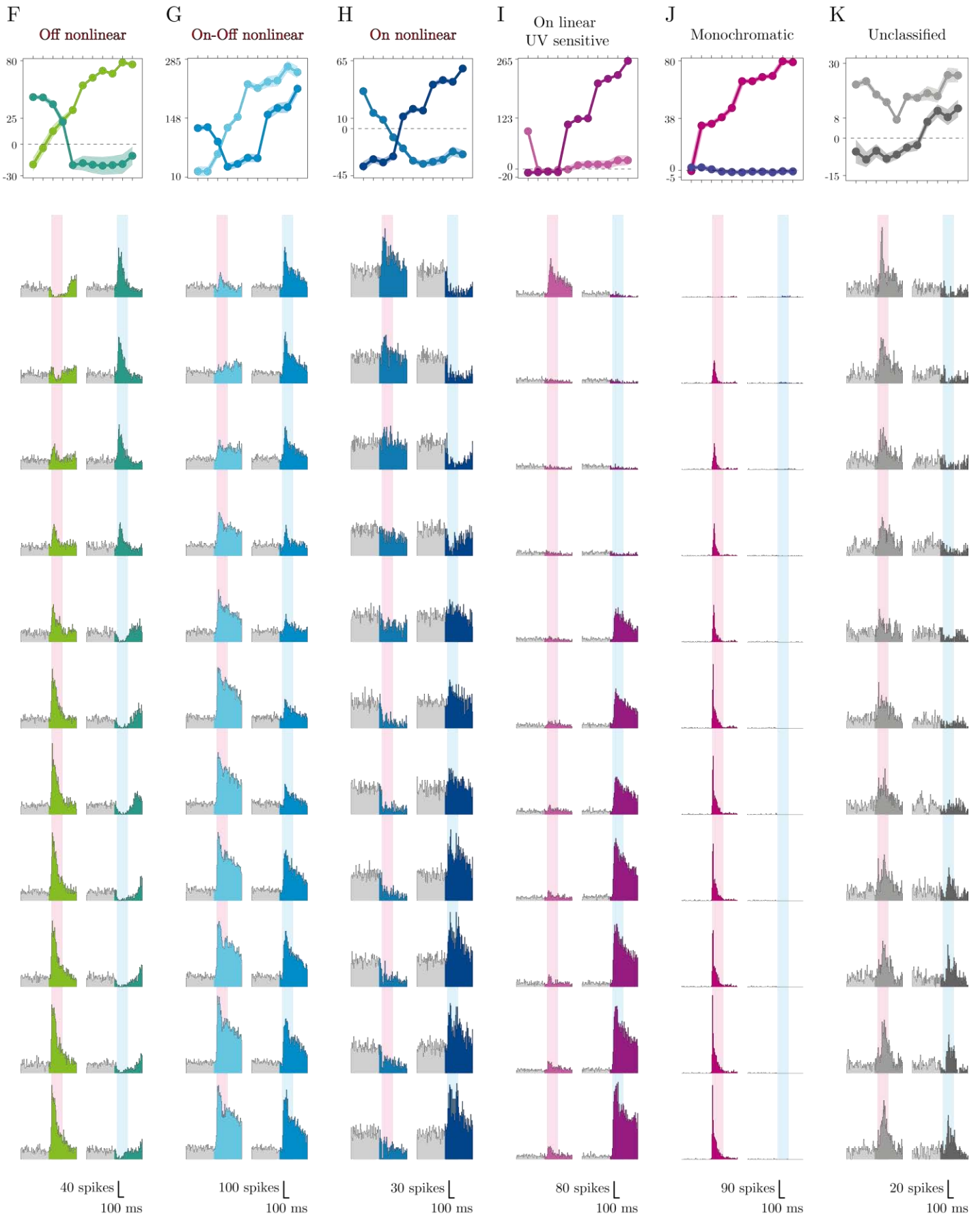


Figure 4.9. Examples for each ganglion cell types based on their chromatic integration properties. The ganglion cells types are: A. Off linear rectifying. B. On linear rectifying. C. Off linear non-rectifying. D. On linear non-rectifying. E. On-Off linear. F. Off nonlinear. G. On-Off nonlinear. H. On nonlinear. I. On linear UV sensitive cell. J. monochromatic and K. un-classified. The upper row of the figure shows the chromatic integration curves for each of the classes. Below are the PSTHs of the ganglion cells to the 11 different steps of the chromatic integration stimulus. In each PSTH, the gray region shows the 500 ms background stimulus before the onset of each contrast step. The bright color of each class corresponds to the green-on, UV-off stimulus set, and the darker shade corresponds to the green-off, UV-on stimulus set. The pink and blue shades in the background of each plot show the response in the time window of 50-250 ms that is used to construct the chromatic integration curves in the upper row. Here, the pink shades correspond to green-on, UV-off and the blue shades correspond to the green-off, UV-on.

Beyond the ganglion cells that were chromatically linear or nonlinear and the monochromatic cells, we found several cells that showed complex and perplexing responses to the chromatic integration stimulus. For example, some cells showed strong responses to both green-on, UV-off and green-off, UV-on stimulus, but they did not have any crossing point or intersection between the two curves (figure 4.8.K). Another group of cells had multiple crossing points, some close to zero (linear integration) and others away from zero (nonlinear integration). In both of these scenarios and in other complex responses, we were not able to classify these cells as simply as before. We therefore grouped these cells into one group of unclassified cells because of their diversity, complexity, and exclusivity of their response. However, further analysis and potentially more robust classification algorithm would be needed to classify all the ganglion cells of the mouse retina completely based on their chromatic integration properties. For the purpose of this study, we focused only on the chromatically linear and nonlinear ganglion cells.

4.4. Classification of retinal ganglion cells based on their chromatic integration characteristics

Until now, we showed that the mouse retinal ganglion cells exhibit diverse and complex responses to the chromatic integration stimulus. We distinguished the ganglion cells from each other based on their chromatic integration properties. This initial separation (figure 4.8) was based on visual inspection of the chromatic integration curves. In our inspection, we focused on the features of the chromatic integration curves that we described before. These features were the crossing point of the chromatic integration curves, the polarity and the rectification of the responses (see section 4.3). Now based on the mentioned three criteria we defined series of indices that allowed us to classify, objectively, the entire population of the recorded ganglion cells.

First: Monochromatic index

Before classifying the cells with these three criteria, it is important to separate the monochromatic cells from the dichromatic cells. This is because the focus of this study is on the dichromatic cells that integrate both colors (green and UV). Therefore, the first step in our automatic, objective classification was to define a measure that allowed us to separate the ganglion cells that respond to both green and UV colors (dichromatic) from the monochromatic ganglion cells. To do so, we defined a monochromatic index that takes the difference between the absolute value of the responses to the strongest green and UV stimuli divided by the sum of them (see methods). This index ranges between -1 (UV sensitive) and 1 (green sensitive). A threshold of -0.8 to 0.8 was defined to separate the cells that integrate both colors from the monochromatic cells (figure 4.10.A). It is worth mentioning that the overall distribution of our data is more slanted toward the UV input rather than the green input. We will address this issue in the following sections.

Second: Nonlinearity index

After separating the monochromatic cells from the rest of the cells, our objective was to define an index that separates the chromatically linear cells from the nonlinear cells. We calculated a nonlinearity index for each ganglion cell as the maximum response of the crossing point's lower bound divided by the strongest response (maximum response among all the contrast steps) of that cell (see methods). We calculated the nonlinearity index for all the recorded ganglion cells and chose the threshold of 0.1 and -0.1 to separate the linear cells from the nonlinear ones (figure 4.10.B). Therefore, the chromatically linear cells have nonlinearity index between -0.1 and 0.1 (figure 4.10.B-inset). Nonlinear cells with robust responses at the crossing point have a nonlinearity index larger than 0.1 and the suppressive nonlinear cells have nonlinearity index smaller than -0.1. Figure 4.10.B shows the distribution of the nonlinearity index for all the recorded ganglion cells. The majority of the cells are linear while we observed populations of nonlinear cells with both positive and negative nonlinearity indices.

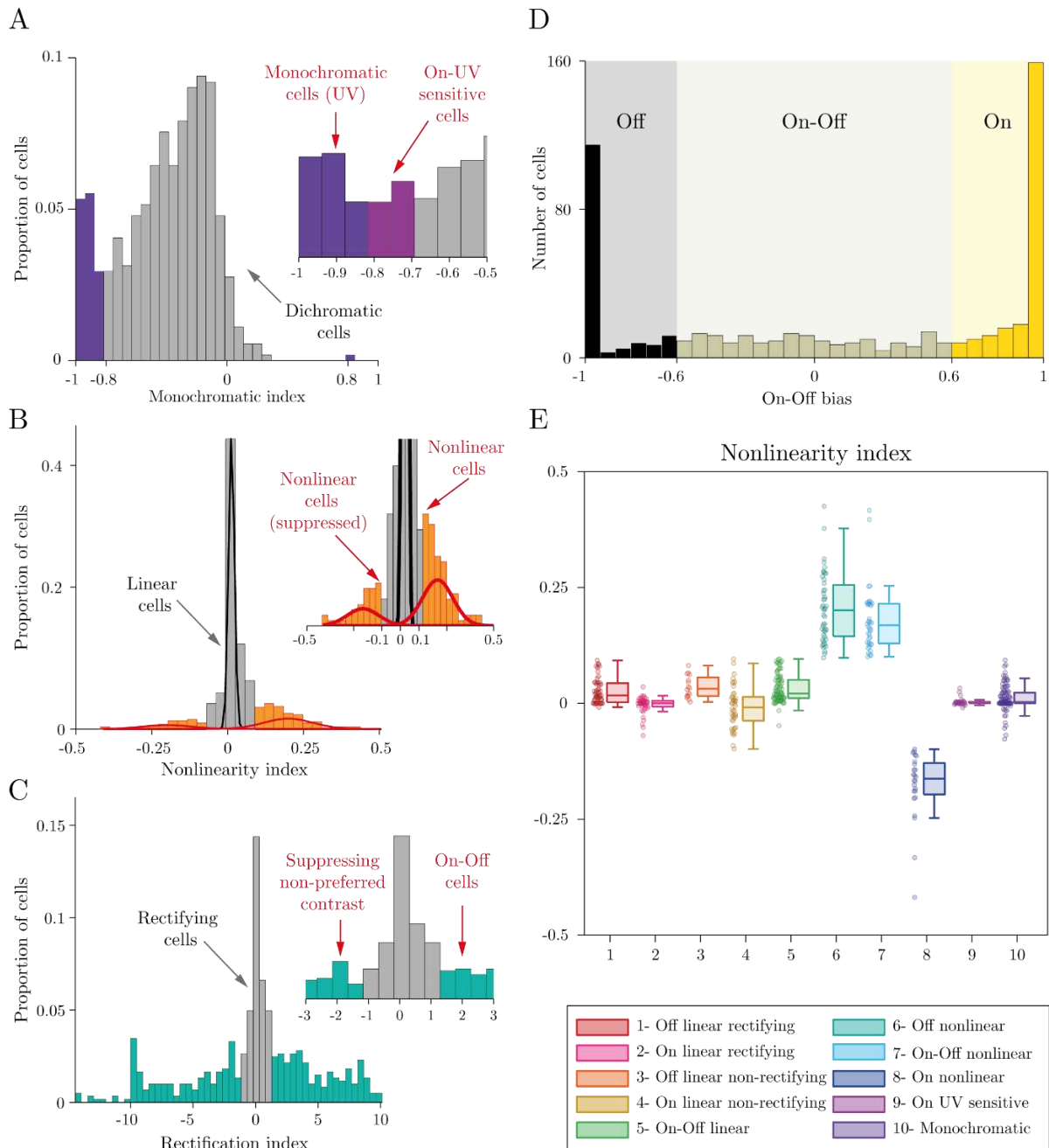


Figure 4.10. Classification of the ganglion cells based on their chromatic integration, response polarity and rectification features. A. Distribution of the monochromatic index for all the recorded ganglion cells shows the shift of the data toward the UV stimulus (-1). This distribution was used to separate the monochromatic cells from the dichromatic cells. B. Distribution of the nonlinearity index for all the ganglion cells. The threshold of the ± 0.1 was used to separate the linear cells from the nonlinear cells. C. Distribution of the rectification index for all the ganglion cells was used to separate the rectifying cells from the non-rectifying and On-Off cells. D. Distribution of the On-Off bias for the ganglion cells shows diversity of the response polarity. We used the threshold of ± 0.6 to classify the cells to On, Off and On-Off cells. E. Nonlinearity indices for the ganglion cells classified based on the indices described in A-D.

Third: On-Off bias

After the nonlinearity indices, we classified the ganglion cells based on their response polarity. In this classification, we used an On-Off bias for the strongest response to either UV or the green stimulus. To calculate the On-Off bias, we first subtracted the baseline activity of the cell from its strongest response and calculated the On-Off bias based on the differences between the cell's response to the increment and decrement of the stimulus divided by the sum of the two (see methods). The On-Off bias ranges from -1 (Off cells) to 1 (On cells) and On-Off cells have the bias closer to 0 (figure 4.10.D). We used a threshold of ± 0.6 to separate On, Off and On-Off cells from each other. As shown in figure 4.10.D for majority of the On and Off cells, the On-Off bias was close to -1 and 1, respectively.

Fourth: Rectification index

In addition to the nonlinearity index and the On-Off bias, we checked how each ganglion cell responds to its non-preferred stimulus. As shown before, some ganglion cells rectify the non-preferred stimulus (figure 4.9.A-B) while others suppress their activity in response to non-preferred stimulus (figure 4.9.C-D). Therefore, to separate the ganglion cells further, we defined a rectification index (see methods) as the response to the stimulus with non-preferred contrast divided by 10% of the strongest response. Based on this index the cells that rectify their non-preferred stimulus have rectification index between -1 and 1, while the non-rectifying cells have rectification index smaller than -1 (suppressive effect of non-preferred stimuli) and On-Off cells have rectification index bigger than 1 (figure 4.10.C). The distribution of the rectification index for all the ganglion cells is shown in the figure 4.10.C. Here, as expected, the majority of the ganglion cells show rectification of the non-preferred stimulus (figure 4.10.C-inset). However, some cells show big values of the rectification index, which corresponds to either reliable On-Off (positive) or strong suppressive (negative) responses. It is important to mention that we labeled the On-Off cells based on their response polarity and we did not consider their rectification in our analysis.

Fifth: Classification

For all the described indices, we selected thresholds for separating the groups in a way that the output of the classification is close to the features of the exemplary cells (figure 4.8). Putting together, the measured indices of the chromatic nonlinearity, On-Off bias and rectification, allowed us to classify the ganglion cells into different groups as shown in table 1.

Class labels	Nonlinearity index		On-Off bias			Rectification index	
	≤ -0.1	≤ 0.1	≤ -0.6	≤ 0.6	≤ -1	≤ 1	
1- Off linear rectifying		✓	✓			✓	

2- On linear rectifying		✓				✓		✓	
3- Off linear non-rectifying		✓		✓			✓		
4- On linear non-rectifying		✓				✓	✓		
5- On-Off linear		✓			✓				✓
6- Off nonlinear			✓	✓			✓	✓	✓
7- On-Off nonlinear			✓		✓		✓	✓	✓
8- On nonlinear	✓					✓	✓	✓	✓

Table 4.1. Summary of the indices and thresholds used to classify the retinal ganglion cells based on their chromatic integration characteristics, response polarity, and their rectification features in response to the non-preferred stimulus.

After careful examination of the ganglion cells in each class, we observed that in the group of On linear rectifying cells, we have a certain population of On cells that showed responses similar to the On UV-sensitive cell (figure 4.9.I). These ganglion cells were very sensitive to small changes (2-4%) of the UV light but only responded to big changes in the green stimulus (20%). Furthermore, the monochromatic index for these cells has values between -0.7 and -0.8. We thus used the monochromatic index to separate these On linear UV-sensitive cells from the rest of the cells.

Until now, we included only the dichromatic ganglion cells. Based on the monochromatic index, we grouped some cells into one broad class of monochromatic cells. For these cells, we did not include the On-Off bias or the rectification index. After classification of the cells, we noticed a small population of cells that did not fit into any described group. These cells generally had none or more than one crossing points the diversity of their responses could not be captured by our indices. Since we could not classify these cells, we put them in a basket with the label of un-classified cells. For most of the parts of this project, we exclude these un-classified cells from our analysis. Yet, more experiments and a more robust classification schema are needed to further study and classify these groups of ganglion cells. Taken together, we added 3 more classes to our 8 classes that were mentioned in the table 4.1. These include:

9. On linear UV sensitive cells: These cells are similar to On linear rectifying cells but they have high sensitivity to UV and very low sensitivity to the green stimulus.

10. Monochromatic cells: these cells integrate one chromatic input and the nonlinearity index for these cells is not informative. This is because, for these cells, the crossing point is at a corner stimuli and the nonlinearity index would not indicate linearity or nonlinearity of chromatic integration. However, these cells have different response polarities such as On, Off or On-Off. Some of these cells do rectify the non-preferred stimulus while others do not.
11. Un-classified cells: these cells come with different polarity and rectification characteristics.

The distribution of the nonlinearity indices of all the classified ganglion cells is shown in figure 4.10.E. All the cells here were classified objectively and based on the defined indices.

4.5. Population analysis of the chromatic integration classes

After classification of the ganglion cells into different chromatic integration classes, we looked at additional fundamental properties of the ganglion cells that would further support our classification. We first analyzed the properties that were measured from the chromatic integration curves and then we looked at the features of the strongest response for each chromatic integration class.

4.5.1. Population analysis based on the chromatic integration curves

We used the chromatic integration stimulus to study the linearity and nonlinearity of chromatic integration. We further looked at the response polarity and rectification of the cells based on this stimulus. In this section, we look at other features of ganglion cells that were measured from the chromatic integration stimulus. This is to check the similarities and differences between our defined chromatic integration classes.

First: Contrast combination at the crossing point

We first studied the contrast combination at the crossing point. Our measurement of the crossing point contrast showed slight deviation from the center contrast combination (figure 4.11.A). For the chromatically linear cells, the crossing point contrast is close to the fifth contrast combination (4.7 ± 0.6 mean and standard deviation, for a range of 1 to 11 contrast combinations) which corresponds to green $\pm 12\%$ and UV $\pm 8\%$ (figure 4.11.A.C5). For the nonlinear cells, we observed more shift towards UV contrast where the average of the crossing point is closer to the fourth contrast set (3.9 ± 0.8) which is the stimulus with green $\pm 14\%$ and UV $\pm 6\%$ (figure 4.11.A.C4). Here, the shift towards the UV means that the s-cone inputs have more weight compared to the m-cone inputs on the overall output of the ganglion cell. Therefore, a stronger contrast of green is needed to cancel out or be equally effective as the response induced by the weaker UV stimulus. For On UV-sensitive ganglion cells, as expected, the

crossing point is even more shifted towards the s-cone inputs (figure 4.11.A.9). In the case of the monochromatic cells, our data was dominated by UV sensitive cells with little to no green sensitive cells. As a result, the contrast of crossing point is shifted to the stimuli sets with small UV changes (1st or 2nd contrast). This on the other hand shows the strong sensitivity of the UV sensitive cells to the UV input with as little as $\pm 2\%$ change in the UV contrast.

Second: Rectification index of the nonlinear cells

Next, we looked at the rectification index for each class of the ganglion cells. We used this index for the classification of the linear cells. The nonlinear cells, however, were only classified based on their chromatic integration properties and their response polarity.

For the chromatically linear cells, as expected, this index separates the rectifying cells from the non-rectifying and On-Off cells (figure 4.11.B.1-5). This is not surprising, since this index was served to define these classes in the first place. Interestingly, for the nonlinear cells, we still observed a separation between the Off, On-Off and On nonlinear cells. The Off nonlinear cells have relatively strong suppression (non-rectifying) in their activity when they face the On stimulus (0.45 ± 0.21 mean and standard deviation of the rectification index). However, a small population of these cells rectifies their responses. For the On nonlinear cells, on the hand, all the cells show strong non-rectifying behavior (0.27 ± 0.06). For the On-Off cells, the majority of cells have strong responses to both stimuli. Therefore, the rectification index for these cells is not a relevant measure. Finally, the monochromatic cells showed a wide range of rectification and potentially further classification in this class is needed to separate these cells based on their rectification properties.

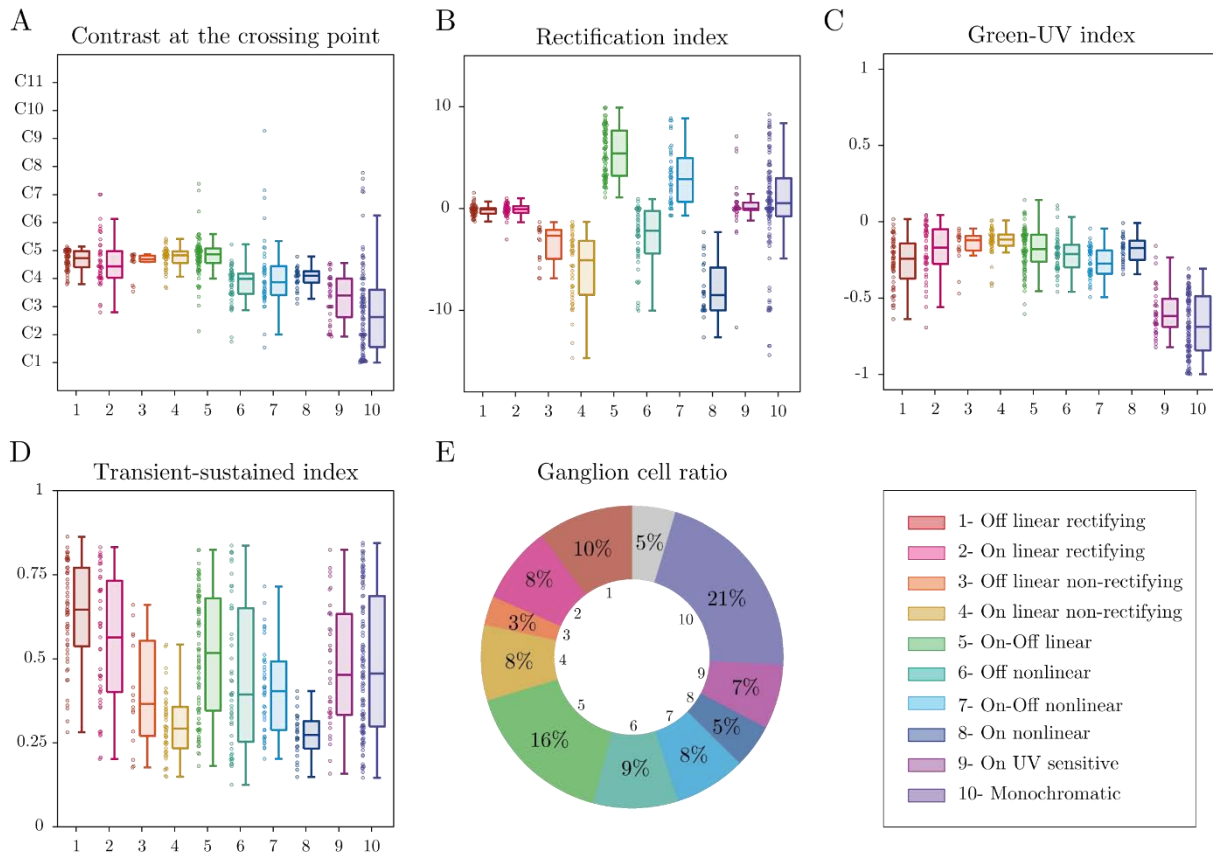


Figure 4.11. Basic properties of the different ganglion cell groups that were classified based on their chromatic integration curves. A. contrast at the crossing point of the green-on, UV-off and the green-off, UV-on curves. This is the contrast of the two stimuli combinations, which elicited the same response. Here C1 is green $\pm 20\%$ and UV 0%, C2 $\pm 18\%$ green and $\pm 2\%$ UV all the way with 2% contrast change for each color to C11 that has 0% green contrast and $\pm 20\%$ UV contrast. B. Rectification index of the different ganglion cell classes. Here both Off nonlinear and On nonlinear cells suppress their response when they face a non-preferred stimulus. C. green-UV ratio shows the contribution of s- and m-cone inputs to each class of the ganglion cells. Here, across the population, there was a slight shift toward the UV stimulus. D. Transience of the ganglion cells response to their preferred stimulus. Among the chromatically linear cells, the rectifying cells show more transience compared to linear non-rectifying cells and among the nonlinear cells, the On nonlinear cells show more sustained responses. E. Relative proportion of each class of the ganglion cells to the overall number of the recorded ganglion cells. Around 55% of the cells were chromatically linear, 20% of them were chromatically nonlinear, and around 20% were the monochromatic cells.

Third: Contribution of the s- and m- opsins on the response of the ganglion cells

After measuring the crossing point's contrast and the rectification index of each ganglion cell, we measured the relative contribution of s- and m- opsins for each cell. We measured a green-UV index as the difference in the strongest response to the green and UV stimuli divided by the sum of the two

(see methods)(Denman et al., 2017). The ganglion cells that respond only to green, have a green-UV index of 1 and the cells that respond only to the UV stimulus have an index of -1. As shown in the figure 4.11.C the majority of our recorded ganglion cells have more relative sensitivity to the UV stimulus. Part of this response bias could be due to the sampling bias in our experiments. This is because some of our data was recorded close to the center or more towards the ventral retina. Thus, our expectation is that the ganglion cells in these regions are more UV sensitive. We investigate this possibility in the following chapter. This shows that the mouse retina has population of ganglion cells that are very sensitive to UV light. This is consistent with previous reports showing that mouse retinal ganglion cells show fast and robust cone-mediated response under UV stimulation (Wang et al., 2011).

Fourth: Transient vs sustained cells

Next, we looked whether the classified ganglion cells showed transient or sustained responses to the chromatic integration stimulus. This separation into transient and sustained is a classical approach to distinguish ganglion cells based on the temporal properties of their response (Cleland et al., 1971). Transient cells encode light changes around the mean while sustained cells encode the mean level of light. It seems that these temporal response features of the ganglion cells are partially inherited from the bipolar cells (Roska and Werblin, 2001). Moreover, previous studies in the primate visual thalamus and mouse lateral geniculate nucleus showed that the color sensitive cells and color opponent cells were more sustained than the achromatic cells (Reid and Shapley, 2002; Denman et al., 2017). A closer look at the PSTHs of the figure 4.9 reveals that some classes such as linear On, Off non-rectifying and all the nonlinear cells showed more sustained responses compared to the rest of the cells. To quantify these observations, we calculated a transient-sustained index as the difference between the peak of the initial 250 ms and the mean of the response, divided by the sum of the two (see methods). Here, similar to previous indices, we chose the PSTH with the strongest response among all the contrast steps, as the base for our index. In this index, the cells with transient responses have values close to one and the sustained cells have values close to zero. A comparison of the transient-sustained index among the different chromatic integration classes showed that the linear On and Off rectifying cells and the linear On-Off cells were more transient than the On and Off linear non-rectifying cells and the chromatically nonlinear cells (figure 4.11.D). Here, what stood out from the rest of the groups were the On nonlinear cells (figure 4.11.D.8). They showed strong sustained response. Statistical comparison of the On nonlinear cells with other nonlinear cells showed significant differences between the groups, with the On nonlinear cells being more sustained (off nonlinear vs On nonlinear: $p=0.0014$ and On-Off nonlinear vs On nonlinear $p<10^{-4}$).

Fifth: Relative proportion of each class

Finally, we looked at the relative proportion of each class of ganglion cells to the overall number of the recorded cells. Figure 4.11.E shows this relative ratio of each class. Together, the chromatically linear cells take the majority of the cells with nearly 55%. The nonlinear cells on the other hand, were

around 20% of the recorded cells similar to the monochromatic ganglion cells. Between the nonlinear cells, the On nonlinear cells are the rarest types. We were not able to classify nearly 5% of our recorded ganglion cells and as mentioned before, further experiments and a more robust classification method could help to classify these cells into more relevant groups.

4.5.2. Population analysis based on the strongest response

In the next step, we focused on the properties of the strongest response. For the strongest response, the stimulus is essentially a chromatically preferred version of the square-wave stimulus that activates the cells robustly.

First: Dynamics of the response

We first assessed the dynamics of the response by inspecting the response latency (time-to-peak) for each class of the ganglion cells (figure 4.12.A). Off and On linear rectifying (1, 2), On linear UV-sensitive (9) and linear On-Off cells (5) showed slightly higher latency compared to the On and Off linear non-rectifying and all the nonlinear cells. This slight delay in the response latency could be due to mechanisms involved in chromatically linearizing these cells such as crossover inhibition. In this case, an amacrine cell modulates the output of the ganglion cells and therefore causes a slight delay in the latency of these linear cells (Molnar et al., 2009; Werblin, 2010). For the nonlinear cells and the On and Off linear non-rectifying cells the latency was very similar.

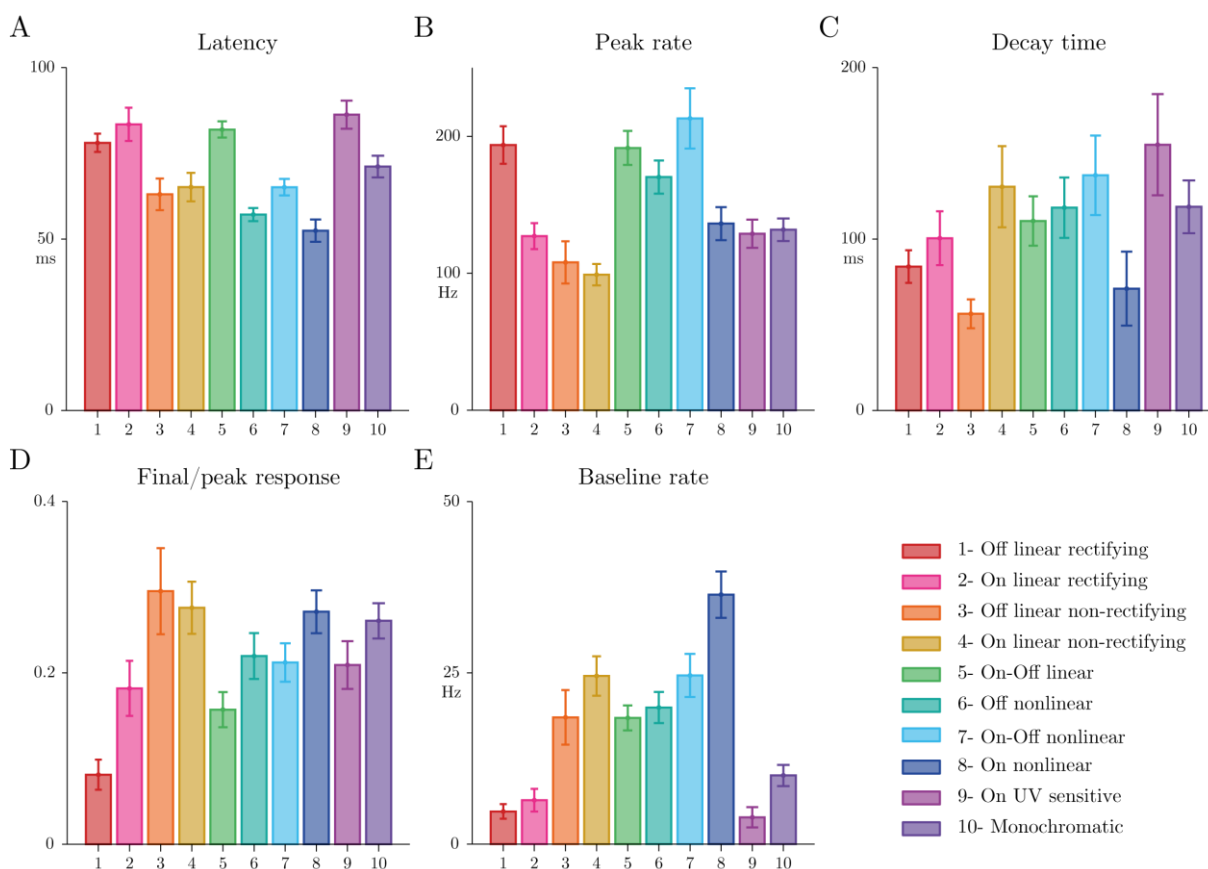


Figure 4.12. Population analysis based on the strongest response to the chromatic integration stimulus. A. Response latency (time-to-peak of the PSTH) for all the chromatic integration classes. The nonlinear cells and linear non-rectifying cells showed faster latency compared to the linear rectifying cells. B. Peak firing rate of the chromatic integration classes. C. Decay time from the peak response measured for the ganglion cells. The On nonlinear and On non-rectifying cells showed faster decay time compared to the rest of the classes. D. Final to peak ratio, which measures the transience of the response. All the nonlinear cells and linear non-rectifying cells showed more sustained responses. E. Baseline activity of all the chromatic integration classes. The linear rectifying cells showed lower firing rate compared to the rest of the classes. On nonlinear cells had high level of spontaneous activity.

Second: Peak of the firing rate

For the peak firing rate of each class, the picture seems to be more complicated. Another observation in figure 4.9 was that some classes of the ganglion cells have higher firing rate while others, especially the On and Off linear non-rectifying cells have lower peak firing rate. The same trend was observed in the population data (figure 4.12.B). Figure 4.12.B shows that the Off linear rectifying cells (see bar 1), On-Off linear cells (5) and Off and On-Off nonlinear cells (6 and 7) have relatively higher peak firing rate. Moreover, all the three classes of the On cells (2, 4, 8 and 9), and Off linear non-rectifying cells

(3) showed much lower peak firing rate. As a result, this measurement seems to be more heterogeneous compared to the previous measurements.

Third: Decay time and Final to peak response

We then looked at the decay time of the strongest response. The decay time shows how fast the cells relax from the peak firing rate (see methods). We observed that the Off linear non-rectifying cells (figure 4.12.C.3) and On nonlinear cells (figure 4.12.C.8) showed fast decay time while other nonlinear cells and the On linear cells have relatively slower decay time. The fast decay time of the Off linear non-rectifying and On nonlinear cells is rather surprising since both of these cells seem to have more sustained responses. Thus, it was expected that these cells have a slow decay time similar to the On linear non-rectifying cells. Part of this discrepancy could be based on the dependency of the transient-sustained index on the mean firing rate. To further investigate this finding, we looked at the transience of the response by defining a new measure. In this measure, we took the ratio of the cells response at the end of each stimulus period (before onset of the background light) and the peak of the response. For the transient cells, this ratio is relatively smaller than the sustained cells (close to 0.5) (Krieger et al., 2017). The advantage of this measurement is that, it is independent of the mean firing rate. Similar to our previous transient-sustained measurement, the On and Off linear non-rectifying cells and the On nonlinear cells were more sustained compared to the rest of the cells. Moreover, Off linear rectifying cells showed clear transience in their response compared to the rest. Therefore, both of the transiency measurements complied were similar to each other to all the classes except the decay time measurement of the Off linear non-rectifying and On nonlinear cells. The potential reason for the fast decay time of these cells could be that they have fast decline in their activity from their high peak firing to a lower sustain rate (Krieger et al., 2017).

Fourth: Baseline rate

Finally, we looked at the baseline rate of the ganglion cells (figure 4.12.E). We measured the baseline rate from the background activity before the onset of the stimulus. As shown in the example cells of the figure 4.8, the Off and On rectifying cells have low baseline activity. Across the population (figure 4.11.E), the On and Off linear non-rectifying cells (see bar 3 and 4) and the nonlinear cells (6, 7 and 8) have higher spontaneous activity. Here, the On nonlinear cells (8) showed the highest level of the baseline activity. The classes that showed higher spontaneous activity also showed more sustain responses. This suggests that these cells especially the nonlinear ones receive synaptic input that is more tonically active even under the background stimulation.

After revising all the measurements from the strongest response, it became clear that the On-Off linear cells (bar 5 in figure 4.12.A-E) seems to be close to the mid-point of all the measurements. In none of the measurements above, they showed unique characteristics that sets them apart from the rest of the groups. The main reason for this could be the limitation in our classification. Because we only classified

the ganglion cells based on their chromatic response into few classes and in the case of the On-Off linear cells, it is possible that more than one type of On-Off cells were put together. Therefore, if these features were different for the potential sub-groups they would have averaged out.

5.

The impact of the receptive field surround on chromatic integration

In this project, we studied how the mouse retinal ganglion cells integrate their inputs from s- and m-cones. Based on the classical studies of spatial integration in the retina, we developed a new stimulus to investigate whether the ganglion cells integrate their chromatic inputs linearly or nonlinearly. In the previous chapter, we found both linear and nonlinear chromatic integration among mouse ganglion cells. Furthermore, we were able to classify the ganglion cells based on their chromatic integration, response polarity and their rectification of non-preferred contrast. The next question that we asked was about the circuit mechanisms of chromatic integration. We asked what mechanisms would cause the linear and nonlinear chromatic integration. Moreover, which processes and computations in the retina would lead to the observed diversity of chromatic integration among the retinal ganglion cells? In this chapter, we address these questions with two different approaches. First, we simulated the chromatic integration properties of the ganglion cells with a simple model. From our simulation, we could speculate about the potential mechanisms and circuitry of the chromatic integration. In our second approach, we looked at the potential role of the receptive field surround in both linear and nonlinear integration of chromatic stimuli. We designed a new grating stimulus based on the chromatic integration stimulus. With this grating stimulus, we were able to stimulate the receptive field center more effectively than the surround. We found out that by reducing the influence of the surround over the center, the linear cells remained chromatically linear. The nonlinear cells, on the other hand, became chromatically linear. Therefore, we found that the receptive field surround has an impact on the nonlinearity of the chromatic integration. We finish this chapter, by studying the receptive field properties of each chromatic integration class. We do so by comparing the spatial and temporal properties of the receptive field among different chromatic integration classes.

5.1. Modelling chromatic signal integration using a nonlinear- linear- nonlinear cascade model

Our initial approach to investigate the potential mechanisms of the chromatic integration was to simulate the different aspects of it with a simple model. Based on the parameters that were used in the model, we could then infer the potential circuitry of the chromatic integration. We constructed the model in way that it was corresponded to the structure of the retina. We used the nonlinear-linear-nonlinear (NLN) model to simulate the chromatic integration of the ganglion cells. This model is an extension of the linear-nonlinear (LN) model, which is commonly used in the retina and vision research (Hunter and Korenberg, 1986; Meister and Berry, 1999; Chichilnisky, 2001; Paninski, 2003) (see methods). The NLN model phenomenologically describes the stimulus-response relation of a ganglion cell. This model assumes series of stimulus filters that each passes through a nonlinear transformation (first level nonlinearity, $N_1(\cdot)$). The output of these nonlinear transformations are being summed together and then passed through another nonlinear transformation (second level nonlinearity, $N_2(\cdot)$). The outcome of the NLN model, similar to the LN model is an instantaneous spike rate, which is used to generate spikes according to a Poisson process (see methods).

The first linear filtering stage of the model corresponds to the inputs of the bipolar cells coming from the photoreceptors. The first nonlinear transformation corresponds to the nonlinearities at synapses between the bipolar cells and the ganglion cells. The summation corresponds to the summation of the inputs that is done by the ganglion cells (dendrite and soma) and the second nonlinear transformation corresponds to the nonlinear spike generation mechanism of the ganglion cell. It is important to mention that, the NLN model assumes linear signal integration and encoding at the level of the photoreceptors and horizontal cells. This is in accordance with previous studies, which have shown that most cone photoreceptors respond to light in a linear fashion (Baylor et al., 1974; Tranchina et al., 1991). Moreover, it has been shown that the ribbon synapses of the photoreceptors play a key role in the linear signal transmission of bipolar cells (DeVries et al., 2006; Shapley, 2009). Since mouse is dichromatic, we assumed two types of inputs (s- and m-cone) to the bipolar cells. Therefore, in our model we defined two types of linear inputs: one for the UV stimulus (S_1) and another for the green (S_2) (figure 5.1.A). Each input was then passed through a nonlinearity ($N_1(\cdot)$ for S_1 and $N_2(\cdot)$ for S_2) and summed together. After this summation, the inputs were transformed by another nonlinearity ($N_2(\cdot)$). Therefore, by using different nonlinear functions for $N_1(\cdot)$ and $N_2(\cdot)$ and comparing the output of the model with the output of our experiments, it was possible to simulate the potential nonlinearities involved in the integration and processing of chromatic stimuli.

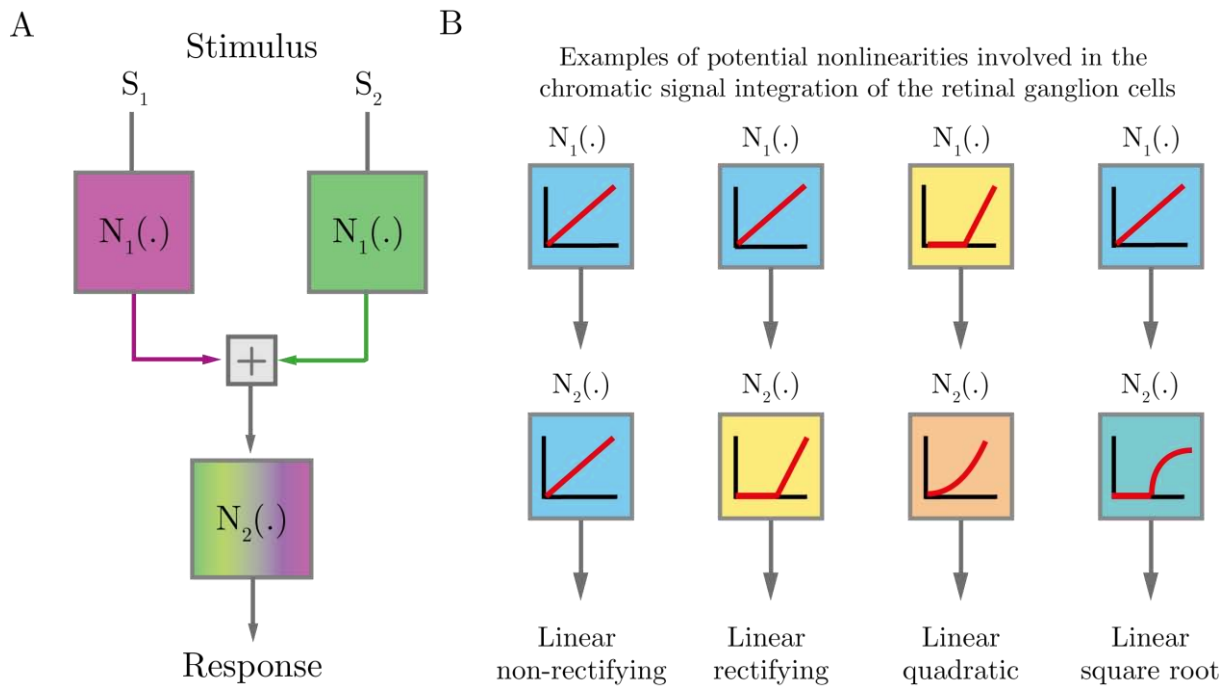


Figure 5.1. Structure of the nonlinear-linear-nonlinear (NLN) model. A. Schematic outline of the NLN model as it was used in this thesis. We defined two types of inputs to the model for the s- and m-cone inputs. These inputs are transformed with a set of nonlinearities $N_1(\cdot)$ and they are summed after the nonlinear transformation. After the summation, the integrated inputs go through a second nonlinearity $N_2(\cdot)$ to generate the output. The $N_1(\cdot)$ corresponds to the nonlinearities at the synapses between bipolar and ganglion cells and the $N_2(\cdot)$ correspond to the spike generating nonlinearities of the ganglion cells. B. Schematic examples of the different nonlinear functions that was used for $N_1(\cdot)$ and $N_2(\cdot)$. Based on the nonlinear functions, the output of the model could show different types of signal integration.

We hypothesized that if only the bipolar cells and ganglion cells were involved in the chromatic integration, we would be able to simulate both linear and nonlinear chromatic integration with this model. However, if other cells of the retina were influencing either linear or nonlinear chromatic integration, the output of the model would not simulate the responses of the ganglion cells from our experiments. Moreover, the functions that were used for $N_1(\cdot)$ and $N_2(\cdot)$ could inform us about the potential input-output nonlinearities for each class of the chromatic integration cells.

We therefore tested our model directly with the identical contrast combinations as the chromatic integration stimulus (figure 4.1) that we used in our experiments. We examined different combinations of nonlinear functions for $N_1(\cdot)$ and $N_2(\cdot)$ in a way that the nonlinearities could potentially describe the output of the neurons in the retina (Bolinger and Gollisch, 2012; Turner and Rieke, 2016) (figure 5.1.B for examples of nonlinear functions). We considered five different nonlinear functions for both $N_1(\cdot)$ and $N_2(\cdot)$. These include:

1. Linear: no changes for both positive and negative (On and Off) inputs.
2. Linear rectifying: no changes in positive inputs but negative inputs were set to zero.
3. Quadratic: quadratic (x^2) operation for positive and negative inputs (amplification).
4. Rectifying quadratic: quadratic (x^2) operation for positive inputs while setting negative inputs to zero (amplification and rectification).
5. Rectifying square root: square root (\sqrt{x}) operation for positive inputs and setting negative inputs to zero (moderate amplification and rectification).

To simplify the model, we assumed same nonlinear function $N_1(\cdot)$, for both green and UV inputs. However, it is possible to use different functions for each input. Since we were interested about the shape of the NLN model's output and the location of the crossing point for the two green-on, UV-off and green-off, UV-on curves, we did not pass the output of the second nonlinearity $N_2(\cdot)$ to a Poisson spike generator.

Figure 5.2 shows the output of the simulation for different combinations of the nonlinearities where each row shows different function for $N_1(\cdot)$ and each column shows different function for $N_2(\cdot)$. Here, the first column (figure 5.2.A) shows the output of the NLN model, which is similar to the response of the chromatically linear cells. However, after introducing any nonlinearity (B-E) in the $N_1(\cdot)$, we observed that the crossing point moves away from zero and the output of the simulation looked like the response of the chromatically nonlinear cells. In the first column, the nonlinear functions after the green and the UV inputs $N_1(\cdot)$ were defined as linear and the second nonlinearities were changing. The first row of the column A shows responses that are similar to the linear non-rectifying cells (figure 4.5 and figure 4.9.C-D).

In this case, both $N_1(\cdot)$ and $N_2(\cdot)$ were defined as linear functions. Since the bipolar cells in the retina have graded potential, it is possible for them to have linear output by having similar level hyperpolarization and depolarization to their inputs. Ganglion cells on the other hand, generate spikes which by its nature is a nonlinear process. However, if a ganglion cell has a high spontaneous activity and adjusts its firing rate based on the changes in the output of the bipolar cells, it can generate a linear output. In our experiments, linear non-rectifying cells showed high level of spontaneous activity (figure 4.12.E). Therefore, for these cells, we propose the model with linear $N_1(\cdot)$ and $N_2(\cdot)$ as a plausible yet simplified model for the mechanism of their chromatic integration (figure 5.2.A first row).

The second, fourth and last rows of the figure 5.2.A show responses that are similar to the linear rectifying cells (figure 4.4 and figure 4.9.A-B). In this case, the $N_2(\cdot)$ is a nonlinear function. Here the second nonlinearity does not affect the linear chromatic integration output of the model or the location of the crossing point, but it defines the shape of the integration curves or the rectification of the outputs. For example, the integration curve from the Off linear rectifying cell that is shown in figure 4.4 has similar shape to the last row of figure 5.2.A. It is possible to infer that the nonlinear input-output function of this ganglion cell is likely to be a square root function. For the ganglion cell of the

figure 4.3, the input-output function has a similar shape to the simulation output with quadratic rectifying $N_2(\cdot)$ function. Therefore, for the linear rectifying cells, the first nonlinearity $N_1(\cdot)$ influences the linearity of the chromatic integration and the second nonlinearity $N_2(\cdot)$ controls the rectification of the output and the shape of the integration curves. Finally, we were able to simulate the response of the On-Off linear cells with the NLN model. This is the case when the both $N_1(\cdot)$ functions were linear and the $N_2(\cdot)$ was nonlinear and non-rectifying (figure 5.2.A third row).

Until now, we assumed a linear function for the first nonlinearity ($N_1(\cdot)$). However, after introducing any nonlinearity for the $N_1(\cdot)$, we observed that the crossing point of the green-on, UV-off and green-off, UV-on curves move away from zero. This is in line with our premise for the chromatically nonlinear cells. A closer inspection of the chromatic integration curves of the Off and On nonlinear cells (figure 4.6 and 4.8) shows that these cells suppress their activity either in response to the non-preferred contrasts (off nonlinear) or at their crossing point (on nonlinear). In our simulations, with the exception of the case with all linear functions, for both $N_1(\cdot)$ and $N_2(\cdot)$, the NLN model failed to show any suppression in its output (figure 5.2.A first row).

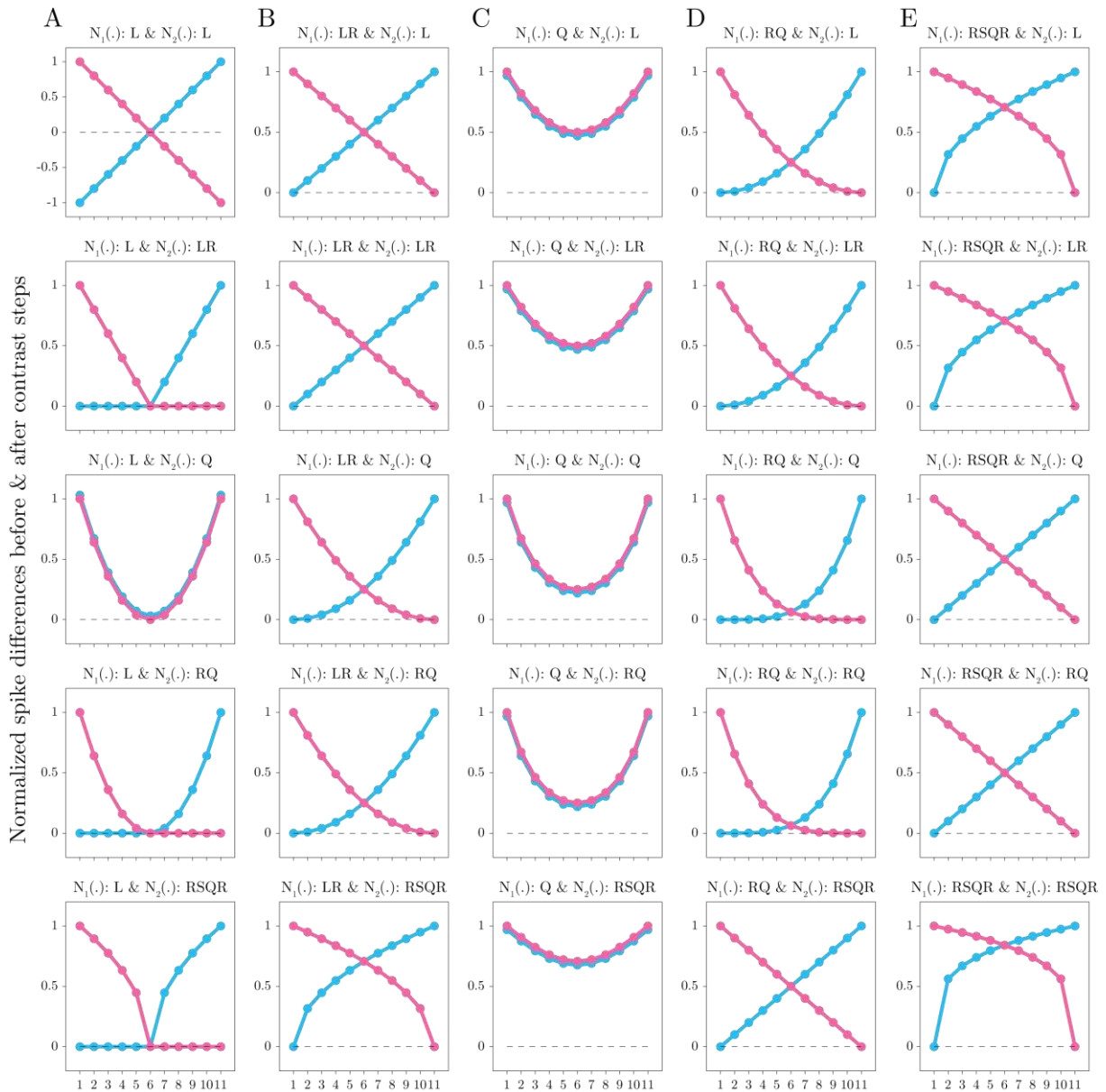


Figure 5.2. Output of the NLN model using different nonlinear functions for $N_1(\cdot)$ and $N_2(\cdot)$. Each column shows a nonlinear function for $N_1(\cdot)$ and each row shows a function for $N_2(\cdot)$. A. The linear integration is observed when the $N_1(\cdot)$ is linear. For these cases, the $N_2(\cdot)$ defines the shape of the integration curve. B-E. The integration becomes nonlinear after introducing any nonlinearity in the $N_1(\cdot)$. However, for all these nonlinear outputs, no suppression (responses below zero) was observed. This is in contrast with our observations from the nonlinear cells (figure 4.6 and 4.8). This led us to assume that other elements of the retina circuitry could be involved in the mechanisms behind the observed nonlinear chromatic integration. Based on the functions of $N_1(\cdot)$ and $N_2(\cdot)$: L=linear, LR=linear rectifying, Q=quadratic, RQ=rectifying quadratic and RSQR=rectifying square root functions.

Thus, for the chromatically nonlinear cells, the NLN model could assume a crossing point above zero. However, it failed to show the suppressive nonlinearities that we observed in the responses of our nonlinear ganglion cells. This suggests that there might be more to the nonlinear output of these cells than we considered by the NLN model. Since NLN model simulates the signal integration between bipolar and ganglion cells, we hypothesized that for the nonlinear cells, the amacrine cells might influence the chromatic nonlinearity of the ganglion cells. Thus, we hypothesized that the observed nonlinearity of the chromatically nonlinear ganglion cells was induced by some amacrine cell-mediated surround effects on the receptive field center of the ganglion cells. We tested this hypothesis in the following section.

Taken together, the NLN model is a powerful tool that helped us to speculate about the mechanisms of the chromatic integration. This model could simulate the output of the chromatically linear cells and even provided information about the shapes of the chromatic integration curves. For the nonlinear cells, on the other hand, the NLN model failed to simulate the suppression observed in the chromatic integration properties of these cells. This led us to speculate about the role of amacrine cells and the effects of the receptive field surround of the ganglion cells on their chromatic integration features.

5.2. The role of the receptive field surround in the chromatic signal integration

In the previous section, we aimed to speculate about the mechanisms of chromatic integration using NLN model. With this model, we were able to hypothesize about the mechanisms of linear chromatic integration. For these cells, we speculated that the chromatic integration linearity is induced by the bipolar cells or at the synapse between the bipolar and the ganglion cells. Moreover, we noticed that the ganglion cell's nonlinearity influences the rectification of the cell with little to no effect on its chromatic signal integration. For the linear non-rectifying cells, the model assumed a linear function for the ganglion cells' nonlinearity and for the rectifying cells, this function was defined as rectifying. For the chromatically nonlinear cells, the NLN model was able to replicate the crossing point differences from zero, but not the suppressions we observed in the chromatic integration curves of the Off and On nonlinear cells. Thus, we hypothesized that an amacrine cell mediated surround effect could affect the output of the nonlinear cells. The effects of the surround on the output of the ganglion cells have been reported since early days of studying retina (Kuffler, 1953). In addition, different pathways (Ichinose and Lukasiewicz, 2005; Zaghoul et al., 2007) and models for the interactions between center and surround of the receptive field have been reported. Some models propose that the surround influences the center linearly with suppressive effects to the preferred stimuli and responsive effects to the non-preferred stimuli (Dayan and Abbott, 2001). Other models suggest direct influence of surround on the local subunits of the receptive field (Enroth-Cugell and Freeman, 1987). Others suggests nonlinear (Takeshita and Gollisch, 2014) or a divisive influence of the surround on the center (Merwine et al., 1995). In term of color processing in the retina, the dominant model is based on the

color opponent cells that have antagonistic center and surround (Dacey and Lee, 1994; Dacey, 1999; Chang et al., 2013). However, the role of the receptive field surround in the chromatic signal integration of the retinal ganglion cells is not yet clear. Here, we first explain a new stimulus that we designed to investigate the role of the surround in the chromatic signal integration of the ganglion cells. We then focus on each chromatic integration class, mainly the nonlinear cells, to check whether their nonlinearity is induced by the surround or it comes from the center of the receptive field.

5.3. Chromatic grating stimulus

In this thesis, we introduced the chromatic integration stimulus as a new approach to study the question of the chromatic integration. As shown in figure 4.1.A, the chromatic integration stimulus is a full-field stimulus with no spatial structure. This stimulus consists of 22 steps of a square wave stimulus with opposing green and UV contrasts. The full-field design of this stimulus was intended to avoid any nonlinearity that might be caused by the nonlinear spatial integration of the ganglion cells (Enroth-Cugell and Robson, 1966). However, because of its full-field design, the chromatic integration stimulus stimulates both the center and the surround of the receptive field. Therefore, we could not use the same stimulus to investigate the role of the surround in the chromatic signal integration. To approach the question of center vs surround, we designed a new stimulus that stimulated the center of the receptive field with the same contrast combinations and properties of the chromatic integration stimulus but do not activate the surround as strong as the full-field stimulus. This stimulus was a slowly moving sinusoidal grating where each bar presents opposite contrasts of green and UV simultaneously. The amplitude or the contrast of each sinusoidal was identical to the chromatic integration stimulus (20% to -20% in steps of 2% change for both green and UV colors). Therefore, we had eleven different contrasts of the stimuli (figure 5.3.G). The width of each period was set to 480-500 μm , which is more than two times bigger than the center of most mouse ganglion cell receptive fields. This is to ensure that each half of the period would cover the center while the surround was covered with more than 1 period. The speed of the movement was set to one period per second. Figure 5.3 shows the design of this stimulus. Here, we depicted a typical mouse ganglion cell with its center and the surround, which is 2-3 times bigger than the center (figure 5.3.A). After the start of the stimulus, the first half of the stimulus period ($0-\pi$) moves and covers the receptive field center of the ganglion cell (figure 5.3.A and C-left). In this situation, what was presented to the center was a green-on, UV-off stimulus, which is similar to one combinations of the chromatic integration stimulus (e.g. green 12%, UV -8%, figure 5.3.D). At the same time, the surround sees 3-4 full period ($0-2\pi$) of the two sinusoidal instead of just half a period (figure 5.3.E and F). Since the two half periods of the sinusoidal have opposing contrasts, the linear sum of these contrasts is similar to the background stimulus. As a result, what was shown to the surround was closer to the background stimulus, which activated the surround not as effective as the full-field stimulus. After 500 ms the second half of the period ($\pi-2\pi$) moves over the receptive center and then the cell sees the opposing contrasts or green-

off, UV-on stimulus (e.g. green -12%, UV 8%, figure 5.3.B-D). The surround at same time sees again 3-4 periods with the opposing contrasts, which together were similar to the background stimulus (figure 5.3.E-F). Since this stimulus is a chromatic sinusoidal grating, for the rest of this thesis we use the term chromatic grating stimulus to refer to it. After repeating each stimulus for nearly 10 periods, the contrast of the stimulus was changed to a new combination of the contrasts. We kept the stimulus for nearly 10 period to make sure that the grating moved through the whole screen in a way that all the ganglion cells saw the stimulus periods more than once. The order of presentation for each contrast combination was selected randomly to avoid any adaptation effects caused by any sequence of the contrasts. Finally, to provide strong statistical support in our measurements, each contrast combination was presented 6-10 times which was equal to 60-100 periods of each contrast combination.

Taken together, we designed a new stimulus that consists of sinusoidal functions with opposing green and UV contrast that slowly moved over the receptive field. In each period of these sinusoidal functions, the receptive field center saw first the green-on, UV-off and then the green Off, UV-on stimulus while the surround saw the sum of these two stimulus combinations. As a result, the responses of the cells were driven by their center with reduced influences from the surround.

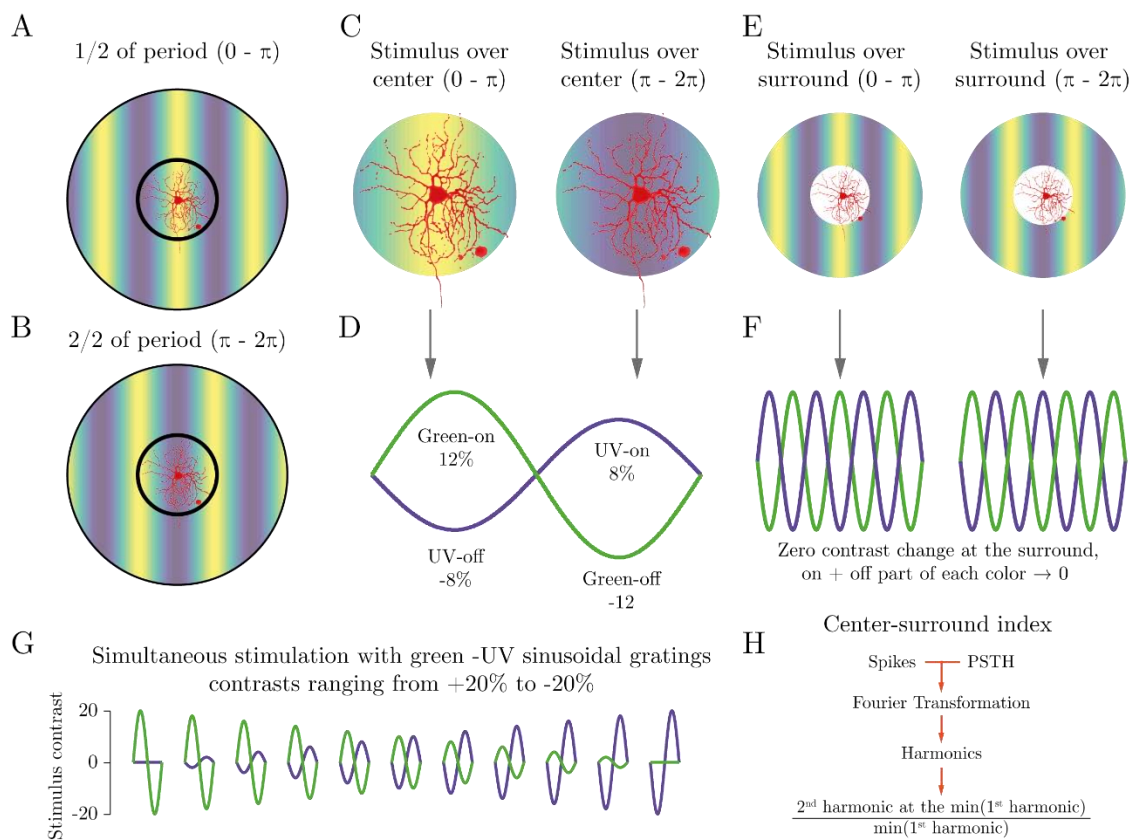


Figure 5.3. Schematic view of the chromatic grating stimulus. A. Illustration of the first half of the stimulus period displayed over a representation of a ganglion cell's receptive center and surround. The width of the grating was designed in a way that each half of a period covers the center of the receptive field. B.

Second half of the period displayed over the receptive center and surround of the ganglion cell. C. Illustration of the stimulus over the receptive field center of the ganglion cell. Here, the cell is stimulated with the green-on, UV-off stimulus on the first half of the period ($0-\pi$) and green-off, UV-on for the second half of the period ($\pi-2\pi$). D. One dimensional representation of the stimulus that was presented over the receptive field center. In this example, only one contrast combination (green $\pm 12\%$, UV $\pm 8\%$) is shown. E and F. Illustration of the stimulus over the receptive field surround of the example ganglion cell. For the first and second halves of the period, the surround was stimulated with multiple On and Off combinations of each color. These combinations thus counter-act each other, which turns them into the background stimulus for the surround. G. Schematic representation of the entire contrast combinations that was presented in each experiment. The contrast combinations are identical to the chromatic integration stimulus (figure 4.1). They cover the 20% to -20% contrasts of green and UV colors. Same as the chromatic integration stimulus, the colors were presented with opposite contrasts in green-on, UV-off and green-off, UV-on arrangement.

H. Diagram for the analysis of the chromatic grating stimulus. For each period of the stimulus, the spikes were counted and from all the trials a PSTH was constructed. The discrete Fourier transformation of the PSTH was taken and a center-surround index was calculated as the magnitude of the second harmonic at weakest first harmonic, divided by magnitude of the weakest first harmonics. The image of the mouse ganglion cell (red) was kindly provided by Helene Schreyer.

5.4. Analysis of chromatic grating stimulus

We analyzed the responses of the ganglion cells to the chromatic grating stimulus based on the same premise as the chromatic integration stimulus. Since we showed the same combination of contrasts, we checked for the cancellation point of the green-on, UV-off and the green-off, UV-on parts of the stimulus. For each trial of the chromatic grating stimulus, we found the spikes during each period of the sinusoidal function. For all the trials of a specific contrast combination, a PSTH with 10 ms time bins was constructed. We took a discrete Fourier transformation of the PSTH and we looked at the first and second harmonics from the Fourier transformation. If a ganglion cell responded robustly to half of the period that matched its preferred polarity (On or Off), the first harmonic for this cell would be larger than the second harmonic. This is because the response frequency was the same as the stimulus frequency. However, if a ganglion cell responded to both On and Off parts of the sinusoidal function or double the stimulus frequency (frequency doubling), the second harmonic is bigger than the first one. Now based on the chromatic integration stimulus, we knew that at the crossing point of the green-on, UV-off and green-off, UV-on curves, the responses of the linear cells are close to zero while the nonlinear cells respond to both combinations of the stimulus.

For analyzing the chromatic grating stimulus, we looked at the combination of the contrasts with weakest responses and there, we compared the first harmonics to the second harmonics. If the magnitude of the first harmonic was bigger than the second harmonic, it was a sign for linear chromatic

integration. If the second harmonic had higher magnitude than the first at the location of the weakest response, it was due to the frequency doubling which we considered it as the sign for nonlinear chromatic integration. Our approach to analyze this stimulus was similar to the previous studies of spatial integration in which the frequency doubling was considered as the sign for nonlinear spatial integration (Enroth-Cugell and Robson, 1966; Hochstein and Shapley, 1976; Carcieri et al., 2003).

If a ganglion cell has no baseline activity or very few spikes at the point, where the opposing colors cancel each other out, the magnitude of both first and second harmonics would be very close to the zero. This led to some error in our measurements because it was possible that with few extra spikes, the second harmonic became bigger than the first one. To avoid this issue, we considered a threshold for our measurements where we defined the weakest response. This threshold was set as the magnitude of the harmonics around 5 Hz. If the cells minimum response was close to zero in a way that the magnitude of both first and second harmonics was below 5 Hz, we considered these cells as chromatically linear. For the rest of the cells that had reliable responses at their cancellation point, we compared the first and second harmonics.

Figure 5.4 shows the responses of two different ganglion cells to the chromatic grating stimulus, with one cell that integrates the chromatic inputs linearly (A-F) and other cell nonlinearly (G-L). For the cell on the left (pink) we observed that this cell encoded the stimulus reliably when the contrast of the stimulus was strong (figure 5.4.F top and bottom rows). As the difference between green and UV contrasts started to reduce, the cell's response started to decline substantially. A closer look at the lowest response for this cell shows few spikes with no clear relation to the stimulus (figure 5.4.A-B). Measuring the harmonics at the lowest response showed higher magnitude for the first harmonic compared to the second harmonic (figure 5.4.C). This relation between the harmonics was also consistent along all the contrast combinations, with first harmonic bigger than second one (figure 5.4.D). Therefore, this cell integrated its chromatic inputs in a linear fashion. Inspection of the responses of this cell to the chromatic integration stimulus shows that this cell is in fact chromatically linear (figure 5.4.F). Therefore, the response of this example cell for both of the chromatic grating stimulus and the chromatic integration stimulus showed linear integration. This means that the receptive field surround does not have a strong effect on the chromatic integration profile of this cell. For the cell on the right side of the figure 5.4 (orange) we observed strong response to both green-on, UV-off and green-off, UV-on parts of the stimulus (figure 5.4.H-I). The harmonic measurements from the weakest response of this cell confirmed this observation with the second harmonic being bigger than the first one. However, the frequency doubling (second harmonic $>$ first harmonic) was not observed for the other contrast combinations (figure 5.4.K). This was expected, since this cell only encodes one polarity of the stimulus. Thus, for the rest of the contrast combinations, the preferred contrast drives the cell's response. This made the first harmonic bigger than the second harmonic for the rest of the contrast combinations.

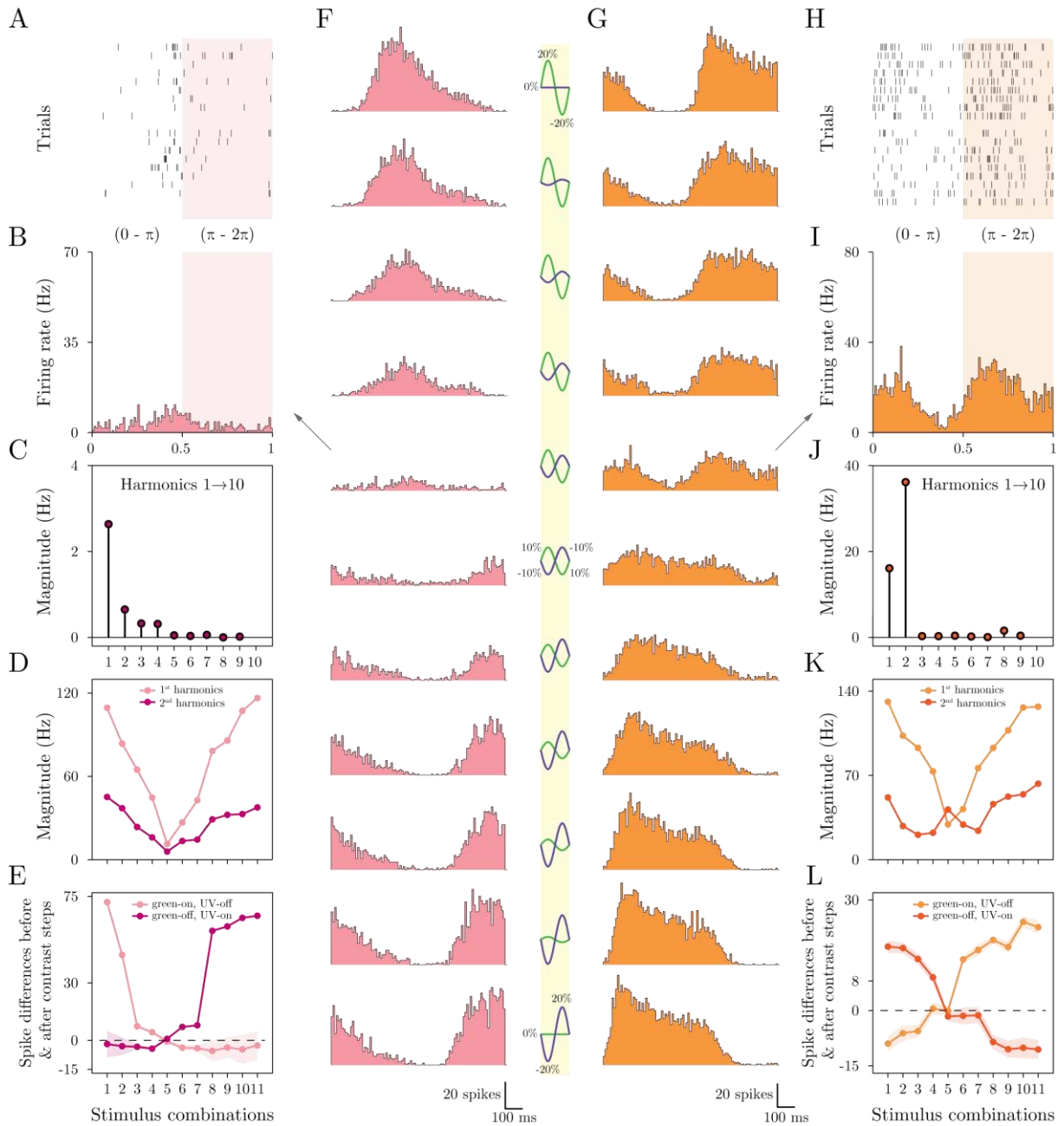


Figure 5.4. Examples of linear and nonlinear chromatic integration in response to the chromatic grating stimulus. A and B. Raster plot and PSTH of the weakest response. C. Output of the discrete Fourier transformation from the PSTH in B. The first harmonic shows higher magnitude compared to the rest. The stronger magnitude of the first harmonic compared to the second harmonic was considered as the sign for linear chromatic integration. We only showed the first 10 harmonic for simplification. D. Magnitudes of the first and second harmonics for all the contrast combinations of the chromatic grating stimulus. For all the contrast combinations, the first harmonics were stronger than the second harmonics. E. Chromatic integration properties of the same ganglion cell show its linear rectification properties.

F. PSTHs from the responses of the ganglion cell to all contrast combinations of the stimulus. The stimulus combinations were depicted in the middle. G. PSTHs from the response of the ganglion cell to all contrast combinations. Here the weakest response shows two response peaks (frequency doubling) while other responses have one peak. H and I. Raster and PSTH from the weakest response of the ganglion cell. J. Fourier transformation of the PSTH shown in I. The second harmonic showed stronger magnitude compared to first harmonic. This was considered as the sign for nonlinear chromatic integration. K. First and second harmonics of responses to all the combinations of the stimulus. For all the combinations, the first harmonics were bigger than the second harmonics, with the expectation of the weakest contrast combination (minimum of the first harmonic). L. Response of this ganglion cell to the chromatic integration stimulus showed linear non-rectifying features. For this specific ganglion cell, the chromatic integration became nonlinear when the center was being stimulated stronger than the surround with the chromatic grating stimulus.

Comparison of this cell's response between the chromatic grating stimulus and the chromatic integration stimulus showed non-matching results. For the chromatic grating stimulus, this cell showed nonlinear chromatic integration while in response to the chromatic integration stimulus this cell showed linear non-rectifying responses (figure 5.4.L). Therefore, for this specific cell, we concluded that the receptive field surround would influence the chromatic integration by making it linear.

Taken together, to analyze the chromatic grating stimulus, for each recorded ganglion cell, we took a discrete Fourier transformation of the weakest response and compared the first and the second harmonics. If the second harmonic at the lowest response was bigger than the first one, it was a sign of nonlinear chromatic integration. Otherwise, we assumed linear integration for that cell. In the next step, we compared the integration features of the cells between the chromatic grating stimulus and chromatic integration stimulus to see whether the receptive field surround has any effects on the linearity or nonlinearity of the chromatic integration.

5.5. Surround's contribution to the chromatic integration of linear and nonlinear ganglion cells

We recorded the responses of 452 ganglion cells from 10 retinas to the chromatic grating stimulus. For each cell, we checked whether it showed linear or nonlinear chromatic integration. We then compared the response of that cell to the chromatic integration stimulus. Finally, we compared the two integration features between the two stimuli. If the chromatic integration properties of each cell stayed the same for both of the stimuli, we assumed that the receptive field surround was not influencing the chromatic integration and the integration was happening at the center. However, if the integration properties of a cell changed between the full-field and the grating stimulus, we associated this change to the receptive field surround. Here, we briefly discuss the responses of the chromatically linear and

nonlinear cells to the chromatic grating stimulus and then compare the changes in the chromatic integration among all the classes.

5.5.1. Linear rectifying and non-rectifying cells

For these cells, the majority of the recorded ganglion cells showed linear chromatic integration in response to the chromatic grating stimulus. For the linear rectifying cells, all the cells showed linear integration to both stimuli. However, for the linear non-rectifying cells, we found some cells that showed nonlinear integration when they face the chromatic grating stimulus. An example for a On linear rectifying cell and also an Off linear non-rectifying is shown in the figure 5.4. Although the example here shows a cell with nonlinear integration profile, over the population, majority of both On and Off non-rectifying cells were chromatically linear for both stimuli (figure 5.7.A).

5.5.2. Nonlinear cells

In the previous section and based on the output of our investigation with the NLN model, we hypothesized that the receptive field surround of the ganglion cells could potentially play a role in the nonlinearity of chromatic integration. Here, what we found among all three groups of the nonlinear cells was a change to linear integration when they responded to the chromatic grating stimulus. Figure 5.5 shows the responses of three nonlinear cells (one from each group) to the chromatic grating stimulus. For all of these cells, we observed reliable responses to a half of the period and substantially higher values for the first harmonic compared to the second harmonic (figure 5.5.B-C). These linear integration outputs of the nonlinear cells were in contrast with their response to the chromatic integration stimulus (figure 5.5.A). Thus, the result of the experiment with chromatic grating stimulus showed that the receptive field surround could potentially cause the nonlinearity of the chromatic integration for Off, On-Off and On nonlinear cells. Over the population, with few exceptions from the Off nonlinear cells, nearly all the chromatically nonlinear cells showed linear integration in response to the chromatic grating stimulus (figure 5.7.A).

5.5.3. Linear On-Off cells

Until now, we found that the linear rectifying and non-rectifying cells did not change their chromatic integration features in response to the chromatic grating stimulus, while nonlinear cells became more linear. For the linear On-Off cells, we found responses that were more heterogeneous. Some On-Off cells showed linear integration while others showed strong nonlinear integration. The main reason for this heterogeneity could come from the On-Off nature of these cells. This is because On-Off cells, by their nature, respond to both On and Off part of the stimulus. Therefore, for these cells, the second

harmonic is bigger than the first harmonic for most contrast combinations. At the weakest response, (small contrast differences) if an On-Off cell has any response, even not so strong, it is a response to both On and Off part of the stimulus. In this case, we cannot separate the potential nonlinearity of the chromatic integration from the On-Off response of the cells. Therefore, for the On-Off cells, the chromatic grating stimulus is not suitable to prove their chromatic integration features.

It is worth mentioning that not all of the recorded On-Off cells showed nonlinear integration and frequency doubling. This is the case for the On-Off cells that have different sensitivity to green and UV colors. For these cells, the half of the stimulus period that has the more preferred color (higher sensitivity) would dominate the response. This makes the first harmonic bigger than the second one. For these cells, our measurement of linearity or nonlinearity could be valid. This is the case for the On-Off nonlinear cells, because these cells showed strong imbalance in their On-Off output (figure 4.6) by having more sensitivity to the UV stimulus than the green. For these cells, the UV response dominates the response to the chromatic grating stimulus (figure 5.5.C). To put together, the measurements based on chromatic grating stimulus is not very relevant for the On-Off cells when they show strong On-Off response to both On and Off part of the stimulus. These cells show strong second harmonics to most of the contrast combinations. However, if the On-Off cells have different sensitivity to different color or polarity of the stimulus, then the measurements from the chromatic grating stimulus becomes more relevant.

5.5.4. Population comparison between the chromatic integration classes

In the last part of our analysis, we checked how chromatic integration classes change their integration characteristics when their receptive field center was being stimulated more effectively than their surround. To do so, we defined a center-surround index for each cell. This index was defined based on the magnitude of the second harmonic from the weakest response divide by the magnitude of the same first harmonic (figure 5.3.H). To find the weakest response, we looked at the minimum of the first harmonics. However, if the magnitude of the minimum of the first harmonic was smaller than 5 Hz, we set the center-surround index to zero. For the ganglion cells that responded linearly to the chromatic grating stimulus, the center-surround index yields a value between zero and one while the ganglion cells with nonlinear integration have center-surround index bigger than one.

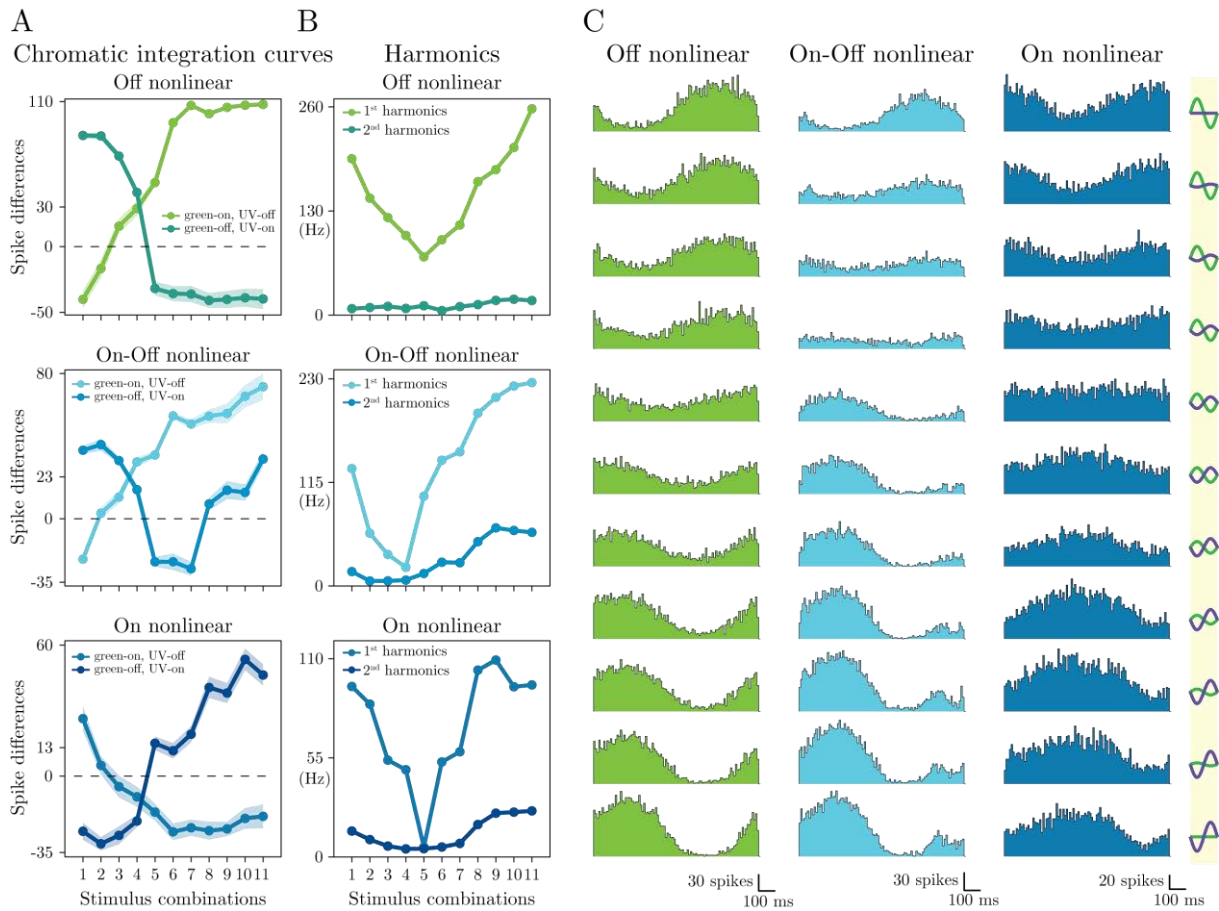


Figure 5.5. The effects of receptive field surround on the chromatic integration properties of the nonlinear cells. A. Chromatic integration curves of Off, On-Off and On nonlinear cells shows nonlinear integration of green and UV stimulus. B. First and second harmonics measured from the response of the cells in A to the chromatic grating stimulus. All of these nonlinear cells had stronger first harmonics across all the contrast combinations. This means that they responded to only one-half of the stimulus as shown in C. Thus, when the center was stimulated more effectively than the surround, the nonlinear cells showed linear chromatic integration instead of nonlinear integration. This points out to the potential role of the surround in the nonlinearity of the chromatic integration for the nonlinear cells.

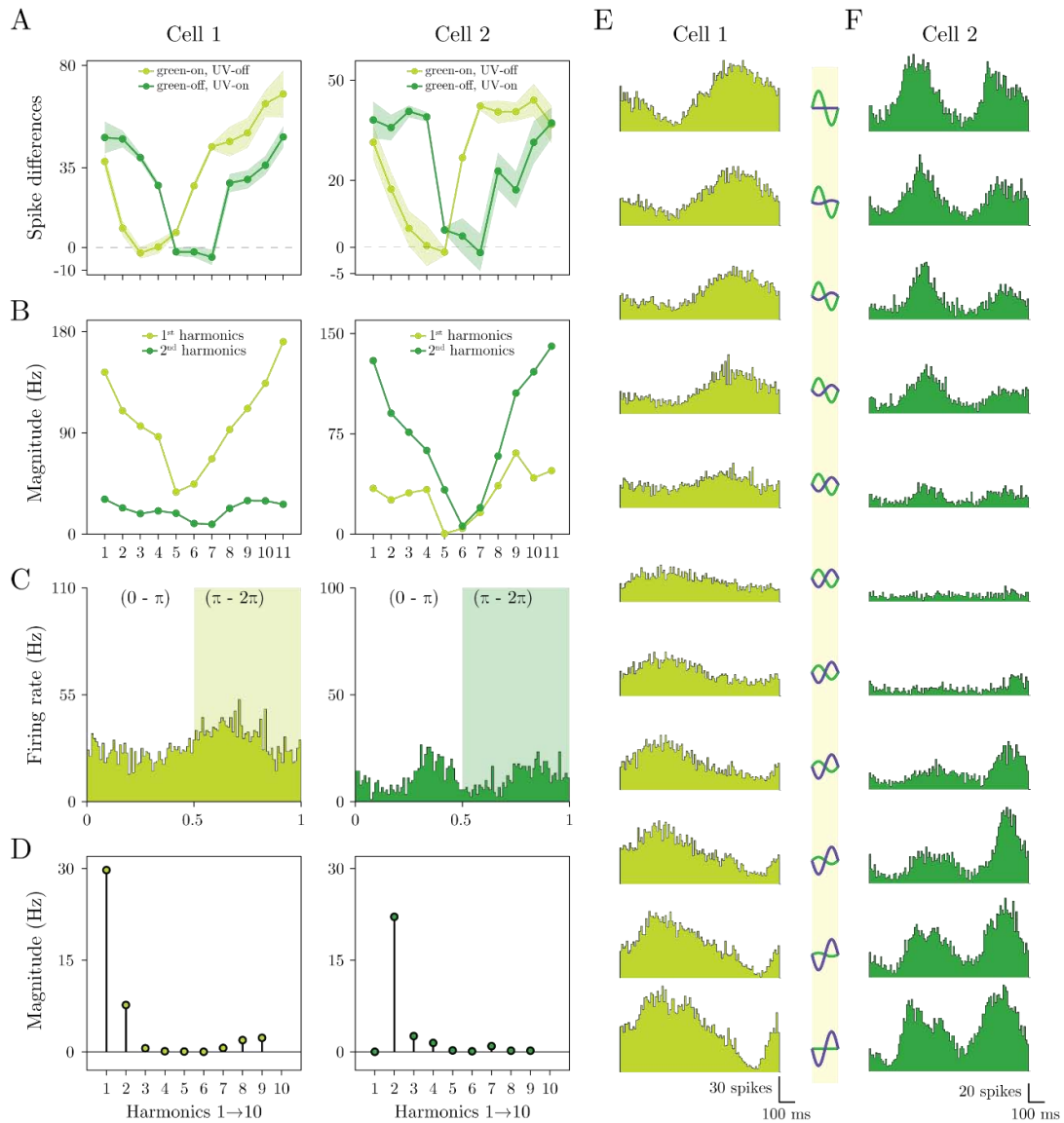


Figure 5.6. Different integration properties of the On-Off linear cells in response to the chromatic grating stimulus. A. Chromatic integration curves of two example cells show their linear and On-Off responses. B. First and second harmonics of cells show different types of responses, with one cell showing strong first harmonic for all the contrast combinations and the other cell shows strong frequency doubling (stronger second harmonic) for most of the contrast combinations. C. PSTHs of the weakest responses show more linear integration for cell 1 and nonlinear integration for cell 2. D. Comparison of the harmonics from the weakest response confirms the linear integration of the cell 1 and nonlinear integration of the cell 2. E. PSTHs from the response of cell 1 and 2 to all the combinations of the chromatic grating stimulus. Cell 1 responded mostly to one-half the stimulus period while cell 2 (as expected from an On-Off cell) responded to both halves of the stimulus period. Since for the On-Off cells, we were not able to separate the On-Off induced frequency doubling from the surround inhibited frequency doubling, we would not draw any conclusion about their chromatic integration properties.

Figure 5.7 shows the center-surround index for all the chromatic integration classes. The On and Off rectifying cells showed linear responses to the chromatic grating stimulus (figure 5.7.A.1-2). The non-

rectifying cells showed more nonlinear responses compared to the rectifying cells (figure 5.7.A.3-4). However, the average of their center-surround index remained below one. This means that for these groups, over the population the surround does not have substantial effect on their chromatic integration characteristics. For some of these non-rectifying cells, on the other hand, the receptive field surround still plays a role in the linearity of their chromatic integration. For the linear On-Off cells, the center-surround index covers a wider range with few cells showed strong nonlinear responses with the majority of the cells showed linear responses. This is reflected in the average of the index. However, as mentioned before, for these cells the center-surround index and the chromatic grating stimulus could not reflect the linear or nonlinear integration features of their receptive field center.

For all the nonlinear cells, we observed linear integration in the center with few Off nonlinear cells only showing nonlinear integration in the center (figure 5.7.A.6-8). Therefore, for the Off, On-Off and the On nonlinear cells, the receptive field surround influences or potentially causes the nonlinearity of chromatic integration. The On UV-sensitive cells showed linear integration for both chromatic grating stimulus and chromatic integration stimulus. Their responses in both cases were similar to the On linear rectifying cells. Finally, for the monochromatic cells, since there is no real integration of the two colors, this measurement is not relevant.

We finally looked at the nonlinear to linear ratio of the cells in each chromatic integration class (Figure 5.7.B). For the Off linear non-rectifying cells, nearly 30% of the cells became nonlinear. For the nonlinear cells, around 10% of the cells stayed nonlinear and the rest became linear when their surround was not stimulated.

Taken together, we investigated the role of the receptive field surround in the chromatic integration properties of different classes of the ganglion cells. We found that for the linear rectifying cells and most of the linear non-rectifying cells the linearity of the integration does not depend on the surround. For the nonlinear cells, on the other hand, the surround is likely to contribute to the nonlinearity of the chromatic integration.

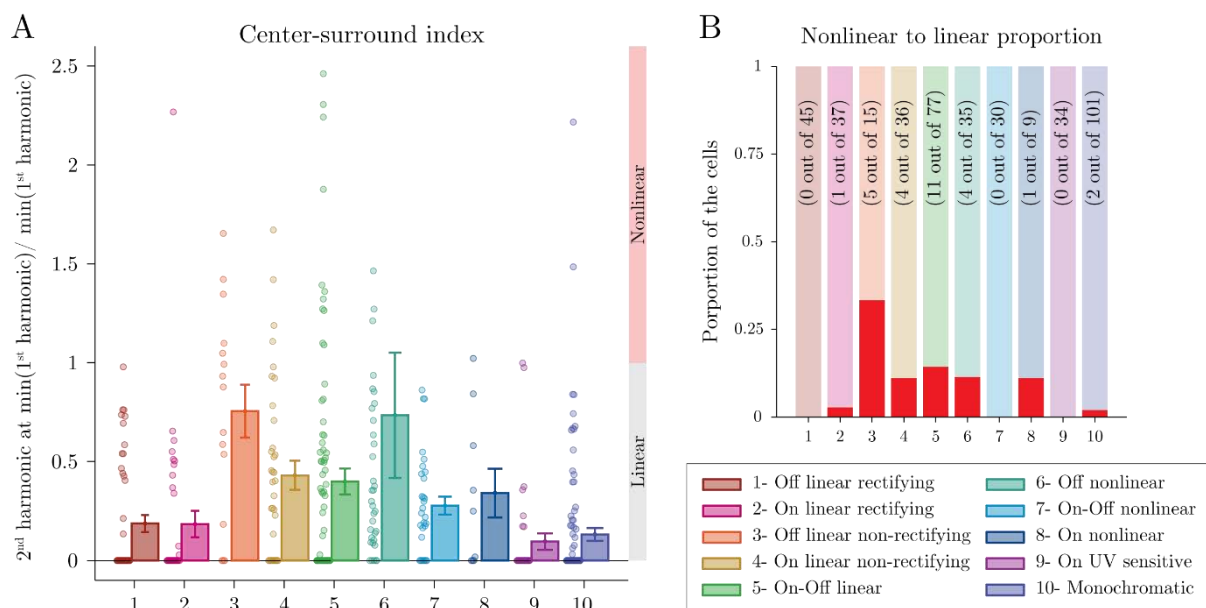


Figure 5.7. Reducing the effects of the receptive field surround linearize the chromatic integration of the nonlinear cells. A. Center-surround index for all the chromatic integration classes showed the integration properties of the cells in response to the chromatic grating stimulus. For all the classes, the chromatic integration on average became linear when the receptive field surround was not stimulated as effectively as the center. Most nonlinear cells (6-8) responded linearly when their center was being stimulated. The Off non-rectifying cells showed nonlinear integration for nearly 30% of their cells. The On-Off linear cells (5) showed complex responses to this stimulus that might be caused by the On-Off nature of these cells. B. The relative proportion of the nonlinear cells in each chromatic integration classes shows that for all the classes except the Off linear non-rectifying (3), less 10% of the cells showed nonlinear responses.

5.6. Receptive field properties of the chromatically linear and nonlinear ganglion cells

Until now, we showed that the ganglion cells in the mouse retina integrate their chromatic inputs in linear or nonlinear fashion. We further showed that the receptive field surround contributes to the nonlinear integration of the nonlinear cells. We classified the cells based on their chromatic integration, response polarity and the rectification of the non-preferred stimulus. However, in our classification, we did not consider the properties of the receptive field. Some of these properties such as receptive field diameter, temporal kinetics of the receptive field and lack of overlap between the receptive fields of the same type (tiling) was used to identify different types of the ganglion cells (Borghuis et al., 2008; Wässle et al., 2009; Masland, 2012; Baden et al., 2016). We therefore checked for the receptive field location of each ganglion cell and inspected the relation between the location on the retina and the chromatic integration properties of that cell. We measured the spatio-temporal receptive field of each

ganglion cell using a chromatic binary white noise stimulus. This stimulus had a mixture of green and UV colors that were displayed on a checkerboard pattern (see methods). We calculated the spatio-temporal receptive field of each ganglion cell with the reverse correlation method (Chichilnisky, 2001; Schwartz et al., 2006). In this approach, we measured the spike-triggered average (STA) from the spatio-temporal white noise stimulus (see methods). We decomposed the spatial and temporal receptive field with the singular value decomposition. For each temporal component of the receptive field, we checked for the polarity of the response, time-to-peak and biphasicness of the temporal filter. We fitted each spatial component of the receptive field with a 2D Gaussian fit and from the fit, the diameter and the location of the receptive field was measured (see methods). In our experiments, we labeled each retina after the enucleation and based on that label we tried to cut the retinas along the ventral-dorsal axis. In a subset of our experiments, we were able to record from both halves of the same retina. Here, we first looked at the temporal features of the receptive fields. We then focused on the relation between the location and the chromatic integration properties of some of the recorded ganglion cells. Finally, we studied the features of the receptive such as diameter, time-to-peak and biphasicness of the temporal receptive field for each chromatic integration class.

5.6.1. Temporal properties of chromatic integration classes

Figure 5.8.A shows the temporal components of the receptive fields from the chromatic integration classes. For all the Off and On classes the polarity of their temporal filter matched the polarity of the response measured from the chromatic integration stimulus. For both linear and nonlinear On-Off cells, the polarities of the temporal components seem to be assigned based on the more dominant responses. This is because the output of the reverse correlation method is either On or Off due to averaging all the stimuli that triggered the response. Our measurement of temporal component's polarity shows that for On and Off cells, the response polarity that were observed was consistent with the polarity of the cells in response to a fast flickering stimulus.

A closer inspection of the temporal filters shows that some classes have more biphasic filter. The biphasic shapes of the filters correspond to how each cell responds to the temporal frequency of the stimulus. Classes such as Off and On rectifying cells and all the nonlinear cells showed more biphasic filters. In the following sections, we will systematically compare the biphasicness of the filters between the chromatic integration classes.

5.6.2. Ganglion cell's location and its chromatic integration

From the groups of recorded retinas (12 retinas), we had two recordings in which we were able to record from both halves of the retina. For these two retinas, we looked at the locations of the ganglion cells relative to the position of the stimulus screen. For each half of the retina, we checked the

distribution of the chromatic integration classes. Since the ventral retina is more dominated by the s-cones, we hypothesized that the cells that have strong bias toward UV stimulus such as On UV-sensitive cells would be more frequent in the ventral retina. Moreover, since the nonlinear cells process their chromatic input in more complex way than the linear cells, we assumed that the nonlinear cells were to be found closer to the center or on the dorsal part of the retina. This assumption was made based on the previous studies that showed the color opponent cells in mouse retina are more common at the center of the retina (Chang et al., 2013). It is important to point out that our measurement here, is a very crude measurement and we sampled only a small region of the retina with limited number of electrodes. Moreover, in some of our recordings, we did not find all the different classes of the cells.

Figure 5.8.B and C shows the distribution of the cells from two different retinas. For each retina, the location of the ventral and dorsal cells were acquired from separated experiments and artificially overlapped onto a schematic view of the retina. After counting the cells based on their chromatic integration features in each retina (figure 5.8.C), we observed that the linear cells were more frequent in the dorsal retina. The Off and On-Off nonlinear cells, on the other hand, were found more frequently on the ventral retina. The On UV sensitive and the UV sensitive monochromatic cells, as expected, were found mostly in the ventral retinas. Here, our observation is partially skewed because one of our recording from the dorsal retina (D1) was devoid of any nonlinear or UV sensitive cells.

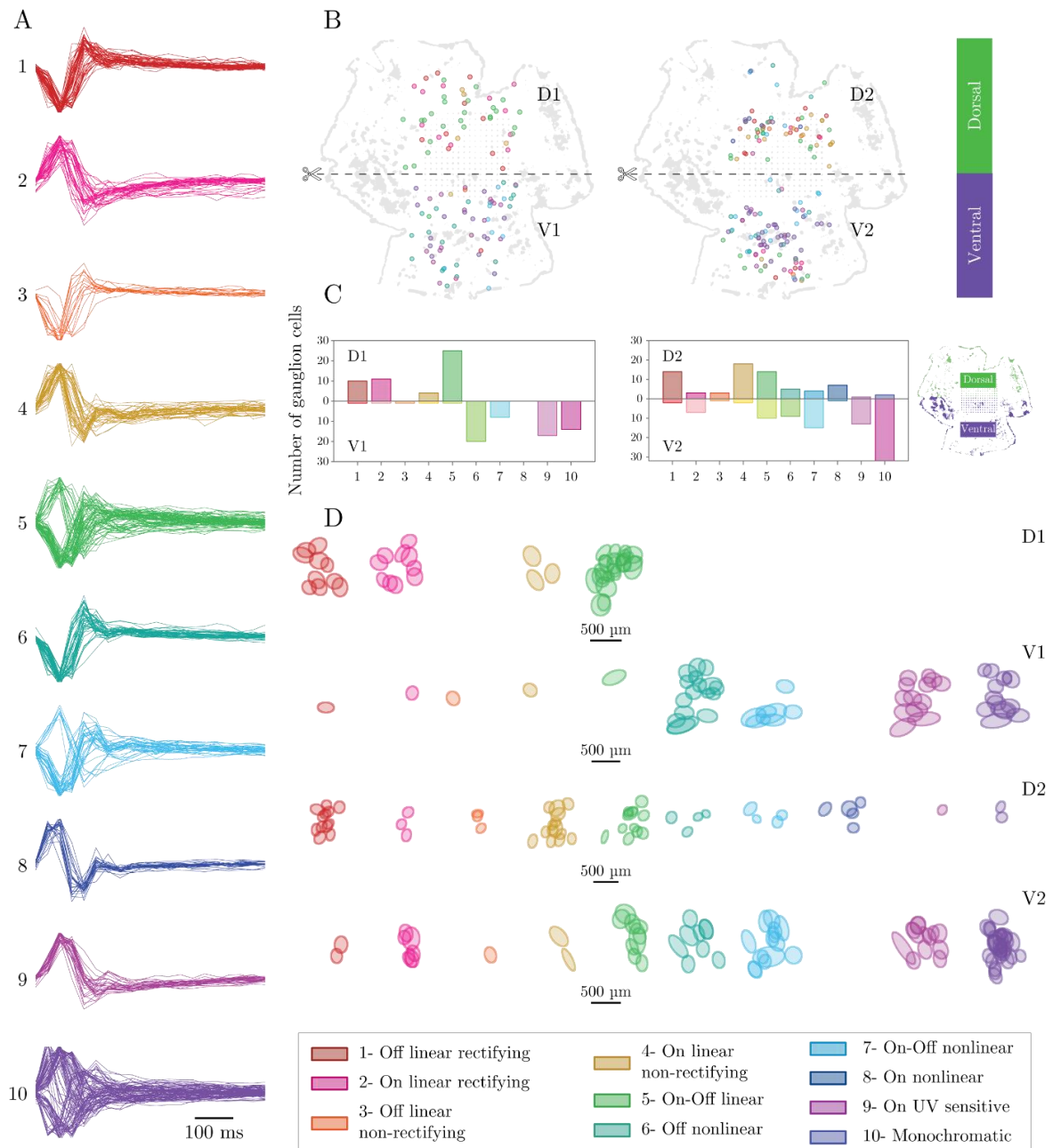


Figure 5.8. Receptive field properties of the chromatic integration classes. A. Temporal components of the spatio-temporal receptive field of the chromatic integration classes showed same response polarity for the chromatic integration stimulus and the flickering white noise stimulus. The nonlinear cells (6-8) showed more biphasic filters compared to the linear cells. B. Distribution of the chromatic integration classes along ventral-dorsal axis of the retina. For each retina, the data for ventral and dorsal retina were acquired in a separate experiment. Here, the schematic view of the retina was constructed from an image of the retina taken after the experiment. As shown in C, the UV sensitive cells (9 and 10) and the Off and On-Off nonlinear cells (6-7) were more frequent in the ventral retina.

D. Receptive field distribution of the ganglion cells from the experiments shown in A and B. Some of the chromatic integration classes showed relative tiling. However, due to limited number of the cells classes per recording, it is not possible to draw a definitive conclusion about the receptive field tiling for all the cell types.

For the On nonlinear cells, we had similar problem. We only found them in one out of four pieces (D2) and they were all located at the dorsal part of the retina. Therefore, our (underdeveloped) conclusion from this measurement was that the UV sensitive cells were more frequent in the ventral retina. Off and On-Off nonlinear cells were also found more in the ventral part. This could potentially explain the shift we observed in their contrast at the crossing point where these nonlinear cells showed more sensitivity toward UV compared to the linear cells (figure 4.11.A). The distribution of the receptive field areas from the ganglion cells presented in the figure 5.8.B is shown in the figure 5.8.D. As mentioned before, some experiments lack certain chromatic integration classes. Moreover, for other classes we had very few (fewer than 4) cells per class. This makes the measurement for the receptive field overlap and tiling not reliable.

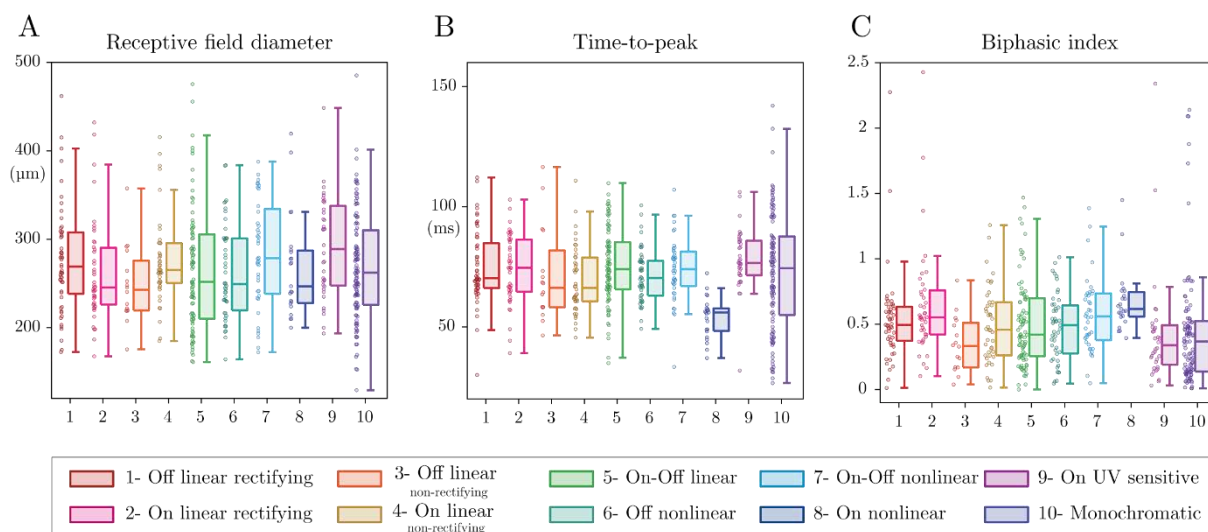


Figure 5.9. Receptive field properties of the chromatic integration classes. A. Measurement of the receptive field diameter of the chromatic integration classes showed no clear differences between the groups. B. Time-to-peak calculation from the temporal filters of the receptive field showed faster response kinetics for the On nonlinear cells. C. Measurement of the biphasicness of the filters showed that the linear rectifying and nonlinear cells were more biphasic than the rest of the chromatic integration classes.

However, for some classes, there were enough cells in one recording that could potentially indicate the receptive field tiling or lack thereof it (e.g. the Off nonlinear cells in D2 and V2 or the Off linear rectifying cells and On linear non-rectifying in all retinas showed tiling). The On-Off linear cells, even though very frequent in our recordings, did not show clear tiling. This goes along with our previous

claim that there might be more than one type of On-Off cells in this class (see 4.5.2). Taken together, for both the location measurements and the tiling, more experiments with the whole retina (instead of half) and stronger recoding methods (array with higher number of electrodes) are needed to sample the retina more efficiently.

5.6.3. Receptive field properties across the population

For the last part of our receptive field analysis, we looked into the properties such as diameter, time-to-peak and the biphasicness of each receptive field. Our measurement of the receptive field diameter showed no specific differences among the chromatic integration classes (figure 5.9.A). For each class, we had cells with relatively big receptive field and cells with rather small ones. Among the linear cells, the Off linear rectifying cells had relatively larger receptive fields. For the nonlinear cells, the On-Off cells showed bigger receptive fields. Therefore, we were not able to separate any classes from the rest based on the receptive field diameter.

Next, we measured the time-to-peak from the temporal component of each receptive field (see methods). This measurement showed how fast the ganglion cells integrate their inputs and it corresponds to the kinetics of their response. Here, we found that the On nonlinear cells showed faster time-to-peak compared to rest of the cells (figure 5.9.B). This is consistent with the latency measurement for the strongest response of the cell to the chromatic integration stimulus. The Off and On rectifying cells showed slight delay in their time-to-peak, however, this difference is not significant from the other linear cells.

In our last measurement, we checked the biphasicness of the temporal components of the receptive fields. The biphasicness measurement, not only shows the sensitivity of the cell to the temporal frequency of the stimulus (Zaghloul et al., 2007), but also, it indicates the influence of the receptive field surround on the cell's output (Sengpiel et al., 1997; Ozeki et al., 2009; Rubin et al., 2015). To measure the biphasicness of each filter we, defined a biphasic index as the absolute of the second peak divided by the first peak (see methods). Monophasic cells have biphasic index close to zero and biphasic cells close to or bigger than one. The comparison of the biphasic index among all the chromatic integration classes showed more biphasic responses from the nonlinear cells. The On nonlinear cells showed clear biphasicness in their temporal filters. Similar to the nonlinear cells, the On and Off rectifying cells showed more biphasic responses. The linear non-rectifying cells, on the other hand, had more monophasic filters.

Taken together, our measurements from the properties of the receptive field showed no clear differences in the receptive field size, faster time-to-peak for the On nonlinear cells and more biphasic responses for the nonlinear and linear rectifying cells.

6.

Discussion

In the nervous system, neurons typically receive multiple inputs that they integrate to generate their output. The functional roles of the neurons are defined based on the way they integrate their inputs. In other words, the functional characteristics of the neurons depend on the computations they do during the integration of the inputs. To understand each neuron and its role in the nervous system, it is important to study their signal integration properties. This means investigating how each neuron encodes or amplifies relevant features of the input while suppressing the non-relevant features. In the visual system and from the first synapse of the retina, the visual inputs are separated into different signals. At each level of the retina and the visual system, these input signals are being integrated by different neurons. In this thesis, we studied the mechanisms of chromatic signal integration in mouse retinal ganglion cells. The retinal ganglion cells are suitable models for studying signal integration. The photoreceptors of the retina separate the light into different chromatic signals and the ganglion cells receive these separated inputs through different bipolar cells. Having two types of chromatic inputs to the ganglion cells is essential for studying signal integration. We focused on the chromatic integration aspect of the ganglion cells, because this way we could study not only the signal integration in the retina, but also we could approach the chromatic processing properties of the retina.

We started this project by developing techniques that allowed us to study chromatic signal integration in the mouse retina. We developed a new projection system (chapter 3) to stimulate mouse s- and m-cones independently. Moreover, we improved upon the previous multi-electrode recording system of our lab by introducing and establishing the perforated multi-electrode recording method for measuring the outputs of the ganglion cells. Alongside these experimental techniques, we introduced the chromatic integration stimulus (figure 4.1) as a new stimulation approach to investigate chromatic integration in the mouse retina. With this stimulus, we asked whether retinal ganglion cells integrate s-cone and m-

cone inputs linearly or nonlinearly. In this stimulation paradigm, we stimulated the retina with combinations of green and UV with opposing contrasts. We found ganglion cells that integrated green and UV stimuli linearly. For these linear cells, the responses induced by the UV stimulus were cancelled out by the opposite green stimulus (chapter 4.3.1). Furthermore, we found two types of responses for the linear cells: some do not respond to non-preferred stimuli (figure 4.4) while others reduced their activity below the spontaneous firing rate (figure 4.5).

In addition to linear cells, we found populations of ganglion cells that integrate chromatic stimuli nonlinearly. Nonlinear ganglion cells showed clear responses to every applied combination of green and UV contrasts (chapter 4.4.2). We classified the nonlinear cells based on the polarity of their responses. Each class of nonlinear cells showed unique type of responses to the chromatic integration stimulus. The Off nonlinear cells showed strong responses when the opposing contrast of green and UV were equally effective (crossing point) (figure 4.6). Moreover, these cells did not rectify the non-preferred stimulus. The On-Off cells showed similar nonlinear integration properties as the Off nonlinear cells but they showed different sensitivity to green and UV colors (figure 4.7). The On nonlinear cells had suppressive nonlinear integration, which was in contrast with the Off and On-Off nonlinear cells. These cells, suppress their activity below spontaneous activity when they face the equally effective stimulus with opposing green and UV contrasts (figure 4.8).

To understand the mechanisms of chromatic signal integration in the retina, we simulated the potential chromatic integration circuitry with the nonlinear-linear-nonlinear cascade (NLN) model. We simulated a ganglion cell that receives two types of chromatic inputs (chapter 5.1). With the NLN model, we were able to simulate the integration properties of the linear cells. For the nonlinear cells, we could simulate their responses at the crossing point of the green-on, UV-off and green-off, UV-on curves. However, for the Off and On nonlinear cells, we were not able to simulate the suppressions that were observed in their chromatic integration curves (figure 4.6 and 4.8). In the NLN model, we only considered the receptive field center and the excitatory cells of the retina. Therefore, the failure of the model in replicating nonlinear integration persuaded us to consider the involvement of other elements of the retina such as the receptive surround and the inhibitory circuitry of the retina. Therefore, we tested the contribution of the receptive field surround to the chromatic integration properties of the ganglion cells. We designed a new stimulus that stimulated the receptive field center similar to the chromatic integration stimulus while it did not effectively stimulated the surround (chapter 4.7.1). By reducing the influence of the surround on the center, we observed that most of the linear cells remained linear, the nonlinear cells, on the other hand, became linear. Therefore, we concluded that the receptive field surround plays an important role in the nonlinear chromatic integration properties of nonlinear ganglion cells.

6.1. Linear chromatic integration

The majority of our recorded ganglion cells showed linear chromatic integration in response to the chromatic integration stimulus (408 out of 543 recorded ganglion cells). We found linear integration among On, Off and On-Off ganglion cells. In this section, we first discuss the potential circuitry of the linear chromatic integration and then we discuss the rectification properties of the linear cells.

First: Potential circuitry of the linear chromatic integration:

Previous studies about spatial integration reported linear spatial integration among the ganglion cells of cat (Enroth-Cugell and Robson, 1966), rabbit (Caldwell and Daw, 1978; Hamasaki et al., 1979; Famiglietti, 2004), guinea pig (Demb et al., 1999; Zaghoul et al., 2007) and monkey (de Monasterio, 1979; Petrusca et al., 2007; Crook et al., 2008). However, little is known about the linear chromatic integration. Based on our data and previous findings about the linear spatial integration, we propose two different scenarios for the linearity of chromatic integration. It is important to mention that achieving linearity among neurons may seem simple at first, but in fact, is rather complicated. This is due to the nonlinear nature of neurons and synaptic transmission (Katz and Miledi, 1967). We propose two different scenarios, which might cause the linear chromatic integration:

In the first scenario, the chromatic integration happens in the outer retina either at the synapses between the photoreceptors and bipolar cells or directly at the photoreceptors. Many mouse photoreceptors co-express s- and m-opsins (Applebury et al., 2000). This means that these s+m-cones respond to both green and UV stimuli. Here, we propose that these cones integrate the green and UV colors linearly. These cones similar to most photoreceptors have depolarization in response to Off stimuli and hyperpolarization to the On stimuli. When a green-on, UV-off stimulus is shown to an s+m-cone, the green-on activates the m-opsins and induces more hyperpolarization. The UV-off, on the other hand, reduce the isomerization of the s-opsins, which leads to more depolarization. If the green-on and UV-off are equally effective, the amount of the hyperpolarization will be similar to the depolarization. For the inverted contrast combination (green-off, UV-on), the s-opsin would cause hyperpolarization and the m-cone depolarization. Therefore, these co-expressing cones could potentially cause linear integration. The bipolar cells and the ganglion cells would just receive the integrated signals from these cones and show no response at the crossing point of green-on, UV-off and green-off, UV-on curves.

Another possible location in the outer retina that could cause linear chromatic integration is at the synapse between the cones and bipolar cells. In this case, the bipolar cell is not cone-selective and connects to both s- and m-cones. The depolarization and hyperpolarization of the s- and m-cones that is caused by the chromatic integration stimulus would be summed linearly by this bipolar cell. Thus, no activation would be observed at the crossing point of the green-on, UV-off and green-off, UV-on curves. In this case, the ganglion cell receives the integrated signals from bipolar cells. Previous studies about the bipolar cell's connectivity to the photoreceptors showed that many bipolar cells are indeed

non-selective (achromatic) and they receive inputs from both s- and m-cones (Haverkamp et al., 2005; Euler et al., 2014; Behrens et al., 2016).

Taken together, in the first scenario, we propose that the linear integration takes place in the outer retina. Here, either the co-expressing (s+m-cones) cones or the non-selective bipolar cells integrate the chromatic inputs linearly and the ganglion cells receive the linearized signal from the bipolar cells.

The second scenario takes place in the inner retina at the synapses between the bipolar and ganglion cells. This scenario is feasible if the outer retina does not linearize the chromatic inputs. This could be the case when the bipolar cells are cone-selective and receive inputs from either s- or m-cones. Moreover, it is possible that a non-selective bipolar cell connects to one type of cones more often than the other cone type. In other words, the bipolar cell does not sample the s- and m-cones equally. This would cause a bias to the s- or m-cone inputs. In the periphery of the primate retina, using multi-electrode recording and small-localized stimuli, it was reported that there is a weak but significant bias among the midget cells (Field et al., 2010). In the center, this bias caused higher chance of weighting one type of cones (l- or m-cone). This bias joined with the mixed (l+m) surround has been reported to generate color opponent responses in the peripheral midget cells. Therefore, it is possible that the non-selective bipolar cells of the mouse retina connect to s- and m-cones in a way that leads to a bias to one type of inputs. For simplicity, for the rest of discussion, we label both the cone-selective bipolar cells and the non-selective bipolar cells with bias to one type of cones as chromatic bipolar cells. Now, if the ganglion cell receives different chromatic signals from the chromatic bipolar cells, the linear integration should be done at the synapse between the bipolar cell and the ganglion cells. Here, we propose three different ways that the output of the chromatic bipolar cells can be integrated linearly by the ganglion cells.

One way to achieve linear integration with the inputs from chromatic bipolar cells is that the synapses of these cells are linear. The ganglion cells receive chromatic signals from different chromatic bipolar cells and integrate these signals linearly. For example, a ganglion cell could receive input from green sensitive Off bipolar cells and UV sensitive On bipolar cells. At the crossing point, when the green-on, UV-off stimulus is shown, the green sensitive bipolar cells hyperpolarize and the UV sensitive cells depolarize their membrane potential. The ganglion cell averages the hyperpolarization and the depolarization and does not change its firing rate. For the inverted green-off, UV-on stimulus the green sensitive bipolar cells show depolarization and the UV sensitive cells have hyperpolarization. The ganglion cell again would average these inputs. For this case to work, it is important that the synapse of the bipolar is linear. This means that the bipolar cell should have similar levels of hyperpolarization and depolarization. However, studies from the synapses of the bipolar cells have reported that this is not the case for most bipolar cells. These studies showed that most bipolar cells have nonlinear synapses with different levels of hyperpolarization and depolarization (Katz and Miledi, 1967). This led us to suggest other ways that linear chromatic integration could be achieved.

The second way to achieve linear chromatic integration with chromatic bipolar cells is with an intervention of an amacrine cell. In this case, the bipolar cells are chromatic and they show some nonlinearity at their synapses. Their output becomes linear through crossover inhibition (Roska and Werblin, 2001; Molnar et al., 2009; Werblin, 2010). In the crossover inhibition, the output of an Off cell is being linearized with an amacrine cell that is activated by an On bipolar cell. Similarly, an On bipolar cell could be linearized through crossover inhibition from an Off bipolar cell. In our case here, the On and Off bipolar cells are chromatic. At the crossing point, when the green-on, UV-off stimulus is shown, the green sensitive On bipolar cell and the UV sensitive Off bipolar cells are activated. The On bipolar cell then activates an amacrine cell, which would linearize the output of the Off bipolar cell. For the inverted stimulus, the ganglion cell should also receive inputs from chromatic bipolar cells with opposite polarity (green sensitive Off bipolar cell and UV sensitive On bipolar cell in our example here).

The third way to achieve linear integration for a ganglion cell that receives inputs from the chromatic bipolar cell is through inhibition that is induced by a suppressive surround. In this case, the ganglion cell has an antagonistic and potentially opponent center-surround receptive field (Rodieck, 1965; Dayan and Abbott, 2001). Here, the surround is activated with opposite color and suppresses the center. Similar linear center-surround interactions have been reported for functions such as local contrast enhancement and redundancy reduction (Srinivasan et al., 1982; Atick and Redlich, 1993; Dan et al., 1996; Tokutake and Freed, 2008). For example, a ganglion cell with a green-off center can have a UV-on surround. When the green-off, UV-on stimulus is shown to this cell, the center is activated by a green-off stimulus and the surround with UV-on stimulus. The surround would suppress the center, which leads to no positive response from the ganglion cells.

Our experimental data from the chromatic grating stimulus showed that reducing the influence of the receptive field surround linearize the output of the center. This means that the center is potentially linear and the nonlinearity is caused by the surround. Our data could not support the case with antagonistic surround. This is because in this case reducing the effect of the surround should lead to nonlinear integration in the center. For the remaining possibilities of the suggested circuitry of the linear integration (linearization in the outer retina or crossover inhibition), we were not able to support one model over the others with our experimental data. However, more experiments such as pharmacological probing of inner and outer retina would be helpful to get more information about the mechanisms of linear integration.

Taken together, we proposed two different mechanisms for the linearity of chromatic integration in the inner and the outer retina. In the outer retina, linear integration could be done by co-expressing cones or non-selective bipolar cells. However, for the cone-selective bipolar cells and the bipolar cells with bias to one type of cone inputs, the linearity could be achieved through crossover inhibition or antagonistic and potentially opponent center-surround interactions.

Based on our simulations of the linear integration, it seems that the ganglion cell's nonlinearity does not influence the linearity of the chromatic integration (chapter 5.1). Instead, the nonlinearity of the ganglion cell defines the shape of the integration curves and the way each cell encodes the preferred or non-preferred stimulus. The ganglion cell nonlinearity, thus, describes the difference between the rectifying and non-rectifying linear cells. For non-rectifying cells, each ganglion cell behaves linearly by increasing and decreasing its activity relative to the spontaneous activity. For rectifying cells, each ganglion cell's nonlinearity could be linear rectifying, rectifying quadratic, or even rectifying square root functions.

Second: rectification properties of linear cells

Among the linear cells, we found some cells that showed rectifying responses and others that showed non-rectifying responses. It is worth mentioning that in the retina, only the ganglion cells and few types of amacrine cells generate spikes. The spike generation is in its nature a rectifying process. This is because of how the voltage sensitive sodium channel works by having a threshold for firing action potentials (Katz and Miledi, 1967). A rectifying ganglion cell starts to fire if the inputs from the bipolar cells are strong enough to pass its spiking threshold. If the bipolar cells are not activated because of a weak or non-preferred stimulus, the ganglion cells will not fire. However, this is not the case for the non-rectifying cells. These cells suppress their activity below their spontaneous level when they face non-preferred stimuli. We hypothesize two different mechanisms for these cells. One is the direct influence of the bipolar cells vesicle release on the output of the ganglion cells. In this case, both decrease and increase of the bipolar cells activity changes the behavior of the ganglion cell respectively. This is possible if the ganglion cell has high spontaneous activity. The constant release of vesicles from the bipolar cell generates the spontaneous activity and the increase in the release rate generates higher firing rate for a ganglion cell. The decrease in the vesicle release of the bipolar cell that is induced by the non-preferred stimulus would then decrease the spontaneous activity of the ganglion cell. Another possible mechanism for the non-rectifying cell is that the inhibitory inputs from the amacrine cells suppress the activity of the ganglion cell when they face the non-preferred stimulus. This scenario is similar to crossover inhibition where the non-preferred stimulus influences the integration of the preferred stimulus through an amacrine cell (Molnar et al., 2009; Werblin, 2010). Moreover, receptive field surround might as well have similar effects on the activity of the ganglion cells. When the inhibition from the non-preferred stimulus is stronger than the excitation induced by the preferred stimulus, the ganglion cell's activity would go below its spontaneous activity. In this case, the ganglion cell may or may not have high spontaneous activity because the suppression affects the excitatory inputs of the cell. From our experiments, we observed that the non-rectifying cells had high spontaneous activity (figure 4.11.E). Moreover, our experiment with the chromatic grating showed that for most non-rectifying cells, the surround does not affect their chromatic integration. Thus, from our data, we cannot rule out any of the mentioned hypotheses and more pharmacological inspections

of the circuitry between bipolar and amacrine cells are needed to describe the integration mechanisms of non-rectifying cells.

6.2. Nonlinear chromatic integration

In our experiments, nearly 20% of the recorded ganglion cells showed nonlinear chromatic integration. We found nonlinear integration among Off, On and On-Off cells, however, each of these classes showed unique responses. The nonlinear integration of the Off and On-Off nonlinear cells were similar to the nonlinear integration of the spatially nonlinear (Y-like) ganglion cells (Enroth-Cugell and Robson, 1966; Demb et al., 1999; Zaghloul et al., 2007). The On nonlinear cells on the other hand, showed nonlinear integration with suppression at the crossing point. This separation of nonlinearities based on the polarity of the response suggests different mechanisms that are involved in the nonlinearity of chromatic integration. For all the nonlinear cells, we found that reducing the influence of the receptive field surround linearized the chromatic integration. This shows that the receptive field center of the nonlinear ganglion cells are likely to be chromatically linear and the surround makes these cells nonlinear. We observed these nonlinear effects in the full field stimulus (chromatic integration stimulus) where both center and surround were being activated. Surround inhibitory effects are created at both synapses of the retina. The horizontal cells inhibit the photoreceptors output to the bipolar cells in the outer retina (Mangel, 1991; McMahon et al., 2004; Duebel et al., 2006). Amacrine cells inhibit bipolar cell terminals and ganglion cell dendrites in the inner retina (Cook and McReynolds, 1998; Dacey et al., 2000).

For the nonlinear chromatic integration, we speculate that the surround effects are mediated by amacrine cells. This is because we observed at least two different types of nonlinearities. For the Off and On-Off cells, we saw the nonlinear effects as an increase in the responses of the ganglion cells to the equally effective stimuli. For the On cells, on the other hand, we saw suppressive nonlinear responses. Since mouse retina has only one type of horizontal cells (Weiler et al., 2000; Thoreson and Mangel, 2012), it is unlikely that they can generate these two different types of nonlinearities. The surround effects that are found in this thesis were nonlinear while it seems that the signal processing of the horizontal cells is linear (Shapley, 2009). Previous studies showed that horizontal cells are likely to have linear integration properties (Tranchina et al., 1981; Baccus et al., 2008). Therefore, we only consider the amacrine cells to be involved in the nonlinearity of the chromatic integration.

The classic view of an antagonistic center-surround receptive field is that the stimulation of the center with the preferred stimulus activates the cell. Further, the cell responds to the stimulation of the surround with the opposite stimulus (Kuffler, 1953; Hartline and Ratliff, 1957; Hubel and Wiesel, 1962; Westheimer, 2004). Since in each step of our stimulus, we presented opposing contrasts at the same

time, the center responds to the preferred color contrast (e.g. green-on) while the surround responds to the opposite color contrast (e.g. UV-off). For the center of a nonlinear cell, there is a combination of contrasts that cancels each other out (linear center). For the surround, on the other hand, no contrast combinations cancel the response (nonlinear surround). This interaction between the center and surround causes the cell to respond to all the contrast combinations, even at the equally effective stimulus. For the Off and On-Off nonlinear cells, the surround is activated and generate the response. For the On nonlinear cells, the activation of the surround leads to the suppression of the spontaneous activity of the cells. This difference is potentially due to the involvement of different amacrine cells for the Off, On-Off and On ganglion cells. We propose two different scenarios for the nonlinear chromatic integration.

In the first scenario, the receptive field center is linearized by an amacrine-mediated crossover inhibition, but the surround has nonlinear effects on the center by inhibiting that amacrine cells. In other words, the inhibition from the surround inhibits the crossover inhibition. As a result, when the surround is not effectively stimulated, the center becomes linear and when the surround is stimulated effectively (full field stimulus), the chromatic integration becomes nonlinear. This could explain the nonlinearities observed in the Off and On-Off nonlinear ganglion cells. However, it fails to provide solution for the suppressive nonlinearities that was observed in On nonlinear cells. The mechanism of inhibition of inhibition or disinhibition has been reported previously for different nonlinear functions of the retina (Werblin, 2010, 2011; Franke and Baden, 2017; Franke et al., 2017). The crossover inhibition is local and involves mostly the glycinergic narrow field amacrine cells while the surround inhibition is likely caused by the GABAergic wide-field amacrine cells. Therefore, it is possible to test this proposed model for the nonlinearity of the chromatic integration with careful pharmacological experiments.

In the second scenario, the receptive field surround only induces the nonlinearity. Here, the surround does not counter-act the center linearly and has nonlinear effects on the center. For this model to support our experimental data, it is important for the center to be linear. If the nonlinearities are caused by the surround, the center is likely to be linear. However, if the center is nonlinear itself and the surround only modifies this nonlinearity then reducing the effect of the surround would not make the integration linear. It is possible that the linearity of the center here is achieved in the outer retina (s+m-cones or non-selective bipolar cells) and the nonlinear effects of the surround happen in the inner retina. Since the surround effects on the center are likely to be inhibitory, the center receives only suppression. This makes the cell to become suppressed with firing rates below the spontaneous activity. We observed such suppressed nonlinearity in the output of the On nonlinear cells (figure 4.8).

Taken together, we proposed two different models to explain the nonlinearities of the chromatic integration. The assumption for these models is that the linear integration of the center takes place in the inner retina and the surround has nonlinear effects on the center. In the first case, we proposed that the surround has nonlinear influence on the center through disinhibition mechanisms. Therefore,

the inhibition from the surround inhibits the crossover inhibition of the center and makes it nonlinear. In the second case, we proposed that the center is chromatically linear and the surround is nonlinear and inhibits the center. The first case could potentially explain the nonlinearities that were observed for Off and On-Off nonlinear cells. The second case, on the other hand, could explain the suppressive nonlinearities of the On nonlinear ganglion cells.

Finally, it is worth mentioning that, in addition to the suggested scenarios for nonlinear integration, it is possible to have nonlinear integration in the center. This is imaginable when the ganglion cells receive chromatic inputs from the cone-selective (chromatic) bipolar cells. However, our experiment with the chromatic grating stimulus does not support this case. This is because, if the center is nonlinear and is not linearized by the surround, reducing the effects of the surround would not affect the center. Therefore, these cells would show nonlinear integration properties in response to both chromatic integration stimulus and chromatic grating stimulus. To check for the possibility of the chromatically nonlinear center, more targeted experiments about the chromatic integration in the receptive field center and surround are needed.

6.3. Functional roles of chromatic linearity and nonlinearity

What could be the potential functional roles of the discovered linear and nonlinear chromatic integration? Since this study is one of the first studies to characterize the nonlinearity of chromatic integration, our knowledge about the functional roles of nonlinear chromatic integration is rather limited. However, linear and nonlinear responses have been described before in the retina. Response properties like motion detection (Barlow and Levick, 1965; Fried et al., 2005; Lee and Zhou, 2006), object-motion detection (Olveczky et al., 2003; Baccus et al., 2008), local edge detection (Levick, 1965; van Wyk et al., 2006) and many other computation features of the retina (Gollisch and Meister, 2010) have been attributed to nonlinear signal integration of the retinal ganglion cells. For most of these studies, the spatial nonlinearities of the ganglion cells provide the particular functionality (Gollisch, 2013) by making the cells sensitive to different spatial structure in the input image. The general idea about nonlinear features in the retina is that they allow different types of the ganglion cells to process different aspects of the input light.

By comparing the discovered chromatic integration features to the spatial integration, we can speculate about the different roles of the chromatic linearity and nonlinearity. One possible role of a chromatic nonlinear integration might be that it provides information about the heterogeneity of the chromatic stimulus. For example, if a certain part of the visual scene has opposite contrasts of green and UV colors with similar brightness, the chromatically linear cells report the average of the two colors and not respond to it. The nonlinear cells, on the other hand, detect these combinations of the colors. Since the chromatically nonlinear ganglion cells, showed different sensitivity to green and UV input, it is imaginable that they are involved in color processing. Since most retinal models of color processing is

based on the opponent ganglion cells (Dacey, 1996; Dacey and Packer, 2003), it is challenging to directly connect nonlinear chromatic integration to color processing.

Beyond the nonlinear processes, some functions of the retina depend on the linear integration of inputs. It has been suggested that functions such as enhancement of edges, distinguishing between contrast and luminance and averaging light across the receptive field (Shapley, 2009; Werblin, 2010) depend on linear signal integration in the ganglion cells. For the chromatically linear cells, it is possible that the function of these cells does not depend much on the chromatic properties of the stimulus. For example, a direction selective cell that encoded the direction of the stimulus may not be interested in the chromatic features of the stimulus. Moreover, linearity of the chromatic integration could potentially help the ganglion cells to separate the luminance from the color information of the input image. For the linear chromatic integration similar to the nonlinear integration very little is known and therefore more studies are needed to understand the functional roles of these nonlinearities in the retina.

6.4. Inference of integration nonlinearities with iso-response measurements

In this project, we aimed at studying the chromatic signal integration nonlinearities of the ganglion cells. However, as shown in our modelling study (chapter 4.6), the signal integration of a ganglion cell possibly takes place before the spike generation nonlinearities of the cells. In the retina, same as in our model, the signal integration happens at the synapse between the bipolar cells, amacrine cells and the dendrites of the ganglion cell. Therefore, the signal integration happens before the spike is being triggered at the axon of the ganglion cell. Thus, what we measured in this project was the integration nonlinearities that passed through the spike generation nonlinearities and not the integration nonlinearities alone. One way to overcome this limitation is to directly measure the integration nonlinearities at the synapses of the inner retina. To do so, one needs to directly record from the bipolar cell synapse and the dendrite of the ganglion cell and measure the output of the bipolar cell and the inward currents of the ganglion cell. However, this way we lose the possibility of recording many neurons and it might be difficult to find all the ganglion cells with different chromatic integration properties. It is possible to overcome these limitations and use multi-electrode recordings to simultaneously record many cells and at the same time access the integration nonlinearities of different ganglion cells with the method of iso-response measurements. This approach has been successfully used for accessing the nonlinearities of spatial integration in the retinal ganglion cells of the salamander (Bolinger and Gollisch, 2012; Takeshita and Gollisch, 2014). In the iso-response measurement of chromatic integration, we would randomly stimulate the retina with diverse combinations of green and UV contrasts with very small changes per contrast steps. We then look at the stimulus combinations that yield identical neuronal responses and try to fit a model for all of the stimulus combinations. The shape of the fitted model for the entire iso-response curve corresponds to the chromatic integration nonlinearity of each ganglion cell. Further, it is possible to use closed-loop experiments to search for

the contrast combinations that lead to the same firing rate. Here, one can apply the iso-response measurements specifically to the receptive center (Bolinger and Gollisch, 2012) or surround (Takeshita and Gollisch, 2014) to dis-entangle the nonlinearities induced by the center or surround.

Taken together, the chromatic integration stimulus that was used in this study gives us important insights about chromatic integration. With this stimulus, we were able to show whether the retinal ganglion cells integrate their chromatic inputs linearly or nonlinearly. Moreover, we observed different types of responses among both linear and nonlinear cells. From these responses and with the help of the chromatic grating stimulus, we were able to speculate about the circuitry of chromatic integration. Therefore, we believe that our approach here with the chromatic integration stimulus has led us to new and interesting findings. Furthermore, our finding about the chromatic integration properties of the ganglion cells form the foundation for further studies. Therefore, the next logical step will be to directly access the integration nonlinearities with iso-response measurements. Moreover, direct iso-response measurement from the receptive field center and surround with closed-loop experiments will help us to get a better understanding about the influence of receptive field surround to overall integration properties of the ganglion cells.

6.5. Comparison to other color processing studies

Chromatic processing has been studied extensively in the primate retina with trichromatic vision. The main focus of these studies was on the function of chromatic opponent cells (Dacey, 1999; Dacey and Packer, 2003). Previous reports showed that the midget pathway in the primate retina shows l- versus m-cone opponency with antagonistic center-surround structure (classical opponency) (Wiesel and Hubel, 1966; Dacey, 1996; Diller et al., 2004). Here, the opponency of the surround is induced from the horizontal cells (Dacey et al., 1996; Crook et al., 2011). In addition to l- vs m-cone opponency, the blue versus yellow opponency has been reported. This type of opponency was found in the small-bistratified ganglion cell which receives input from the Off bipolar cell that contacts m- and l-cones (yellow) as well as On bipolar cell that selectively contacts s-cones (blue) (Dacey and Lee, 1994; Packer et al., 2010). In the dichromatic mammals with a gradient of opsins in the retina such as guinea pig (Yin et al., 2009), ground squirrel (DeVries et al., 2006; Li and DeVries, 2006) and mouse (Breuninger et al., 2011; Chang et al., 2013) chromatic opponency has been reported. For these dichromatic mammals, the chromatic opponency around the center of the retina is generated through an amacrine-mediated surround. At the edges of the retina of the guinea pig, a rare population (nearly 1%) of ganglion cells showed classical horizontal-mediated center-surround opponency (Yin et al., 2009). Thus, for animals with regionalized opsin distribution, the diversity of color processing depends mostly on the amacrine cells that sample different regions of the retina (Chang et al., 2013). Beyond chromatic opponency and its relevant mechanisms in the retina, not much is known about chromatic signal integration of the retinal ganglion cells. Thus, this thesis put forth a new approach for studying color

processing in the retina. In terms of mechanisms, we proposed the role of amacrine cells in mediating nonlinear chromatic interactions. This is potentially similar to the way mouse color opponent cells respond to green and UV colors.

It is important to mention that, in our study we rarely found cells with opponent characteristics. One reason for this could be the design of our chromatic integration stimulus. Because this stimulus showed green and UV color with nearly equal opposing contrast, we think that this stimulus could not stimulate the opponent cells effectively. Another reason for having very few opponent cells in our recordings was our sampling of the ganglion cells. Since we cut the retina in two halves and generally recorded from the center of each half, we were not able to efficiently sample the mid-region of the retina. This mid-region is the region with the most color opponent retinal ganglion cells (Chang et al., 2013). Taken together, previous studies about color processing have focused on the color opponency as the main mechanisms of color processing in the retina. These studies showed both horizontal-mediated and amacrine-mediated opponency in the retinas of primate and dichromatic mammals. Here, we focused mainly on the chromatic integration and we rarely found opponent cells in our recording. This could be due to our design of the stimulus or our sampling bias in our recordings. Therefore, we believe more experiments with both the chromatic integration stimulus and the classical color exchange stimulus (Lee et al., 1989; Shapley and Hawken, 2002; Denman et al., 2017), which was used to find color opponent cells, will help us to find the relation between the chromatic integration and color opponency in the retina.

6.6. UV stimulus and the mouse retina

To study mechanisms of chromatic signal integration in the mouse retina, we used stimuli that had contrast combinations of green and UV colors. Over the course of this project, we observed that the majority of our cells showed higher sensitivity to UV inputs (figure 4.10.A). Moreover, close to 30% of our recorded cells showed a strong bias toward the UV stimulus (on UV sensitive cells and UV monochromatic cells). This is consistent with previous studies about mouse s- and m-cone distributions, which reported 95% of mouse cones are co-expressing (s and m opsins) and 5% of them are genuine s-cones (Rohlich et al., 1994; Applebury et al., 2000; Haverkamp et al., 2005; Nikonov et al., 2006). Furthermore, a study of cone-mediated responses in the mouse retina showed that ganglion cells have faster and more robust responses when the retina is being stimulated with UV stimuli (Wang et al., 2011). We also observed fast temporal integration of stimuli in our time-to-peak measurement from the temporal component of the receptive fields (figure 4.20). The range of the time-to-peak (50-60 ms) in our experiments was consistent with the data from the mentioned study (Wang et al., 2011). However, many previous studies of the mouse retina used the conventional projectors to stimulate the retina. This type of black and white stimulus could not drive the s-opsin strongly (Grubb and Thompson, 2003; Niell and Stryker, 2008; Umino et al., 2008; Baden et al., 2016).

Further, we found that nearly 20% of our data showed monochromatic responses with a strong bias for s-cone inputs. For these cells, it is possible that they receive inputs from bipolar cells that selectively connect to s-cones or m-cones. Previous studies in the mouse retina have reported that the type 1 bipolar cell is Off m-cone selective and type 9 is an On s-cone selective bipolar cell (Haverkamp et al., 2005; Behrens et al., 2016). It is possible that our UV sensitive monochromatic cells receive inputs mainly from these bipolar cells. However, Haverkamp et al. showed that the type 9 bipolar cell is distributed randomly in the mouse retina. This is in contrast with our measurement, which showed that most UV sensitive ganglion cells were found in the ventral retina (figure 4.19). A potential reason for this discrepancy could be that the dichromatic ganglion cells in the dorsal retina connect to other dichromatic bipolar cells in addition to the type 9 bipolar cell. It is worth mentioning that the type 9 is an On bipolar cell and there is no report of an s-cone specific Off bipolar cell. This could explain why we had only On UV sensitive cells and no Off or On-Off counterpart for these cells. For the monochromatic cells, on the other hand, we found both Off and On-Off UV responding cells. This means that other mechanisms such as surround suppression and other cells such as amacrine cells could be involved in the chromatic exclusive responses of our monochromatic ganglion cells. A similar example of chromatic sensitivity in specific region of retina without having a specific cone or bipolar cell type can be found in the fovea of primates. In the primate fovea, the s-cones are nearly absent (Curcio et al., 1991) and they appear in the region around the fovea. However, blue color perception is present in this region (Hibino, 1992; Calkins, 2001). Overall, similar to the previous studies (Breuninger et al., 2011; Wang et al., 2011; Chang et al., 2013), our study here shows the importance of s-cone signals in the output of the mouse ganglion cells. For UV sensitive and monochromatic cells, the connection to s-cone selective bipolar cells (type 9) or other chromatically inclusive mechanisms such as center-surround interactions could cause their monochromatic integration properties.

6.7. Classification of the ganglion cells beyond chromatic integration

In this thesis, we classified the ganglion cells based on their chromatic integration properties. This classification was based on the linearity or nonlinearity of chromatic integration, response polarity and rectification properties of each ganglion cell. Based on these criteria, we group the recorded ganglion cells in eleven separate groups. This number is smaller than the reported number of ganglion cells in the mouse retina. Previous studies reported nearly 40 different types of ganglion cells in the mouse retina (Baden et al., 2016). The main reason for the difference between our classification and the general classification of ganglion cells is that in our classification, we just focused on the chromatic properties of the cells using only the chromatic integration stimulus. As a result, many cells with specific functionality such as direction selective cells, orientation selective cells, edge detectors etc. were possibly assigned to the same chromatic integration class. Moreover, our stimulus was a full-field stimulus with no spatial structure and many of the mentioned cell types of the retina are responsive to spatial stimuli. Therefore, our analysis over-simplifies the responses of ganglion cells. Yet, for the

purpose of this thesis, it was effective enough to separate more than 90% of the recorded ganglion cells. Such simplified classification approaches have been previously used to study specific aspects of the retinal computations (Della Santina et al., 2013; Sabharwal et al., 2017). It is worth mentioning that most classification studies of the mouse ganglion cells have used black and white stimuli for their stimulation and did not consider UV stimuli. As our data and previous studies showed (Wang et al., 2011), the mouse retina is sensitive and rather optimized in encoding UV stimuli. Thus, matching our measured responses and our classification to previous classification studies of the retina would not be very easy. As a complementary to our classification, it is possible to use the same stimulus set as the previous classification studies and classify the ganglion cells. Then look at the chromatic integration properties of each cell type and try to match it to the classification. This comprehensive classification approach would help us to get a better understanding about the mechanism and role of the chromatic integration for the different ganglion cell types in the retina.

7.

Outlook

In this project, we studied linear and nonlinear chromatic integration in the mouse retina. We designed a new projection system and established a new stimulation approach to investigate chromatic integration in the mouse retina. We found both chromatically linear and nonlinear ganglion cells and we found that the receptive field surround influences the nonlinear integration of chromatically nonlinear cells. A significant part of this project and this thesis was devoted to the development and optimization of the projection system (chapter 3). In fact, the aim of chapter 3 is to provide a guideline for making the same projection system. From our experiments and other studies (Wang et al., 2011; Chang et al., 2013), it became clear that the mouse retina is very sensitive to UV light with specific cells dedicated to process UV stimuli. Thus, we think that using conventional projection systems for studying visual system in the mouse retina undermines the abilities of the mouse retina and influences our interpretations about different aspects of the mouse visual system. Since it is hard to find a commercially available projection system with UV LED and optimized UV-fusing optics, we hope that the technical parts of this thesis provide useful information for developing similar projection systems.

Beyond the projection system, we established a new approach for studying linearity and nonlinearity of signal integration. We looked for the linearity of integration by searching for a cancellation point of the two opposing stimuli. For this approach to work, two different stimuli should be defined as opposite of each other. In our case, we defined On and Off parts of each color as the two opposing stimuli (green-on, UV-off and green-off and UV-on). We presume that the same stimulation approach is possible in other stages of the visual processing and other sensory systems such as hearing.

Apart from the technical parts of this project, we address the question of chromatic integration using multi-electrode recordings and classify our cells into linear and nonlinear groups. Based on the

integration properties and polarity of the responses and rectification features, we classified the ganglion cells into 11 different groups. However, our classification approach was a practical approach and could not verify whether our classes are indeed specific ganglion cell types of the mouse retina. Therefore, the next possible step in this project would be to identify the ganglion cell type of each chromatic integration class. Based on the identity of each cell, one can access the anatomy of each cell and look at the connections of each cell to other cells of the retina. From the input and output of each cell, one can study the properties of the chromatic integration thoroughly. Another finding of this thesis is the role of the receptive field surround in the nonlinearity of the chromatic integration. Here, due to experimental limitation, we were not able to study the neuronal components of the surround. Although we speculated about the role of the amacrine cells in both linearity and nonlinearity of the chromatic integration, we could not report any specific amacrine cell type or specific retinal circuitry of the surround. This opens the way for more research about the receptive field surround and its role in chromatic integration. Thus, to understand the neuronal mechanisms of chromatic integration, it is important to study the receptive field surround and its influence on the center extensively.

Another possible direction for studying chromatic integration would be about the impact of the signals from the linear and nonlinear cells on higher visual areas. Which cells in the cortex receive information from linear cells and which cells from nonlinear cells? Do we find similar linearity and nonlinearity of chromatic integration in the higher visual areas? What is the behavioral impact of the linear and nonlinear cells? How much does each cell contribute to chromatically guided behavior? Do nonlinear cells contribute to color vision? Based on the output of this project, it is therefore possible to investigate the properties of the chromatic integration in the higher visual areas.

In this project, we used only the mouse retina. Although the mouse visual system is a well-studied model of vision (Huberman and Niell, 2011; Baker, 2013; Seabrook et al., 2017), many classical studies of color processing were done in the primate retina (Dacey, 1996, 1999; Dacey and Packer, 2003). An interesting step after this work would be to apply the measurements from this thesis to the primate retina. Since old world primates have trichromatic vision, the stimulus and the analysis need to be modified for trichromatic vision. Therefore, for the primate retina, similar to this project, one could search for linear and nonlinear chromatic integration. Moreover, one could study the relation between the chromatic integration and color-opponent responses of the ganglion cells. Finally, one could investigate the behavior impacts of the chromatically linear and nonlinear cells. Beyond the basic research aspects of this thesis, it is possible to consider some applications from the findings of the thesis. The linear and nonlinear processes that are described here could be used in the design of devices that are used to mimic the function of the retina. For example, the retina prosthetics aim to help the visually impaired patient to recover their vision. Our understanding about the functions of the retina could eventually help us to optimize the internal functions of these devices in a way that they can restore color vision as close as possible to the natural vision.

Closure

At beginning of this thesis, we aimed at studying mechanisms of the chromatic integration in mouse retina. We did so by developing a new projection system and establishing a new stimulation paradigm. We found that the mouse retinal ganglion cells integrate their chromatic inputs both linearly and nonlinearly. We found different types of responses for linear and nonlinear ganglion cells. For the nonlinear ganglion cells, we found that the receptive field surround influences the nonlinearity of their chromatic integration. From the technical point of view, our study provides new guidelines for developing a stimulation system that is more optimized for the mouse retina. Moreover, our stimulation approach and stimulus design could provide more information about investigating signal integration in the nervous system. Beyond that, our study here shows, on the one hand, new types of nonlinear processes in the retina and on the other hand, it provides new insights about the parallel processing properties of the retina. Furthermore, our study provides more evidence about the complexity of the interactions between the receptive field center and the surround. Our results, therefore, bolster the notion that the retina is not just a simple light sensor, but that it computes and processes complex features of the visual world. The identification of new response types in the retina could offer more information and insights about the signal encoding properties of the neurons. We hope that the technical and analytical parts of this project alongside its results pave the way for more interesting findings about the mechanisms of color processing and signal integration of the neurons in vision research and other areas of neuroscience.

Bibliography

- Hartline, H.K. (1938). The response of single optic nerve fibers of the vertebrate eye to illumination of the retina. *American Journal of Physiology--Legacy Content* 121, 400-415.
- Kuffler, S.W. (1953). Discharge patterns and functional organization of mammalian retina. *Journal of Neurophysiology* 16, 37-68.
- Hartline, H.K., and Ratliff, F. (1957). Inhibitory interaction of receptor units in the eye of *Limulus*. *J Gen Physiol* 40, 357-376.
- Hubel, D.H., and Wiesel, T.N. (1962). Receptive fields, binocular interaction and functional architecture in the cat's visual cortex. *The Journal of Physiology* 160, 106-154.
- Barlow, H., and Levick, W.R. (1965). The mechanism of directionally selective units in rabbit's retina. *The Journal of Physiology* 178, 477-504.
- Levick, W.R. (1965). Receptive Fields of Rabbit Retinal Ganglion Cells. *Am J Optom Arch Am Acad Optom* 42, 337-343.
- Rodieck, R.W. (1965). Quantitative analysis of cat retinal ganglion cell response to visual stimuli. *Vision Res* 5, 583-601.
- Enroth-Cugell, C., and Robson, J.G. (1966). The contrast sensitivity of retinal ganglion cells of the cat. *The Journal of Physiology* 187, 517-552.
- Wiesel, T.N., and Hubel, D.H. (1966). Spatial and chromatic interactions in the lateral geniculate body of the rhesus monkey. *Journal of Neurophysiology* 29, 1115-1156.
- Katz, B., and Miledi, R. (1967). A study of synaptic transmission in the absence of nerve impulses. *The Journal of Physiology* 192, 407-436.
- Kolb, H. (1970). Organization of the outer plexiform layer of the primate retina: electron microscopy of Golgi-impregnated cells. *Philos Trans R Soc Lond B Biol Sci* 258, 261-283.
- Cleland, B.G., Dubin, M.W., and Levick, W.R. (1971). Sustained and transient neurones in the cat's retina and lateral geniculate nucleus. *The Journal of Physiology* 217, 473-496.
- Baylor, D.A., Hodgkin, A.L., and Lamb, T.D. (1974). The electrical response of turtle cones to flashes and steps of light. *The Journal of Physiology* 242, 685-727.
- Hochstein, S., and Shapley, R.M. (1976). Quantitative analysis of retinal ganglion cell classifications. *The Journal of Physiology* 262, 237-264.
- Caldwell, J.H., and Daw, N.W. (1978). New properties of rabbit retinal ganglion cells. *The Journal of Physiology* 276, 257-276.
- de Monasterio, F.M. (1978). Properties of concentrically organized X and Y ganglion cells of macaque retina. *Journal of Neurophysiology* 41, 1394-1417.

- de Monasterio, F.M. (1979). Asymmetry of on- and off-pathways of blue-sensitive cones of the retina of macaques. *Brain Res* 166, 39-48.
- Hamasaki, D.I., Tasaki, K., and Suzuki, H. (1979). Properties of X- and Y-cells in the rabbit retina. *Jpn J Physiol* 29, 445-457.
- Shapley, R., and Victor, J. (1979). Nonlinear spatial summation and the contrast gain control of cat retinal ganglion cells. *The Journal of Physiology* 290, 141-161.
- Tranchina, D., Gordon, J., Shapley, R., and Toyoda, J. (1981). Linear information processing in the retina: a study of horizontal cell responses. *Proceedings of the National Academy of Sciences* 78, 6540-6542.
- Estevez, O., and Spekreijse, H. (1982). The "silent substitution" method in visual research. *Vision Res* 22, 681-691.
- Srinivasan, M.V., Laughlin, S.B., and Dubs, A. (1982). Predictive coding: a fresh view of inhibition in the retina. *Proceedings of the Royal Society of London B: Biological Sciences* 216, 427-459.
- Enroth-Cugell, C., and Robson, J.G. (1984). Functional characteristics and diversity of cat retinal ganglion cells. Basic characteristics and quantitative description. *Invest Ophthalmol Vis Sci* 25, 250-267.
- Remtulla, S., and Hallett, P.E. (1985). A schematic eye for the mouse, and comparisons with the rat. *Vision Res* 25, 21-31.
- Hood, D., and Finkelstein, M. (1986). Sensitivity to light, *Handbook of Perception and Human Performance*, KR Boff, L. Kaufman, and JP Thomas, eds. (Wiley).
- Hunter, I.W., and Korenberg, M.J. (1986). The identification of nonlinear biological systems: Wiener and Hammerstein cascade models. *Biol Cybern* 55, 135-144.
- Nathans, J., Thomas, D., and Hogness, D.S. (1986). Molecular genetics of human color vision: the genes encoding blue, green, and red pigments. *Science* 232, 193-202.
- Enroth-Cugell, C., and Freeman, A. (1987). The receptive-field spatial structure of cat retinal Y cells. *The Journal of Physiology* 384, 49-79.
- Lee, B.B., Martin, P.R., and Valberg, A. (1989). Nonlinear summation of M- and L-cone inputs to phasic retinal ganglion cells of the macaque. *J Neurosci* 9, 1433-1442.
- Wikler, K.C., Williams, R.W., and Rakic, P. (1990). Photoreceptor mosaic: number and distribution of rods and cones in the rhesus monkey retina. *J Comp Neurol* 297, 499-508.
- Curcio, C.A., Allen, K.A., Sloan, K.R., Lerea, C.L., Hurley, J.B., Klock, I.B., and Milam, A.H. (1991). Distribution and morphology of human cone photoreceptors stained with anti-blue opsin. *J Comp Neurol* 312, 610-624.
- Kolb, H., and Dekorver, L. (1991). Midget ganglion cells of the parafovea of the human retina: a study by electron microscopy and serial section reconstructions. *J Comp Neurol* 303, 617-636.
- Mangel, S.C. (1991). Analysis of the horizontal cell contribution to the receptive field surround of ganglion cells in the rabbit retina. *The Journal of Physiology* 442, 211-234.
- Tranchina, D., Sneyd, J., and Cadenas, I.D. (1991). Light adaptation in turtle cones. Testing and analysis of a model for phototransduction. *Biophys J* 60, 217-237.
- Hibino, H. (1992). Red-green and yellow-blue opponent-color responses as a function of retinal eccentricity. *Vision Res* 32, 1955-1964.
- Jonas, J.B., Schneider, U., and Naumann, G.O. (1992). Count and density of human retinal photoreceptors. *Graefes Arch Clin Exp Ophthalmol* 30, 505-510.
- Atick, J.J., and Redlich, A.N. (1993). Convergent algorithm for sensory receptive field development. *Neural Computation* 5, 45-60.
- Kolb, H., and Nelson, R. (1993). OFF-alpha and OFF-beta ganglion cells in cat retina: II. Neural circuitry as revealed by electron microscopy of HRP stains. *J Comp Neurol* 329, 85-110.
- Dacey, D.M., and Lee, B.B. (1994). The 'blue-on' opponent pathway in primate retina originates from a distinct bistratified ganglion cell type. *Nature* 367, 731-735.
- Kolb, H. (1994). The architecture of functional neural circuits in the vertebrate retina. The Proctor Lecture. *Invest Ophthalmol Vis Sci* 35, 2385-2404.

- Rohlich, P., van Veen, T., and Szel, A. (1994). Two different visual pigments in one retinal cone cell. *Neuron* *13*, 1159-1166.
- Lapuerta, P., and Schein, S.J. (1995). A four-surface schematic eye of macaque monkey obtained by an optical method. *Vision Res* *35*, 2245-2254.
- Merwine, D.K., Amthor, F.R., and Grzywacz, N.M. (1995). Interaction between center and surround in rabbit retinal ganglion cells. *Journal of Neurophysiology* *73*, 1547-1567.
- Baylor, D. (1996). How photons start vision. *Proc Natl Acad Sci U S A* *93*, 560-565.
- Dacey, D.M. (1996). Circuitry for color coding in the primate retina. *Proc Natl Acad Sci U S A* *93*, 582-588.
- Dacey, D.M., Lee, B.B., Stafford, D.K., Pokorny, J., and Smith, V.C. (1996). Horizontal cells of the primate retina: cone specificity without spectral opponency. *Science* *271*, 656-659.
- Dan, Y., Atick, J.J., and Reid, R.C. (1996). Efficient coding of natural scenes in the lateral geniculate nucleus: experimental test of a computational theory. *J Neurosci* *16*, 3351-3362.
- Szel, A., Rohlich, P., Caffè, A.R., and van Veen, T. (1996). Distribution of cone photoreceptors in the mammalian retina. *Microsc Res Tech* *35*, 445-462.
- Sengpiel, F., Sen, A., and Blakemore, C. (1997). Characteristics of surround inhibition in cat area 17. *Exp Brain Res* *116*, 216-228.
- Ahnelt, P.K. (1998). The photoreceptor mosaic. *Eye (Lond)* *12 (Pt 3b)*, 531-540.
- Cook, P.B., and McReynolds, J.S. (1998). Lateral inhibition in the inner retina is important for spatial tuning of ganglion cells. *Nat Neurosci* *1*, 714-719.
- Jeon, C.J., Strettoi, E., and Masland, R.H. (1998). The major cell populations of the mouse retina. *J Neurosci* *18*, 8936-8946.
- Lewicki, M.S. (1998). A review of methods for spike sorting: the detection and classification of neural action potentials. *Network* *9*, R53-78.
- Boycott, B., and Wässle, H. (1999). Parallel processing in the mammalian retina: the Proctor Lecture. *Invest Ophthalmol Vis Sci* *40*, 1313-1327.
- Dacey, D.M. (1999). Primate retina: cell types, circuits and color opponency. *Prog Retin Eye Res* *18*, 737-763.
- Demb, J.B., Haarsma, L., Freed, M.A., and Sterling, P. (1999). Functional circuitry of the retinal ganglion cell's nonlinear receptive field. *J Neurosci* *19*, 9756-9767.
- Meister, M., and Berry, M.J., 2nd (1999). The neural code of the retina. *Neuron* *22*, 435-450.
- Nathans, J. (1999). The evolution and physiology of human color vision: insights from molecular genetic studies of visual pigments. *Neuron* *24*, 299-312.
- Oyster, C.W. (1999). *The human eye*. Sunderland, MA: Sinauer.
- Roorda, A., and Williams, D.R. (1999). The arrangement of the three cone classes in the living human eye. *Nature* *397*, 520-522.
- Applebury, M.L., Antoch, M.P., Baxter, L.C., Chun, L.L., Falk, J.D., Farhangfar, F., Kage, K., Krzystolik, M.G., Lyass, L.A., and Robbins, J.T. (2000). The murine cone photoreceptor: a single cone type expresses both S and M opsins with retinal spatial patterning. *Neuron* *27*, 513-523.
- Dacey, D., Packer, O.S., Diller, L., Brainard, D., Peterson, B., and Lee, B. (2000). Center surround receptive field structure of cone bipolar cells in primate retina. *Vision Res* *40*, 1801-1811.
- Weiler, R., Potttek, M., He, S., and Vaney, D.I. (2000). Modulation of coupling between retinal horizontal cells by retinoic acid and endogenous dopamine. *Brain Res Brain Res Rev* *32*, 121-129.
- Calkins, D.J. (2001). Seeing with S cones. *Prog Retin Eye Res* *20*, 255-287.
- Chichilnisky, E.J. (2001). A simple white noise analysis of neuronal light responses. *Network* *12*, 199-213.
- Dayan, P., and Abbott, L.F. (2001). *Theoretical neuroscience*, Vol 806 (Cambridge, MA: MIT Press).
- Passaglia, C.L., Enroth-Cugell, C., and Troy, J.B. (2001). Effects of remote stimulation on the mean firing rate of cat retinal ganglion cells. *J Neurosci* *21*, 5794-5803.

- Roorda, A., Metha, A.B., Lennie, P., and Williams, D.R. (2001). Packing arrangement of the three cone classes in primate retina. *Vision Res* *41*, 1291-1306.
- Roska, B., and Werblin, F. (2001). Vertical interactions across ten parallel, stacked representations in the mammalian retina. *Nature* *410*, 583-587.
- Pouzat, C., Mazor, O., and Laurent, G. (2002). Using noise signature to optimize spike-sorting and to assess neuronal classification quality. *J Neurosci Methods* *122*, 43-57.
- Reid, R.C., and Shapley, R.M. (2002). Space and time maps of cone photoreceptor signals in macaque lateral geniculate nucleus. *J Neurosci* *22*, 6158-6175.
- Shapley, R., and Hawken, M. (2002). Neural mechanisms for color perception in the primary visual cortex. *Curr Opin Neurobiol* *12*, 426-432.
- Carcieri, S.M., Jacobs, A.L., and Nirenberg, S. (2003). Classification of retinal ganglion cells: a statistical approach. *Journal of Neurophysiology* *90*, 1704-1713.
- Dacey, D.M., and Packer, O.S. (2003). Colour coding in the primate retina: diverse cell types and cone-specific circuitry. *Curr Opin Neurobiol* *13*, 421-427.
- Grubb, M.S., and Thompson, I.D. (2003). Quantitative characterization of visual response properties in the mouse dorsal lateral geniculate nucleus. *Journal of Neurophysiology* *90*, 594-607.
- Olveczky, B.P., Baccus, S.A., and Meister, M. (2003). Segregation of object and background motion in the retina. *Nature* *423*, 401-408.
- Paninski, L. (2003). Convergence properties of three spike-triggered analysis techniques. *Network* *14*, 437-464.
- Poynton, C.A. (2003). *Digital Video and HDTV: Algorithms and Interfaces* (Morgan Kaufmann Publishers).
- Diller, L., Packer, O.S., Verweij, J., McMahan, M.J., Williams, D.R., and Dacey, D.M. (2004). L and M cone contributions to the midget and parasol ganglion cell receptive fields of macaque monkey retina. *J Neurosci* *24*, 1079-1088.
- Famiglietti, E.V. (2004). Class I and class II ganglion cells of rabbit retina: a structural basis for X and Y (brisk) cells. *J Comp Neurol* *478*, 323-346.
- McMahon, M.J., Packer, O.S., and Dacey, D.M. (2004). The classical receptive field surround of primate parasol ganglion cells is mediated primarily by a non-GABAergic pathway. *J Neurosci* *24*, 3736-3745.
- Schmucker, C., and Schaeffel, F. (2004). A paraxial schematic eye model for the growing C57BL/6 mouse. *Vision Res* *44*, 1857-1867.
- Wassle, H. (2004). Parallel processing in the mammalian retina. *Nat Rev Neurosci* *5*, 747-757.
- Westheimer, G. (2004). Center-surround antagonism in spatial vision: retinal or cortical locus? *Vision Res* *44*, 2457-2465.
- Fried, S.I., Munch, T.A., and Werblin, F.S. (2005). Directional selectivity is formed at multiple levels by laterally offset inhibition in the rabbit retina. *Neuron* *46*, 117-127.
- Haverkamp, S., Wassle, H., Duebel, J., Kuner, T., Augustine, G.J., Feng, G., and Euler, T. (2005). The primordial, blue-cone color system of the mouse retina. *J Neurosci* *25*, 5438-5445.
- Ichinose, T., and Lukasiewicz, P.D. (2005). Inner and outer retinal pathways both contribute to surround inhibition of salamander ganglion cells. *The Journal of Physiology* *565*, 517-535.
- Lukats, A., Szabo, A., Rohlich, P., Vigh, B., and Szel, A. (2005). Photopigment coexpression in mammals: comparative and developmental aspects. *Histol Histopathol* *20*, 551-574.
- Peichl, L. (2005). Diversity of mammalian photoreceptor properties: adaptations to habitat and lifestyle? *Anat Rec A Discov Mol Cell Evol Biol* *287*, 1001-1012.
- DeVries, S.H., Li, W., and Saszik, S. (2006). Parallel processing in two transmitter microenvironments at the cone photoreceptor synapse. *Neuron* *50*, 735-748.
- Duebel, J., Haverkamp, S., Schleich, W., Feng, G., Augustine, G.J., Kuner, T., and Euler, T. (2006). Two-photon imaging reveals somatodendritic chloride gradient in retinal ON-type bipolar cells expressing the biosensor Clomeleon. *Neuron* *49*, 81-94.

- Gold, C., Henze, D.A., Koch, C., and Buzsaki, G. (2006). On the origin of the extracellular action potential waveform: A modeling study. *Journal of Neurophysiology* *95*, 3113-3128.
- Lee, S., and Zhou, Z.J. (2006). The synaptic mechanism of direction selectivity in distal processes of starburst amacrine cells. *Neuron* *51*, 787-799.
- Li, W., and DeVries, S.H. (2006). Bipolar cell pathways for color and luminance vision in a dichromatic mammalian retina. *Nat Neurosci* *9*, 669-675.
- Nikonov, S.S., Kholodenko, R., Lem, J., and Pugh, E.N., Jr. (2006). Physiological features of the S- and M-cone photoreceptors of wild-type mice from single-cell recordings. *J Gen Physiol* *127*, 359-374.
- Schwartz, O., Pillow, J.W., Rust, N.C., and Simoncelli, E.P. (2006). Spike-triggered neural characterization. *J Vis* *6*, 484-507.
- Solomon, S.G., Lee, B.B., and Sun, H. (2006). Suppressive surrounds and contrast gain in magnocellular-pathway retinal ganglion cells of macaque. *J Neurosci* *26*, 8715-8726.
- van Wyk, M., Taylor, W.R., and Vaney, D.I. (2006). Local edge detectors: a substrate for fine spatial vision at low temporal frequencies in rabbit retina. *J Neurosci* *26*, 13250-13263.
- Yin, L., Smith, R.G., Sterling, P., and Brainard, D.H. (2006). Chromatic properties of horizontal and ganglion cell responses follow a dual gradient in cone opsin expression. *J Neurosci* *26*, 12351-12361.
- Field, G.D., and Chichilnisky, E.J. (2007). Information processing in the primate retina: circuitry and coding. *Annu Rev Neurosci* *30*, 1-30.
- Petrusca, D., Grivich, M.I., Sher, A., Field, G.D., Gauthier, J.L., Greschner, M., Shlens, J., Chichilnisky, E.J., and Litke, A.M. (2007). Identification and characterization of a Y-like primate retinal ganglion cell type. *J Neurosci* *27*, 11019-11027.
- Zaghloul, K.A., Manookin, M.B., Borghuis, B.G., Boahen, K., and Demb, J.B. (2007). Functional circuitry for peripheral suppression in Mammalian Y-type retinal ganglion cells. *Journal of Neurophysiology* *97*, 4327-4340.
- Baccus, S.A., Olveczky, B.P., Manu, M., and Meister, M. (2008). A retinal circuit that computes object motion. *J Neurosci* *28*, 6807-6817.
- Borghuis, B.G., Ratliff, C.P., Smith, R.G., Sterling, P., and Balasubramanian, V. (2008). Design of a neuronal array. *J Neurosci* *28*, 3178-3189.
- Crook, J.D., Peterson, B.B., Packer, O.S., Robinson, F.R., Troy, J.B., and Dacey, D.M. (2008). Y-cell receptive field and collicular projection of parasol ganglion cells in macaque monkey retina. *J Neurosci* *28*, 11277-11291.
- Davenport, C.M., Detwiler, P.B., and Dacey, D.M. (2008). Effects of pH buffering on horizontal and ganglion cell light responses in primate retina: evidence for the proton hypothesis of surround formation. *J Neurosci* *28*, 456-464.
- Niell, C.M., and Stryker, M.P. (2008). Highly selective receptive fields in mouse visual cortex. *J Neurosci* *28*, 7520-7536.
- Tokutake, Y., and Freed, M.A. (2008). Retinal ganglion cells—spatial organization of the receptive field reduces temporal redundancy. *European Journal of Neuroscience* *28*, 914-923.
- Umino, Y., Solessio, E., and Barlow, R.B. (2008). Speed, spatial, and temporal tuning of rod and cone vision in mouse. *J Neurosci* *28*, 189-198.
- Molnar, A., Hsueh, H.A., Roska, B., and Werblin, F.S. (2009). Crossover inhibition in the retina: circuitry that compensates for nonlinear rectifying synaptic transmission. *J Comput Neurosci* *27*, 569-590.
- Munch, T.A., da Silveira, R.A., Siebert, S., Viney, T.J., Awatramani, G.B., and Roska, B. (2009). Approach sensitivity in the retina processed by a multifunctional neural circuit. *Nat Neurosci* *12*, 1308-1316.
- Ozeki, H., Finn, I.M., Schaffer, E.S., Miller, K.D., and Ferster, D. (2009). Inhibitory stabilization of the cortical network underlies visual surround suppression. *Neuron* *62*, 578-592.
- Passaglia, C.L., Freeman, D.K., and Troy, J.B. (2009). Effects of remote stimulation on the modulated activity of cat retinal ganglion cells. *J Neurosci* *29*, 2467-2476.

- Shapley, R. (2009). Linear and nonlinear systems analysis of the visual system: why does it seem so linear? A review dedicated to the memory of Henk Spekreijse. *Vision Res* *49*, 907-921.
- Volgyi, B., Chheda, S., and Bloomfield, S.A. (2009). Tracer coupling patterns of the ganglion cell subtypes in the mouse retina. *J Comp Neurol* *512*, 664-687.
- Wassle, H., Puller, C., Muller, F., and Haverkamp, S. (2009). Cone contacts, mosaics, and territories of bipolar cells in the mouse retina. *J Neurosci* *29*, 106-117.
- Yin, L., Smith, R.G., Sterling, P., and Brainard, D.H. (2009). Physiology and morphology of color-opponent ganglion cells in a retina expressing a dual gradient of S and M opsins. *J Neurosci* *29*, 2706-2724.
- Field, G.D., Gauthier, J.L., Sher, A., Greschner, M., Machado, T.A., Jepson, L.H., Shlens, J., Gunning, D.E., Mathieson, K., Dabrowski, W., *et al.* (2010). Functional connectivity in the retina at the resolution of photoreceptors. *Nature* *467*, 673-677.
- Gollisch, T., and Meister, M. (2010). Eye smarter than scientists believed: neural computations in circuits of the retina. *Neuron* *65*, 150-164.
- Guo, C., Hirano, A.A., Stella, S.L., Jr., Bitzer, M., and Brecha, N.C. (2010). Guinea pig horizontal cells express GABA, the GABA-synthesizing enzyme GAD 65, and the GABA vesicular transporter. *J Comp Neurol* *518*, 1647-1669.
- Lee, B.B., Martin, P.R., and Grunert, U. (2010). Retinal connectivity and primate vision. *Prog Retin Eye Res* *29*, 622-639.
- Packer, O.S., Verweij, J., Li, P.H., Schnapf, J.L., and Dacey, D.M. (2010). Blue-yellow opponency in primate S cone photoreceptors. *J Neurosci* *30*, 568-572.
- Pitulescu, M.E., Schmidt, I., Benedito, R., and Adams, R.H. (2010). Inducible gene targeting in the neonatal vasculature and analysis of retinal angiogenesis in mice. *Nat Protoc* *5*, 1518-1534.
- Wei, W., Elstrott, J., and Feller, M.B. (2010). Two-photon targeted recording of GFP-expressing neurons for light responses and live-cell imaging in the mouse retina. *Nat Protoc* *5*, 1347-1352.
- Werblin, F.S. (2010). Six different roles for crossover inhibition in the retina: correcting the nonlinearities of synaptic transmission. *Vis Neurosci* *27*, 1-8.
- Breuninger, T., Puller, C., Haverkamp, S., and Euler, T. (2011). Chromatic bipolar cell pathways in the mouse retina. *J Neurosci* *31*, 6504-6517.
- Crook, J.D., Manookin, M.B., Packer, O.S., and Dacey, D.M. (2011). Horizontal cell feedback without cone type-selective inhibition mediates "red-green" color opponency in midget ganglion cells of the primate retina. *J Neurosci* *31*, 1762-1772.
- Huberman, A.D., and Niell, C.M. (2011). What can mice tell us about how vision works? *Trends Neurosci* *34*, 464-473.
- Wang, Y.V., Weick, M., and Demb, J.B. (2011). Spectral and temporal sensitivity of cone-mediated responses in mouse retinal ganglion cells. *J Neurosci* *31*, 7670-7681.
- Werblin, F.S. (2011). The retinal hypercircuit: a repeating synaptic interactive motif underlying visual function. *The Journal of Physiology* *589*, 3691-3702.
- Williams, D.R. (2011). Imaging single cells in the living retina. *Vision Res* *51*, 1379-1396.
- Bolinger, D., and Gollisch, T. (2012). Closed-loop measurements of iso-response stimuli reveal dynamic nonlinear stimulus integration in the retina. *Neuron* *73*, 333-346.
- Masland, R.H. (2012). The neuronal organization of the retina. *Neuron* *76*, 266-280.
- Schwartz, G.W., Okawa, H., Dunn, F.A., Morgan, J.L., Kerschensteiner, D., Wong, R.O., and Rieke, F. (2012). The spatial structure of a nonlinear receptive field. *Nat Neurosci* *15*, 1572-1580.
- Sher, A., and DeVries, S.H. (2012). A non-canonical pathway for mammalian blue-green color vision. *Nat Neurosci* *15*, 952-953.
- Thoreson, W.B., and Mangel, S.C. (2012). Lateral interactions in the outer retina. *Prog Retin Eye Res* *31*, 407-441.
- Vaney, D.I., Sivyver, B., and Taylor, W.R. (2012). Direction selectivity in the retina: symmetry and asymmetry in structure and function. *Nat Rev Neurosci* *13*, 194-208.

- Zhang, C., and McCall, M.A. (2012). Receptor targets of amacrine cells. *Vis Neurosci* *29*, 11-29.
- Baden, T., Schubert, T., Chang, L., Wei, T., Zaichuk, M., Wissinger, B., and Euler, T. (2013). A tale of two retinal domains: near-optimal sampling of achromatic contrasts in natural scenes through asymmetric photoreceptor distribution. *Neuron* *80*, 1206-1217.
- Baker, M. (2013). Neuroscience: Through the eyes of a mouse. *Nature* *502*, 156-158.
- Borghuis, B.G., Marvin, J.S., Looger, L.L., and Demb, J.B. (2013). Two-photon imaging of nonlinear glutamate release dynamics at bipolar cell synapses in the mouse retina. *J Neurosci* *33*, 10972-10985.
- Chang, L., Breuninger, T., and Euler, T. (2013). Chromatic coding from cone-type unselective circuits in the mouse retina. *Neuron* *77*, 559-571.
- Della Santina, L., Inman, D.M., Lupien, C.B., Horner, P.J., and Wong, R.O. (2013). Differential progression of structural and functional alterations in distinct retinal ganglion cell types in a mouse model of glaucoma. *J Neurosci* *33*, 17444-17457.
- Farrow, K., Teixeira, M., Szikra, T., Viney, T.J., Balint, K., Yonehara, K., and Roska, B. (2013). Ambient illumination toggles a neuronal circuit switch in the retina and visual perception at cone threshold. *Neuron* *78*, 325-338.
- Gollisch, T. (2013). Features and functions of nonlinear spatial integration by retinal ganglion cells. *J Physiol Paris* *107*, 338-348.
- Euler, T., Haverkamp, S., Schubert, T., and Baden, T. (2014). Retinal bipolar cells: elementary building blocks of vision. *Nat Rev Neurosci* *15*, 507-519.
- Puller, C., Haverkamp, S., Neitz, M., and Neitz, J. (2014). Synaptic elements for GABAergic feed-forward signaling between HII horizontal cells and blue cone bipolar cells are enriched beneath primate S-cones. *PLoS One* *9*, e88963.
- Reinhard, K., Tikidji-Hamburyan, A., Seitter, H., Idrees, S., Mutter, M., Benkner, B., and Munch, T.A. (2014). Step-by-step instructions for retina recordings with perforated multi electrode arrays. *PLoS One* *9*, e106148.
- Seung, H.S., and Sumbul, U. (2014). Neuronal cell types and connectivity: lessons from the retina. *Neuron* *83*, 1262-1272.
- Takeshita, D., and Gollisch, T. (2014). Nonlinear spatial integration in the receptive field surround of retinal ganglion cells. *J Neurosci* *34*, 7548-7561.
- Vlasits, A.L., Bos, R., Morrie, R.D., Fortuny, C., Flannery, J.G., Feller, M.B., and Rivlin-Etzion, M. (2014). Visual stimulation switches the polarity of excitatory input to starburst amacrine cells. *Neuron* *83*, 1172-1184.
- Vroman, R., Klaassen, L.J., Howlett, M.H., Cenedese, V., Klooster, J., Sjoerdsma, T., and Kamermans, M. (2014). Extracellular ATP hydrolysis inhibits synaptic transmission by increasing pH buffering in the synaptic cleft. *PLoS Biol* *12*, e1001864.
- Wang, T.M., Holzhausen, L.C., and Kramer, R.H. (2014). Imaging an optogenetic pH sensor reveals that protons mediate lateral inhibition in the retina. *Nat Neurosci* *17*, 262-268.
- Rubin, D.B., Van Hooser, S.D., and Miller, K.D. (2015). The stabilized supralinear network: a unifying circuit motif underlying multi-input integration in sensory cortex. *Neuron* *85*, 402-417.
- Sanes, J.R., and Masland, R.H. (2015). The types of retinal ganglion cells: current status and implications for neuronal classification. *Annu Rev Neurosci* *38*, 221-246.
- Veleri, S., Lazar, C.H., Chang, B., Sieving, P.A., Banin, E., and Swaroop, A. (2015). Biology and therapy of inherited retinal degenerative disease: insights from mouse models. *Dis Model Mech* *8*, 109-129.
- Baden, T., Berens, P., Franke, K., Roman Roson, M., Bethge, M., and Euler, T. (2016). The functional diversity of retinal ganglion cells in the mouse. *Nature* *529*, 345-350.
- Behrens, C., Schubert, T., Haverkamp, S., Euler, T., and Berens, P. (2016). Connectivity map of bipolar cells and photoreceptors in the mouse retina. *Elife* *5*.
- Joesch, M., and Meister, M. (2016). A neuronal circuit for colour vision based on rod-cone opponency. *Nature* *532*, 236-239.

- Turner, M.H., and Rieke, F. (2016). Synaptic Rectification Controls Nonlinear Spatial Integration of Natural Visual Inputs. *Neuron* *90*, 1257-1271.
- Viets, K., Eldred, K.C., and Johnston, R.J., Jr. (2016). Mechanisms of Photoreceptor Patterning in Vertebrates and Invertebrates. *Trends Genet* *32*, 638-659.
- Denman, D.J., Siegle, J.H., Koch, C., Reid, R.C., and Blanche, T.J. (2017). Spatial Organization of Chromatic Pathways in the Mouse Dorsal Lateral Geniculate Nucleus. *J Neurosci* *37*, 1102-1116.
- Franke, K., and Baden, T. (2017). General features of inhibition in the inner retina. *The Journal of Physiology* *595*, 5507-5515.
- Franke, K., Berens, P., Schubert, T., Bethge, M., Euler, T., and Baden, T. (2017). Inhibition decorrelates visual feature representations in the inner retina. *Nature* *542*, 439-444.
- Krieger, B., Qiao, M., Rousso, D.L., Sanes, J.R., and Meister, M. (2017). Four alpha ganglion cell types in mouse retina: Function, structure, and molecular signatures. *PLoS One* *12*, e0180091.
- Liu, J.K., Schreyer, H.M., Onken, A., Rozenblit, F., Khani, M.H., Krishnamoorthy, V., Panzeri, S., and Gollisch, T. (2017). Inference of neuronal functional circuitry with spike-triggered non-negative matrix factorization. *Nat Commun* *8*, 149.
- Sabharwal, J., Seilheimer, R.L., Tao, X., Cowan, C.S., Frankfort, B.J., and Wu, S.M. (2017). Elevated IOP alters the space-time profiles in the center and surround of both ON and OFF RGCs in mouse. *Proc Natl Acad Sci U S A* *114*, 8859-8864.
- Seabrook, T.A., Burbridge, T.J., Crair, M.C., and Huberman, A.D. (2017). Architecture, Function, and Assembly of the Mouse Visual System. *Annu Rev Neurosci* *40*, 499-538.